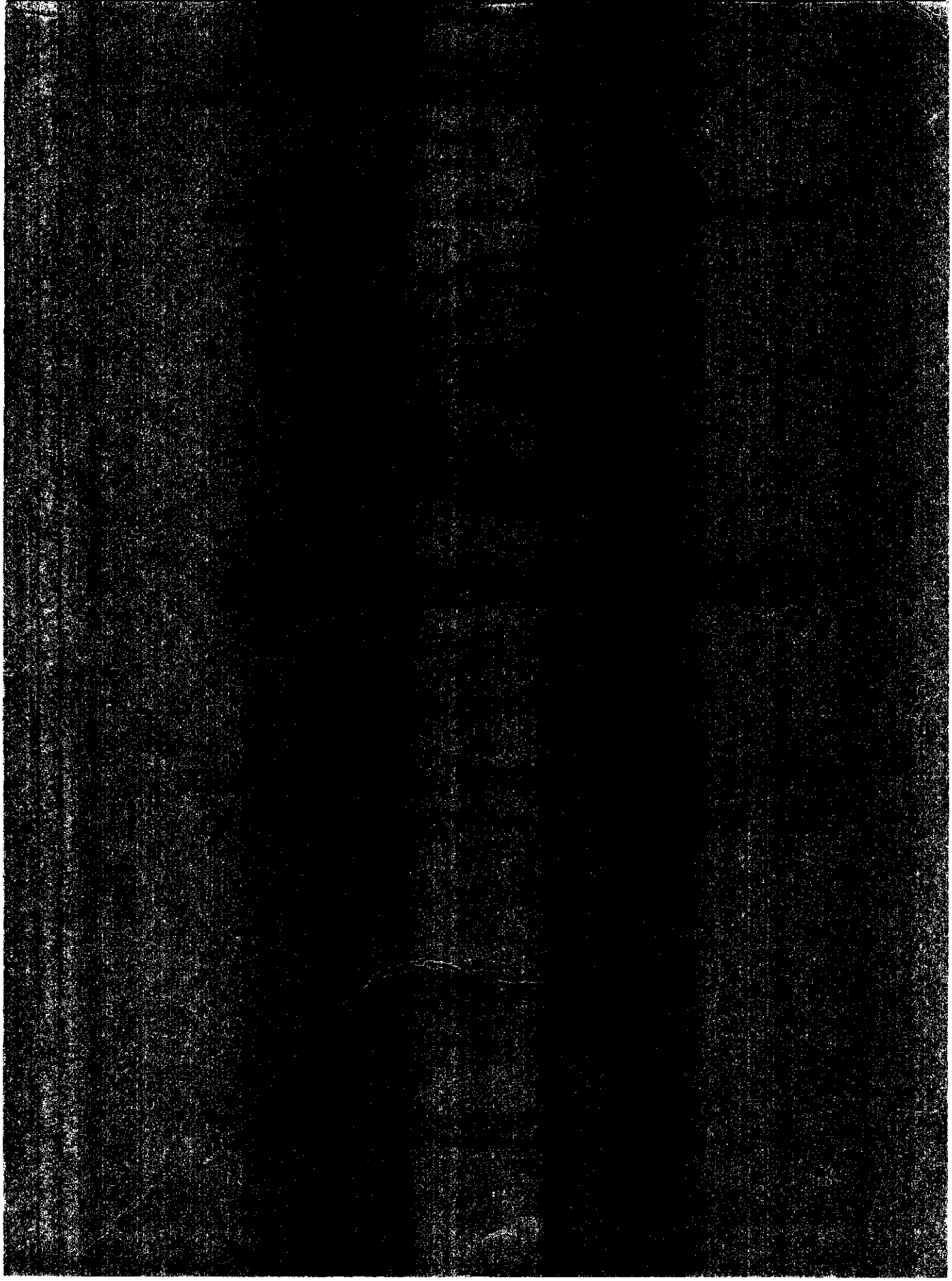

PUBLICATIONS
OF THE
ANTARCTIC DIVISION, DEPARTMENT OF EXTERNAL AFFAIRS

EDITOR: P. G. Law, Director

ASSISTANT EDITOR: M. R. O. Millett, Publications Officer

Reports are now published in three categories:

ANARE SCIENTIFIC REPORTS
ANARE INTERIM REPORTS
ANARE DATA REPORTS

These are classified as follows:

Series A	(I)	Narrative
	(II)	Geography
	(III)	Geology
	(IV)	Glaciology
Series B	(I)	Zoology
	(II)	Botany
	(III)	Oceanography
	(IV)	Medical Science
Series C	(I)	Terrestrial Magnetism
	(II)	Cosmic Rays
	(III)	Upper Atmosphere Physics
Series D		Meteorology

In general, it is the policy of the Division to publish in the regular scientific journals all articles suitable for such media. The ANARE SCIENTIFIC REPORTS provide a medium for publication of comprehensive works and for specialized studies not catered for by appropriate journals. The ANARE INTERIM REPORTS cater for scientific and technical articles, descriptions of instruments etc. which, because of the preliminary nature of the work or for other reasons, are likely to be of relatively lower long-term importance. The ANARE DATA REPORTS contain numerical or graphical data with only very limited discussion.

Copies of Reports and a list of Reports published are available from the Publications Officer, Antarctic Division, Department of External Affairs, 568 St. Kilda Road, Melbourne, S.C.3, Victoria, Australia.

COMMONWEALTH OF AUSTRALIA
DEPARTMENT OF EXTERNAL AFFAIRS

AUSTRALIAN NATIONAL ANTARCTIC RESEARCH EXPEDITIONS

ANARE SCIENTIFIC REPORTS

SERIES A (IV) GLACIOLOGY

PUBLICATION No. 88

GLACIOLOGICAL STUDIES IN THE REGION OF WILKES, EASTERN ANTARCTICA, 1961

by
W. F. BUDD

ISSUED BY THE ANTARCTIC DIVISION
DEPARTMENT OF EXTERNAL AFFAIRS, MELBOURNE
1966

CONTENTS

LIST OF FIGURES*

* An abridgement of each longer explanatory caption accompanying the respective figure.

GLACIOLOGICAL STUDIES IN THE REGION OF WILKES, EASTERN ANTARCTICA, 1961

By

W. F. BUDD

Antarctic Division, Department of External Affairs, Melbourne

(Manuscript received 15 December 1965)

ABSTRACT

An analysis of the glaciological work at Wilkes initiated by U.S. glaciologists in 1957–58 and continued and extended by ANARE to 1962 is presented.

The climate at Wilkes, as indicated by the three climatic elements, temperature, wind speed and precipitation, is shown to vary considerably from one year to another. This has an important influence on the pattern of snow stratification of the inland plateau. The pattern of higher temperatures over summer and higher wind speeds over winter are the prime factors which allow pit data to be used to indicate annual accumulation layers.

Accumulation measurements using stakes over a 5-year period from Wilkes to 80 km inland show that the position of the snow line varies from one year to another. The result is zero net accumulation to about 400 m elevation. From here the average net accumulation increases to 10 g cm^{-2} 20 km inland and then more gradually to 14 g cm^{-2} 80 km inland, elevation 1100 m. One year results further inland (100 km) show that there is a region of high accumulation (80 g cm^{-2}) over a topographical depression. This high rate gradually decreases to 30 g cm^{-2} by 300 km and 20 g cm^{-2} 500 km inland.

Measurements of wind speed and snow drift at various levels above the surface, both at Wilkes and on the inland plateau, show that the variation in drift density conforms with the theory of turbulent snow transport discussed by Dingle and Radok (1960). As the wind speed increases from 13 to 27 m sec^{-1} the drift density at the 400 cm level increases from 0·1 to 1·5 g cm^{-3}, and at the 12·5 cm level from 12 to 65 g cm^{-3}. The total drift content (1 cm to 100 m) increases from 25 to 63 g m^{-2}. The total drift transport rate (1 m to 100 m) increases from 0·6 to 10·4 g cm^{-1} sec^{-1}.

The annual drift transport past Wilkes and S2 are calculated as $2{\cdot}1 \times 10^7$ and $3{\cdot}5 \times 10^7$ g cm^{-1} yr^{-1}. The variation in wind speed over the local ice cap allows the variation in net accumulation due to snow drift to be calculated.

Temperatures in the firn, to 7 m depth, were measured to 500 km inland, elevation 3000 m. The variation in temperature with depth is studied. The effect of the high accumulation at the surface and the varying diffusivity with depth are considered in obtaining estimates of annual mean temperature. This temperature is found to decrease with elevation at the rate of 0·9°C/100 m near the coast, and 1·2°C/100 m, 500 km inland. Temperature gradients between 10 and 30 m depth at the ice cap surface were found to decrease gradually from +2·8°C/100 m near the coast to +0·4°C/100 m 60 km inland. Further inland, higher negative temperature gradients prevail. The import of these temperature gradients is discussed in relation to the ice thickness, movement and accumulation rate. The basal temperatures are calculated to be just below melting point.

Several years' data on the compaction of the snow in the 35 m deep pit at the inland station S2 are analysed and related to the changes in the density profile and the accumulation rate. The compaction rates decrease from 3·0% yr^{-1} at 4 m to 0·5 at 10 m and 0·25 at 30 m. Contraction of the 2 m diameter tunnel at the 30 m depth has been decreasing in time. The variation in contraction rate along the tunnel allows estimates of the ice flow parameters to be made.

The ice cap surface at S2 has a maximum strain rate ($+3 \times 10^{-4}$ yr^{-1}) perpendicular to the direction of maximum slope and a minimum along the slope. Near the coastal ice cliffs there is a higher strain rate of 1% yr^{-1} in the direction of flow. Surface waves along the Vanderford Glacier are moving with the velocity of the glacier.

Mass budget considerations of the Wilkes region suggest that the local area (to 200 km inland) appears to be approximately in balance, but further inland there appears to be a net gain.

PREFACE

Prior to 1957, little was known about the large sector of East Antarctica between Mawson (longitude approximately 63°E) and Dumont D'Urville (140°E) (cf. Fig. 0.1). With the beginning of the I.G.Y. three further permanent coastal stations were established in this region: Wilkes (66° 15'S, 110° 35'E), Mirny (66° 33'S, 93° 00'E), and Davis (68° 33'S, 77° 56'E).

The present report deals with various aspects of the glaciology of the ice cap in the Wilkes region. In order to broaden the picture a comparison is made with data drawn from coastal stations, and their associated inland bases, of a large part of Eastern Antarctica.

The broad objectives of the glaciological research programme are to determine the shape and size of the ice cap in this region, its past history, what is happening to it now (its "regime" or mass and heat budgets) and the mechanisms of special physical processes related to these problems. With these aims in mind, this report analyses the results of glaciological work carried out by the writer during 1961. As much of this work is a continuation and extension of previous studies at Wilkes, the analysis amounts to a synthesis of results from measurements and observations made over the period 1957 to 1962.

The arrangement of these results and the order in which different subjects are treated are somewhat arbitrary. Therefore an outline of the previous work carried out at Wilkes and a synopsis of the report as a whole are given in the Introduction.

0. INTRODUCTION

0.1. BACKGROUND

0.1.1. Glaciological work 1957-58

As part of the I.G.Y. programme the U.S.A. established Wilkes station in January 1957 on Clark Peninsular of the Windmill Islands (cf. Fig. 0.2). From Wilkes as base, studies were initiated in the following sciences: glaciology, geology, oceanography, meteorology, ionospherics, aurora, geomagnetism, local seisms.

The glaciology programme, carried out by a team of three glaciologists in each of 1957 and 1958, covered a wide range of topics, including

(i) Topography and geomorphology

(ii) Snow accumulation

(iii) Meteorology of the ice cap

(iv) Ice movement

(v) Glacial geology and geochronology

(vi) Sea ice observations

(vii) Field traverse surface and subsurface observations.

As this early work provides a background for the later investigations an outline will be given of the results of the major work carried out in each of these sections.

(i) Topography. The Windmill Islands (cf. Fig. 0.3)are an extensive rock exposure contained within a rectangle approximately 51 km N–S and 14 km E–W. "The summits of the islands are generally accordant at 250 ft. (76 m) and may represent remnants of an old erosion surface. This surface is now dissected by shallow U-shaped valleys and broad, deeper valleys which, at present, form arms of the sea." (Robertson (1959), p.2).

This coastal rock is, in general, joined to the ice plateau by a steep ice 'ramp'. In the northern area of the islands this join of the ramp and ice plateau is characterised by a shear moraine at approximately 160 m elevation (cf. Fig. 0.2).

Topographic surveys to obtain the form of the rock and ice profile, and to fix certain positions for movement studies, resulted in the Northern Area map (cf. Fig. 0.4). In this are shown the positions which were fixed by triangulation, and by subtense, relative to a point B2 at Wilkes on Clerk Peninsular, which was established astronomically at

$$66^\circ\ 15'\ 24''\ \pm\ 03''\ \text{S}$$
$$110^\circ\ 31'\ 31''\ \pm\ 03''\ \text{E}$$

(Hollin *et al.* (1961), p.8).

The ice plateau rises gradually less steeply inland of the moraine. The surface topographic survey was extended to 80 km inland at an elevation of 1160 m where a

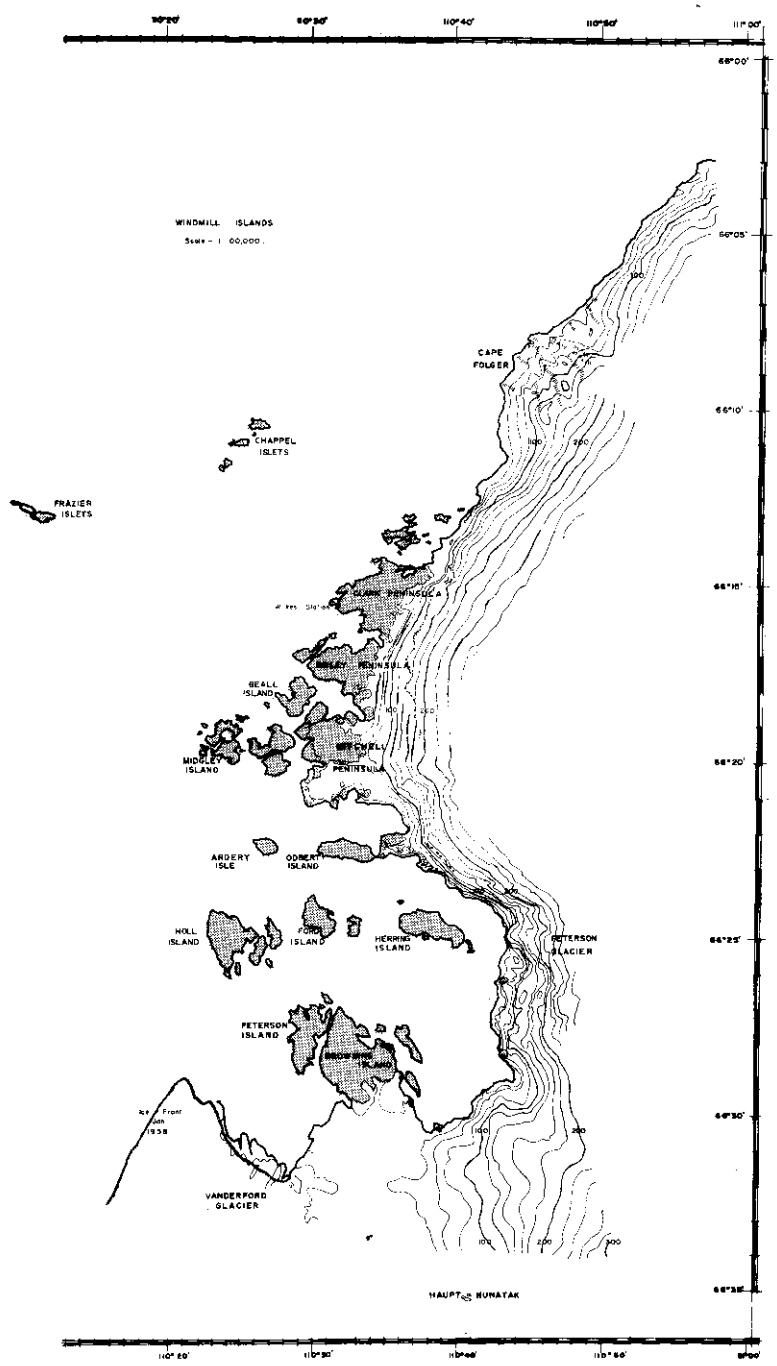

FIG. 0.2. THE WINDMILL ISLANDS. This group is an outcrop of rock at the edge of the ice cap consisting of some islands which are free of ice in summer, as well as some rock peninsulas which are permanently joined by ice to the mainland ice cap. Wilkes station is situated on one such rock outcrop—Clark Peninsula.

satellite station S2 was established in 1957. No exposed rock occurs inland further than Haupt Nunatak which is a cluster of rock outcrops covering approximately 0.2 sq km and is situated approximately 12 km from the coast, just north of the Vanderford Glacier (cf. Fig. 0.2).

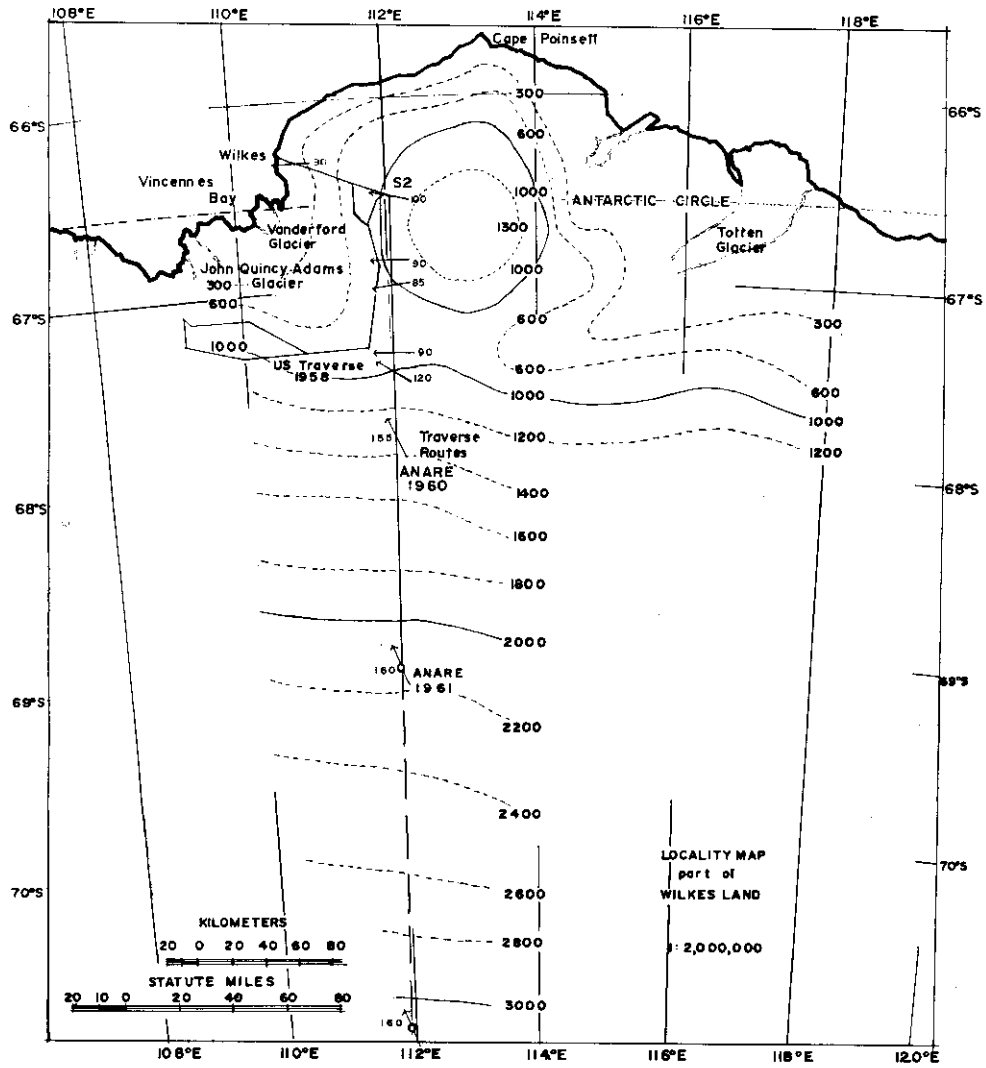

FIG. 0.3. THE WILKES REGION OF THE ANTARCTIC ICE CAP. The glaciological traverse routes of 1958–60–61 are shown. The arrows show the predominant sastrugi directions measured in 1961.

(ii) Snow accumulation. Over 1957 and 1958 systems of stakes were established and detailed accumulation measurements were carried out at the coast, along the S2 trail, and at S2. To determine the pattern of snow accumulation of the past, and also the properties of this accumulated snow, a pit was excavated at S2 to a depth of 35 m. By studying the snow stratigraphy exposed by the pit the annual layers

the accumulation in recent years.

Temperatures in the firn had previously been measured to about 10 m depth in the Wilkes region to obtain estimates of the annual mean temperature at the

were traced back as far as 1783 and the annual accumulation rates from that time were determined (Cameron *et al.* (1959).

Further information on the accumulation of the region was obtained from pits and subsurface observations made on the inland trips.

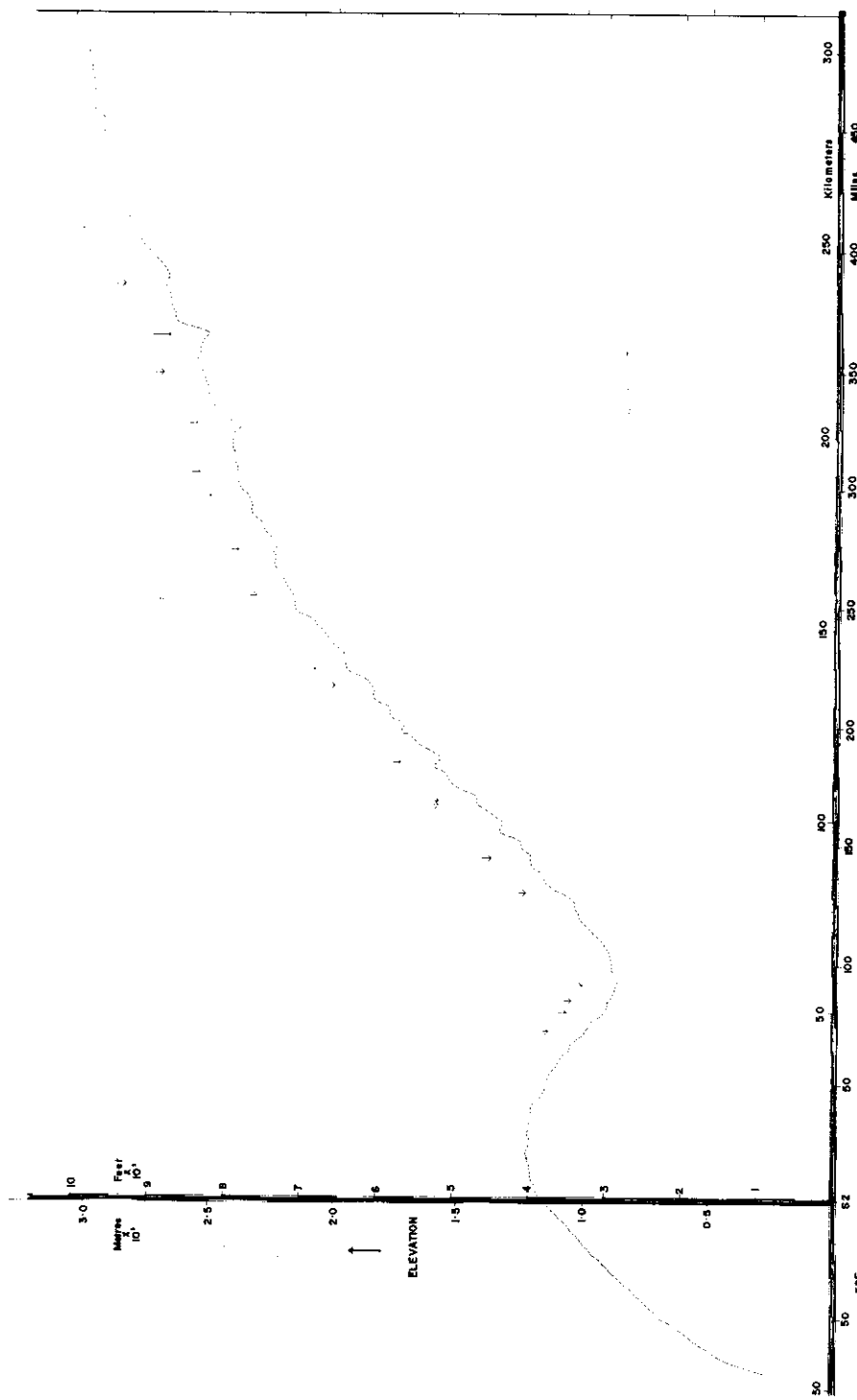

FIG. 0.5. THE ICE PLATEAU ELEVATION PROFILE INLAND OF WILKES. The results have been taken from the 1961 observations of Jewell. The arrows indicate positions of high sastrugi.

(vii) Traverses. In 1957 a traverse in December was made by dog sledge, on the sea ice, following the coastal ice cliffs north from Wilkes to Cape Poinsett. In 1958 a traverse was made inland of the Vanderford and John Quincy Adams Glaciers (cf. Fig. 0.3). Surface and sub-surface glaciological observations were carried out. The terrain encountered included many domed and crevassed areas.

0.1.2. Glaciological work since 1958

Following the I.G.Y. period, the Australian National Antarctic Research Expeditions 1959, 1960 and 1961 have continued glaciological activities at Wilkes, the glaciological programme being largely organised by the Department of Meteorology of the University of Melbourne.

In 1959, accumulation measurements were continued in the local area, S2 was visited for pit compaction measurements, and apparatus for measuring the amount of blowing snow at various levels from the ground was installed and operated.

In 1960, the local area accumulation measurements were continued, the S2 trail stakes were remeasured, and the 12 relative movement stakes at S2 were located, surveyed, and measured for accumulation. Compaction and contraction measurements were carried out in the pit and tunnel. In November and December 1960 a field traverse was made from Wilkes to S2 and 180 miles (290 km) south of S2. Accumulation stakes were placed at each mile (1.6 km) intervals and snow surface observations were recorded.

Programme of 1961

(i) Geophysical exploration. In 1961, the field geophysical programme commenced. This work, undertaken by the Australian Bureau of Mineral Resources Geology and Geophysics, aims at determining by a series of traverses over several years the ice cap elevations (barometrically), the ice thickness (by seismic reflection and gravity observations) and the distribution of seismic wave velocities in the ice (by seismic refraction). The region covered by the 1961 seismic survey is shown in Figure 0.3. Ice thicknesses were determined at 20-mile (32 km) intervals from Wilkes to S2 and 300 miles (480 km) south of S2.

Preliminary results of this geophysical work are presented in an unpublished report of the Australian Bureau of Mineral Resources Geology and Geophysics by Jewell (1962). cf. also Figure 4.4.

(ii) Glaciological work. Accummulation measurements were continued on all the existing stake systems in 1961, and the 1960 stake line was extended to 480 km south of S2. Movement studies were continued in the Vanderford Glacier area, at Cape Folger, and inland at S2 with the relative movement strain grid and the deep pit. The study of drifting snow, commenced at Wilkes in 1959, was continued in 1961 and extended to inland on the plateau at S2. Along the traverse route surface and subsurface observations were made and a series of pits were excavated and the usow stratigraphy studied along the accumulation profile from Wilkes to S2 and 480 km south of S2 to provide information on weather conditions inland as well as the accumulation in recent years.

Temperatures in the firn had previously been measured to about 10 m depth in the Wilkes region to obtain estimates of the annual mean temperature at the

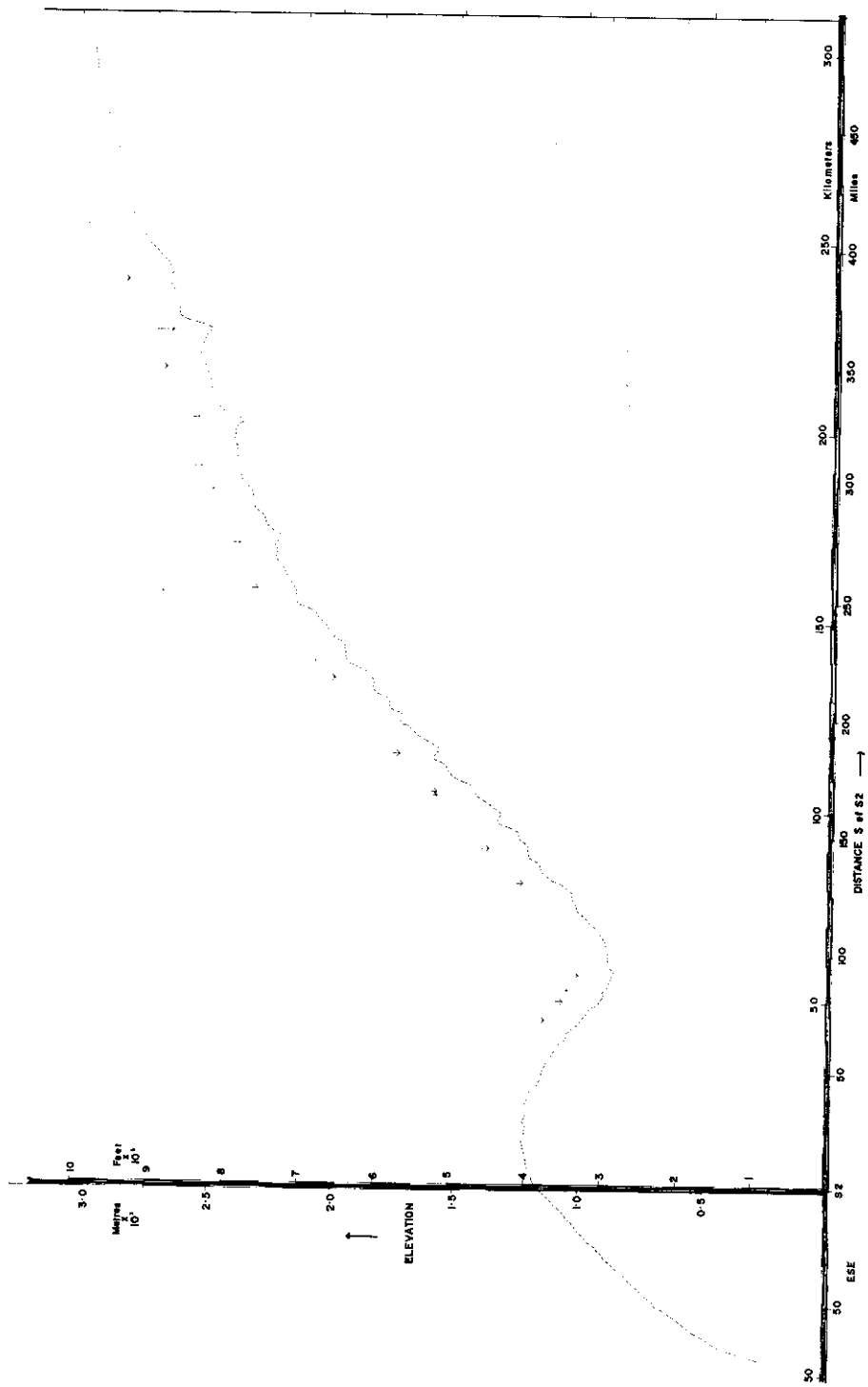

FIG. 0.5. THE ICE PLATEAU ELEVATION PROFILE INLAND OF WILKES. The results have been taken from the 1961 observations of Jewell. The arrows indicate positions of high sastrugi.

(vii) Traverses. In 1957 a traverse in December was made by dog sledge, on the sea ice, following the coastal ice cliffs north from Wilkes to Cape Poinsett. In 1958 a traverse was made inland of the Vanderford and John Quincy Adams Glaciers (cf. Fig. 0.3). Surface and sub-surface glaciological observations were carried out. The terrain encountered included many domed and crevassed areas.

0.1.2. Glaciological work since 1958

Following the I.G.Y. period, the Australian National Antarctic Research Expeditions 1959, 1960 and 1961 have continued glaciological activities at Wilkes, the glaciological programme being largely organised by the Department of Meteorology of the University of Melbourne.

In 1959, accumulation measurements were continued in the local area, S2 was visited for pit compaction measurements, and apparatus for measuring the amount of blowing snow at various levels from the ground was installed and operated.

In 1960, the local area accumulation measurements were continued, the S2 trail stakes were remeasured, and the 12 relative movement stakes at S2 were located, surveyed, and measured for accumulation. Compaction and contraction measurements were carried out in the pit and tunnel. In November and December 1960 a field traverse was made from Wilkes to S2 and 180 miles (290 km) south of S2. Accumulation stakes were placed at each mile (1.6 km) intervals and snow surface observations were recorded.

Programme of 1961

(i) Geophysical exploration. In 1961, the field geophysical programme commenced. This work, undertaken by the Australian Bureau of Mineral Resources Geology and Geophysics, aims at determining by a series of traverses over several years the ice cap elevations (barometrically), the ice thickness (by seismic reflection and gravity observations) and the distribution of seismic wave velocities in the ice (by seismic refraction). The region covered by the 1961 seismic survey is shown in Figure 0.3. Ice thicknesses were determined at 20–mile (32 km) intervals from Wilkes to S2 and 300 miles (480 km) south of S2.

Preliminary results of this geophysical work are presented in an unpublished report of the Australian Bureau of Mineral Resources Geology and Geophysics by Jewell (1962). cf. also Figure 4.4.

(ii) Glaciological work. Accummulation measurements were continued on all the existing stake systems in 1961, and the 1960 stake line was extended to 480 km south of S2. Movement studies were continued in the Vanderford Glacier area, at Cape Folger, and inland at S2 with the relative movement strain grid and the deep pit. The study of drifting snow, commenced at Wilkes in 1959, was continued in 1961 and extended to inland on the plateau at S2. Along the traverse route surface and subsurface observations were made and a series of pits were excavated and the usow stratigraphy studied along the accumulation profile from Wilkes to S2 and 480 km south of S2 to provide information on weather conditions inland as well as the accumulation in recent years.

Temperatures in the firn had previously been measured to about 10 m depth in the Wilkes region to obtain estimates of the annual mean temperature at the

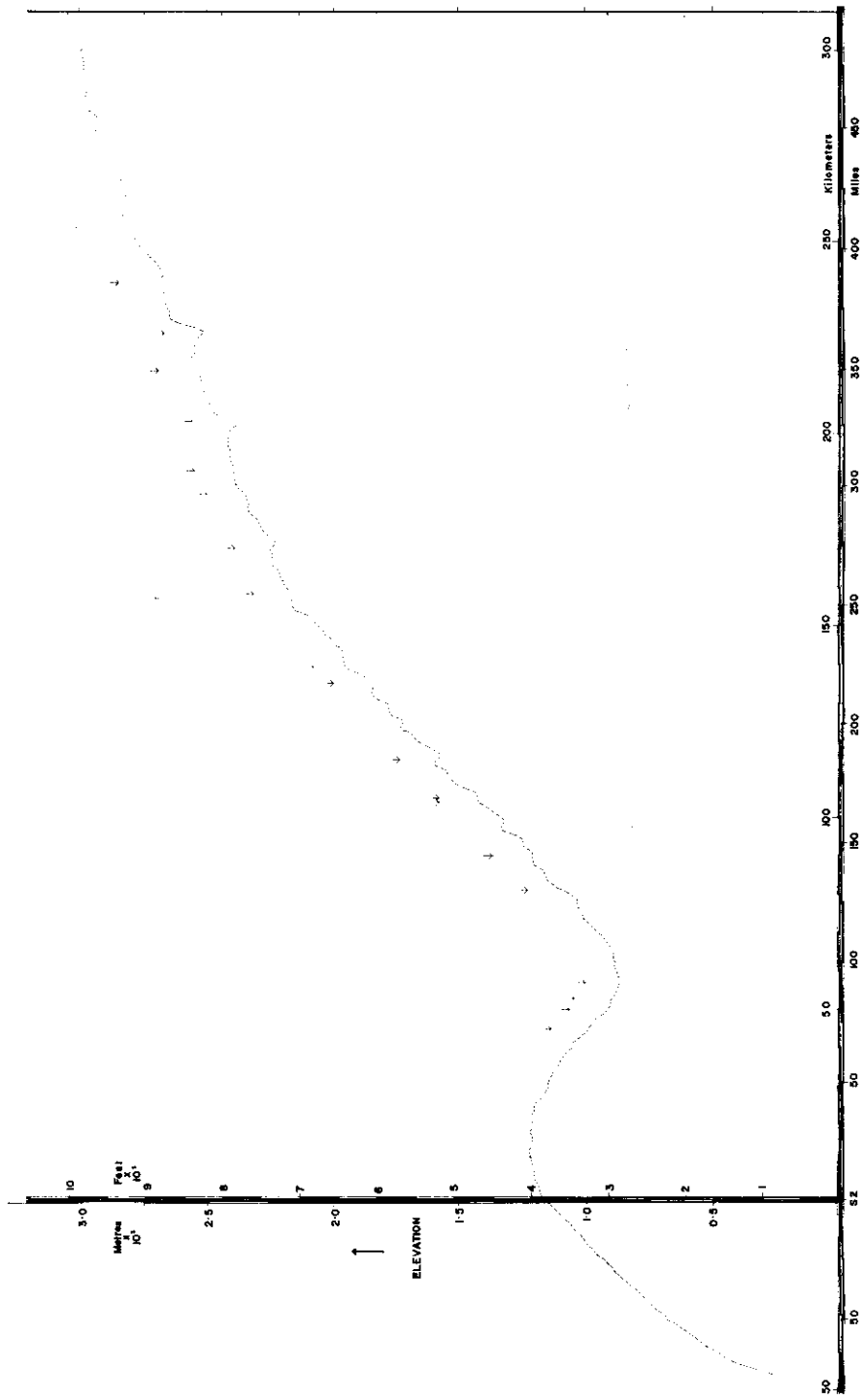

FIG. 0.5. THE ICE PLATEAU ELEVATION PROFILE INLAND OF WILKES. The results have been taken from the 1961 observations of Jewell. The arrows indicate positions of high sastrugi.

surface. These surface measurements were extended to approximately latitude 71°S in 1961. To procure further information concerning the temperature and movement regime of the ice cap, temperature gradients to the depth of 30 m in the firn were measured in boreholes from Wilkes to S2.

Sea ice observations were continually being interrupted when the strong winds broke up and removed the sea ice from around Clark Peninsula. The longest period during which the sea ice remained intact was less than one month and the maximum thickness reached was 41 cm. This occurred in October, which was the coldest and least windy month of 1961. These details are given here because sea ice data will not be treated in this report.

This completes the outline of the glaciological work carried out at Wilkes up to 1961. A synopsis is now presented of the following sections which treat separately the different aspects of this work, the analysis of the results and their implications concerning the broader aims of glaciological studies outlined in the preface.

0.2. SYNOPSIS

The order in which the various sections are presented is largely arbitrary. Since all sections are concerned at least indirectly with the mass and heat budgets of the ice cap all are partly inter-related. Consequently there is frequent cross reference from one section to another.

The order chosen is to discuss in the first three sections Climate, Snow stratigraphy and Drifting snow, all of which have some bearing on the fourth section Accumulation. Section 5 discusses temperature profiles in the firn, making use of the accumulation results and providing information on ice movement and temperature inland. Finally, Section 6 treats snow and ice movement, and by incorporating the results of the accumulation section leads up to a preliminary mass budget study for the Wilkes region.

1. Climatology

In considering the mass budget the gain to the ice surface comes from some form of precipitation. Precipitation, however, is difficult to measure directly by conventional snow gauges because of the windy conditions prevailing in the Antarctic. Instead, a direct measure of *net* gain may be obtained from the results of net accumulation measurements made at a large number of positions over the plateau surface. The net accumulation measurements give the resultant gain or loss to the surface from precipitation, drift transport, melt and sublimation. Because the meteorological factors affecting these (temperature, wind speed, precipitation, in particular) vary widely with position, the net accumulation also varies with position.

In order to understand the distribution of the net snow accumulation with topography, and to compare Wilkes climate with that of other positions a short analysis of climate variables (wind speed, temperature and precipitation) has been made. This analysis shows how the climate varies throughout the year at Wilkes, from one year to another, from Wilkes going inland on the ice cap, and between Wilkes and other coastal East Antarctic stations.

2. Stratigraphy

With a knowledge of how the climate varies through the year and with position, a study of the effect of the climate on the snow stratigraphy is next carried out.

Information on the climate further inland is obtained from the pit stratigraphic data and surface observations obtained on the traverse. The annual variation of climate, as reflected in the snow stratigraphy, allows the annual net accumulation rate to be estimated along the traverse profile.

3. Drifting snow

From the accumulation stake measurements it is apparent that the accumulation rate varies markedly with topography. The cause of this seems to be the variation of wind speed with surface topography, and the variation of drift snow content with wind speed. Hence, in order to understand the distribution of accumulation rate with wind speed, it is necessary to know the mechanism of snow drift.

The analysis of the drift measurements, largely taken at S2, represents an extension of the work by Mellor and Radok (1960) and Dingle and Radok (1961). It determines, among other things, the variation with wind speed of the following quantities: the parameters of the logarithmic wind profile—the drift density at various heights—the average fall velocity of the snow particles—the snow supply at the surface—the total drift content—the total drift transport rate.

From the topography in the Wilkes region, estimates of the wind conditions are made and are combined with the variation of drift content with wind speed to construct a theoretical accumulation profile for comparison with the actual accumulation profile of the S2 trail.

A further important use of the drift measurements in the Wilkes region is for the calculation of the potential quantities of drift snow blowing past each of S2 and Wilkes per year. The latter quantity gives the annual loss of snow from the ice cap by drift.

4. Accumulation

From the accumulation measurements from 1957 onwards, extending from the coast to as far inland as S2, Section 4 shows how the snow accumulation rate varies during the year, from one year to another, and from the coast to S2. From the shorter term results of measurements south of S2 the following are also determined: the general trend of decrease of accumulation rate with distance inland, the variation of accumulation rate with major topographic features, and the variation of net accumulation over an undulating slope.

Finally, an accumulation contour map of the Wilkes region is constructed from the accumulation results together with the results of the climatology and topographical surveys.

5. Ice cap temperature profiles

Surface temperatures above 10 m depth measured along the traverse route provide information from which the annual mean temperature can be estimated. However, the calculation of the annual mean temperature is complicated by the snow accumulating on the surface (up to 2 m of snow per year in some positions) and also by the variation in density (and hence diffusivity) with depth. Therefore, corrections to the theoretical temperature profile with depth for these effects are investigated.

The relationship between the temperature gradient at the surface (below 10 m) of an ice cap, its accumulation rate, movement, thickness, and the geothermal flux have been discussed, among others by Robin (1955) and by Jenssen and Radok (1960,

1963). Temperature gradients measured between Wilkes and S2 in 1961 are analysed together with the measurements of elevation, ice thickness, and accumulation to provide further information on the movement of the inland ice, as well as fundamental information regarding basal temperatures, geothermal flux, and the heat budget of the ice cap. An estimate is then made of the movement rate inland.

6. Ice Movement

(a) Inland movement. Information on stress and strain relations of the inland ice is deduced from the relative movement strain grid network and from the deep pit and tunnel at S2. The strain grid shows the relative deformation at the surface and from very broad assumptions estimates of the inland surface movement rates are made.

From the measurements of contraction rates in the tunnel at S2 the variation of closure rate with time, distance along the tunnel, and direction across the tunnel provide information on the flow parameters of ice of that type and its change as it densifies with time.

The study of the mechanism of the change of the surface firn into dense ice is provided by the change of compaction rates, measured at different levels in the deep pit, over time. The compaction rate depends upon the initial surface density, the accumulation rate, and the depth, for given snow type and climate. The type of snow and climate effects are judged from the comparison of the S2 results with those from other regions.

(b) Coastal movement. As there has been very little *net* ablation in the Wilkes region over the period 1957 to 1962, the chief mechanism for loss of ice from the plateau has been the calving of ice bergs from the ice cliffs north of Wilkes and from the glacier tongues to the south. To obtain the amount of ice lost from calving, it would be necessary to know the change in the coast line (i.e. the extent and depth of the ice) over the period, as well as the movement rate of the ice. As this mapping control has not yet been carried out the loss is estimated directly from the rate of outward flow.

For the purpose of the mass balance the thickness of the ice is also required. No thickness values are available in the Vanderford Glacier area but for the Cape Folger region a single gravity thickness result is used.

Theoretical arguments are outlined to show that if sufficient information were available about the flow parameters of ice for known conditions of temperature, stress, and ice type, an estimate of the ice thickness for the given flow rates could be made. Alternatively if sufficient information were available on the ice shape as well as the flow rates, then estimates could be made of the flow law parameters. In this way, from the movement results from Cape Folger and the Vanderford Glacier, estimates are made of both flow parameters and thickness and then the rate of ice loss. But evidently, until more measurements of ice thickness become available, this stage can only be regarded as accurate to the nearest order of magnitude.

Finally, with the estimates of ice loss from the movement surveys and the estimates of gain from the accumulation profile contours, a mass budget is drawn up for two regions of the Wilkes area which appear to be self-contained in so far as there is no inflow of ice into them.

1. CLIMATOLOGY

1.0. INTRODUCTION

The most important meteorological variables for the study of the ice mass budget are temperature, wind and precipitation. The supply of snow comes only from precipitation (here understood to include all types of deposition) in its various forms, but in the Antarctic precipitation is difficult to measure directly because the wind makes it difficult to distinguish between precipitation and snow blown off the plateau surface. The snow remaining on the surface can be measured by systems of stake networks giving the resultant net accumulation. The amount of snow removed depends largely upon the wind and the temperature.

From a limited set of meteorological data available at this stage a survey will be made of these three meteorological variables with the intention of throwing some light on

(i) how the temperature, wind and precipitation vary throughout the year at Wilkes,

(ii) how the temperature, wind and precipitation patterns have varied from one year to another at Wilkes from 1957 to 1962,

(iii) how these meteorological variables change from the coast at Wilkes to inland on the plateau at S2,

(iv) how the climate at Wilkes compares with that of similarly situated Eastern Antarctic bases,

(v) the relation between the climatic variables, snow drift and accumulation.

The brief survey that follows is of a preliminary nature only. Zimmerman (1960) has already made a general study of the climatic tendencies at Wilkes for the years 1957 and 1958. A more detailed analysis will be possible when the complete Australian National Antarctic Research Expeditions meteorology reports are published by the Antarctic Division. It should be noted that any general annual cycle characteristics observed in the climatic data will be particularly important for the study of annual strata from pit stratification data.

1.1. VARIATION IN THE METEOROLOGICAL ELEMENTS AT WILKES DURING THE YEAR

In Tables 1.I, 1.II and 1.III are listed the values of monthly mean temperature, mean wind speed, and total precipitation, respectively from 1957, together with the row and column means and standard deviations. These mean values are plotted in Figure 1.2.

(a) Temperature. From Table 1.I it may be seen that the mean temperature rises to about 0°C in the summer (December–January) and falls to about −15 to −20°C over winter (June–September). The mean temperature over the whole period has been −9·3°C.

TABLE 1.I.

WILKES PRECIPITATION (MM) OF WATER.

	1957	1958	1959	1960	1961	1962	Mean	SD.
J	(8)	6	20	10	2	2	8	8
F	(8)	20	10	5	2	5	8	7
M	122	0	80	30	40	20	49	45
A	48	9	11	20	30	55	29	19
M	50	61	27	10	10	16	29	22
J	24	18	41	20	50	6	27	16
J	50	78	13	30	40	8	27	26
A	45	17	27	10	1	30	22	16
S	23	9	5	10	100	28	29	36
O	31	19	29	10	2	48	23	16
N	42	22	16	10	10	20	20	12
D	6	5	19	0	4	20	9	8
av./month	38·1	22·0	24·8	13·8	24·3	21·5	23·3	
ANNUAL TOTALS								
Wilkes	457	264	298	165	291	258	280	
Mawson	453	495						
Davis		56	119	76				

TABLE 1.II.

WILKES MONTHLY MEAN TEMPERATURES (− °C).

	1957	1958	1959	1960	1961	1962	Mean	SD.
J	(0·6)	+0·3	0·8	0·6	0·6	1·5	0·6	0·6
F	(2·1)	1·9	3·9	2·3	1·8	0·4	2·1	1·3
M	4·6	4·9	8·9	10·0	4·9	4·3	6·3	2·5
A	6·4	7·3	8·9	9·0	9·4	13·1	9·1	2·3
M	11·8	8·5	11·9	16·1	10·0	17·6	12·7	3·5
J	17·6	21·3	15·1	17·3	13·3	16·5	16·9	2·7
J	17·6	15·0	15·2	17·3	11·1	20·8	16·2	3·3
A	12·5	17·3	17·2	13·9	12·9	15·0	14·8	2·1
S	11·2	20·4	22·1	14·6	11·3	11·8	15·2	4·9
O	9·4	12·7	9·6	10·8	14·2	10·0	11·1	1·9
N	4·6	5·3	6·1	4·5	5·9	5·5	5·3	0·7
D	0·1	1·5	0·8	1·4	2·4	1·7	1·3	0·8
ANNUAL AVERAGES								
Wilkes	(8·2)	9·7	10·0	9·8	8·2	9·9	9·3	
Mawson	10·0	11·1	10·8	12·7	9·6	12.5	11·1	
Davis		10·1	10·2	11·6	8·7	11.8	10·5	
Dumont D'Urville	10·8	11·3			10·9			

TABLE 1.III.

WILKES MONTHLY MEAN WIND SPEEDS (M/SEC).

	1957	1958	1959	1960	1961	1962	Mean	SD.
J	(4·8)	4·4	3·7	5·1	6·0	5·3	4·9	1·0
F	(5·3)	3·6	4·5	5·1	8·2	6·5	5·6	2·0
M	5·1	4·2	5·6	5·3	6·7	4·9	5·3	2·3
A	7·0	7·3	4·9	3·9	4·7	6·8	5·8	1·5
M	6·2	7·5	7·1	4·4	8·0	4·5	6·3	1·4
J	4·0	4·4	8·5	4·3	10·4	6·3	6·3	2·9
J	4·7	5·1	6·0	4·5	12·2	5·5	6·3	3·2
A	6·7	3·5	4·9	3·3	8·8	11·0	6·4	2·3
S	8·1	2·8	6·8	4·7	5·2	5·9	5·8	1·7
O	5·2	4·8	6·5	4·6	3·6	7·0	5·3	1·1
N	3·8	4·0	7·8	5·5	5·2	(5·3)	5·3	1·6
D	3·2	3·4	3·9	5·5	4·6	5·5	4·4	1·4
				ANNUAL AVERAGES				
Wilkes	(5·3)	5·0	5·9	4·7	7·0	6·2	5·6	
Mawson	10·1	10·5	9·8	9·5	10·5	8·9	10·0	
Davis		4·7	5·2	4·8	5·4	4·7	5·0	

One important point concerning the temperature variation during the year is that at the start of a blizzard the temperature often rises and stays high while the wind speed is high. Hence the maximum (extreme) temperature for each month is generally quite high even during winter. This is illustrated in Figure 1.5 showing the monthly extreme maxima and minima and means for Wilkes 1961. The monthly extreme maxima vary much less than the means or extreme minima. This feature was also observed in the temperature measured throughout the year at the inland station S2 (cf. Fig. 1.6).

(b) Precipitation. The pattern of precipitation varies greatly from one year to another but is often characterised by an exceptionally large snow fall in a single month, the particular month varying from year to year. Thus a large snow fall occurred in March 1959, with little precipitation in other months, whereas in 1961 September had by far the greatest precipitation. The resulting monthly means computed for the whole period show much variation between different years and little variation between months.

This large variation between months in different years largely obscures any general annual cycle. However, from the monthly means over the whole period 1957 to 1962 it may be seen that the largest falls appear to occur in autumn to spring, while over the summer months, December, January and February, the precipitation has been comparatively small.

(c) Wind. The monthly mean wind speeds also show wide variations from one year to another but the general variation throughout the year may be seen from Figures 1.1 and 1.2. The summer months, November, December, January and February, all have mean wind speeds (1957 to 1961) below the annual mean, with December having the lowest. The windiest period appears to be from late autumn to

early spring, but this varies widely from year to year. The mean wind speed over the whole period has been 5·5 m/sec.

The mean wind speed, however, is not a good indicator of the wind conditions at Wilkes, because of the extreme nature of the blizzards. Between blizzards the weather may be relatively calm with mean wind speeds below 2 m/sec; during a blizzard (lasting one to five days) the average wind speed may be as high as 20 or 30 m/sec. This is brought out more clearly by the extremely skew frequency distribution of the daily wind means for Wilkes for 1961, given in Table 1.IV below and plotted in Figure 1.4 together with the corresponding distribution for S2.

TABLE 1.IV.

V	m/sec:	0–2	2–4	4–6	6–8	8–10	10–12	12–14	14–16
F		52	121	67	21	25	17	17	6
V		16–18	18–20	20–22		22–24	24–26	26–28	28–30
F		7	9	4		4	5	4	1
V		30–32	32–34	34–36		36–38			
F		1	0	0		2			

(V = wind speed range, F = number of days per year).

It is during the periods of very high winds that most of the snow on the surface is removed. The actual dependence of drift on wind speed is discussed in Section 3 (also cf. Fig. 1.7).

1.2. VARIATION IN WILKES CLIMATE FROM ONE YEAR TO ANOTHER

The general variation in the main meteorological elements at Wilkes from 1957 to 1962 may be seen from the values of the annual means for different years. These have been plotted from Tables 1.I to 1.III in Figure 1.3.

(a) Temperature. The years 1957 and 1961 were "warm" years with average temperatures more than 1.5°C higher than those of 1958, 1959, 1960 and 1962. From Figure 1.1 it may be seen that the mean summer temperatures do not vary very much from year to year, whereas the winter temperatures fluctuate greatly. The stability of the summer temperatures may be regarded to be largely a result of the absorption of heat by melting. January 1958 was the only month with the mean above 0°C, and this was reported to have been accompanied by extensive ablation (Hollin *et al.* (1961) p. 112).

The general annual cycle remains fairly constant from one year to another. The temperature maximum occurs about January; the temperature goes below the annual mean in April–May, and rises above it in October–November.

(b) Precipitation. The precipitation total was high in 1957 and low in 1960. For the other three years total precipitation was between 25 and 30 cm of water. As mentioned earlier, the period during the year over which maximum precipitation occurs varies from autumn to spring but there are generally one or two occasions of heavy precipitation.

(c) Wind. The wind pattern varies considerably from one year to another. Hence only few general observations may be made. The average wind speed over the summer months is substantially less than over autumn, winter and spring (1960

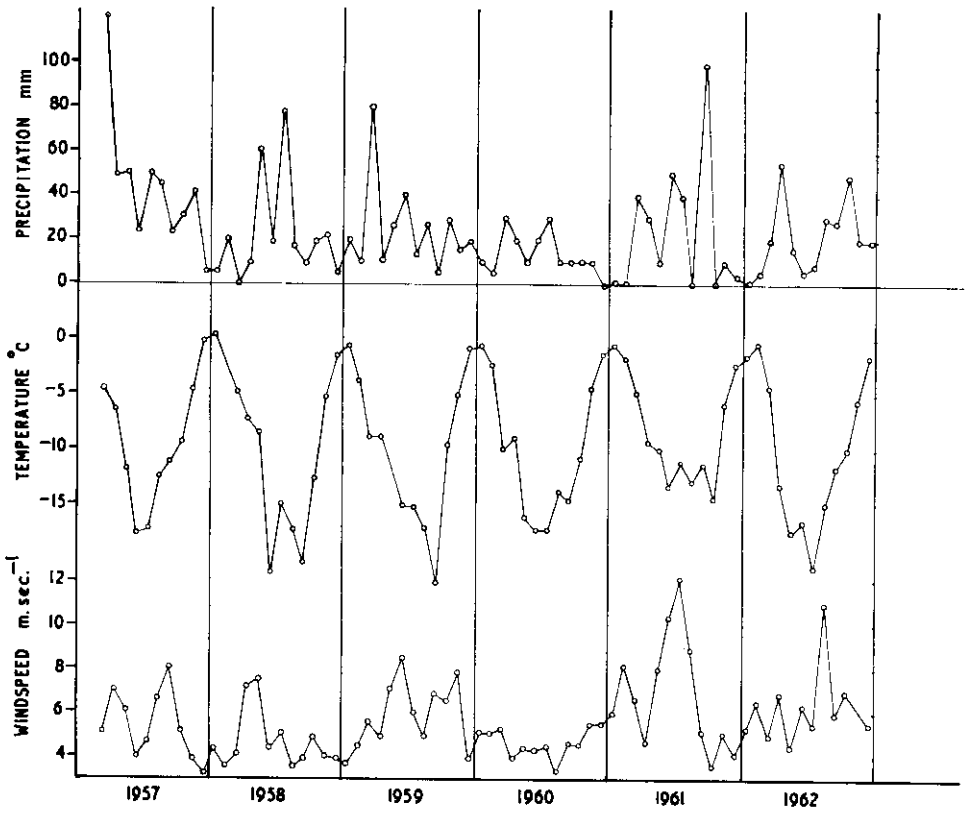

FIG. 1.1. WILKES CLIMATE 1957–62. The monthly mean values of temperature and wind speed have been plotted with monthly total precipitation from March 1957 to December 1962.

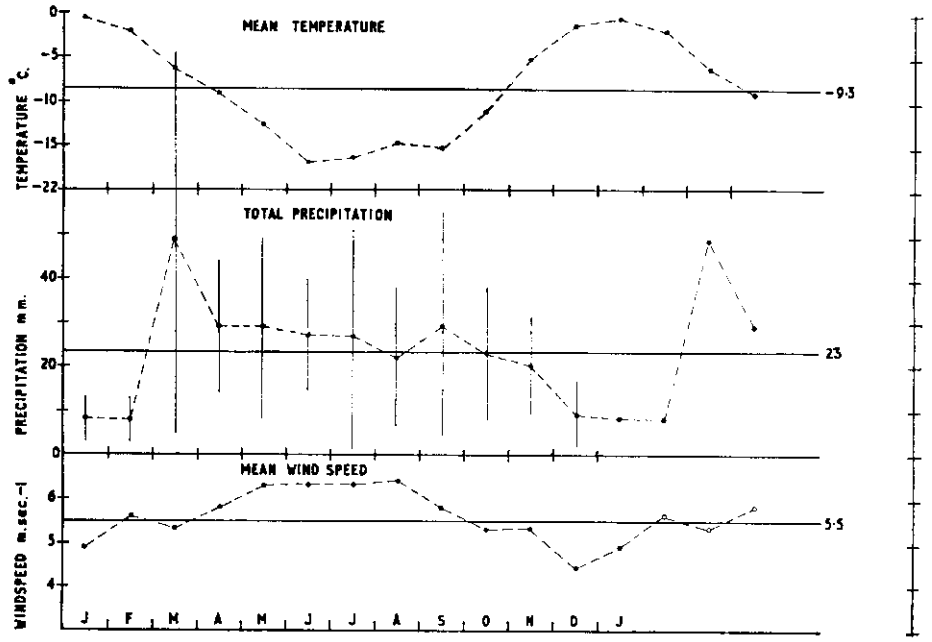

FIG. 1.2. VARIATION OF WILKES CLIMATE DURING THE YEAR. The value of each of the three climate variables considered has been averaged over the six years for each month to show the general pattern of variation during the year.

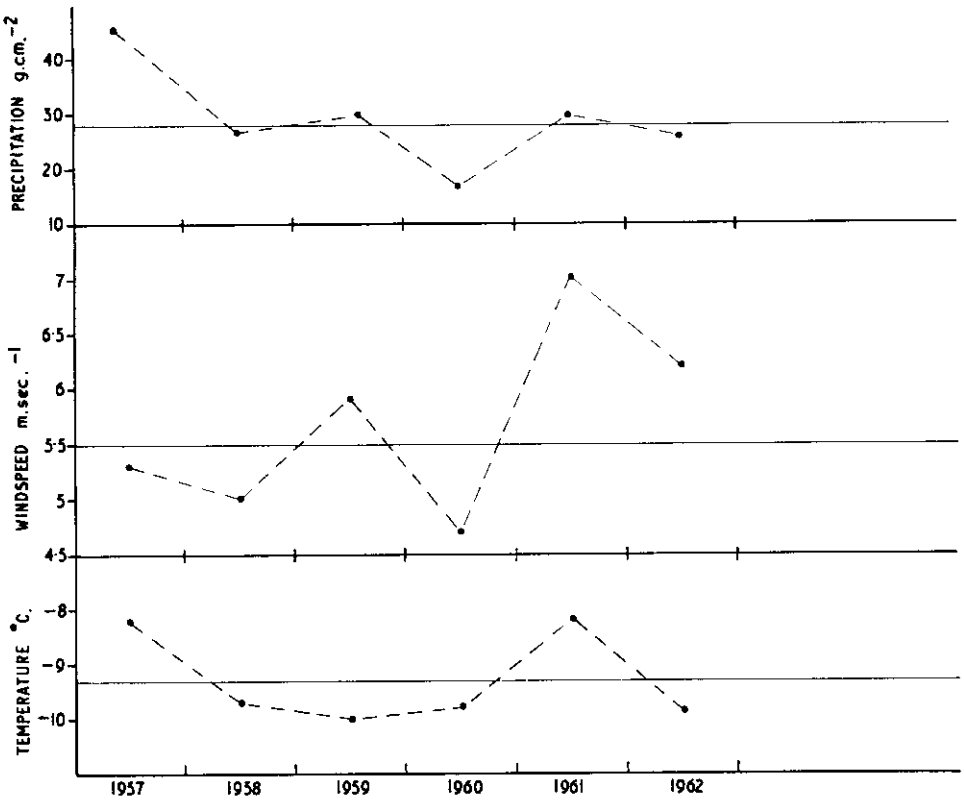

FIG. 1.3. VARIATION IN WILKES CLIMATE FROM ONE YEAR TO ANOTHER. The annual mean wind speed and temperature and total precipitation are plotted for each of the years 1957 to 1962 to show broadly how any year differed from the others.

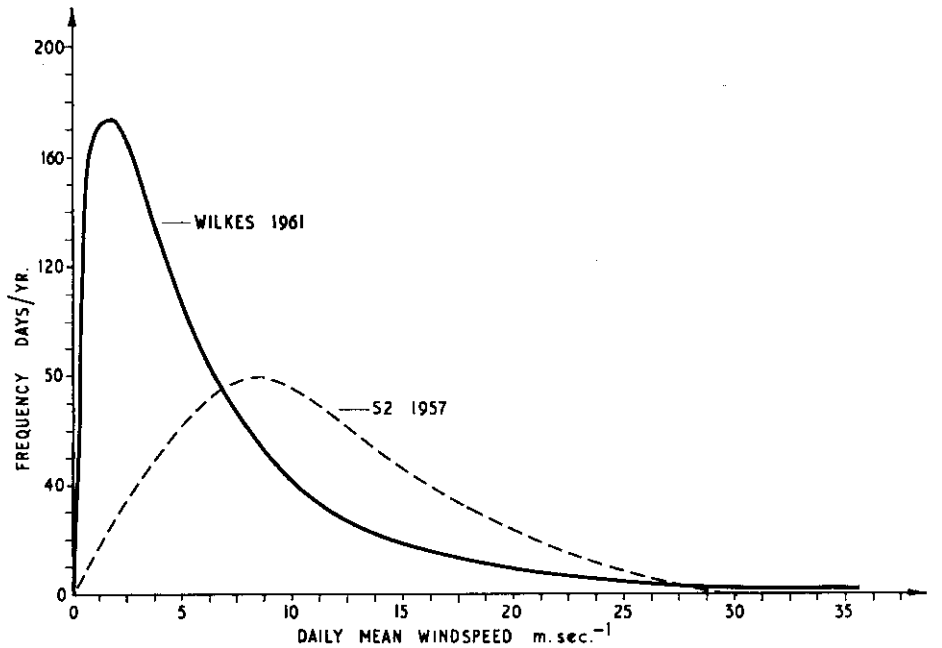

FIG. 1.4. DAILY MEAN WIND SPEED FREQUENCY DISTRIBUTIONS FOR WILKES AND S2.

was a notable exception). The period of greatest wind also fluctuates widely from year to year, occurring apparently anywhere between autumn and spring.

1.3. VARIATION IN CLIMATE FROM WILKES ON THE COAST TO INLAND ON THE ICE CAP

From the weather data of 1957–8 collected at S2 by Cameron *et al.* (1959), values of monthly mean winds, monthly extreme temperatures and the accumulation have been plotted in Figure 1.6.

The most notable contrast to Wilkes (apart from the lowering of temperature, due mainly to an elevation increase to 1,160m) is the much higher wind speed. It will be seen in the next section that the Wilkes wind speed is less than that of most coastal Antarctic stations. This appears to result from a channelling of the wind from the Wilkes-S2 route (the line of the predominant wind direction) north over the region of Cape Folger and south over the low region of the Vanderford Glacier. The theory of the topographical channelling of katabatic winds has been discussed by Ball (1960) who shows how the wind speed would depend on the slope of the ice plateau surface.

The weaker winds at Wilkes as compared with those on the plateau may also be partly explained as the effect of stationary hydraulic jumps ("Loewe's phenomenon"), cf. Ball (1956) and Valtat (1960). This phenomenon appears to be characteristic of many parts of the Antarctic coast and although it has been observed in the Wilkes region by Black in 1960 and the present author in 1961, no data are at present available for making a more detailed study. Within this limitation the average wind speed at S2 is lowest over summer and highest from autumn to spring, just as at the coast.

The difference between the winds inland on the ice cap and at the coast is further illustrated by the frequency distributions of daily mean wind speeds for Wilkes and S2 (cf. Fig. 1.4). The S2 wind distribution is much less skew than that of Wilkes. In other words, S2 does not have the extreme high winds of Wilkes but the wind blows there consistently moderately high over long periods.

Because of the consistently high winds at S2, precipitation measurements have not been made there. Instead, cumulative accumulation has been recorded at close intervals from March 1957 to January 1958 (cf. Cameron *et al.* (1959). The most rapid accumulation rates occurred in April–May and September–October. From October to January net ablation took place. This is discussed more fully in the accumulation section.

Between Wilkes and S2 little information is available at this stage. However, simultaneous measurements taken from January 3rd to February 2nd, 1959, at Wilkes and S1 (9 km inland, elevation 260 m) gave average wind speeds of 3·6 m/sec at Wilkes and 5·0 m/sec at S1. For S2 the average wind speed over January was 8·9 m/sec.

The higher winds at S1 in comparison with Wilkes suggests that the katabatic wind stream may pass over Wilkes at some altitude and only occasionally (during blizzards) sweeps across the Wilkes ground level at the foot of the ice plateau.

The variation in the annual mean temperature at the surface of the ice cap going inland from Wilkes has been found from the measurement of temperatures in the firn. This will be discussed in Section 5.

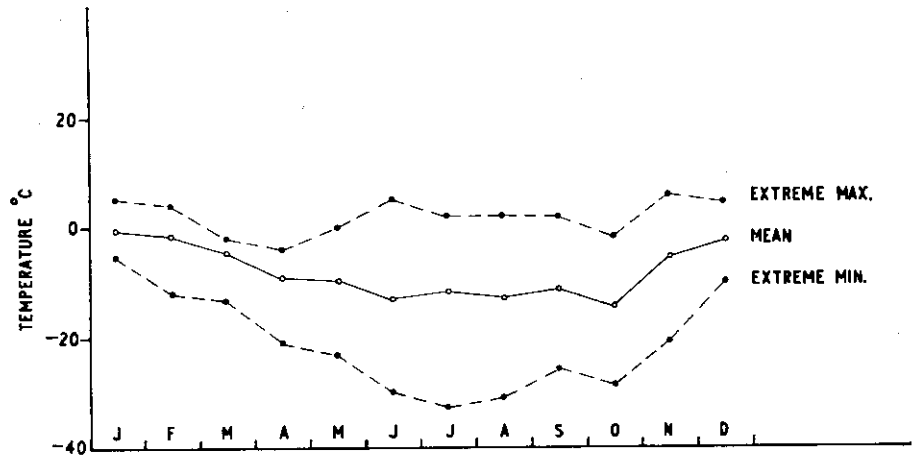

FIG. 1.5. TEMPERATURE VARIATION DURING THE YEAR, WILKES, 1961. The monthly extreme maximum and minimum temperatures are plotted with the mean for each month of 1961, showing how the minima have a wide range whereas the maxima vary only slightly from summer to winter.

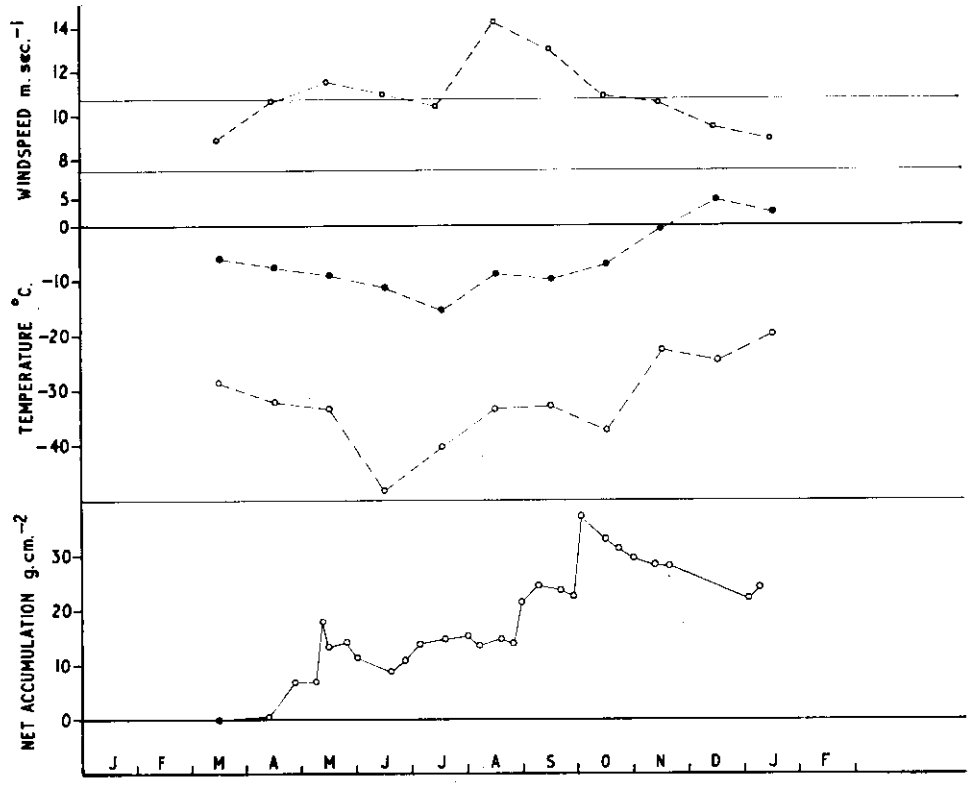

FIG. 1.6. S2 METEOROLOGICAL DATA. The variation during the year in average wind speed, maximum and minimum temperature, and net accumulation rate are plotted from the data gathered in 1957 by Cameron et al. (1959).

1.4. COMPARISON OF WILKES REGION CLIMATE WITH THAT OF OTHER EASTERN ANTARCTIC STATIONS

A brief comparison will be made of the Wilkes region climatology with that of similarly situated Eastern Antarctic stations: Dumont D'Urville, Mirny, Mawson and Davis at the coast, and Charcot and Pioneerskaya inland. Table 1.V below lists the relevant parameters for each of these stations.

Considering the inland station first, it can be seen that the climate of S2 appears to be typical for an Antarctic station situated about half way between the coast and the inland stations exemplified by Charcot and Pioneerskaya.

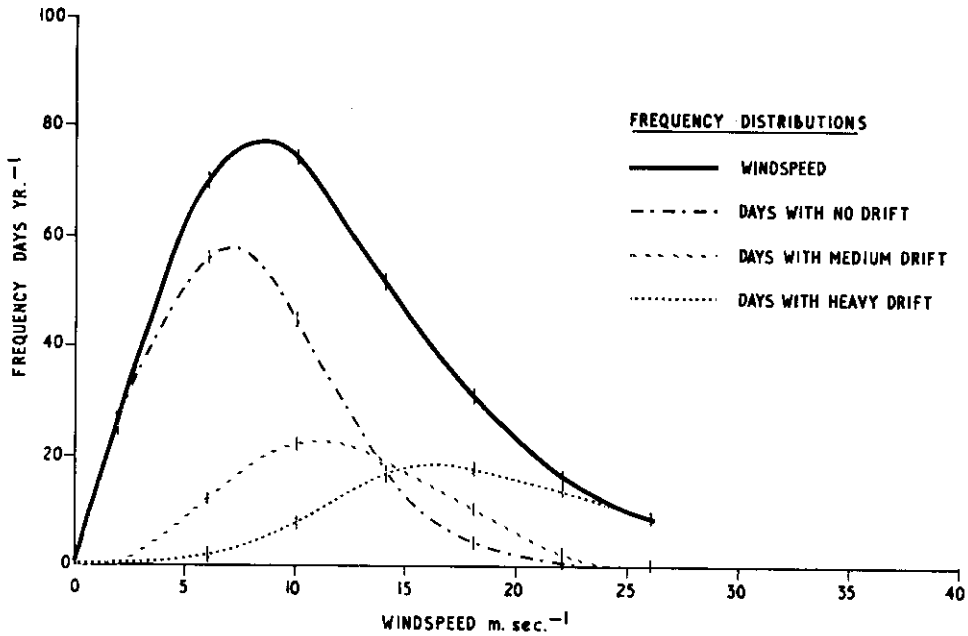

FIG. 1.7. WIND SPEED AND SNOW DRIFT FREQUENCY DISTRIBUTIONS. From the 1957 meteorological data for S2 from Cameron et al. (1959), for each subrange of wind velocity, the number of days per year have been calculated on which no drift, medium drift, and heavy drift were observed. Heavy drift predominated after 15 m sec^{-1} and became universal by 25 m sec^{-1}.

Tauber (1960) lists the mean wind velocity over the period June to September 1958 for Russian stations going inland from the coast and these are shown in Table 1.VI.

The decrease in wind speed inland from the coast has important consequences regarding drift transport and net accumulation as will be shown in Sections 3.4 and 4.3.4. The relation between the wind speed and snow drift frequencies for S2 is illustrated in Figure 1.7.

The weather data from S2, together with the pit stratigraphic data from the 1961 traverse, confirm this general trend of wind velocity; i.e. surface katabatic winds prevail in coastal regions where the plateau surface slope is considerable but tend to disappear by about 450 km inland where the plateau slope becomes small.

Another similarity of Pioneerskaya with S2 is that for both regions the wind speed is greater over winter. Tauber (1960) states: "In winter, when Antarctica does not receive any solar heat, the katabatic winds increase their intensity with a steady constancy and with no noticeable diurnal variation in the speed".

TABLE I.V.

COMPARATIVE ANNUAL CLIMATIC DATA.

Station	Location	Elevation m	Mean Temp. −°C	Mean Wind m/sec	Net Accum. g. cm^{-2}	Total Precip. g. cm^{-2}
Wilkes	66° 15′S 110° 32′E	12	9·8	5·5	0	28
Dumont D'Urville	66° 40′S 140° 01′E	40	11·2	10·4		
Mirny	66° 33′S 93° 00′E	30	9·5	11·6		
Mawson	66° 36′S 62° 53′E	46	11·2	10·7	−60	47
Davis	68° 35′S 77° 59′E	15	10·6	4·5		8
S2	66° 31′S 112° 13′E	1166	19·6	10·7	14	
Charcot	69° 23′S 139° 01′E	2800	37·5	9·2	10–18	
Pioneer-skaya	69° 44′S 95° 30′E	2700	39·2	10·7	16	

TABLE 1. V1.

VARIATION OF WIND SPEED WITH DISTANCE INLAND.

Station		Mirny	Pioneerskaya	Komsomolskaya	Vostok
Dist. from Coast	km	0·2	375	815	1410
Elevation	m	30	2704	3416	3416
Wind Speed	m/sec	13·6	10·6	3·8	4·0

The wind speed at these inland stations is also consistently moderately high, in contrast to the coastal stations where the average wind speed is smaller but often reaches extremely high values during blizzards.

Considering next the coastal stations, it appears that Wilkes cannot be directly compared with Mirny, Mawson and Dumont D'Urville because Wilkes is approximately 3·5 km from the foot of the ice ramp. That this distance is significant may

be seen from the difference in wind speeds between Wilkes and S1. Tauber (1960, p.62) states: "The energy of the air stream flowing downslope dissipates very quickly

In the sections on snow drift (3.3, 3.5) it is shown how the amount of drift content, and therefore the amount of snow picked up or deposited, varies with the wind speed for steady state saturated conditions. The results of sections 3.3 and 3.5 suggest that ablation would be highest where acceleration of the wind is highest. For katabatic winds this occurs where the convex curvature of the ice plateau is greatest, i.e. near the coast. However, ice slopes, such as that inland of Mawson (which consists largely of a "blue ice" surface), would rarely have sufficient snow supply to maintain saturated conditions of drift. Hence the amount of surface removed here may be related more to the magnitude of the wind velocity rather than to its rate of change.

70

2. PIT STRATIFICATION DATA

2.0. INTRODUCTION

Along the 1961 traverse route from Wilkes (cf. map Fig. 0.3) each 32 km a 2 m pit was dug in the firn in order to determine the properties of the accumulated snow. For each pit position the following data were recorded:

(i) at the surface: the distance from the coast, latitude, longitude, elevation, surface slope, annual mean temperature (from 7 m bore-hole temperatures) and the accumulation rate (as far as 290 km S of S2).

(ii) subsurface: pit stratification, ram hardness, density, grain size and temperatures.

These values for each pit have been plotted in pit diagrams, Figures 2.1 to 2.18.

In order to interpret the pit stratification data reference will be made to the results of the climatology survey. For the first 12 pits direct reference could be made to the accumulation rate measured over the year at the stake next to the pit. When the results of the 1962 accumulation are available the examination may be extended to the 6 pits from 290 to 480 km south of S2, while for the earlier pits the variability in annual accumulation, and therefore in the annual stratification, may be studied.

STRATIGRAPHIC KEY FOR PIT DIAGRAMS,

FIGS. 2.1 TO 2.18.

Annual Layer Markers <

Very Small Crystals

Small Crystals

Medium Crystals

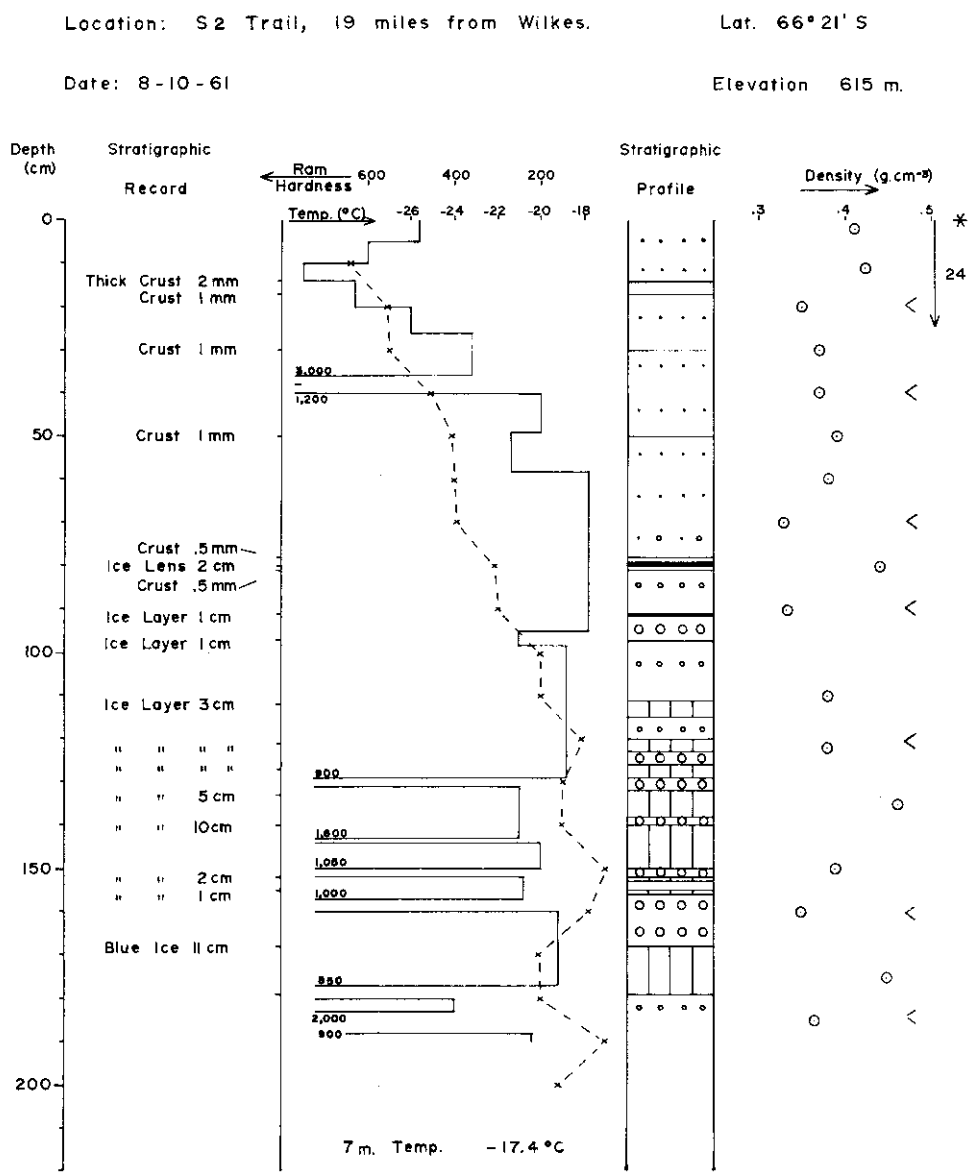

FIG. 2.1.

* Where a stake has been used next to the pit, the previous years accumulation rate has been indicated by an arrow.

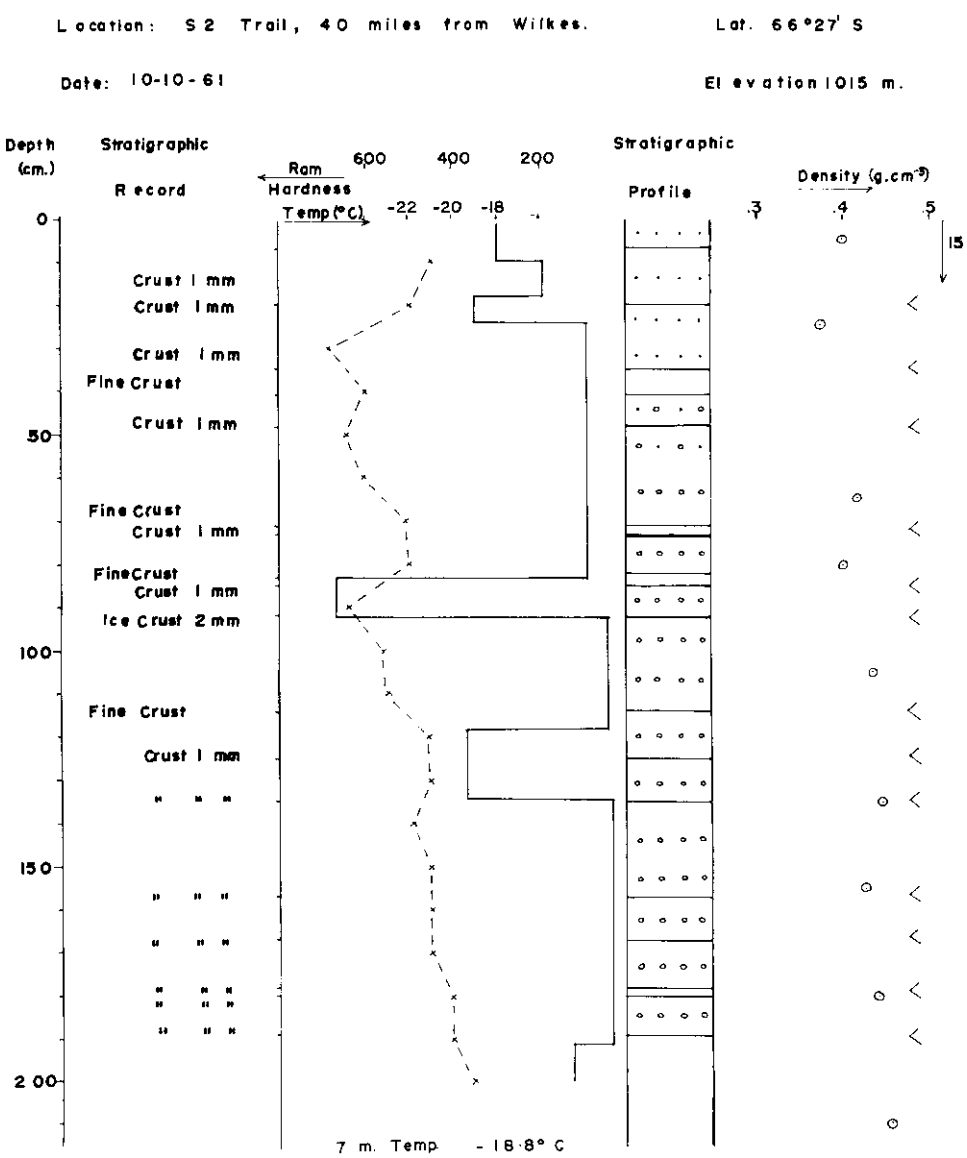
Location: S 2 Trail, 40 miles from Wilkes.
Lat. 66°27' S
Date: 10-10-61
Elevation 1015 m.
Depth (cm.)
Stratigraphic Record
Ram Hardness
Temp (°C)
600
400
200
-22
-20
-18
Stratigraphic Profile
Density (g.cm⁻³)
.3
.4
.5
15
0
50
100
150
200
Crust 1 mm
Crust 1 mm
Crust 1 mm
Fine Crust
Crust 1 mm
Fine Crust
Crust 1 mm
FineCrust
Crust 1 mm
Ice Crust 2 mm
Fine Crust
Crust 1 mm
7 m. Temp. - 18·8° C

FIG. 2.2.

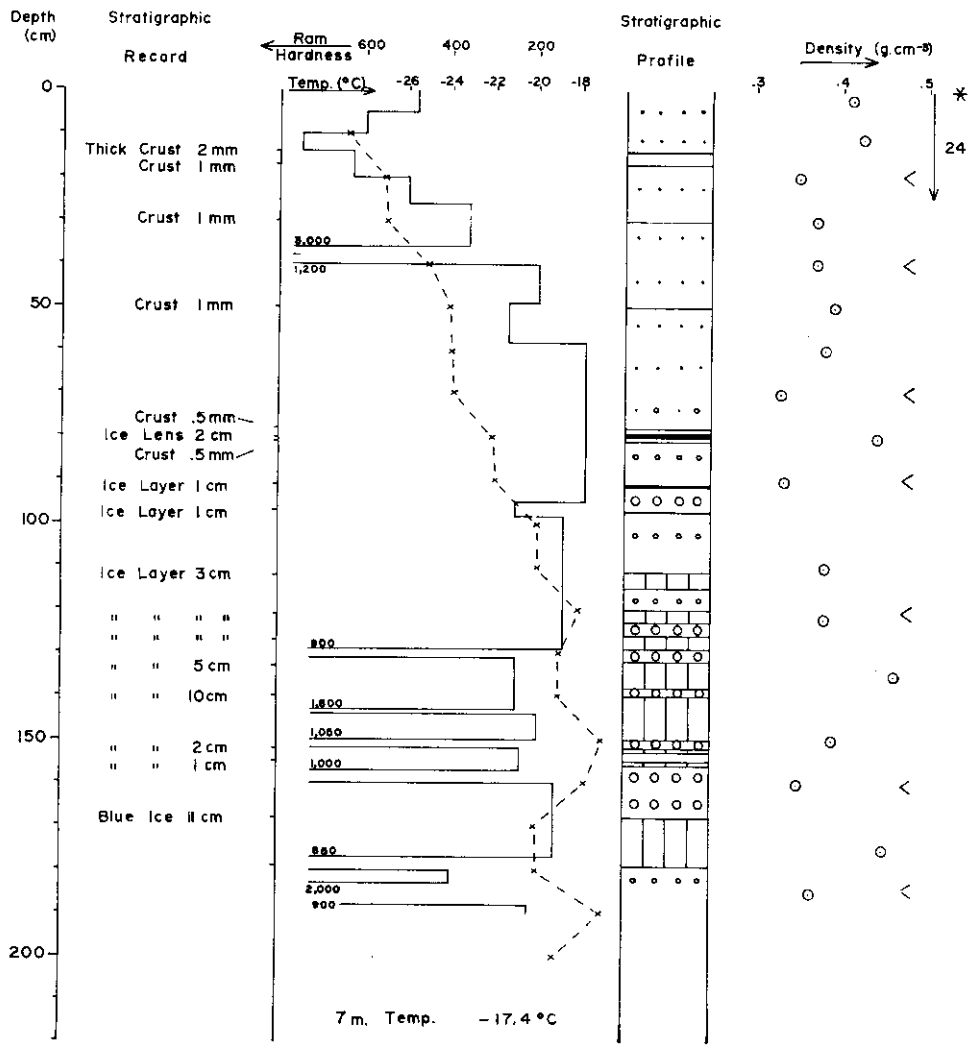

FIG. 2.1.

* Where a stake has been used next to the pit, the previous years accumulation rate has been indicated by an arrow.

Location S 2

Lat. 66° 31' S

Date 15-10-61

Elevation 1162 m.

Depth
(cm)

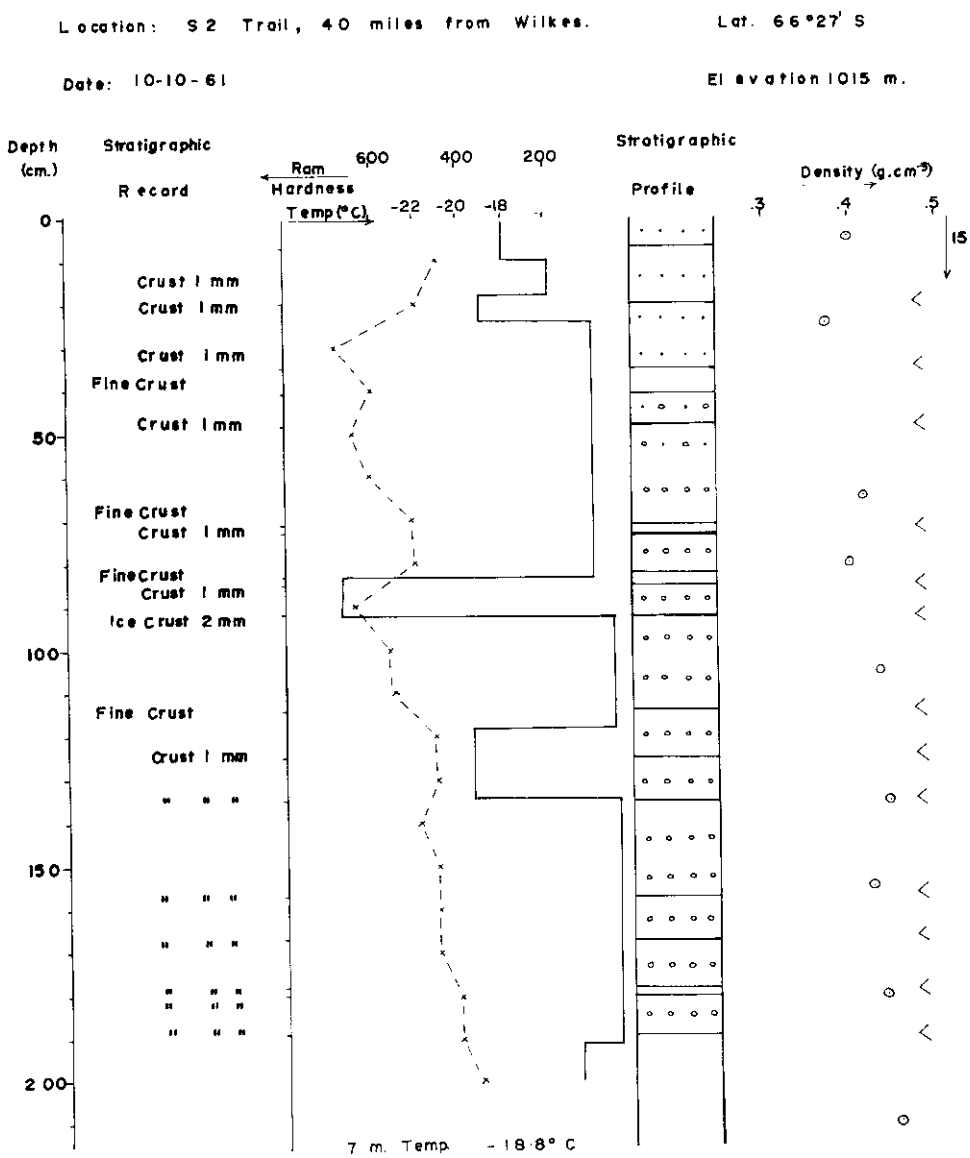
Location: S 2 Trail, 40 miles from Wilkes.
Lat. 66°27' S
Date: 10-10-61
Elevation 1015 m.
Depth (cm.)
Stratigraphic Record
Ram Hardness
Temp(°C)
Stratigraphic Profile
Density (g.cm⁻³)
Crust 1 mm
Crust 1 mm
Crust 1 mm
Fine Crust
Crust 1 mm
Fine Crust
Crust 1 mm
Fine Crust
Crust 1 mm
Ice Crust 2 mm
Fine Crust
Crust 1 mm
7 m. Temp -18·8° C

FIG. 2.2.

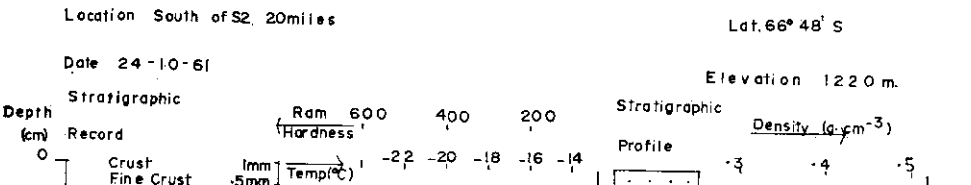
Location South of S2, 20miles
Lat. 66° 48' S
Date 24-10-61
Elevation 1220 m.
Depth (cm)
Stratigraphic Record
Ram Hardness
Temp(°C)
Stratigraphic Profile
Density (g.cm⁻³)
Crust
Fine Crust

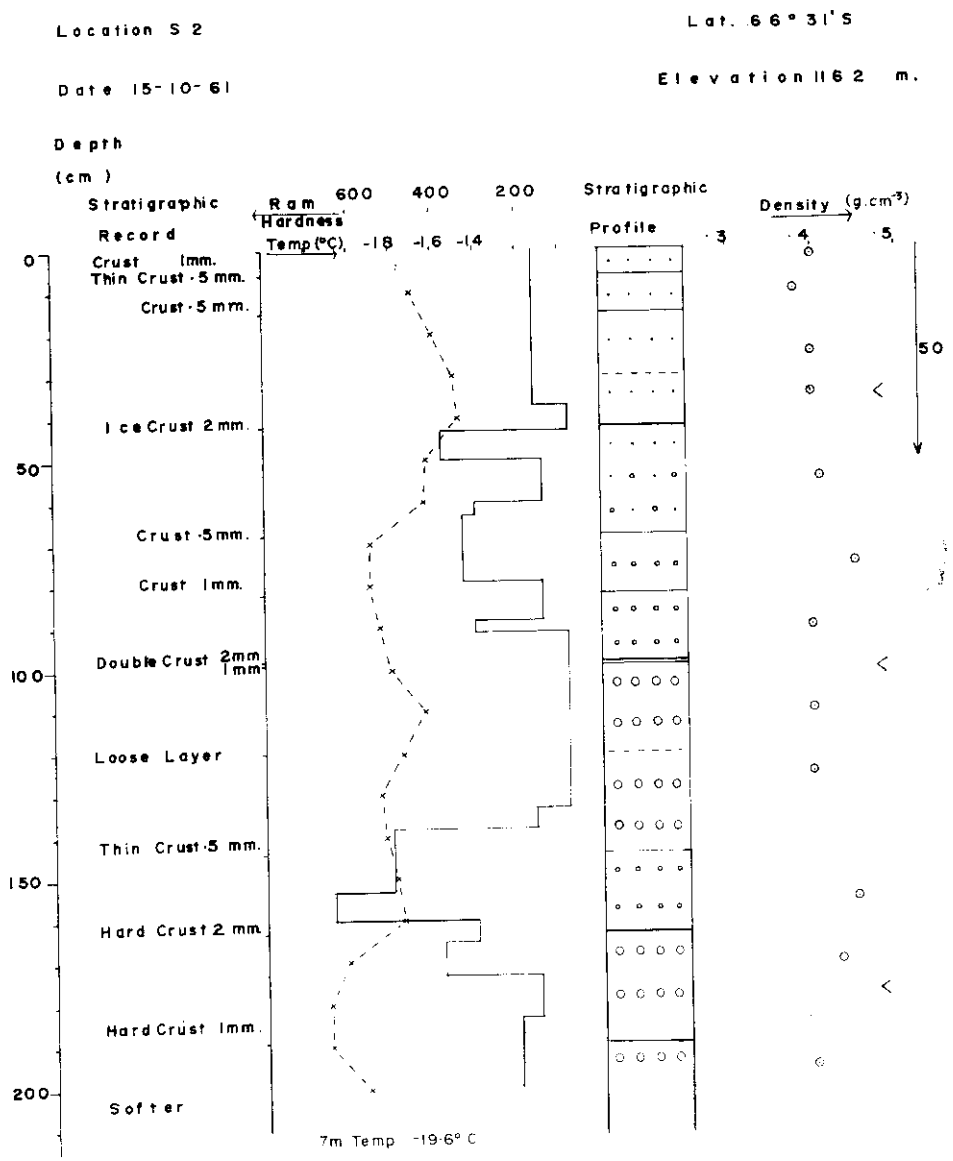
Location S 2
Lat. 66° 31'S
Date 15-10-61
Elevation 1162 m.
Depth (cm)
Stratigraphic Record
Ram Hardness
Temp (°C)
-1.8 -1.6 -1.4
600 400 200
Stratigraphic Profile
Density (g.cm⁻³)
.3 .4 .5
Crust 1mm.
Thin Crust .5 mm.
Crust .5 mm.
Ice Crust 2 mm.
Crust .5mm.
Crust 1mm.
Double Crust 2mm 1mm
Loose Layer
Thin Crust .5 mm.
Hard Crust 2 mm.
Hard Crust 1mm.
Softer
0
50
100
150
200
50
7m Temp -19.6° C

FIG. 2.3.

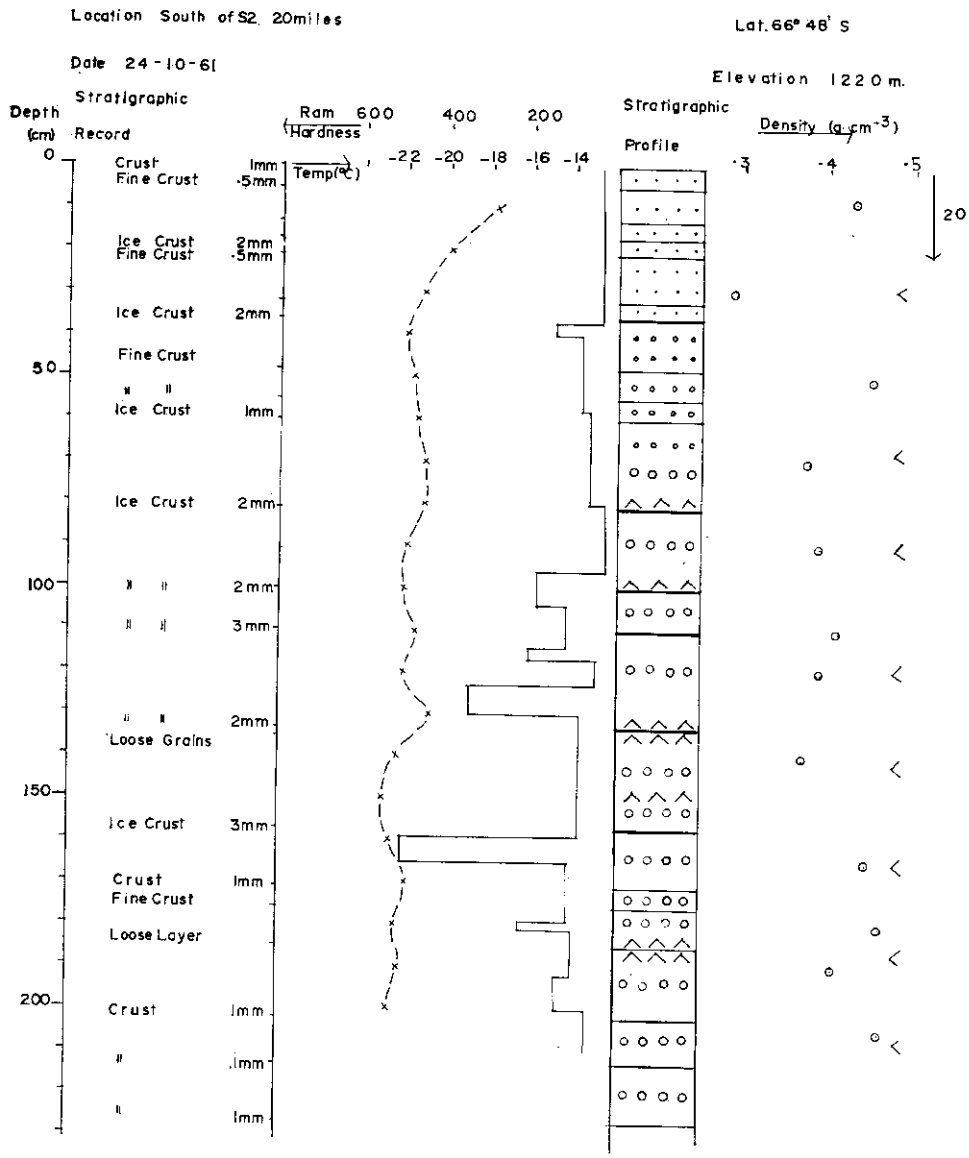
Location South of S2. 20miles
Lat. 66° 48' S
Date 24-10-61
Elevation 1220 m.
Stratigraphic Record
Depth (cm)
Ram Hardness
Temp(°C)
Stratigraphic Profile
Density (g·cm⁻³)
Crust
Fine Crust
Ice Crust
Fine Crust
Ice Crust
Fine Crust
Ice Crust
Ice Crust
Loose Grains
Ice Crust
Crust
Fine Crust
Loose Layer
Crust

FIG. 2.4.

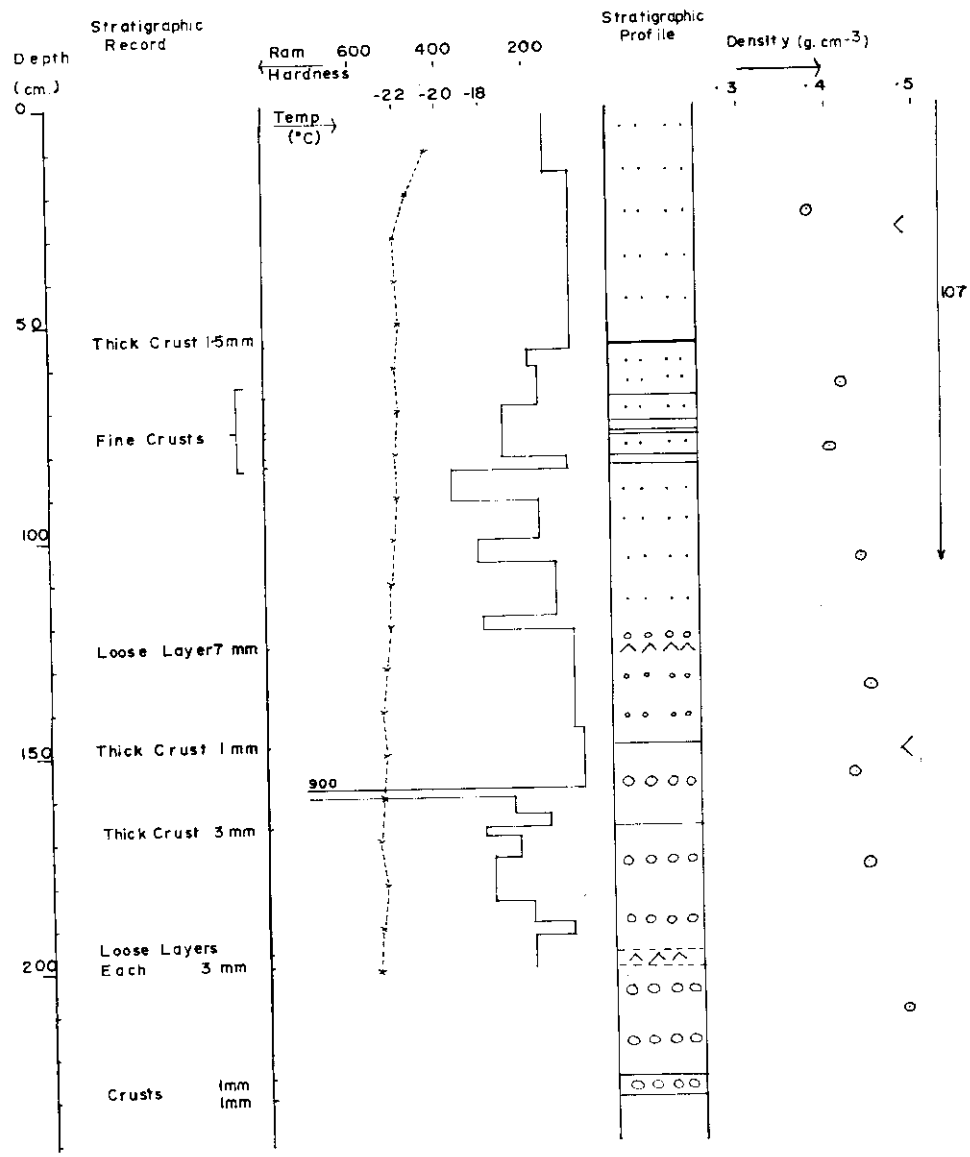
Location South of S2 40 miles
Lat. 67°05'S
Date 25-10-61
Elevation 1059 m.
Stratigraphic Record
Depth (cm.)
Ram Hardness
600
400
200
Temp (°C)
-22
-20
-18
Stratigraphic Profile
Density (g. cm-3)
·3
·4
·5
0
50
100
150
200
Thick Crust 1·5mm
Fine Crusts
Loose Layer 7 mm
Thick Crust 1 mm
Thick Crust 3 mm
Loose Layers Each 3 mm
Crusts 1mm 1mm
900
107

FIG. 2.5.

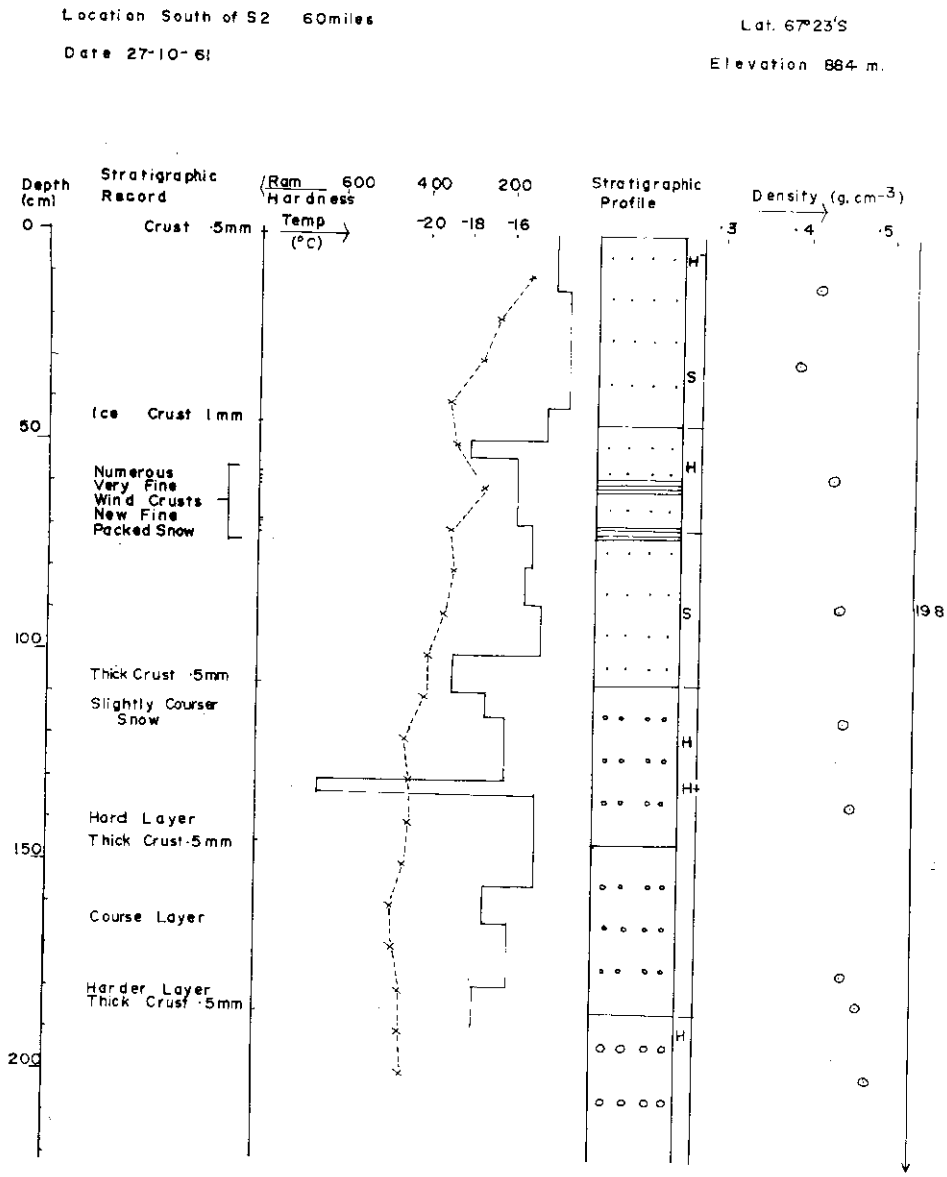
Location South of S2 60miles
Lat. 67°23'S
Date 27-10-61
Elevation 884 m.
Depth (cm)
Stratigraphic Record
Ram Hardness
600
400
200
Temp (°C)
-20
-18
-16
Stratigraphic Profile
Density (g. cm⁻³)
·3
·4
·5
Crust ·5mm
Ice Crust 1mm
Numerous Very Fine Wind Crusts New Fine Packed Snow
Thick Crust ·5mm
Slightly Courser Snow
Hard Layer
Thick Crust·5mm
Course Layer
Harder Layer
Thick Crust ·5mm
0
50
100
150
200
H
S
H
S
H
H+
H
198

FIG. 2.6.

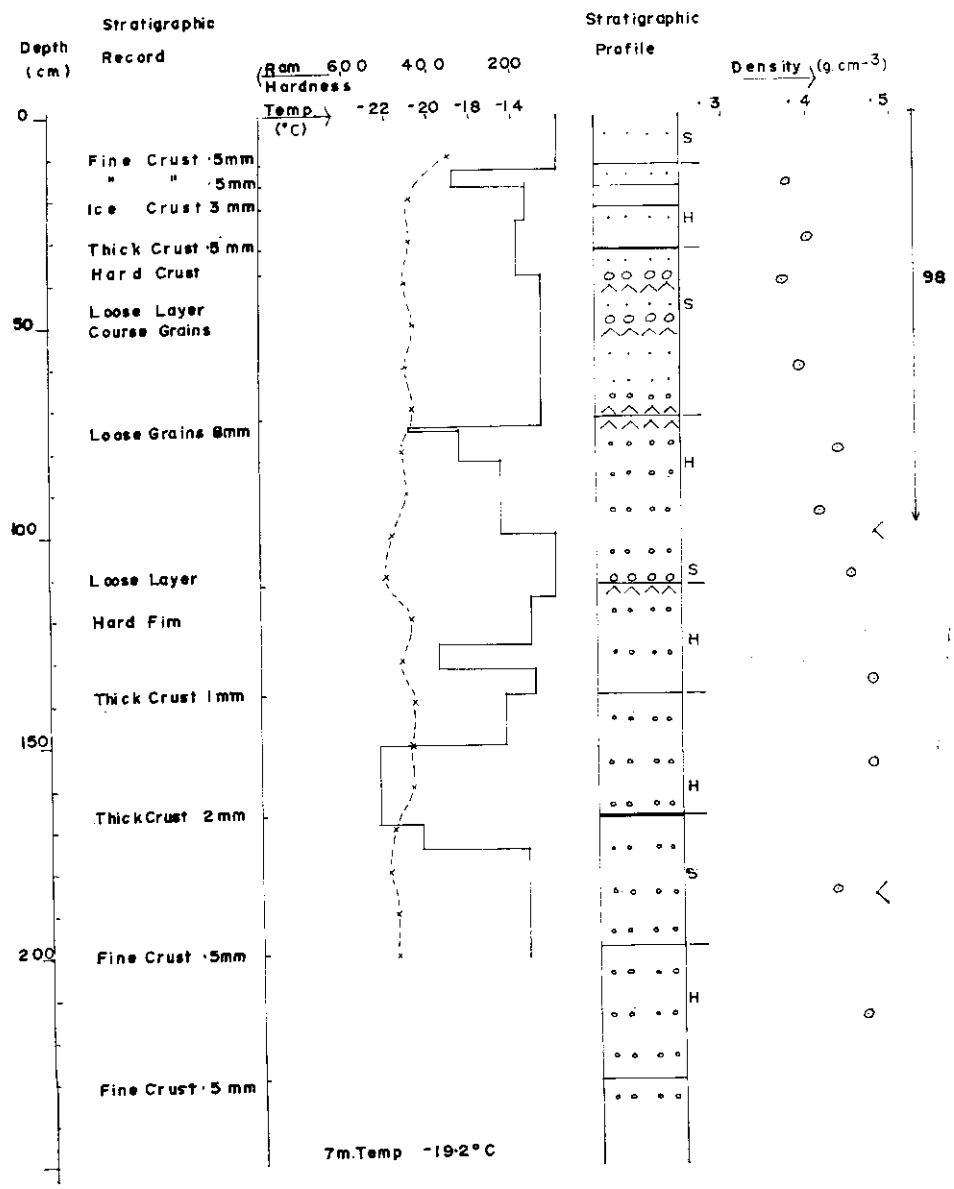
Location South of S2 80 miles
Lat. 67° 40' S
Date 1-11-61
Elevation 1062 m.
Stratigraphic Record
Depth (cm)
Ram Hardness
600 400 200
Temp (°C)
-22 -20 -18 -14
Stratigraphic Profile
Density (g cm-3)
·3 ·4 ·5
Fine Crust ·5mm
" " ·5mm
Ice Crust 3 mm
Thick Crust ·5 mm
Hard Crust
Loose Layer
Course Grains
Loose Grains 8mm
Loose Layer
Hard Fim
Thick Crust 1mm
Thick Crust 2mm
Fine Crust ·5mm
Fine Crust ·5 mm
0
50
100
150
200
S
H
S
H
S
H
H
S
H
98
7m. Temp -19·2° C

FIG. 2.7.

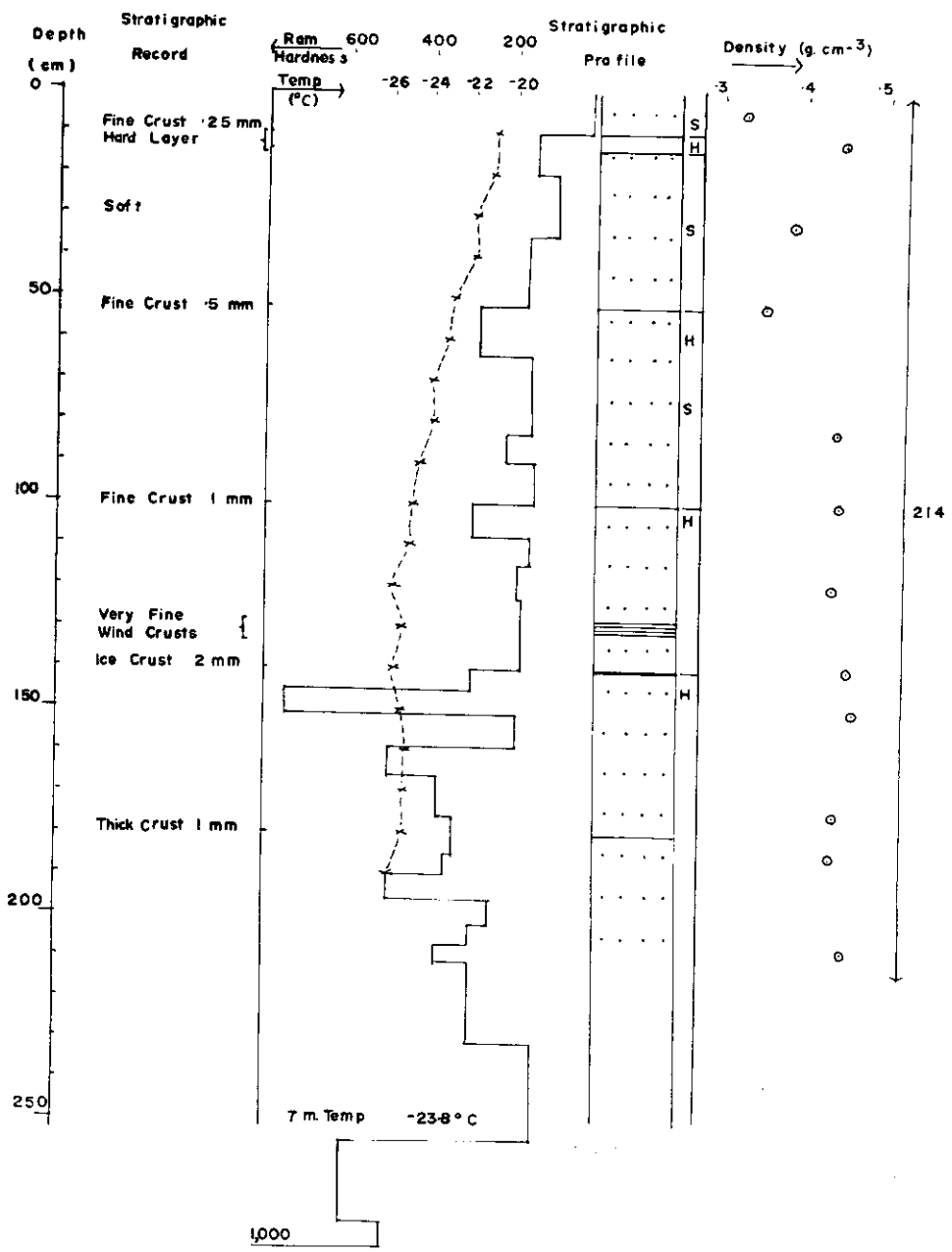
Location South of S2 100miles
Lat. 67°57' S
Date 5-II-61
Elevation 1339 m.
Depth (cm)
Stratigraphic Record
Ram Hardness
Temp (°C)
Stratigraphic Profile
Density (g. cm-3)
Fine Crust ·25 mm
Hard Layer
Soft
Fine Crust ·5 mm
Fine Crust 1 mm
Very Fine Wind Crusts
Ice Crust 2 mm
Thick Crust 1 mm
7 m. Temp -23·8° C
214

FIG. 2.8.

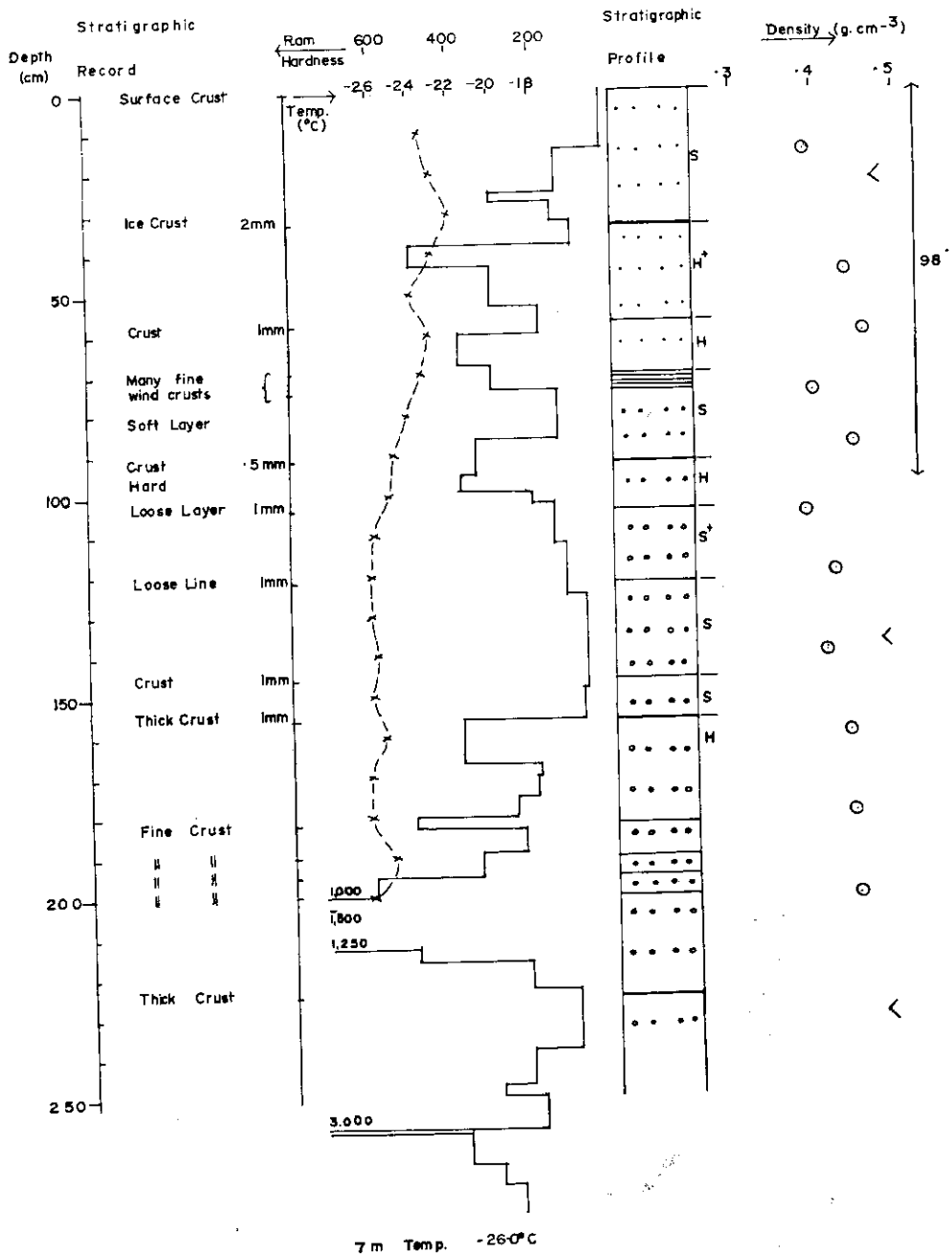
Location South of S2 120 miles
Lat. 68°15'S
Date 19-11-61
Elevation 1668m.
Stratigraphic Record
Depth (cm)
Surface Crust
Ice Crust
Crust
Many fine wind crusts
Soft Layer
Crust
Hard
Loose Layer
Loose Line
Crust
Thick Crust
Fine Crust
Thick Crust
Ram Hardness
Temp. (°C)
Stratigraphic Profile
Density (g.cm⁻³)
1,000
1,800
1,250
3,000
7 m Temp. -26·0°C

FIG. 2.9.

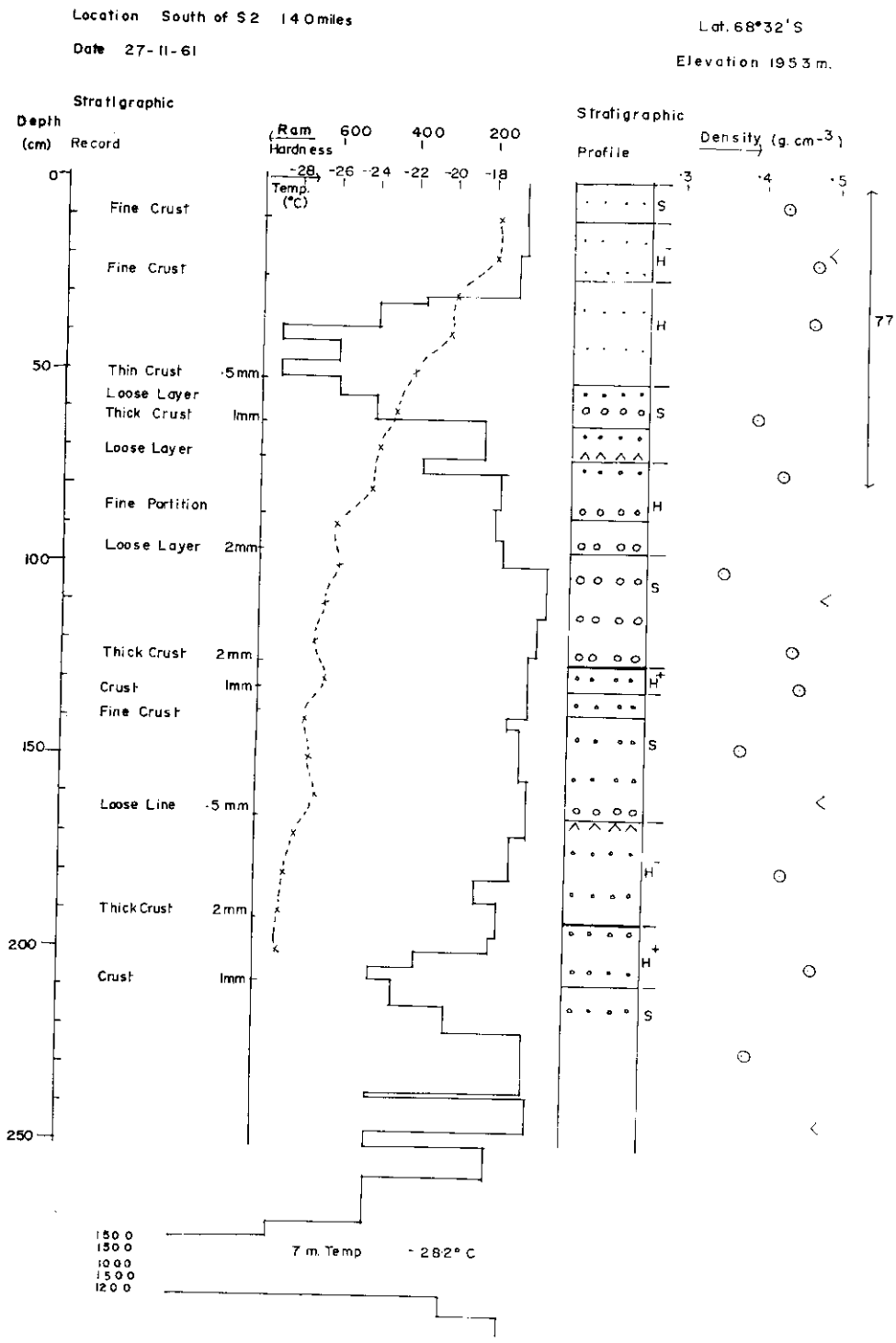
Location South of S2 140miles
Lat. 68°32'S
Date 27-11-61
Elevation 1953 m.
Stratigraphic
Depth (cm)
Record
Ram Hardness
600
400
200
-28
-26
-24
-22
-20
-18
Temp. (°C)
Stratigraphic Profile
Density (g. cm-3)
·3
·4
·5
77
0
50
100
150
200
250
Fine Crust
Fine Crust
Thin Crust
·5mm
Loose Layer
Thick Crust
1mm
Loose Layer
Fine Partition
Loose Layer
2mm
Thick Crust
2mm
Crust
1mm
Fine Crust
Loose Line
·5 mm
Thick Crust
2mm
Crust
1mm
S
H
H
S
H
S
H+
S
H
H+
S
1500
1500
1000
1500
1200
7 m. Temp
-28·2° C

FIG. 2.10.

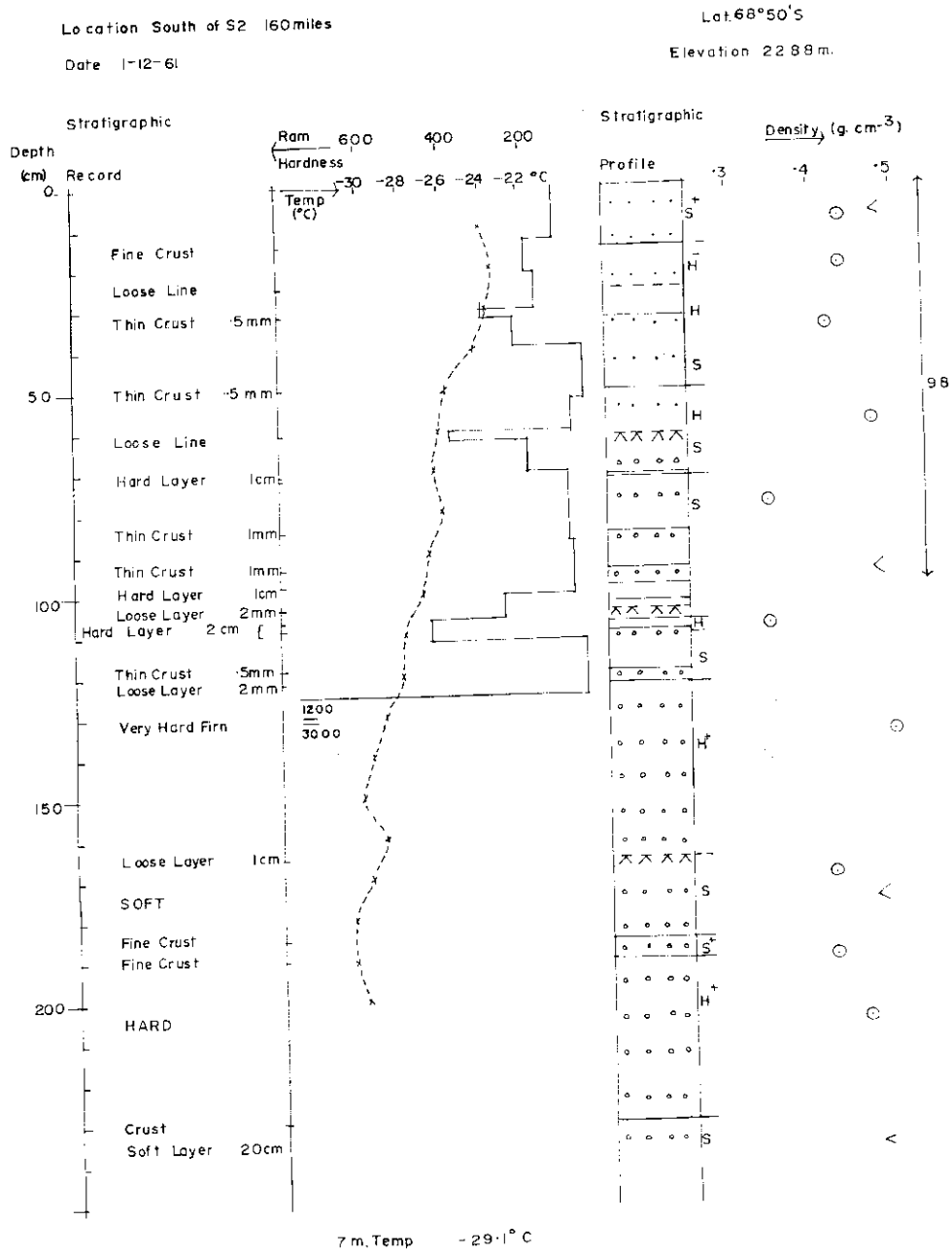
Location South of S2 160miles
Date 1-12-61
Lat.68°50'S
Elevation 2289m.
Stratigraphic Record
Depth (cm)
Ram Hardness
Temp (°C)
Stratigraphic Profile
Density (g. cm⁻³)
Fine Crust
Loose Line
Thin Crust 5mm
Thin Crust 5mm
Loose Line
Hard Layer 1cm
Thin Crust 1mm
Thin Crust 1mm
Hard Layer 1cm
Loose Layer 2mm
Hard Layer 2cm
Thin Crust 5mm
Loose Layer 2mm
Very Hard Firn
Loose Layer 1cm
SOFT
Fine Crust
Fine Crust
HARD
Crust
Soft Layer 20cm
1200
3000
98
7m. Temp -29·1°C

FIG. 2.11.

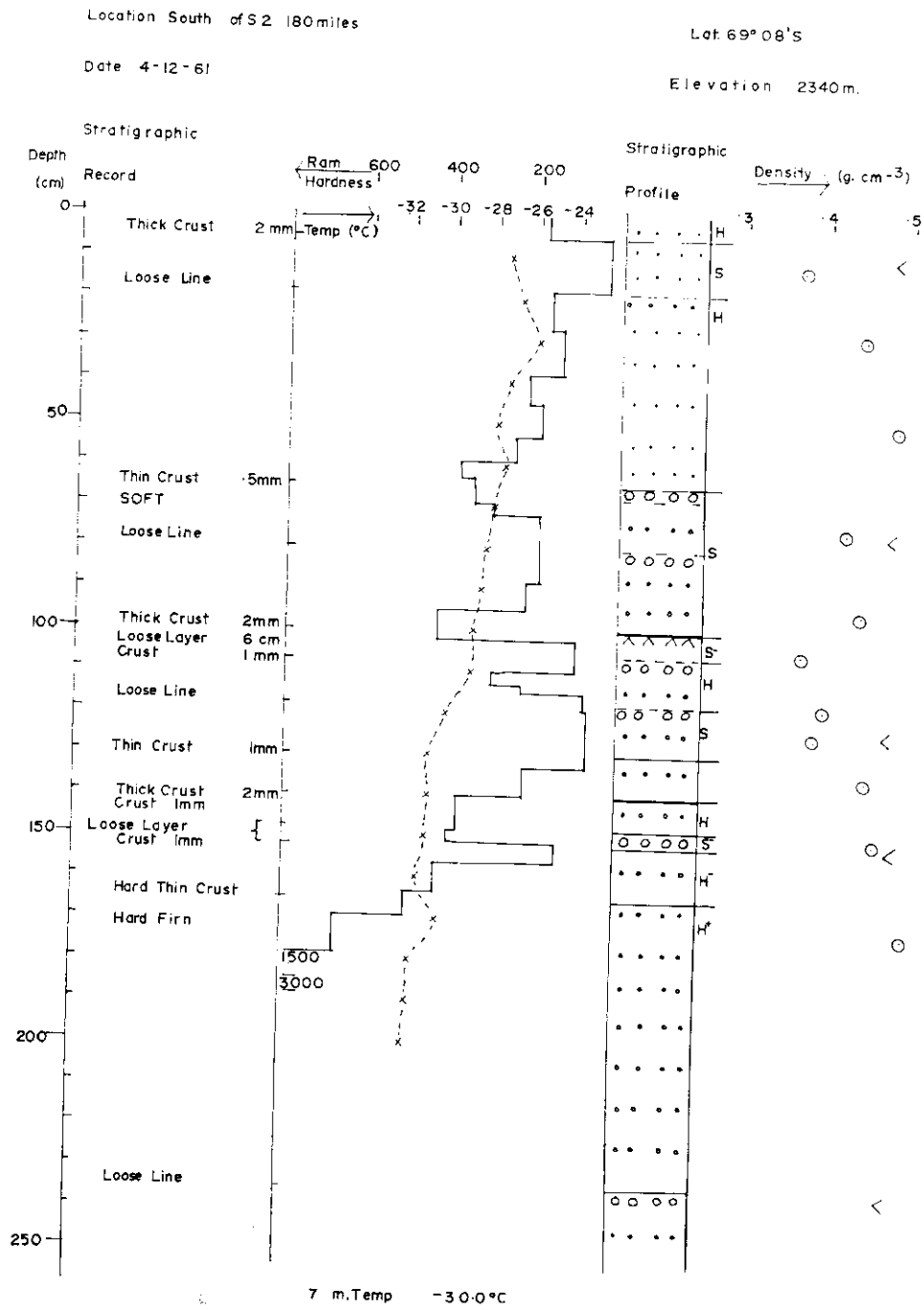
Location South of S 2 180 miles
Lat. 69° 08' S
Date 4-12-61
Elevation 2340 m.
Stratigraphic Record
Depth (cm)
Ram Hardness
Temp (°C)
Stratigraphic Profile
Density (g. cm-3)
Thick Crust
Loose Line
Thin Crust SOFT
Loose Line
Thick Crust
Loose Layer
Crust
Loose Line
Thin Crust
Thick Crust Crust
Loose Layer Crust
Hard Thin Crust
Hard Firn
Loose Line
2 mm
·5mm
2mm
6 cm
1 mm
1mm
2mm
1mm
1500
3000
7 m. Temp -30·0°C

FIG. 2.12.

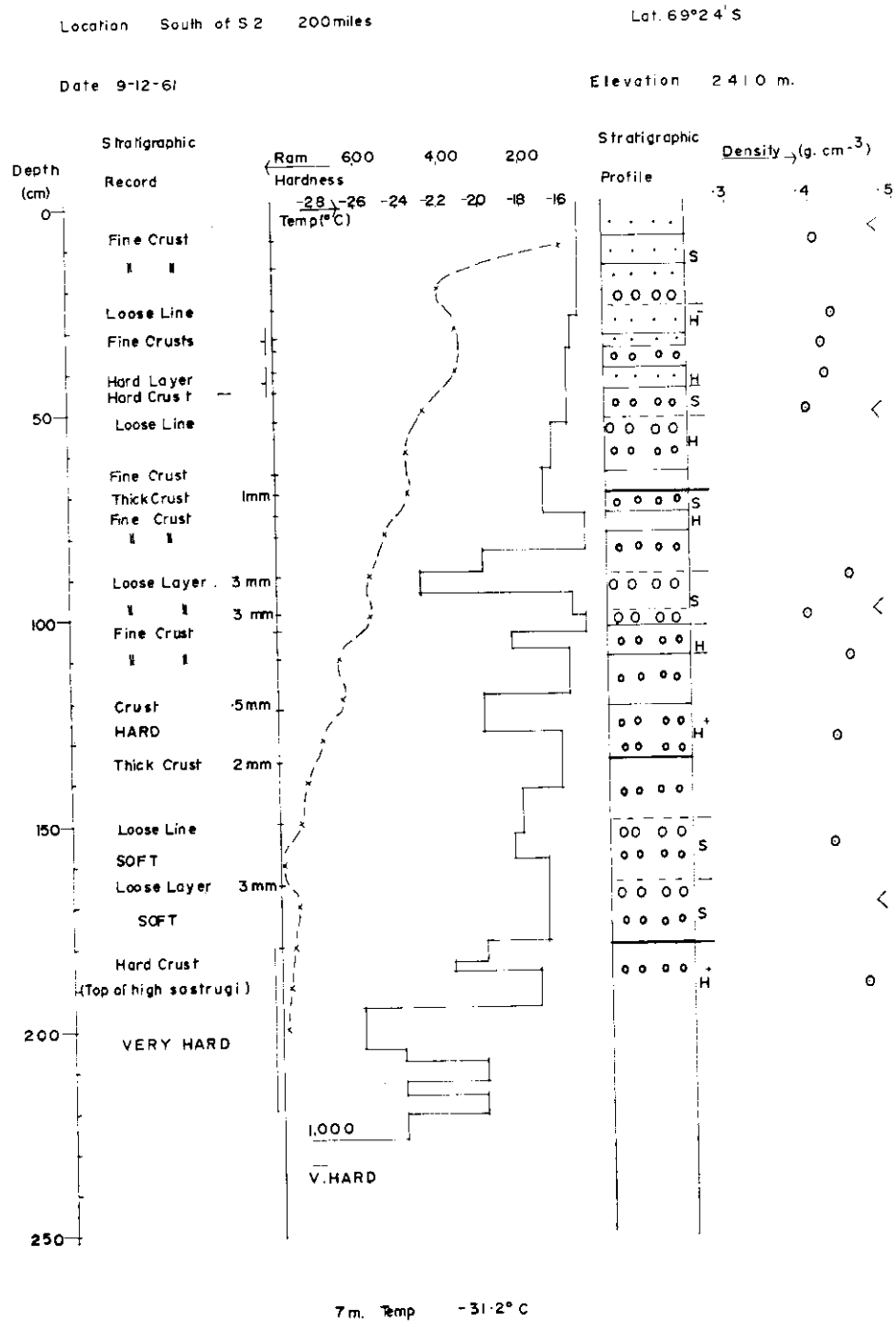
Location South of S 2 200 miles
Lat. 69°24'S
Date 9-12-61
Elevation 2410 m.
Depth (cm)
Stratigraphic Record
Ram 6.00 4.00 2.00
Hardness
-28 -26 -24 -22 -20 -18 -16
Temp(°C)
Stratigraphic Profile
Density (g. cm-3)
·3 ·4 ·5
Fine Crust
Loose Line
Fine Crusts
Hard Layer
Hard Crust
Loose Line
Fine Crust
Thick Crust
Fine Crust
Loose Layer
Fine Crust
Crust
HARD
Thick Crust
Loose Line
SOFT
Loose Layer
SOFT
Hard Crust
(Top of high sastrugi)
VERY HARD
1mm
3 mm
3 mm
·5mm
2mm
3mm
1,000
V.HARD
0
50
100
150
200
250
7m. Temp -31·2° C

FIG. 2.13.

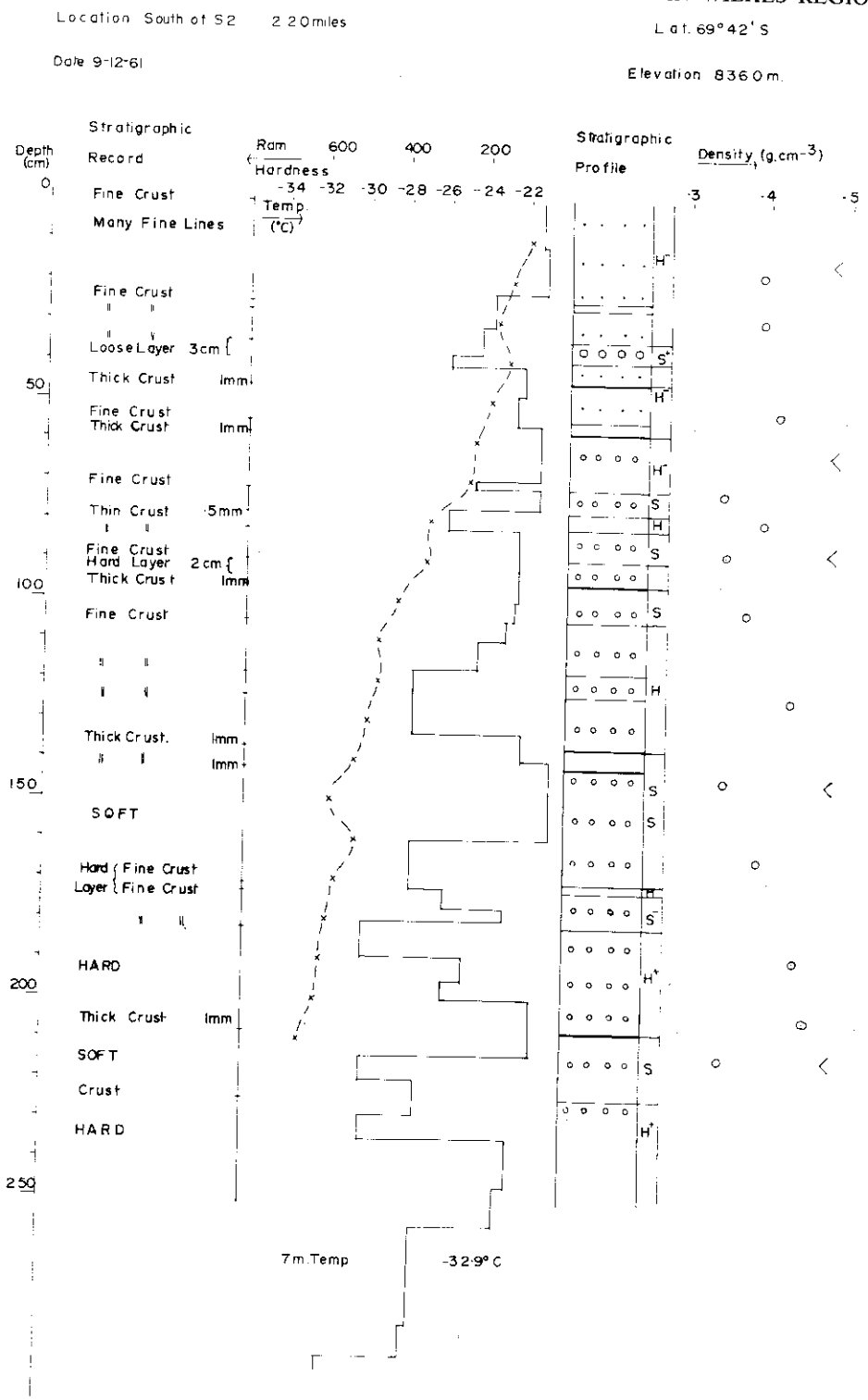
Location South of S2 2 2 0 miles
Lat. 69°42' S
Date 9-12-61
Elevation 836 0 m.
Depth (cm)
Stratigraphic Record
Ram Hardness
600 400 200
Temp. (°C)
-34 -32 -30 -28 -26 -24 -22
Stratigraphic Profile
Density (g.cm⁻³)
·3 ·4 ·5
Fine Crust
Many Fine Lines
Fine Crust
Loose Layer 3cm
Thick Crust 1mm
Fine Crust
Thick Crust 1mm
Fine Crust
Thin Crust ·5mm
Fine Crust
Hard Layer 2cm
Thick Crust 1mm
Fine Crust
Thick Crust. 1mm
1mm
SOFT
Hard Layer { Fine Crust
Fine Crust
HARD
Thick Crust 1mm
SOFT
Crust
HARD
7m Temp -32·9° C
0
50
100
150
200
250

FIG. 2.14.

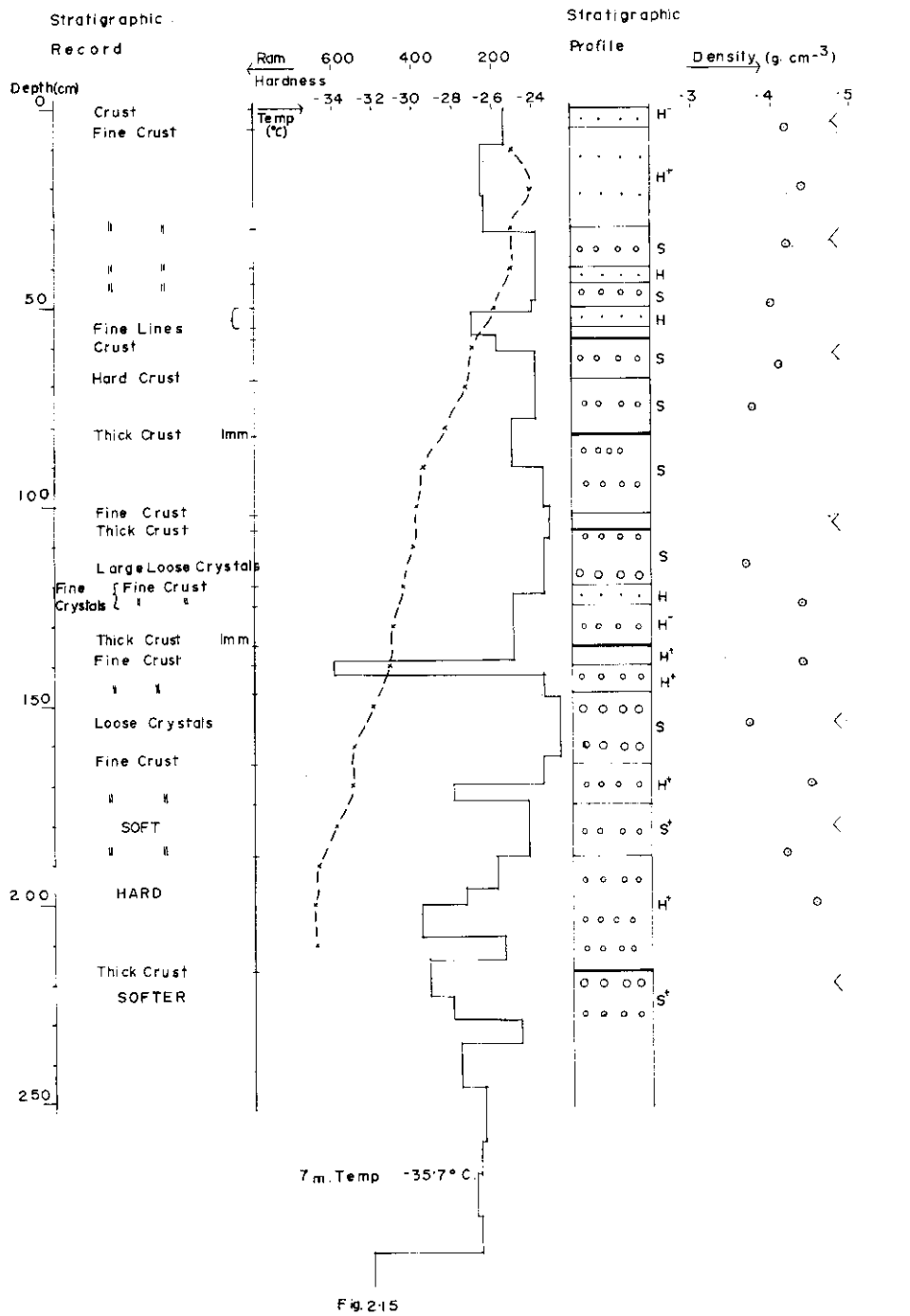
Location South of S2 240 miles
Lat. 69°59'S
Date 11-12-61
Elevation 2680 m.
Stratigraphic Record
Stratigraphic Profile
Depth(cm)
Ram Hardness
Temp (°C)
Density (g. cm⁻³)
Crust
Fine Crust
Fine Lines Crust
Hard Crust
Thick Crust
Fine Crust
Thick Crust
Large Loose Crystals
Fine Crystals
Fine Crust
Thick Crust
Fine Crust
Loose Crystals
Fine Crust
SOFT
HARD
Thick Crust
SOFTER
7m. Temp -35·7° C.

FIG. 2.15.

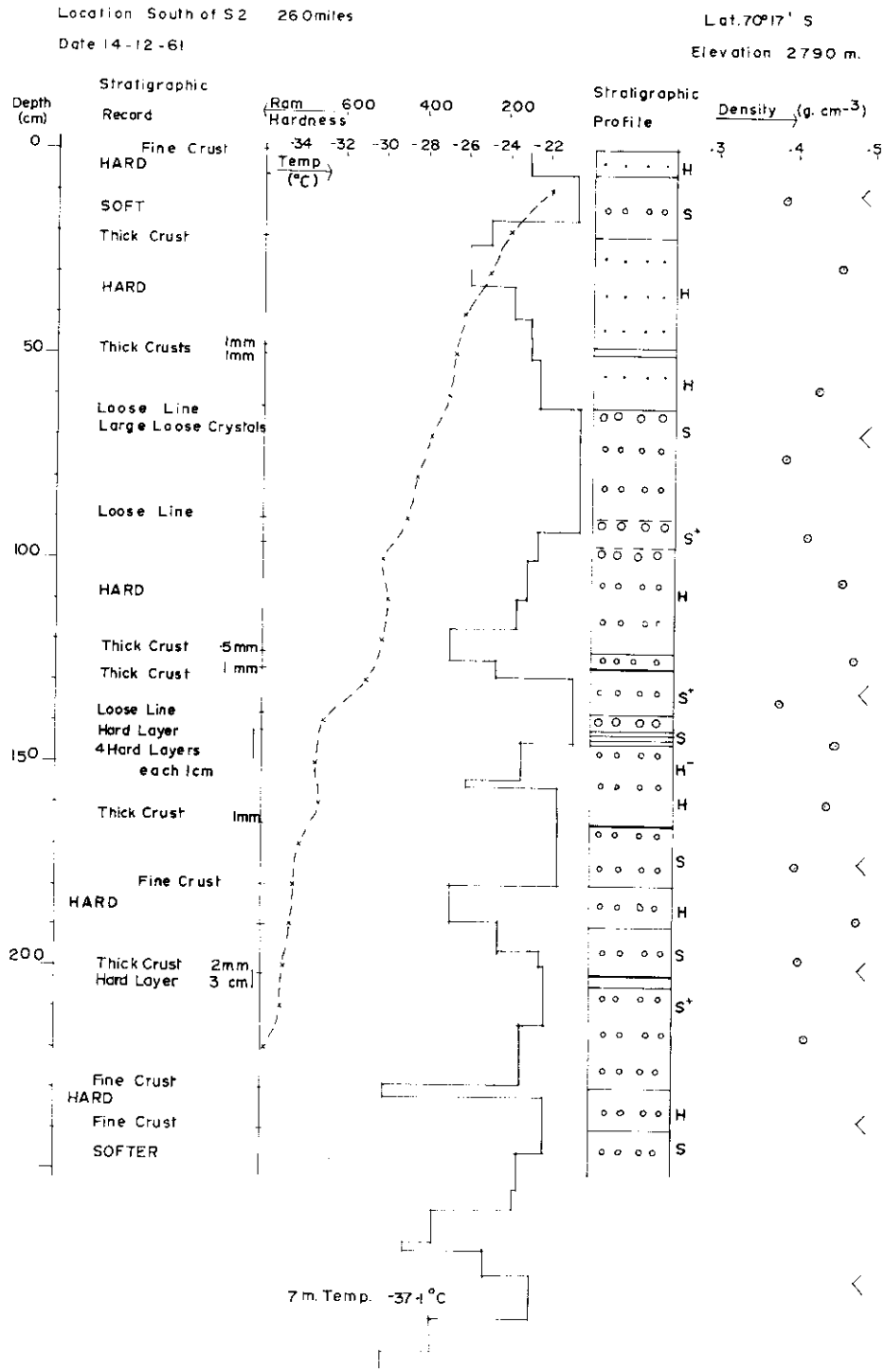
Location South of S2 26 0miles
Lat. 70°17' S
Date 14-12-61
Elevation 2790 m.
Depth (cm)
Stratigraphic Record
Ram Hardness
600
400
200
Temp (°C)
-34 -32 -30 -28 -26 -24 -22
Stratigraphic Profile
Density (g. cm-3)
·3 ·4 ·5
0
50
100
150
200
Fine Crust
HARD
SOFT
Thick Crust
HARD
Thick Crusts 1mm 1mm
Loose Line
Large Loose Crystals
Loose Line
HARD
Thick Crust ·5mm
Thick Crust 1 mm
Loose Line
Hard Layer
4 Hard Layers each 1cm
Thick Crust 1mm
Fine Crust
HARD
Thick Crust 2mm
Hard Layer 3 cm
Fine Crust
HARD
Fine Crust
SOFTER
H
S
H
H
S
S+
H
S+
S
H-
H
S
H
S
S+
H
S
7 m. Temp. -37·1 °C

FIG. 2.16.

Location South of S2 280 miles Lat.70°34'S.

Date 17-12-61 Elevation 2935 m.

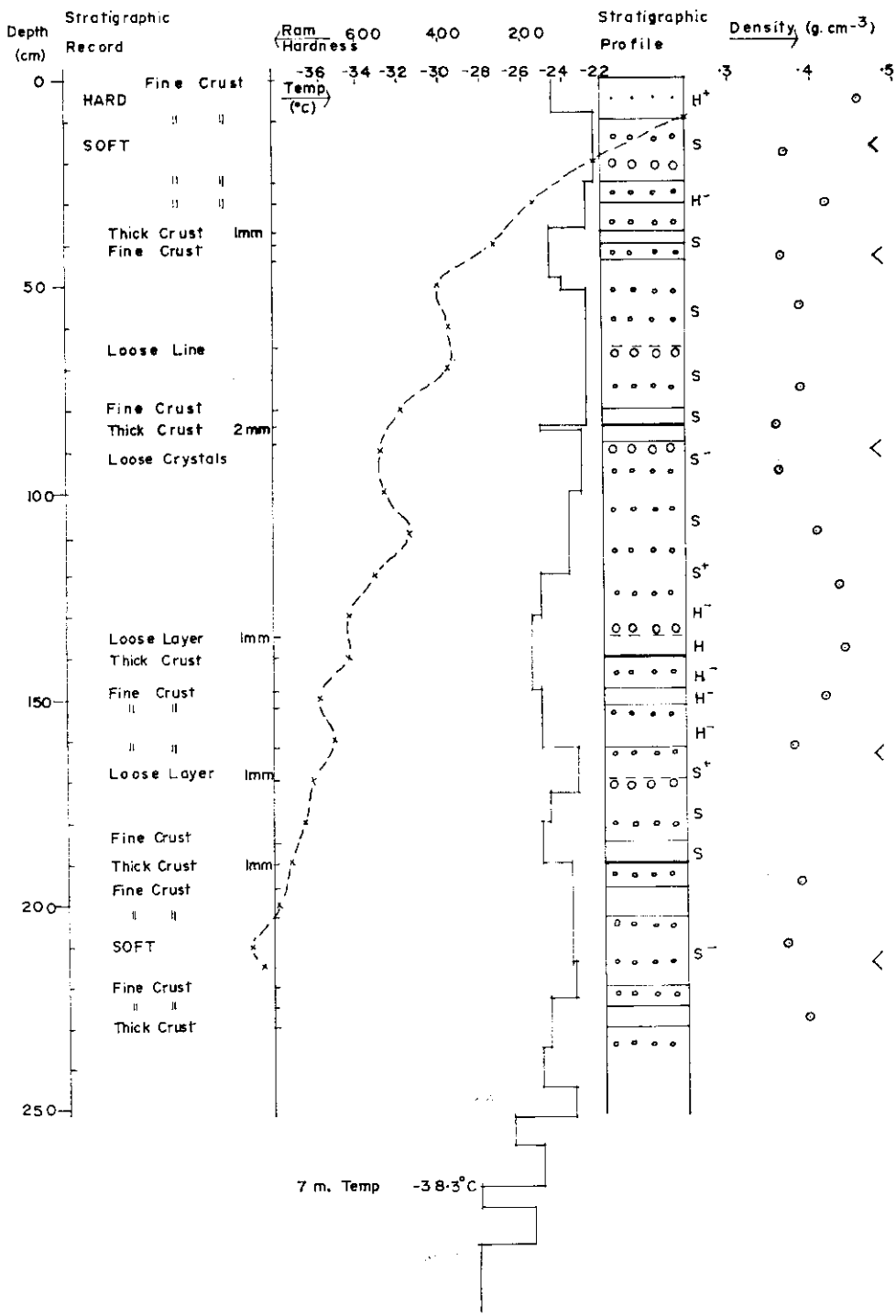

FIG. 2.17.

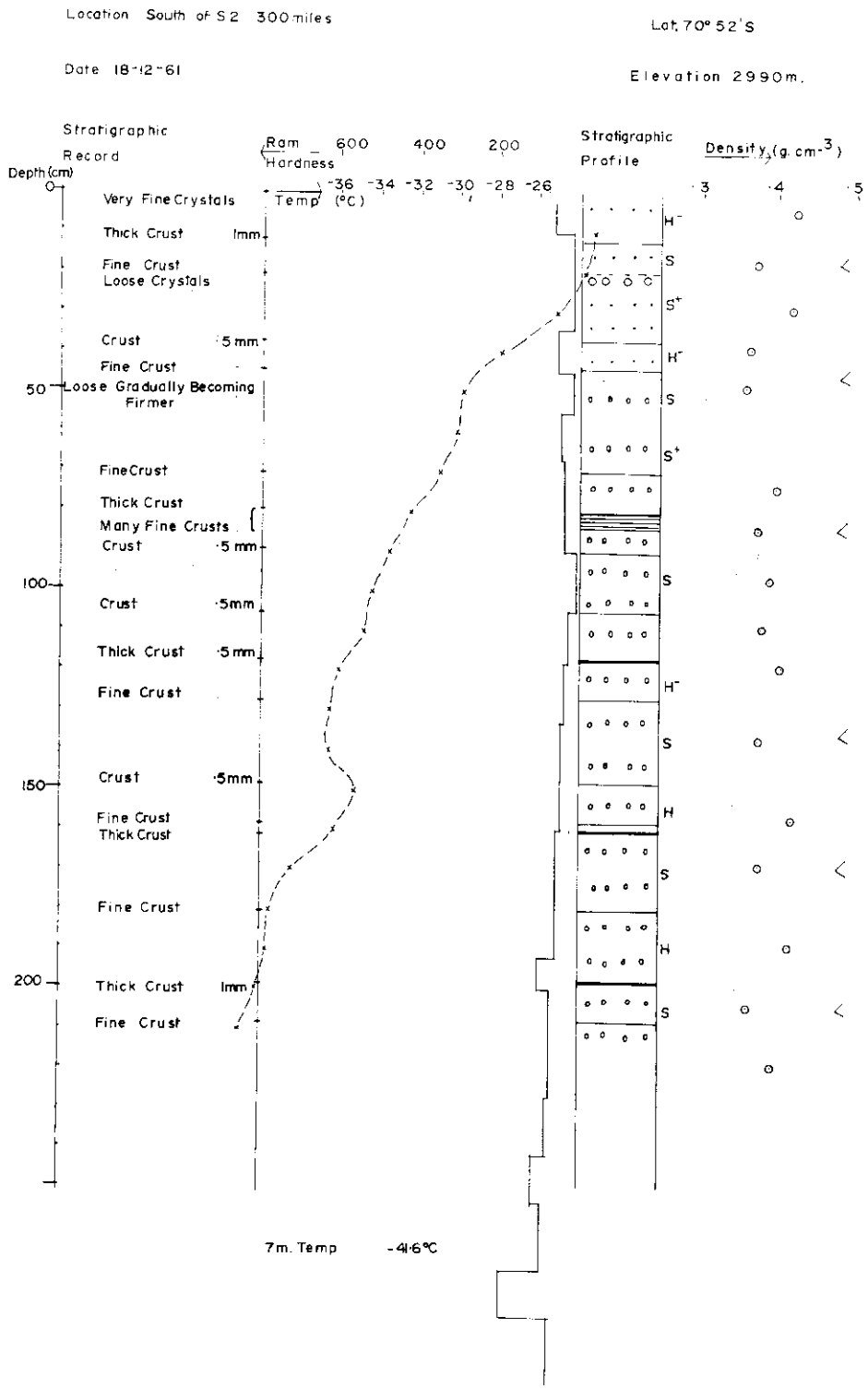
Location South of S2 300 miles
Lat. 70° 52'S
Date 18-12-61
Elevation 2990m.
Stratigraphic Record
Depth (cm)
Ram Hardness
600 400 200
Temp (°C)
-36 -34 -32 -30 -28 -26
Stratigraphic Profile
Density (g. cm-3)
·3 ·4 ·5
Very Fine Crystals
Thick Crust 1mm
Fine Crust
Loose Crystals
Crust ·5 mm
Fine Crust
Loose Gradually Becoming Firmer
Fine Crust
Thick Crust
Many Fine Crusts
Crust ·5 mm
Crust ·5mm
Thick Crust ·5 mm
Fine Crust
Crust ·5mm
Fine Crust
Thick Crust
Fine Crust
Thick Crust 1mm
Fine Crust
50
100
150
200
H⁻ S S⁺ H⁻ S S⁺ S H⁻ S H S H S
7m. Temp -41·6°C

FIG. 2.18.

2.1. DEPENDENCE OF STRATIFICATION UPON CLIMATE

It was found that no single subsurface variable was sufficient to determine the annual layers. Only by a close association of all the variables could a confident estimate of the annual strata be made. This follows from the climatic survey, Section 1, which showed that the variability in precipitation, wind speed, and temperature in different years is high. Therefore it is necessary to use the few general results which seem to apply from year to year. Three notable results are

(i) the temperature is definitely higher over summer;

(ii) the precipitation is slightly lower over summer;

(iii) the wind speed is slightly lower over summer.

The consequences of these with respect to stratification are:

(i) The summer layer is smaller. In fact, near the coast there is no summer layer in the sense that a new snow layer is deposited, for ablation occurs and part of the winter layer is removed. However, at the same time the top part of the winter layer may become metamorphosed by radiation and higher temperature, giving an artificial "summer layer".

(ii) (a) For positions sufficiently low in elevation near the coast, where for some time during the year the temperature rises above 0°C, a melt layer may form on the surface. Inland from Wilkes the ice layers varied from almost continuous ice at S1, through 5 cm layers 32 km inland, to 2 mm layers at S2. Beyond 32 km south of S2 no evidence of summer melting was discerned.

(b) Even in the absence of melt the effect of the higher temperatures over summer tends to create larger crystals with larger pore spaces between them, in contrast to small compacted crystals of the winter layer. Underneath relatively impermeable crusts large loose hexagonal crystals often grow from sublimation processes. These are termed sublimation crystals and may be several mm across.

(iii) Due to the high winter winds the thicker winter layers may have numerous "wind crusts" throughout the layer. This also leads to harder-packed denser snow layers during winter in contrast to the softer, looser, but larger-grained snow of the summer.

Similar features have been noted for firn stratification in different parts of inland Antarctica by Schytt (1958), Hoinkes (1961), Lorius (1962) and Crary *et al.* (1962).

Again it must be stressed that these general features are subject to wide variation in different years. For example, at Wilkes in 1960 the average wind appeared no stronger in winter than in summer and also the precipitation was less than half that of 1957. The accumulation along the S2 trail and at S2 was smaller over 1960 than in the neighbouring years. This variability of climatic conditions in different years suggests that annual layers may fluctuate in size to the same extent, and that the typical hard-packed, fine-crusted winter layer may be absent or may be merged indistinguishably with the summer layer.

Schytt (1958, p. 37) found a relative variability (ratio of the standard deviation to the mean) of 25% from pit data over 17 years at Maudheim and quotes the accumulation figures of Sorge (1935) from the pit at Eismitte as giving a relative

variability of 11% and those of Etienne (1940) giving a variability of 18% over 9 years. For station Charcot, Lorius (1962) obtained values of accumulation rates from core structures ranging from 13·4 cm water over 10 years to 28·1 over 24 years.

In the present study, even though surface meteorological observations were carried out during the 1961 traverse (October to December), the basis for the interpretation of the pit stratification has been provided mainly by the weather data recorded at Wilkes and at S2. Much further inland the weather situation may in general be very different. If this is so it is expected to be revealed in the pit stratification data.

2.2. INTERPRETATION OF PIT DATA

2.2.1. Surface layer

One difficulty in interpreting the pit data is that the surface snow (at the top of the pit) may not necessarily be directly comparable with the region of the pit one annual layer below. This is because the surface may still have to undergo metamorphosis. On the 1961 traverse the pits between S2 and 290 km south were dug in November 1961. The stakes along this route had been placed in November 1960, yet the type of snow at the surface did not correspond directly to that at the initial mark of the stake next to the pit. The snow at this lower level had undergone the summer metamorphosis which the surface snow was just commencing to undergo.

2.2.2. Ramsonde

The ramsonde record for each pit is continuous but may miss small layers due to the impetus of the weight carrying the instrument right through a layer. Furthermore, the ramsonde values do not correspond exactly to the other pit values because the ramsonde was used about 20 cm from the wall studied. On many occasions large steep, sastrugi were discerned in the pit wall. These caused complications in the interpretation of the pit data.

2.2.3. Densities

The firn density was measured at each observable layer of greater thickness than the diameter of the sampler (7 cm). On the average the density determinations were made about 15 cm apart. The summer layers generally show up on the density profile as small, less dense layers. But this less dense summer snow is not regularly a feature and generally, right through the pit, thin hard dense layers alternate with soft layers.

2.2.4. Stratification

The winter layers in the region 32 to 380 km south of S2 had many fine wind crusts, mostly embedded in hard dense firn. In some annual layers there appeared to be no typical hard layer, whereas in a soft summer layer there would sometimes be many fine wind crusts. In each layer there were often more than a dozen different hard, thin crusts. Only by an overall association of these with the other parameters, density, crystal size and hardness, could the annual layers be distinguished.

2.2.5. Crystals (grain sizes)

In the pits near the coast the surface snow had the small crystals of wind-packed firn. Deeper down, the crystals were larger and ice bands alternated with loose layers and hard, dense firn.

In pit No. 5 (64 km south of S2) and those further south the crystals in general were small, although sublimation crystals were observed in a thin layer (2–3 mm) often below a thin crust.

There appeared to be a slight increase in crystal size (as well as in density and hardness) with depth on going into the previous year's accumulation. However, crystal sizes were only measured qualitatively on the traverse and in, order to establish such a variation firmly, it would be necessary to obtain a large number of precise measurements and treat them statistically (cf. Vickers (1961)).

2.2.6. The pit temperature profiles

(a) The most noticeable feature of the temperature profiles to 2 m was the gradual change from slightly positive gradients at the beginning of the traverse (early October) to highly negative gradients at the end of the traverse (late December). This is a result of the surface temperature rising over the period and of the time lag for this effect to reach the 2 m depth. The general shape of this temperature profile may be used to estimate the annual mean temperature at the surface and its annual range.

(b) The smaller fluctuations in the slope of the temperature/depth profile going down the pit appear to be a result of two factors. Firstly, the random large fluctuations of the surface temperature from day to day are quickly damped out when transmitted downwards into the snow and hence are particularly noticeable in the first 20 to 50 cm of the pits (cf. conduction theory, Section 5.1). Secondly, the conductivity of the firn increases with density. Hence often through a hard layer the temperature gradient becomes small whereas through a soft layer it is large.

2.3. GENERAL RESULTS FROM 1961 TRAVERSE

2.3.1. Variation of strata and accumulation inland

(1) For the region from the coast to 32 km south of S2 the past accumulation could be determined by the melt layers. The annual strata for this region were small and the pits extended therefore further back into the past than the pits in the high accumulation region 90 to 200 km south of S2 (cf. Section 2.3.4). The past accumulation can be seen from the pit diagrams to be of the same magnitude as that measured by the stakes, with the expected random variation in different years. In particular, some "summer" layers were characterised by a single thick ice layer whereas others had several smaller ice layers.

(2) Further south from 32 km south of S2 the accumulation increased to values in excess of 2 m of snow per year. Whenever the pits extended deeply enough, evidence was obtained of similar accumulation rates for the previous year. For the higher accumulation rates it will be necessary to wait for longer term measurements to see if they are not exceptional. The study of the pattern of accumulation over undulating slopes, Section 4.3.4., suggests that these high rates are not exceptional but a property of the topographical position.

Some extremely hard layers were encountered in this region, so hard that the ramsonde, after registering over 3,000 kg wt. resistance, would not penetrate without suffering damage.

(3) Still further inland (beyond 290 km south of S2) the elevation still increased but the accumulation and slope decreased. The ram hardness and density in the pits also decreased, cf. Pit Diagrams, Figures 2.15 to 2.18. This decrease in hardness and density seems to be a result of the wind being weaker in this region. This is in agreement with the absence of large, hard wind-packed sastrugi here. The pits in this inland region generally reached 3 or 4 annual layers, as determined from the hardness, density and stratification. The accumulation rates estimated for these pits have been obtained from the means of the annual layers excavated.

2.3.2. Variation of climate inland, from pit strata

Dolgushin (1961, p. 64) has described the climate and accumulation of inland Antarctica. His discussion indicates that the main climatic features of central Antarctica are lower temperatures, less precipitation, lighter winds, smaller accumulation and softer, less dense snow.

The results of the pit and accumulation stake measurements along the 1961 traverse route confirm this and appear to show a similar climate situation to that inland of Mirny and inland of Dumont D'Urville (cf. Dolgushin (1961), Kotlyakov (1961), Lorius (1962)). From the graph of Figure 4.4 it may be seen that the slope of the ice plateau surface gradually decreases inland from 120 km south of S2. From this it may be expected that the katabatic winds decrease inland from this position. This is confirmed by the sastrugi observations and the decrease in snow hardness. The decrease in accumulation rate inland seems to be a direct result of the wind decrease inland; that is to say, the high accumulation values between 90 and 120 km south of S2 are a result of snow being transported down slope by strong winds. From the accumulation and drift studies (Sections 3 and 4) it follows that the amount of snow accumulation depends on the rate of change of wind velocity, i.e., where the wind increases snow will be picked up, whereas it will be deposited where the wind velocity decreases. Hence where the slope of the ice surface is convex (cf. Fig. 4.4) and the wind speed may be expected to increase, the snow would be transported to the positions of concave slope. This is well brought out by the accumulation profile, cf. Figure 4.4.

An alternative explanation to that in terms of wind transport, for the decrease of accumulation inland, is that the precipitation may decrease going inland on the ice cap. This is reported to apply between Mirny and Vostok, but at this stage there are not sufficient data available inland of Wilkes to confirm such a decrease, since the decrease in accumulation might be entirely a result of drift transport. The results from the Wilkes 1962 traverse from Wilkes to Vostok should throw light on this problem.

3. DRIFTING SNOW

3.0. INTRODUCTION

Following the measurements of drift density initiated at Mawson in 1957 (Mellor and Radok (1960)) and extended to Wilkes in 1959 (Dingle and Radok (1961)) using the snow collection traps described by Mellor (1960), an attempt was made in 1961 to measure the part played by blowing snow in the mass budget of the Wilkes region.

Drift density and wind profile measurements were made at Wilkes station, along the S2 trail and at S2. The prevailing wind direction here is very close to the S2—Wilkes route direction. In July, simultaneous measurements were attempted at S2 and Wilkes to obtain the variation in drift from inland to the coast. However, it was found that the weather conditions varied greatly over the region so that strong wind at one station was not necessarily accompanied by windy conditions at the other even though S2 appears to be almost directly upwind of Wilkes station. Over a three-week period in July–August almost continuous drift was encountered at S2, whereas Wilkes station only had a few days of strong winds.

As mentioned earlier (Section 1.3), experience gained during other field journeys north and south of Wilkes suggests that the katabatic winds may be strongly channelled at the coast into the low Vanderford Glacier area or north of Cape Folger, thus missing Wilkes located between them. This means that, although detailed information may be available about the drift at an inalnd station and at the coast, it is still not possible to give an accurate account of the transport of snow over the region until much more information is obtained about the surface winds over the area.

In the following sections the mechanism of drifting snow at a single station will first be analysed in detail; in the final section the result will be used, together with a very approximate representation of the winds over the area, to make a calculation of the effect of the wind-blown drift on the snow accumulation profile from the inland station to the coast.

An attempt was made to study how the drift density varies with 3 main variables:

(i) the height above the surface;

(ii) the wind velocity;

(iii) the "local parameters" such as the amount of loose snow available, particle fall velocities, the roughness of the surface and surface topography.

For the first two variables, the results obtained show close agreement with the theoretical treatment of steady-state turbulent drift transport (cf. Loewe (1956), Mellor and Radok (1960), Dingle and Radok (1961)). The third, however, is much more difficult to treat exactly because of the difficulty of attaching precise measures to the various factors. The conditions of surface snow appear to undergo wide random variation during a large number of measurements in the one place. But although the individual measurements of drift and the local parameters exhibit wide

variations, their averages over a large number of measurements, for each sub-range of wind speed, supply good estimates of typical drift conditions for each of these wind speed ranges.

Total drift transports have hence been calculated from these average drift densities as a function of wind velocity for typical local conditions. From the daily mean wind distributions of Wilkes and S2, for certain years, estimates of the potential loss of snow by wind have been calculated on the assumption that the supply of snow at the surface has been maintained. A comparison is then made between this value and the expected loss of snow obtained from the difference between the total precipitation recorded at Wilkes and the net accumulation measured at the various accumulation stakes from Wilkes to S2.

3.1. DRIFT DENSITY

3.1.1. Drift density as a function of height

Following Dingle and Radok (1961), the following symbols are used:

z vertical co-ordinate above the surface
w particle fall velocity
n_z drift density at height z
V_z wind velocity at height z
u_* shear velocity of the wind
k von Karman's constant
ρ density of the air
A_z turbulent coefficient of exchange at height z

For steady conditions (n_z constant with time) the amount of snow falling across unit area per unit time is balanced by the amount spread upwards by turbulent diffusion, cf. Shiotani and Arai (1953) and Loewe (1956),

$$wn_z + A_z\rho \frac{\partial n}{\partial z} = 0. \tag{3.1}$$

For a logarithmic wind profile near the ground the exchange coefficient A_z is given by:

$$A_z = ku_* \frac{z}{\rho}. \tag{3.2}$$

(cf. e.g. Sutton (1953)).

This gives

$$wn_z + ku_* z \frac{\partial n_z}{\partial z} = 0; \tag{3.3}$$

hence

$$\frac{n_z}{n_{z_1}} = \left(\frac{z}{z_1}\right)^{-\frac{w}{ku_*}} \tag{3.4}$$

as given by Dingle and Radok (1961).

3.1.2. Wind profile and roughness length

The logarithmic wind profile corresponding to equation (3.2) has the form

$$V_z = \frac{u_*}{k} \log_e \frac{z}{z_0}. \tag{3.5}$$

where z_0 is the "roughness length"—the height at which the velocity is zero, a parameter describing local surface conditions.

For all the drift measurements carried out by the author in 1961 the velocity was measured at 3 or, on most occasions, 4 levels and was found to agree with the logarithmic wind profile. The roughness length was found to vary largely independently of wind speed or drift density. For this reason the antilog of the mean log value for all the drift runs was taken as a typical value and regarded as a constant with respect to wind speed; z_0 had the mean value of 0·75 cm and ranged from 0·04 to 1·5 cm. These values are higher than those found from the 1959 Wilkes results and appear to be a result of sastrugi up to about 10 cm high which were present during a large number of the measurements, especially at S2. This type of surface, together with the variation in surface due to either erosion, or deposition, made measurements in the lowest layer (below 10 cm) more difficult to interpret.

3.1.3. Variation of shear velocity with wind speed

Having taken a constant value (0·75 cm) for z_0, we now see that the shear velocity u_* varies *linearly* with the velocity at a given level. In particular, if V_{10} m/sec is the velocity at the 10 m level, then

$$V_{10} = \frac{u_*}{\cdot 4} \ln \left(\frac{10000}{0{\cdot}75} \right)$$

or

$$u_* = \frac{V_{10}}{18{\cdot}3} \text{ m/sec.} \tag{3.6}$$

This linear increase of u_* with V_z is illustrated in Figure 3.1. Similar results have been obtained by Liljequist (1957, p. 200) (z_0 = 0·01 to 0·58 cm for V_{10} = 10 to 33 cm/sec).

3.1.4. Variation of fall velocity (w) with height

From equation (3.4) it may be seen that in any given steady drift run (constant wind profile hence V_{10} and u_* constant) the value of $\log \frac{n_z}{n_{z_1}}$ is proportional to $\log \frac{z}{z_1}$, provided the fall velocity w does not vary significantly with height, i.e. the variation in the regression of $\log \frac{n_z}{n_{z_1}}$ on $\log \frac{z}{z_1}$ is a measure of the variation of w with height. For the levels studied in 1961 between 10 and 800 cm no systematic variation of w was detected from the 3 or 4 drift density height values observed; hence for a given wind profile the fall velocity has been regarded as a constant with height. Actually the fall velocity of the particles will depend upon their diameter and may be expected to be similarly distributed. Consideration of this leads to a refinement of the present drift profile (equation (3.4)) and indicates also how the distribution of fall velocity varies with height (cf. Budd (1966)).

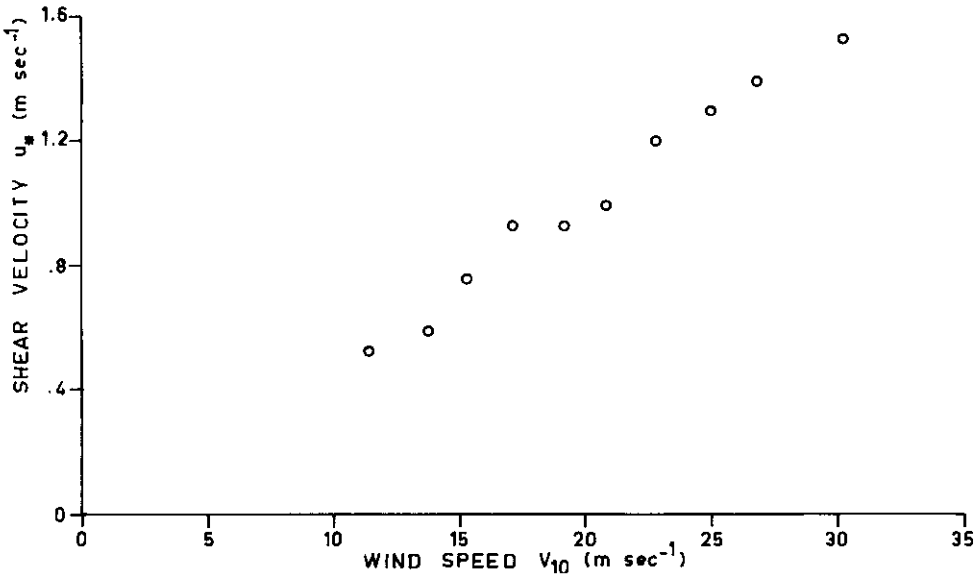

FIG. 3.1. SHEAR VELOCITY VERSUS WIND SPEED. The wind speed measurements carried out in conjunction with the drift measurements at S2 have been fitted to a logarithmic profile of the form $V_z = u_*/k \log z/z_0$. The parameter u_* has then been plotted against V_{10} (the velocity at the 10 m level) showing an approximately linear relation between the two.

Lister (1960) obtained only a very small variation in particle size distribution with height to 6 m for drift particles at South Ice. However, by studying a larger number of levels Dingle and Radok (1960) and Budd, Dingle and Radok (1966) found a distinct variation in fall velocity with height.

For the present study, w was assumed constant with height and, using this, the least squares regression lines for $\log \frac{n_z}{n_{z_1}}$ on $\log \frac{z}{z_1}$ were calculated from the n_z values of the 3 or 4 drift densities measured between 10 and 800 cm. Using this straight line, n_z values were then calculated for the following corresponding heights (z) for each run: 12·5, 25, 50, 100, 200, 400 and 10,000 cm.

3.1.5. Variation of drift density with wind speed

It may be seen from equation (3.4) that drift density for different wind profiles will vary with u_*. This will be illustrated by the change of the slope $\left(-\frac{ku_*}{w}\right)$ of the $\log z - \log n_z$ lines, which for constant w would increase linearly with u_* and therefore wind speed. The drift densities obtained at S2 have been logarithmically averaged for 6 velocity ranges between 10 and 30 m/sec and are shown in Table 3.I. The same values are also plotted in Figure 3.2 using $\log n_z$ $\log z$ axes.

The values in Table 3.I and Figure 3.2 show how the drift density decreases with height and increases with wind speed. In Table 3.Ia and Figure 3.2a some average

TABLE 3.I.

S2 DRIFT DENSITY ($g\,m^{-3}$) V. HEIGHT (z cm) AND WIND SPEED ($v\,m\,sec^{-1}$).

V	13·4	16·1	17·2	19·1	21·0	24·6	27·2
z							
400	0·010	0·09	0·16	0·25	0·38	0·67	1·55
200	0·042	0·29	0·46	0·68	0·98	1·57	3·2
100	0·18	0·90	1·36	1·86	2·54	3·74	6·9
50	0·73	2·8	4·0	5·10	6·53	8·87	14·6
25	3·0	8·6	11·6	14·0	16·8	21·0	30·9
12·5	12·5	26·4	34·0	38·3	43·2	50·0	65·3

values from the results of Dingle and Radok (1961) for Wilkes are shown for comparison. The drift density values in the lower layers (12·5 cm) for corresponding wind speeds show close agreement for Wilkes and S2. For the higher levels, however,

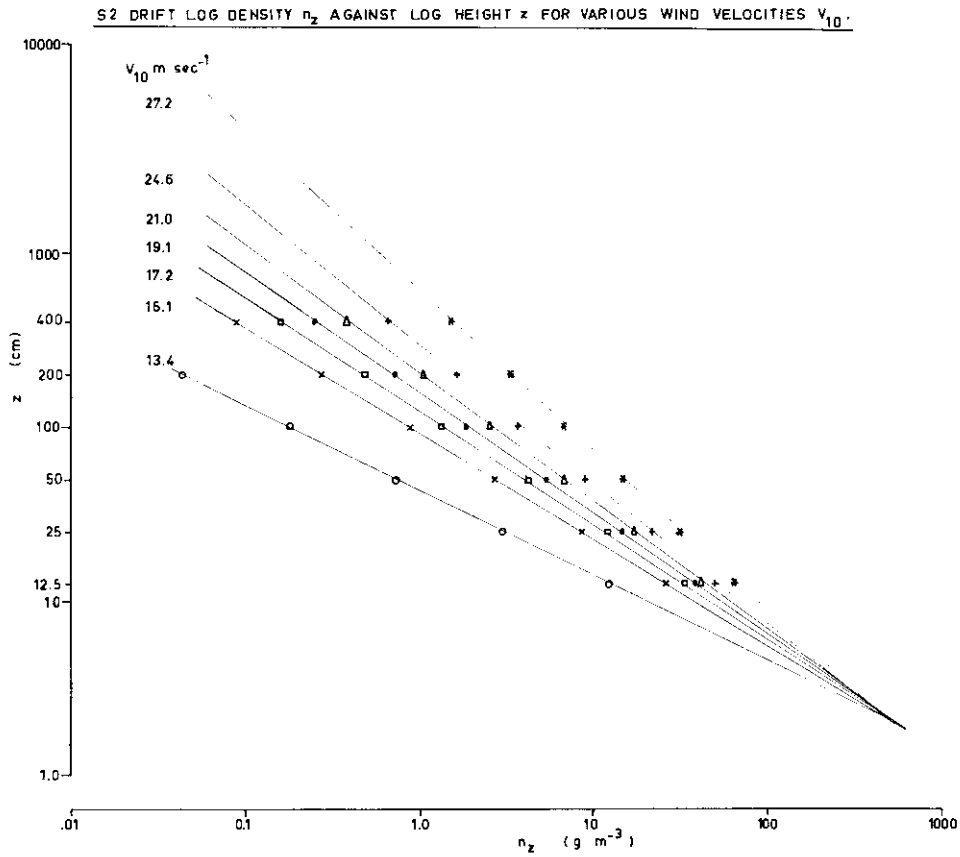

FIG. 3.2. DRIFT DENSITY VERSUS HEIGHT. The average drift densities from S2 for increasing subranges of velocity are plotted against the height above the snow surface. The values plotted are from the computed linear regression of log n_z on log z. Hence the plotted lines are necessarily straight. The slope of the lines increases with wind velocity following u_*.

the Wilkes values are somewhat larger. This may first of all be due to the straight line regression used in the reduction of the S2 values although the individual values obtained at Wilkes show a definite upward curvature for the upper levels, especially

TABLE 3.I.a.

WILKES DRIFT DENSITY (g m^{-3}) v. HEIGHT (z cm) AND WIND SPEED (v m sec^{-1}), (FROM DINGLE AND RADOK (1961)).

V	16·5	20·9	22·7	23·9	25·4	28·0
z						
400	0·320	3·14	1·29	2·76	4·11	8·05
200	0·543	5·30	3·40	4·90	6·59	12·0
100	0·975	8·56	4·12	7·98	9·40	19·1
50	1·34	14·1	7·43	15·0	16·2	29·6
25	6·34	32·6	21·0	30·7	32·6	60·5
12·5	22·8	72·3	61·5	79·0	72·9	107·0

for the lower wind speeds. This type of curvature would result from a slight decrease of particle fall velocity with height (cf. Budd (1966)).

The other reason that would account for the lower drift densities for the higher levels for S2 is that the average particles were larger at S2; their fall velocities would then be greater and hence the drift density would decrease more rapidly with height.

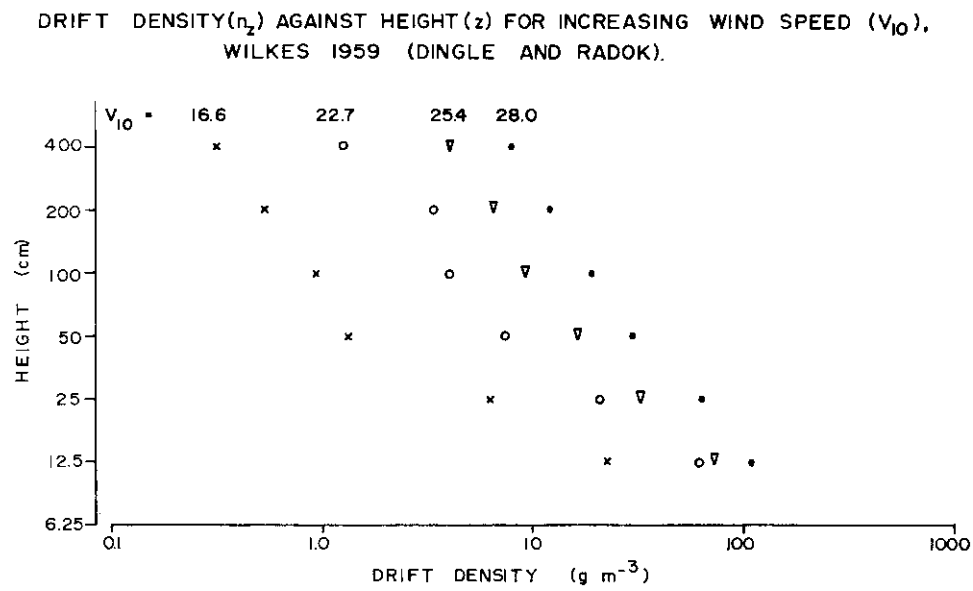

FIG. 3.2a. DRIFT DENSITY VERSUS HEIGHT (WILKES, 1959). From the results of Dingle and Radok (1961) the actual *measured* drift density-height profile has been averaged (logarithmically) for different wind speed ranges and then plotted similarly as in Fig. 3.2. In spite of the scatter each profile shows evidence of slight curvature which decreases for increasing wind speed.

3.1.6. Variation of fall velocity with wind speed

From the drift density values in Table 3.I the fall velocity w has been calculated for each velocity range by using equation (3.4) in the form

$$w = ku_* \frac{\log \frac{z}{z_1}}{\log \frac{n_z}{n_{z_1}}}. \tag{3.7}$$

Only a slight variation with wind velocity was obtained for w as illustrated in Table 3.II which lists the average values for the different velocity ranges.

TABLE 3.II.

FALL VELOCITY (w) V. WIND SPEED (V_{10}).

V_{10}	m/sec	13·4	16·1	17·2	19·1	21·0	24·6	27·2
w	m/sec	0·59	0·58	0·58	0·61	0·62	0·66	0·64

The small increase in w may be due to slightly larger particles, on the average, being carried with stronger winds. These values of w are somewhat higher than those found from the Wilkes measurements of 1959 (Dingle and Radok (1961)) and may be characteristic of the conditions at S2 in contrast to those at Wilkes.

3.1.7. Increase in drift density with wind speed (assuming w *constant)*

Figure 3.1 shows the almost linear increase in slope of the $\log z - \log n_z$ lines as the velocity increases. This is a result of w varying only slightly with wind speed, whereas u_* increases linearly. The figure also illustrates how an increase in velocity increases the drift density at the surface only slightly, whereas at high levels the density increases greatly. The effect of a wind velocity increase is to carry the drift higher and spread it more evenly along the vertical. This implies that, if V were to increase beyond limit, then the total drift *content* would increase beyond limit (for unlimited height) but the drift *density* would tend to a finite limit, its maximum value for the surface conditions at the time, i.e. n_{z_0}. This follows from equation (3.4) in the form

$$n_z = n_{z_0}\left(\frac{z}{z_0}\right)^{-\frac{w}{ku_*}} \tag{3.8}$$

and the fact that as u_* is proportional to V

$$n_z = n_{z_0}\left(\frac{z}{z_0}\right)^{-\frac{c}{V}} \tag{3.9}$$

where c is constant. Equation (3.8) shows that $n_z \to n_{z_0}$ as V becomes large.

3.1.8. Variation of n_{z_0} *with wind velocity*

Values of n_{z_0} have been obtained by the extrapolation of the $\log z - \log n_z$ relation, equation (3.4), down to z_0. Table 3.III shows the result of this calculation for the S2 data.

TABLE 3.III.

SURFACE DRIFT DENSITY (n_{z_0}) AS A FUNCTION OF WIND SPEED.

V_{10}	m/sec	13·4	16·1	17·2	19·1	21·0	24·6	27·2
n_{z_0}	10^2g/m^3	34·7	28·6	26·4	24·3	18·9	15·6	13·5

The values of n_{z_0} vary within each velocity range but the general trend is a *decrease* of n_{z_0} with wind velocity. This implies that on the average the surface supply of snow tends to be less for the higher wind speeds. Much of the present theory deals with the variation of the drift parameters with wind speed, on the assumption that the surface conditions remain constant. However, the S2 drift results indicate that it is more realistic to regard the supply of snow in general as decreasing with wind speed. The reason for this will be more clearly seen when the variation of drift *content* with wind speed is considered in the next section, 3.2.

3.1.9. Limiting drift density for strong winds

If n_{z_0} were to remain constant then it may be seen from equation (3.4), written in the form

$$n_z = n_{z_0} e^{-\frac{w}{ku_*} \ln \frac{z}{z_0}}, \tag{3.10}$$

that the drift density at any level would tend asymptotically towards n_{z_0} as the wind speed (and hence u_*) increases. The rate of the approach to n_{z_0} increases with height, so that the density at the lower levels changes only slightly with wind speed, while at higher levels it increases rapidly. This result has been illustrated by Figure 3 in the paper by Radok and Dingle (1961) by plotting log n_z against $\frac{1}{V_z}$ for various levels, obtaining approximate linear relationships with increasing slopes for higher levels.

However, as n_{z_0} for the S2 drift values was not constant, the plot log n_z against $\frac{1}{V}$ in Figure 3.3 showed marked deviation from the straight line. Therefore, in the present case the quantity $\log \frac{n_z}{n_{z_0}}$ has been plotted against reciprocal wind velocity $\frac{1}{V_{10}}$ in Figure 3.3a. This shows that the log drift densities at all levels approach one another as the wind increases. The figure shows the linear relation between $\log \frac{n_z}{n_{z1}}$ and $\frac{1}{V_{10}}$ to be closely realized and that the slopes of the lines for different levels (z) are proportional to $\log_e \frac{z}{z_1}$.

3.2. Drift content in the air

The total snow content Γ_{z_0-z} in the air from the surface (z_0) to height z for a particular run (constant wind speed, hence u_* constant) per unit area of the surface is given by

$$\Gamma_{z_0-z} = \int_{z_0}^{z} n_z \, dz = \int_{z_0}^{z} n_{z_0} \left(\frac{z}{z_0}\right)^{-\frac{w}{ku_*}} dz. \tag{3.11}$$

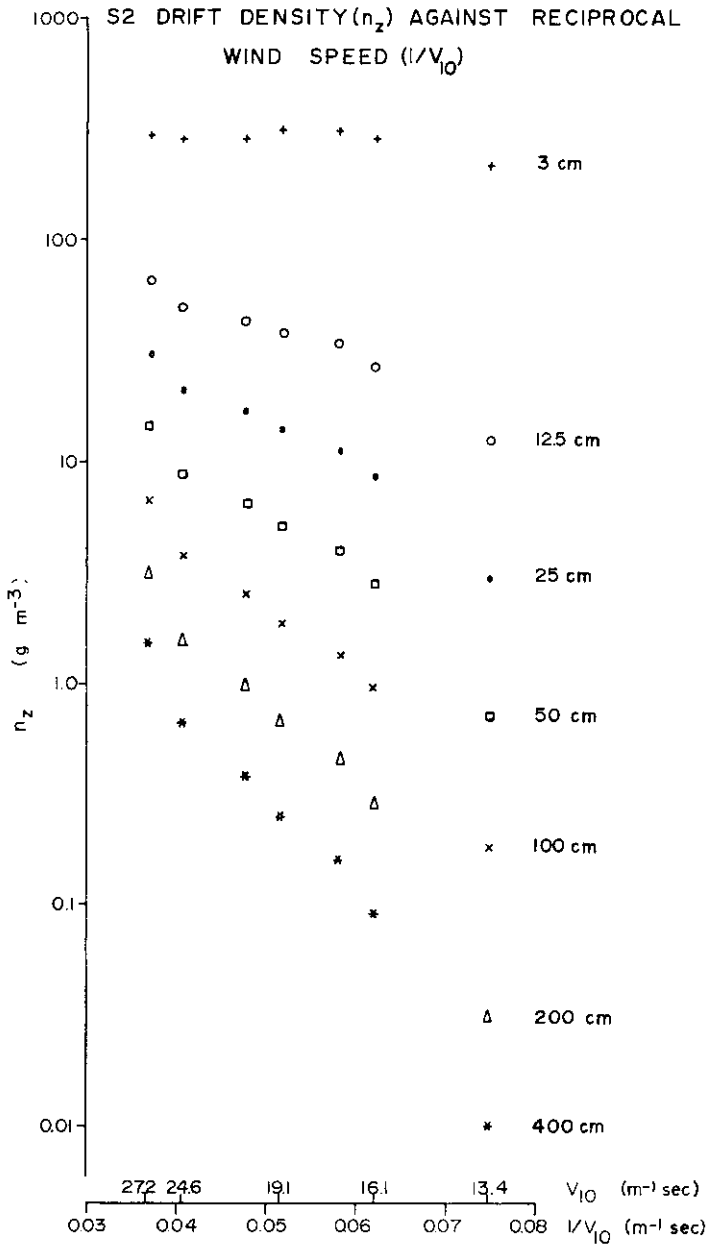

FIG. 3.3. LOG DRIFT DENSITY VERSUS RECIPROCAL WIND VELOCITY. From Table 3.I the log drift densities have been plotted against $1/V_{10}$, the reciprocal of the wind speed at the 10 m level, for each of the 6 heights from 12.5 to 400 cm, and also the 3 cm level. The slope of the regression lines for each level increases with the height above the surface. Extrapolating these lines for very high wind speeds gives maximum drift densities from about 20 g m^{-3} for the higher levels to 400 g m^{-3} for the low levels.

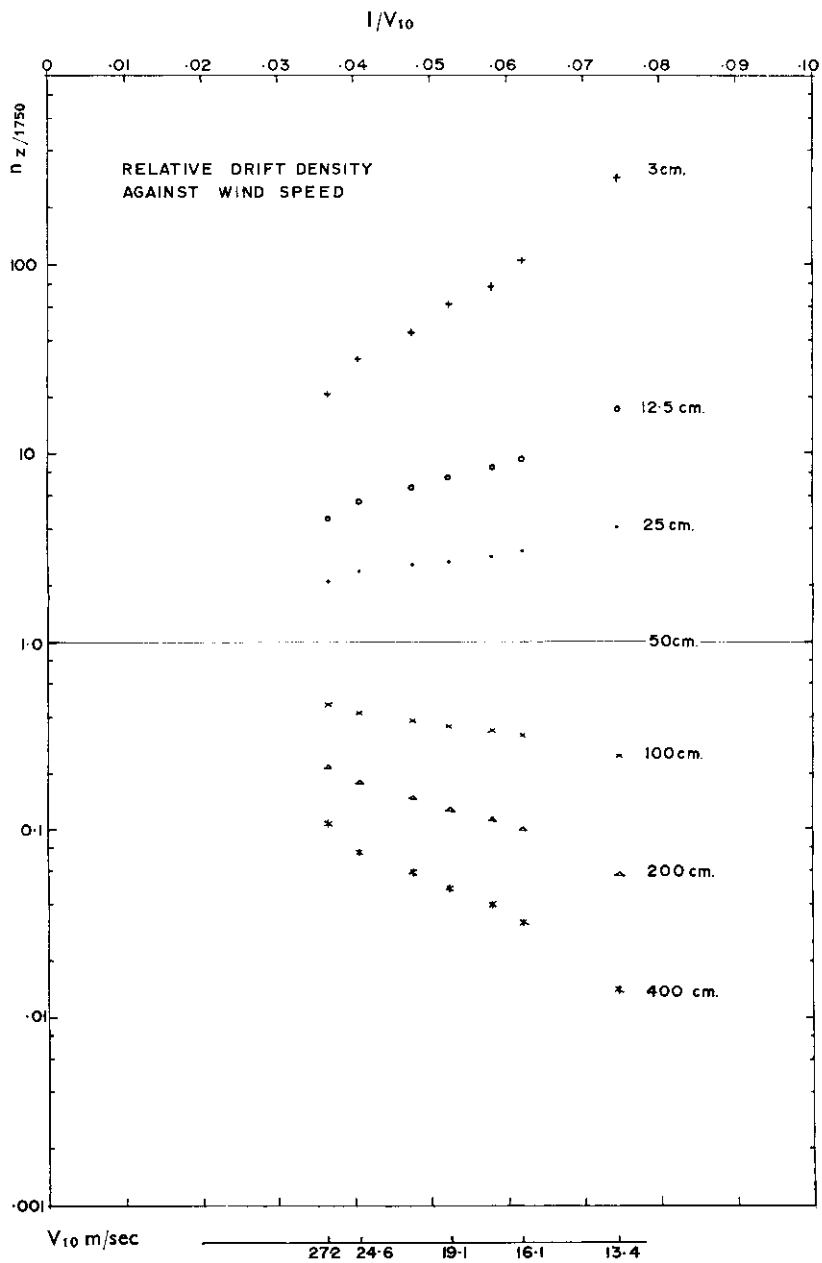

FIG. 3.3a. LOG DRIFT DENSITY RATIO VERSUS RECIPROCAL WIND SPEED. Using the ratio of the drift density at a level to that at a particular level (in this case the 50 cm level) gives straight line plots, on a log scale, against reciprocal wind velocity. This procedure eliminates the variability due to the change of snow supply at the surface which is present in Fig. 3.3.

The solution of this integral depends on the relative magnitudes of ku_* and w. Three cases must be distinguished:

(i) $ku_* < w$ (light to strong winds, $V_{10} < 28$ m/sec)

(ii) $ku_* = w$ (critical velocity $V_{10} = 28$ m/sec)

(iii) $ku_* > w$ (very strong winds)

(i) $ku_* < w$. In this case

$$\Gamma_{z_0-z} = \frac{z_0 n_{z_0}}{ku_* - w}\left(\frac{z}{z_0}\right)^{1-\frac{w}{ku_*}}\Bigg|_{z_0}^{z}$$

i.e.
$$\Gamma_{z_0-z} = \frac{ku_*}{w - ku_*}(z_0 n_{z_0} - z n_z). \tag{3.12}$$

Now the important result here is that for $ku_* < w$, $zn_z \to 0$ as $z \to \infty$ and so the expression for the total drift content reduces to

$$\Gamma_{z_0-z} = \frac{z_0 n_{z_0} ku_*}{w - ku_*}. \tag{3.13}$$

From this it can be seen that as the wind speed increases ($ku_* \to w$) the total drift content increases very rapidly provided the snow supply (n_{z_0}) remains constant. This is due to the great height to which the drift would be carried if equation (3.3) were to hold. In practice, however, this would be expected to break down at the level where the logarithmic wind profile loses its validity ($\sim$100 m at Wilkes, cf. Section 3.3 below), so that for high wind velocities the upper limit of the above integral for calculating total drift content will be taken as $z = 100$ m.

(ii) $ku_* = w$. In this case, for the content of drift between any two levels z_1 and z_2 we obtain

$$\Gamma_{z_1-z_2} = n_{z_0} z_0 \ln \frac{z_2}{z_1}. \tag{3.14}$$

This value of drift content increases indefinitely as z_2 increases and no longer converges to a finite value as in case (i).

(iii) $ku_* > w$. In this case we obtain

$$\Gamma_{z_0-z} = \frac{ku_*}{ku_* - w}(z n_z - z_0 n_{z_0}). \tag{3.15}$$

This value also increases indefinitely with height z. The drift content, however, does not increase indefinitely with wind speed (u_*). In fact,

$$\text{as } V \text{ or } u_* \to \infty, \frac{ku_*}{ku_* - w} \to 1, n_z \to n_{z_0} \text{ and } \Gamma_{z_0-z} \to n_{z_0}(z - z_0), \text{ so}$$

that the drift content tends to a finite limit as the wind speed increases if the snow supply at the surface remains constant. The rate of change of drift content with wind speed is proportional to

$$\frac{d\Gamma}{du_*} = \frac{n_{z_0} z_0 kw}{(w - ku_*)^2}. \tag{3.16}$$

Thus, the rate of increase of drift content of an infinite layer increases to a maximum at the critical value ($ku_* = w$) then decreases for greater wind speeds. This result becomes important when the effect of snow drift on accumulation is considered, for if the drift content increases, snow must be picked up from the surface, while if drift content decreases, snow must be deposited.

For the values obtained from the drift measurements at S2, ku_* was always less than w, and so the drift content was easily calculated for different wind speeds. These values are listed in Table 3.IV and plotted in Figure 3.4.

TABLE 3.IV.

DRIFT CONTENT, Γ, V. WIND SPEED, V.

V	m/sec	13·4	16·1	17·2	19·1	21·0	24·6	27·2
Γ_{z_0-100m}	g/m²	25·0	33·0	37·0	39·0	39·0	47·0	63·0

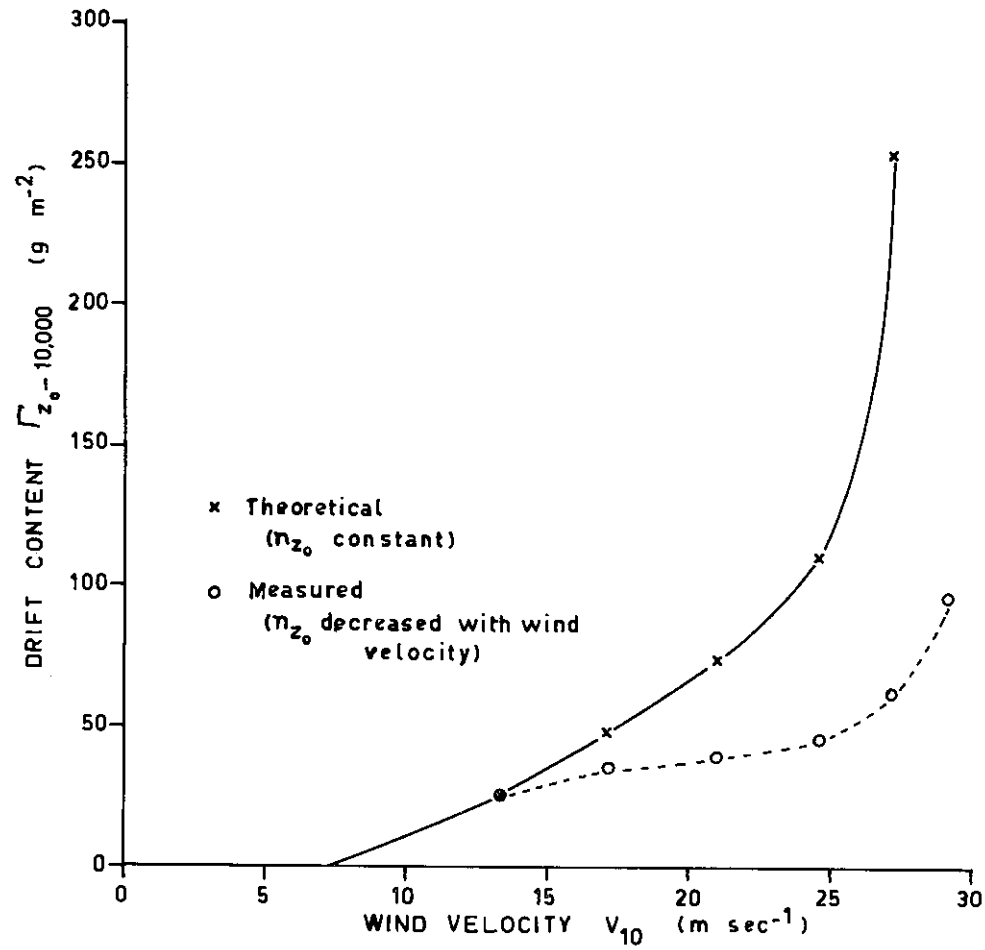

FIG. 3.4. DRIFT CONTENT VERSUS WIND SPEED. The two curves show the difference between the total content of snow in the air and that which would be there if the snow supply at the surface were maintained. In spite of the decrease of snow supply at the surface, the rapid increase in drift content is observed as V_{10} approaches 29 m sec^{-1} where $ku_* = w$.

The solution of this integral depends on the relative magnitudes of ku_* and w. Three cases must be distinguished:

(i) $ku_* < w$ (light to strong winds, $V_{10} < 28$ m/sec)

(ii) $ku_* = w$ (critical velocity $V_{10} = 28$ m/sec)

(iii) $ku_* > w$ (very strong winds)

(i) $ku_* < w$. In this case

$$\Gamma_{z_0-z} = \frac{z_0 n_{z_0}}{ku_* - w}\left(\frac{z}{z_0}\right)^{1-\frac{w}{ku_*}}\Bigg|_{z_0}^{z}$$

i.e.
$$\Gamma_{z_0-z} = \frac{ku_*}{w - ku_*}\cdot(z_0 n_{z_0} - z n_z). \tag{3.12}$$

Now the important result here is that for $ku_* < w$, $zn_z \to 0$ as $z \to \infty$ and so the expression for the total drift content reduces to

$$\Gamma_{z_0-z} = \frac{z_0 n_{z_0} ku_*}{w - ku_*}. \tag{3.13}$$

From this it can be seen that as the wind speed increases ($ku_* \to w$) the total drift content increases very rapidly provided the snow supply (n_{z_0}) remains constant. This is due to the great height to which the drift would be carried if equation (3.3) were to hold. In practice, however, this would be expected to break down at the level where the logarithmic wind profile loses its validity ($\sim$100 m at Wilkes, cf. Section 3.3 below), so that for high wind velocities the upper limit of the above integral for calculating total drift content will be taken as $z = 100$ m.

(ii) $ku_* = w$. In this case, for the content of drift between any two levels z_1 and z_2 we obtain

$$\Gamma_{z_1-z_2} = n_{z_0} z_0 \ln\frac{z_2}{z_1}. \tag{3.14}$$

This value of drift content increases indefinitely as z_2 increases and no longer converges to a finite value as in case (i).

(iii) $ku_* > w$. In this case we obtain

$$\Gamma_{z_0-z} = \frac{ku_*}{ku_* - w}(z n_z - z_0 n_{z_0}). \tag{3.15}$$

This value also increases indefinitely with height z. The drift content, however, does not increase indefinitely with wind speed (u_*). In fact,

$$\text{as } V \text{ or } u_* \to \infty,\ \frac{ku_*}{ku_* - w} \to 1,\ n_z \to n_{z_0} \text{ and } \Gamma_{z_0-z} \to n_{z_0}(z - z_0), \text{ so}$$

that the drift content tends to a finite limit as the wind speed increases if the snow supply at the surface remains constant. The rate of change of drift content with wind speed is proportional to

$$\frac{d\Gamma}{du_*} = \frac{n_{z_0} z_0 kw}{(w - ku_*)^2}. \tag{3.16}$$

Thus, the rate of increase of drift content of an infinite layer increases to a maximum at the critical value ($ku_* = w$) then decreases for greater wind speeds. This result becomes important when the effect of snow drift on accumulation is considered, for if the drift content increases, snow must be picked up from the surface, while if drift content decreases, snow must be deposited.

For the values obtained from the drift measurements at S2, ku_* was always less than w, and so the drift content was easily calculated for different wind speeds. These values are listed in Table 3.IV and plotted in Figure 3.4.

TABLE 3.IV.

DRIFT CONTENT, Γ, V. WIND SPEED, V.

V	m/sec	13·4	16·1	17·2	19·1	21·0	24·6	27·2
Γ_{z_0-100m}	g/m²	25·0	33·0	37·0	39·0	39·0	47·0	63·0

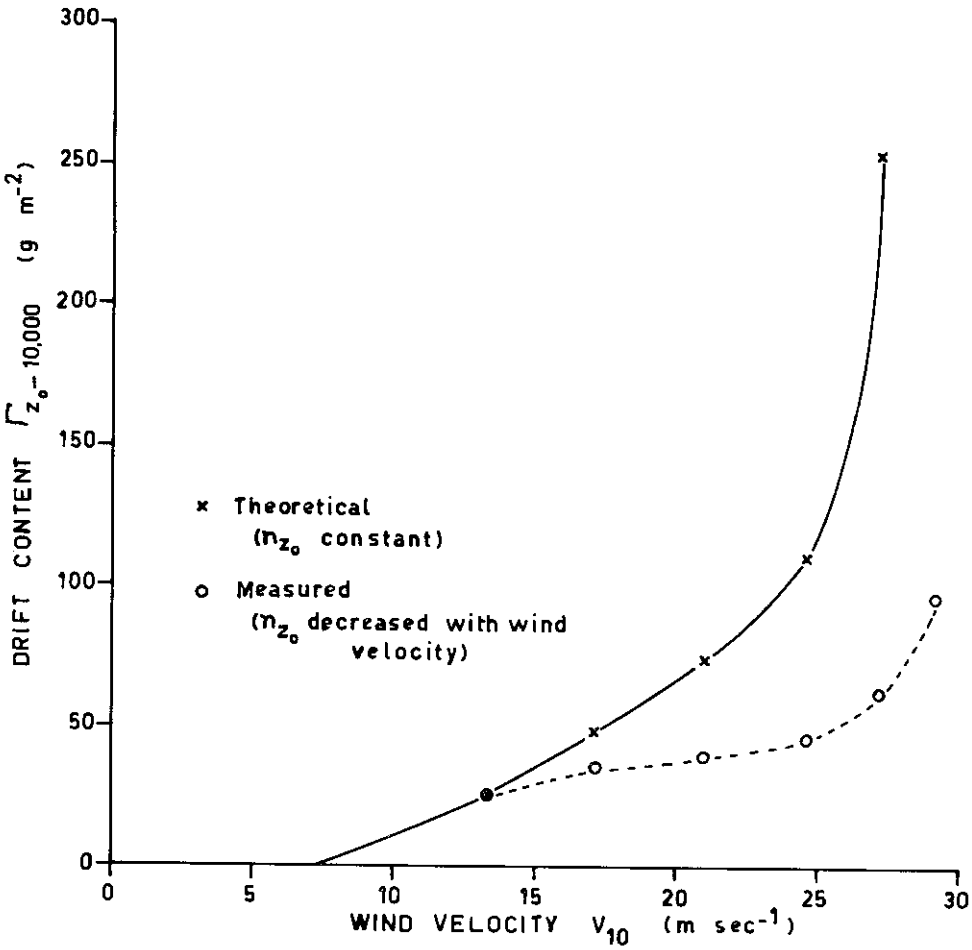

FIG. 3.4. DRIFT CONTENT VERSUS WIND SPEED. The two curves show the difference between the total content of snow in the air and that which would be there if the snow supply at the surface were maintained. In spite of the decrease of snow supply at the surface, the rapid increase in drift content is observed as V_{10} approaches 29 m sec^{-1} where $ku_* = w$.

Figure 3.4 also shows the theoretical increase of the infinite-layer drift content with wind for n_{z_0} constant. For high wind speeds this value of drift content increases very rapidly. In practice however, the snow supply at the surface does not stay constant and n_{z_0} actually decreases on the average with wind speed and consequently the measured values of drift content are lower. The rate of increase of drift content with wind speed still shows the expected increase as $ku_* \to w(V_{10} \to 28$ m/sec).

3.3 DRIFT TRANSPORT

To obtain the amount of snow removed by the wind we require the total drift transport for any given wind profile. The drift transport is defined as the mass of snow flowing across unit length, perpendicular to the wind velocity, per unit time, that is to say, the drift transport is given by

$$Q_z = \int n_z V_z \, dz \tag{3.17}$$

over the appropriate height range, provided the wind retains the same direction over that height range (cf. Dingle and Radok (1961)).

$$n_z V_z = n_{z_1} \frac{u_*}{k} \left(\frac{1}{z_1}\right)^{-\frac{w}{ku_*}} z^{-\frac{w}{ku_*}} \log \frac{z}{z_0} = cz^{-a} \ln \frac{z}{z_0},$$

say, where

$$c = n_{z_1} \frac{u_*}{k} \left(\frac{1}{z_1}\right)^{-\frac{w}{ku_*}}$$

and

$$a = \frac{w}{ku_*}$$

and, therefore, for $a \neq 1$

$$Q_z = c \frac{1}{-a+1} z^{-a+1} \left(\ln \frac{z}{z_0} - \frac{1}{-a+1}\right);$$

substituting for a and c gives

$$Q_z = \frac{n_{z_1}}{1 - \frac{w}{ku_*}} z \left(\frac{z}{z_1}\right)^{-\frac{w}{ku_*}} \frac{u_*}{k} \left(\ln \frac{z}{z_0} - \frac{1}{1 - \frac{w}{ku_*}}\right) \tag{3.18}$$

or, expressing this in the form used by Dingle and Radok (1961),

$$Q_z = \left(1 - \frac{w}{ku_*}\right)^{-1} z n_z \left(V_z - \frac{u_*}{k}\left(1 - \frac{w}{ku_*}\right)^{-1}\right). \tag{3.19}$$

We now need to consider the limits of z over which the integration is to be taken. At the surface, z_0, we have from (3.19)

$$Q_{z_0} = z_0 n_{z_0} \frac{ku_*^3}{(w - ku_*)^2}. \tag{3.20}$$

For the upper limit we note

$$Q_\infty = \lim_{z\to\infty} Kz^{1-\frac{w}{ku_*}}\left(\ln\frac{z}{z_0} - \frac{1}{1-\frac{w}{ku_*}}\right), \tag{3.21}$$

where $K = \dfrac{n_{z_1}}{1-\dfrac{w}{ku_*}}\, z_1^{\frac{w}{ku_*}}\dfrac{u_*}{k}$ is independent of z.

Now $\lim_{z\to\infty} z^a \ln z = 0$ for $\log a < 0$, i.e. $\dfrac{w}{ku_*} < 1$ and therefore for $ku_* < w$, $Q_\infty = 0$. Hence Q_z is the total drift transport (from z to ∞) above z, and converges to a finite value for $ku_* < w$, i.e. $V_{10} < 28$ m/sec for the S2 data.

In order to study how drift transport varies with wind velocity we note that

$$Q_z = zn_z\left(\frac{ku_*^3}{(w-ku_*)^2} + \frac{u_*^2}{w-ku_*}\ln\frac{z}{z_0}\right) \tag{3.22}$$

and recall that u_* is proportional to the wind velocity at a given level.

In particular, until the wind velocity becomes very strong the total drift transport converges and is given by

$$Q_{z_0} = z_0 n_{z_0}\frac{ku_*^3}{(w-ku_*)^2}.$$

For n_{z_0} remaining constant with wind speed (on the average) this last result shows that the total drift transport increases very rapidly with wind speed, especially as ku_* approaches w. This is mainly because the drift *content* becomes very large under these conditions.

To see how the drift transport increases for higher velocities we note that

$$Q_{z_0} - Q_{z_1} = \frac{ku_*^3}{(w-ku_*)^2}(z_0 n_{z_0} - n_{z_1}z_1) - \frac{u_*^2}{w-ku_*}\left(n_{z_1}z_1\ln\frac{z_1}{z_0}\right) \tag{3.23}$$

gives the drift transport up to level z_1. This level z_1 will be taken as the height at which the log wind profile breaks down. From a set of 32 detailed radiosonde wind measurements in the lowest kilometer made at Wilkes from 1959 to 1961 it appears that, for the stronger winds at Wilkes, the logarithmic profile holds well to about 100 m after which u_* may remain zero to 500 m or even turn negative. Hence in absence of further information on how the drift varies at greater heights the calculations of drift transport have been taken to 100 m.

For S2 the drift transport values for different velocity ranges are listed in Table 3.V. These values are somewhat lower than the drift transport values given by Dingle and Radok (1961) and by Mellor and Radok (1960). This follows from the result that the drift density values were lower for the S2 data, especially at the higher levels. This becomes even more accentuated when the drift densities are extrapolated to 100 or 300 m.

TABLE 3.V.

DRIFT TRANSPORT g cm^{-1} sec^{-1} BETWEEN VARIOUS LEVELS (z cm) FOR INCREASING WIND SPEEDS (V_{10} m/sec) AT S2.

z / V_{10}	0·75	3	12·5	400	10,000	30,000
13·4	0·36	0·16	0·10	0·005	0·0002	
16·1	0·56	0·19	0·30	0·06	0·008	
17·2	0·24	0·46	0·66	0·17	0·02	
19·1	0·33	0·58	0·88	0·33	0·05	
21·0	0·37	0·48	1·4	0·63	0·13	
24·6	0·44	0·63	2·5	1·6	0·19	
27·2	0·70	1·20	3·6	3·8	1·1	

From equation (3.23) it can be seen that, as the wind velocity increases, the drift transport increases more and more rapidly until $ku_* = w$ for which direct integration of equation (3.17) gives

$$Q_{z_1} - Q_{z_0} = z_0 n_{z_0} \frac{w}{2k^2} \ln^2 \frac{z_1}{z_0}. \tag{3.24}$$

For still higher velocities we note from equation (3.23) that as V_{10} or u_* becomes large

$$Q_{z_0} - Q_{z_1} \to \frac{u_*}{k} n_{z_0} z_1 \left(\ln \frac{z_1}{z_0} - 1 + \frac{z_0}{z_1} \right), \tag{3.25}$$

a value which increases linearly with wind speed. This gives a drift transport wind relation, below a given level, the general form of which is shown in Figure 3.5a. Thus, for snow supply (n_{z_0}) constant, the drift transport increases with wind speed, with the rate of increase tending to a limit that depends on the height of the upper boundary of the drift layer.

For the S2 results the highest velocity range was 27·2 m/sec, and ku_* became equal to w when V_{10} was about 28 m/sec, so that only the first part of Figure 3.5a has been verified.

The results of the drift transport calculation from the S2 data are given in Table 3.VI showing how the drift transport below different levels increases with wind speed. These values are plotted in Figure 3.5 and show close agreement with the first part of the curve of Figure 3.5a.

TABLE 3.VI.

S2 DRIFT TRANSPORT Q_{z_0-z}(g/cm/sec) v. WIND SPEED V_{10}(m/sec).

V_{10} / z	13·4	16·1	17·2	19·1	21·0	24·6	27·2
12·5 cm	0·52	0·75	0·70	0·91	0·85	1·07	1·90
400 cm	0·62	1·06	1·36	1·8	2·2	3·6	5·5
100 m	0·63	1·12	1·53	2·1	2·9	5·2	9·3
300 m	0·63	1·13	1·55	2·2	3·0	5·4	10·4

These total drift transport figures are lower than the values obtained (Dingle and Radok (1960)) for Wilkes for corresponding velocities, as expected from the

results for individual levels (Table 3.V). Values of total drift transport rate reported by various workers for different parts of the Antarctic are listed in Table 3.VII. The large variation between the results of the various authors seems to be due, firstly, to the different types of gauges used and, secondly, to the lack of information concerning the drift density at the high levels (above 10 m).

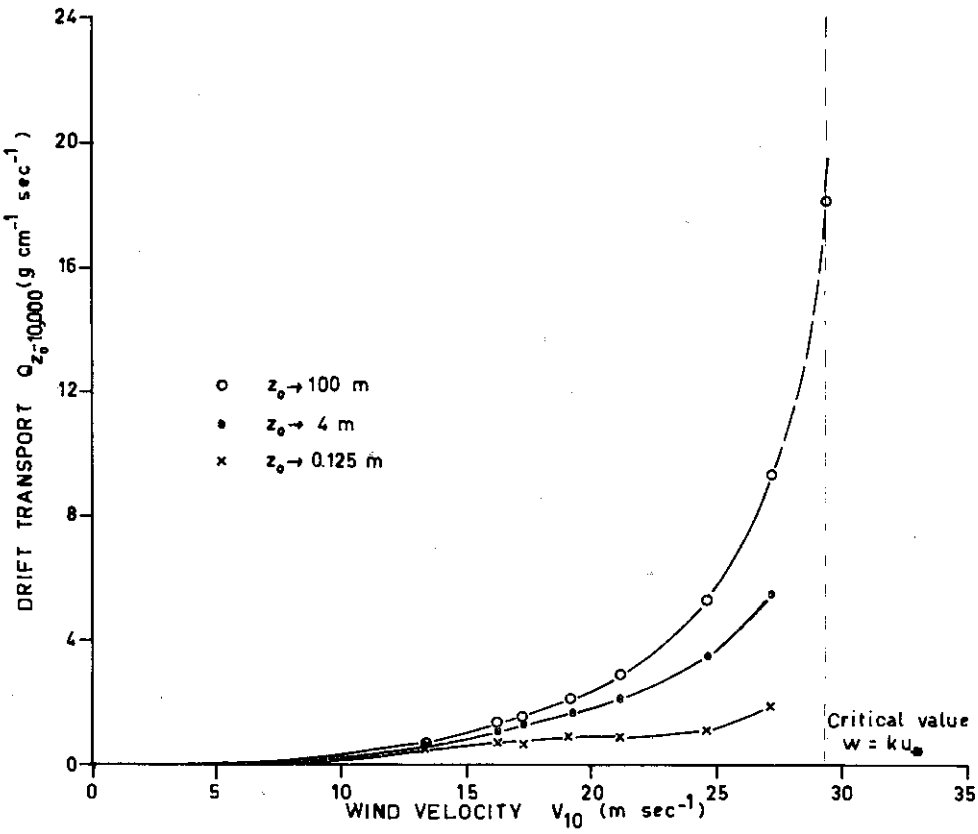

FIG. 3.5. S2 DRIFT TRANSPORT VERSUS WIND SPEED. The drift transport for various wind speeds has been calculated from the drift density and wind speed measurements extrapolated to 100 m. The results show general agreement to the expected form, as shown schematically in Fig. 3.5a, but the wind speed range does not extend far enough to verify the remainder of the schematic diagram for high winds.

The drift transport between the lower levels z_0 to 3 cm and 3 cm to 12·5 cm varies only slightly with wind speed (i.e. on the average, or assuming local conditions constant). This is because the drift density at these levels varies insignificantly with the 10 m wind speed V_{10}, and also because the wind speed itself only varies slightly at these low levels.

For higher levels the drift transport increases very rapidly with wind speed. This is, firstly, because the drift density increases more rapidly with wind for the higher levels and, secondly, because a larger V_{10} corresponds to an even greater wind

velocity at the higher levels in the logarithmic wind profile. A third point is that the height above which there is negligible drift increases with velocity until a substantial proportion of the snow reaches 100 m (cf. Fig. 3.6).

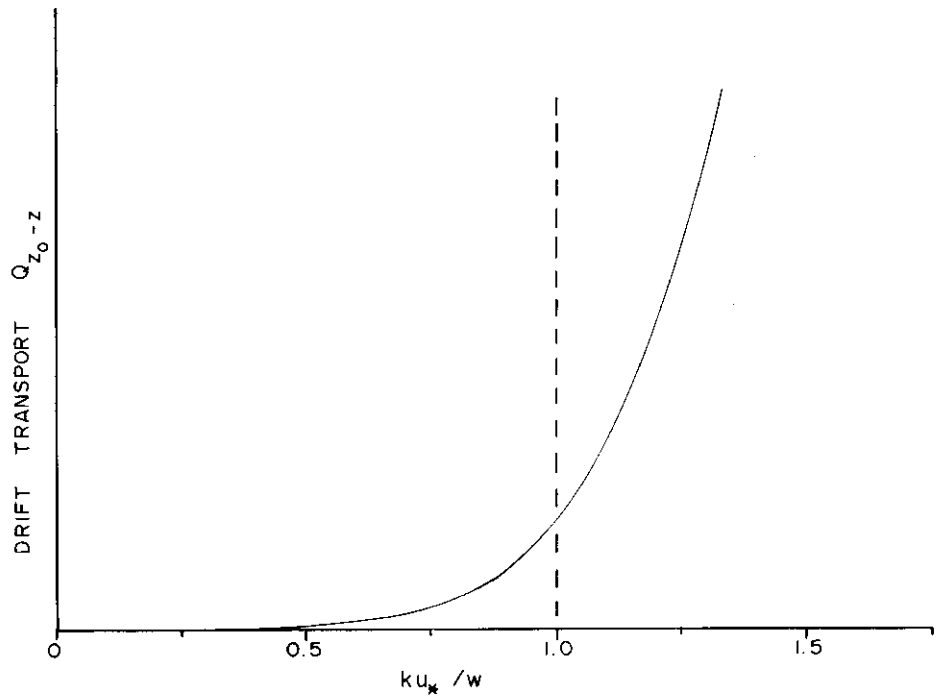

FIG. 3.5a. DRIFT TRANSPORT VERSUS WIND SPEED (SCHEMATIC). The general form of the drift transport wind relation is shown for the height range $z = z_0$ to 100 m, assuming snow supply at the surface (n_{z0}) as constant. The horizontal scale is in units of ku_*/w with the vertical line drawn for $ku_* = w(V_{10} \sim 29$ m sec^{-1} for S2 data). For higher winds the slope of the curve still increases, showing the great effect the high winds have on the transport of drift.

3.3.1. Loss of snow by drift

Having found how drift transport varies in general with wind, the potential amount of snow which blows past S2 has been calculated from the distribution of the wind speeds as measured at S2 over the 11-month period March 1957 to February 1958.

This is listed in Table 3.VIII, together with a similar calculation of the potential drift snow blowing past Wilkes. The calculation assumes that the supply of snow has kept up. At Wilkes this may be particularly in error because a large part of the surface is blue ice and often, after the surface snow is removed, strong winds are experienced carrying very little drift. Neglecting this complication the result of the annual drift transport for Wilkes provides an estimate for the loss of snow by wind across the coasline. (The wind direction here is approximately perpendicular to the coastline.) Table 3.IX shows the estimated annual loss of snow by drift across the coastline obtained from a variety of sources.

TABLE 3.VII.

DRIFT TRANSPORT RATES QUOTED FOR PARTS OF ANTARTICA.

Location	Drift Transport Q g cm^{-1} sec^{-1}	Wind Speed V m sec^{-1}	Source
Wilkes	94	28	Dingle & Radok (1961)
	580	36	
Mawson	156	28	Mellor & Radok (1960)
Port Martin	28	36	Loewe (1956)
South Ice	0·08	10·3	Lister (1960)
	0·5	15·5	
	3·6	20·6	
Dumont D'Urville	0·02	10·3	Lorius (1962)
	0·32	16·2	

TABLE 3.VIII.

ANNUAL SNOW TRANSPORT, WILKES AND S2.

Wind Speed m sec^{-1} daily mean	Frequency days yr^{-1}		Transport Rate g cm^{-1} sec^{-1}	g cm^{-1} day^{-1}	Annual Transport g cm^{-1} yr^{-1} × 10^6	
	Wilkes	S2			Wilkes	S2
0	0	0	0·00	0·00	0	0
2	99·8	16·7	0·00	0·00	0	0
4	76·8	32·8	0·01	$8{\cdot}64 \times 10^2$	0·06	0·03
6	50·7	45·3	0·04	$3{\cdot}46 \times 10^3$	0·17	0·16
8	34·7	49·3	0·10	$8{\cdot}64 \times 10^3$	0·30	0·42
10	24·1	48·4	0·15	$1{\cdot}30 \times 10^4$	0·31	0·63
12	16·4	41·8	0·50	$4{\cdot}32 \times 10^4$	0·71	1·81
14	13·2	33·8	0·75	$6{\cdot}48 \times 10^4$	0·86	2·19
16	10·7	26·5	1·08	$9{\cdot}33 \times 10^4$	1·00	2·47
18	8·6	20·3	1·74	$1{\cdot}50 \times 10^5$	1·29	3·05
20	7·1	15·0	2·48	$2{\cdot}14 \times 10^5$	1·52	3·21
22	5·9	10·9	8·40	$2{\cdot}94 \times 10^5$	1·73	3·20
24	4·9	8·0	4·68	$4{\cdot}04 \times 10^5$	1·98	3·24
26	4·0	5·8	6·65	$5{\cdot}75 \times 10^5$	2·30	3·33
28	3·1	4·2	10·80	$9{\cdot}33 \times 10^5$	2·89	3·92
30	2·4	3·0	13·0	$1{\cdot}12 \times 10^6$	2·70	3·37
32	1·7	2·1	14·2	$1{\cdot}23 \times 10^6$	2·09	2·58
34	0·7	1·4	15·1	$1{\cdot}30 \times 10^6$	0·91	1·83
	365	365	Total		20·8	34·5

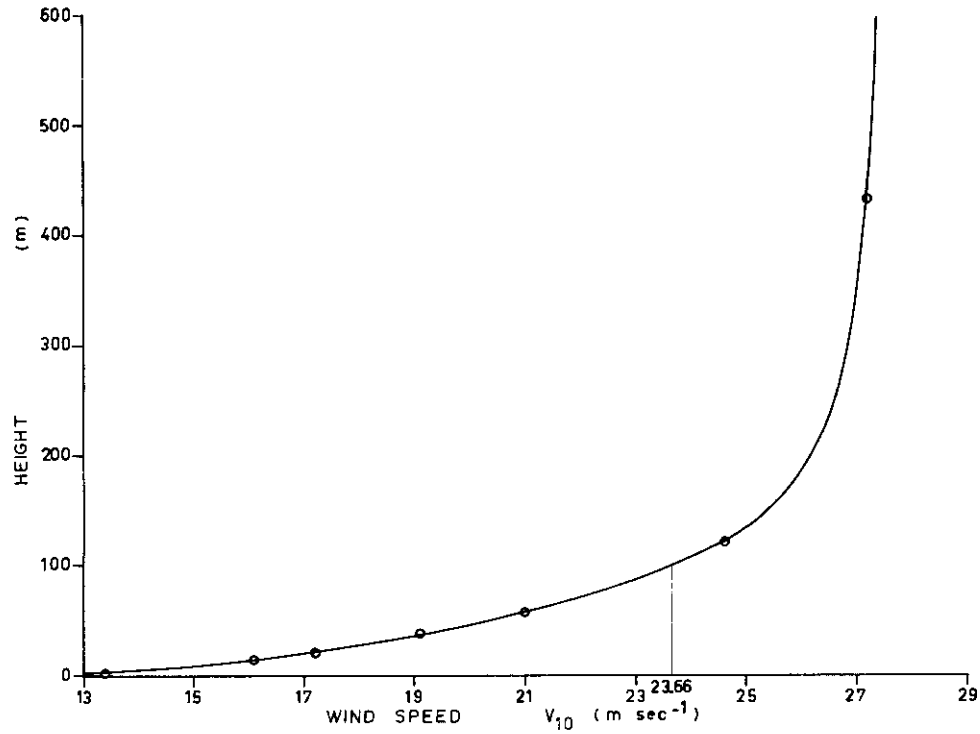

FIG. 3.6. VERTICAL TRANSPORT OF SNOW DRIFT. The height to which the drift is spread by increasing wind speed is illustrated by the height at which the drift density is less than a certain value, here 0.01 g m^{-3} (the lowest density measured), plotted against wind speed. As $ku_* \rightarrow w$ this height increases rapidly (theoretically tending to infinity if the wind profile stayed logarithmic). The drift density reaches this value at the 100 m level (the average height at which the log wind profile broke down) when $V_{10} \approx 24$ m sec^{-1}.

TABLE 3.IX.

LOSS OF SNOW ACROSS THE ANTARTIC COASTLINE BY DRIFT.

Location	Drift Transport gm cm^{-1} yr^{-1} × 10^7	Mean Wind Speed m sec^{-1}	Source
S2	3·4	10·7	Budd
Wilkes	2·1	5·5	Budd
Terre Adélie	18	18	Loewe (1956)
Mawson	15	10·7	Mellor (1958)
South Ice	1·5	11·1	Lister (1960)
Mirny	1·5	11·6	Kotlyakov (1961)
Mirny	3·85	(11)	Shchepilov (1963)

The amount of snow blowing past S2 is not directly related to the amount of snow removed from S2 but rather a measure of the amount of drift transported from further inland. It is expected that erosion would occur with accelerating winds, and deposition with decelerating winds. Because of the general topographic features of the Wilkes–S2 area it is possible to define a region from which the drift could come and the direction in which it would go. It appears that snow will be removed from the high dome region of the Budd coast and be transported downwind, across the coast into Vincennes Bay, cf. map, Figure 0.3.

An estimate may be made of the average ablation over the area caused by drift. Consider a sector from the dome to the coast (radius $r = 100$ km). If q gm cm^{-1} yr^{-1} is the rate of snow loss, and l the length of coastline, then the total loss is given by

$$Q = lq. \tag{3.26}$$

Now if the sector has angle θ, then

$$l = r\theta \tag{3.27}$$

and the area is given by

$$A = \tfrac{1}{2}r^2\theta. \tag{3.28}$$

Hence the average ablation over the area is given by

$$a = \frac{r\theta q}{\frac{1}{2}r^2\theta}. \tag{3.29}$$

Substituting for r from above and q from Table 3.VIII yields

$$a = \frac{2q}{r} = \frac{2 \times 2{\cdot}1 \times 10^7}{100 \times 10^5} \doteq 4 \text{ g cm}^{-2},$$

a result which is not too unrealistic for the region considered.

3.4. SNOW DRIFT AND ACCUMULATION

The rate at which snow is picked up or deposited, if the velocity gradually changes so that steady conditions are maintained, may be calculated from the way the drift content varies with u_*. We restrict discussion to winds such that $ku_* < w$ (i.e. $V_{10} < 28$ m/sec) which will include most of the relevant conditions.
From equation (3.13)

$$\Gamma = \frac{n_{z_0} z_0 k u_*}{w - k u_*}$$

$$\frac{d\Gamma}{du_*} = \frac{z_0 n_{z_0} k w}{(w - k u_*)^2}. \tag{3.30}$$

Now, if it is known how the wind speed varies with topography or slope (α), then, provided this variation is sufficiently slow to maintain steady saturated conditions,

$$\frac{d\Gamma}{d\alpha} = \frac{z_0 n_{z_0} k w}{(w - k u_*)^2} \frac{du_*}{d\alpha}. \tag{3.31}$$

For uniform katabatic flow typical for an Antarctic ice cap, Ball (1960) has derived the relation

$$V^3 = \frac{Qg^*\alpha}{k}, \tag{3.32}$$

where Q = rate of volume flow of air,
g^* = modified gravitational acceleration,
α = surface slope,
k = friction constant,
V = wind speed.

Considering a stream of wind from the centre of the dome region to the coast, the plateau accumulation should be related to $\frac{d\Gamma}{dx}$ where x is the distance from the centre.

From this the variation in accumulation may be expected to follow variation in slope. In the high region beyond S2 the accumulation is small. From S2 to about 20 km inland the slope has very little change and the accumulation is approximately constant. From here to the coast the slope increases very rapidly and the accumulation rate decreases. This is expected from the acceleration of the wind with increased slope.

From the daily wind speed frequency distributions for S2 and for Wilkes (cf. Climatology section, Fig. 1.4), it can be seen that the wind speed is in general greater at S2. Because of this it is presumed that a channelling of the winds occurs from the S2 trail to the south into the low region of the Vanderford Glacier. Hence, in order to calculate the amount of snow removed along the S2 trail, it would be necessary to have much more data on the variation in the wind speed between S2 and Wilkes.

In absence of further data the effect of the varying slope on the wind speed and drift, and hence on the resulting accumulation, may be studied by considering the effect of the acceleration of a typical inland katabatic along the trail. For a typical inland katabatic on a slope of 10^{-2}, Ball (1960, p. 12) takes a wind speed of 15 m/sec. This wind speed will be used here for illustration.

Now, since the average wind speed actually decreases from S2 to Wilkes, the effect of the change in drift content with slope along the S2 trail will be considered for a 15 m/sec wind velocity all along the trail. The acceleration will be assumed to effect only the component of the wind perpendicular to the S2 trail, so that the wind speed along the trail remains constant at 15 m/sec. In order to obtain the change in drift content along the trail due to the acceleration of the wind we note

$$\frac{d\Gamma}{dx} = \frac{d\Gamma}{dV} \cdot \frac{dV}{d\alpha} \cdot \frac{d\alpha}{dx}, \tag{3.33}$$

where α is the slope of the plateau surface at distance x from the centre dome. Now $\frac{d\Gamma}{du_*}$ has already been obtained and, as u_* may be taken to be a linear function of V, $\frac{d\Gamma}{dV}$ is easily calculated. $\frac{dV}{d\alpha}$, as a function of α, and $\frac{d\alpha}{dx}$ along the S2 trail have been

obtained graphically from the S2 trail height profile. From these the values of $\frac{d\Gamma}{dx}$ have been calculated in Table 3.X.

Now the time taken for a 15 m/sec wind to travel from the centre dome to Wilkes is 0·089 days. Hence these changes in Γ with distance x would correspond to changes in accumulation along the route over this time (0·089 days). To obtain an estimate of the corresponding change per year we multiply by the number of times a 15 m/sec wind would need to travel from centre to coast in a year to give the mean of the annual wind totals at Wilkes and S2. This amounts to about 2,000 times. Hence the annual change in the accumulation rate along the S2 trail due to drift may be obtained from the $\frac{d\Gamma}{dx}$ values above by multiplying by 2,000.

TABLE 3.X.

ESTIMATED VARIATION OF DRIFT CONTENT ALONG THE S2-WILKES TRAIL.

x km	α	$\frac{d\Gamma}{dV}$ g m^{-2}/m sec^{-1} (V = 15m/sec)	$\frac{dV}{d\alpha}$ m sec^{-1}	$\frac{d\alpha}{dx}$ km^{-1}	$\frac{d\Gamma}{dx}$ g m^{-2} km^{-1}	$\frac{d\Gamma}{dx}$/yr g cm^{-2} km^{-1} yr^{-1}
0	0·001	0·46	$17{\cdot}6 \times 10^{2}$	$1{\cdot}6 \times 10^{-3}$	1·3	0·26
10	0·009		$6{\cdot}0 \times 10^{2}$	$2{\cdot}0 \times 10^{-4}$	0·54	0·11
20	0·010		$5{\cdot}7 \times 10^{2}$	$2{\cdot}5 \times 10^{-5}$	0·065	0·013
30	0·010		$5{\cdot}7 \times 10^{2}$	0·0	0·000	0·000
40	0·010		$5{\cdot}7 \times 10^{2}$	$1{\cdot}3 \times 10^{-5}$	0·032	0·006
50	0·010		$5{\cdot}7 \times 10^{2}$	$2{\cdot}5 \times 10^{-5}$	0·065	0·013
60	0·011		$5{\cdot}4 \times 10^{2}$	$5{\cdot}8 \times 10^{-5}$	0·14	0·027
70	0·012		$5{\cdot}2 \times 10^{2}$	$1{\cdot}3 \times 10^{-4}$	0·31	0·062
80	0·014		$4{\cdot}8 \times 10^{2}$	$3{\cdot}5 \times 10^{-4}$	0·77	0·15
90	0·023		$3{\cdot}7 \times 10^{2}$	$1{\cdot}15 \times 10^{-3}$	1·98	0·40
100	0·044		$2{\cdot}7 \times 10^{2}$	$2{\cdot}7 \times 10^{-3}$	3·3	0·66

Using these values of $\frac{d\Gamma}{dx}$ the accumulation rates along the route may be calculated in terms of the accumulation rate at one position. The most reliable accumulation rate to use would be the value found for the S2 station grid (over an area of 12 sq km) of 14·2 g cm^{-2} yr^{-1} (cf. Section 4.3.3). Anticipating the results of Section 4.3.2, the theoretical and actual accumulation rates for the profile are listed in Table 3.XI and are plotted in Figure 3.7.

The variability among the actual accumulation results is high. This is largely because there is only one accumulation stake per five miles along the profile and because the accumulation value at each of these stakes is dependent not only upon the distance from the coast but also on the minor topographical features of the position of the stake. However, the general trend of the accumulation pattern seems to follow that of the theoretical. This general trend is for little change in accumulation rate between S2 and about 30 km from the coast because the change in slope over this section is slight. However, further inland and at the coast the slope changes are greater and so is the change in accumulation rate. Furthermore, the magnitude of the calculated losses is quite compatible with the changes actually occurring.

In order to obtain a more exact relationship between snow drift and resulting accumulation it would be necessary to know the wind speeds in greater detail, the effect of sublimation along the trail, and a more detailed accumulation profile between

TABLE 3.XI.

SNOW DRIFT, ACCUMULATION AND TOPOGRAPHY.

					S2									
Distance from Centre Dome	km	5	15	25	35	45	55		65	75	85		95	105
Accumulation (calculated)	g cm^{-2} yr^{-1}	10·4	13·0	14·1	14·2	14·1	14·0		13·7	13·1	11·6		7·6	1·0
Distance from Centre Dome	km				35	43	51	59	67	75	83	91	99	107
Distance along southern trail	km	24	16	8										
Accumulation (measured)	g cm^{-2} yr^{-1}	6·0	4·0	14·0	14·2	8·3	12·3	10·9	12·0	9·6	11·6	9·4	7·3	0

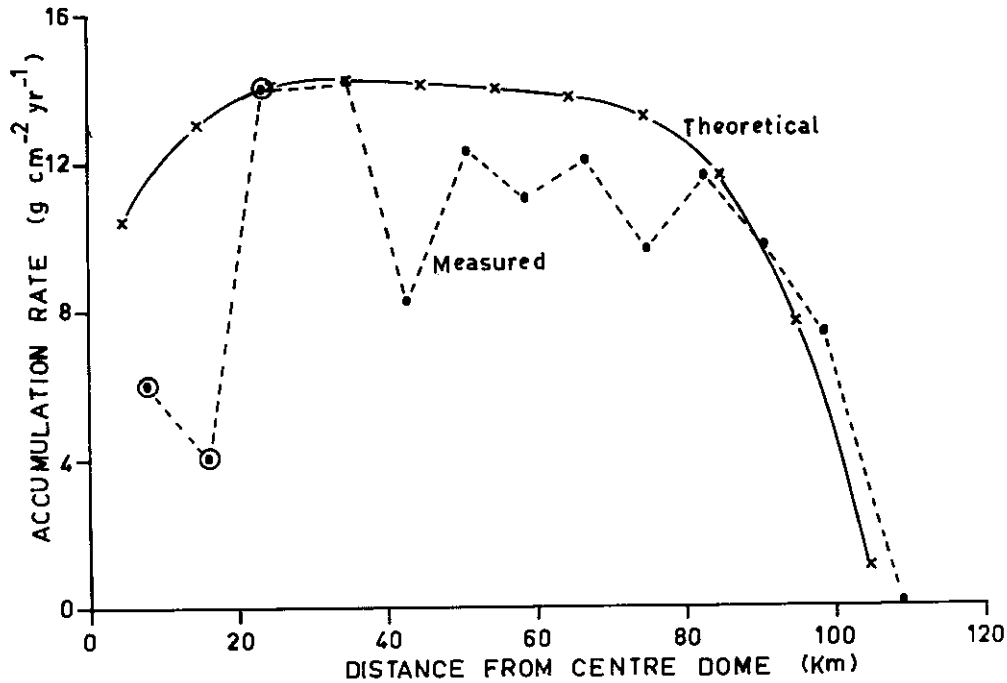

FIG. 3.7. ACCUMULATION OVER WILKES ICE CAP. The ablation of snow due to snow drift has been calculated over the Wilkes dome and has then been localised to the net accumulation rate at S2 to give the corresponding accumulation rates over the rest of the dome. The scatter in the measured values is believed to be largely due to minor topographical irregularities at the stake positions, not considered in the theoretical calculations.

Wilkes and S2. Then, by using the theoretical variation in drift with wind and slope, the amount of snow removed could be calculated for the whole wind speed distribution rather than just the typical 15 m/sec value taken here. Accumulation measurements to be taken further inland over the dome during 1963 should supply the data necessary to test the predicted results.

4. SNOW ACCUMULATION

4.0. INTRODUCTION

With the stake networks set up over the I.G.Y. period by the U.S. glaciological parties in the Wilkes region (cf. Hollin and Cameron (1961), members of the Australian National Antartic Research Expeditions have continued accumulation stake measurements to 80 km inland on the plateau (latitude 66° 31′) and extended them south 480 km (to latitude 71°). This section analyses the results of these stake measurements, supplemented by pit data and surface observations, to supply a comperhensive account of the accumulation in this region, how it builds up during the year, how it varies from year to year, and how it is affected by topography.

4.1. PLATEAU TOPOGRAPHY

Wilkes is situated on a rock peninsular, 10 m elevation, at 66° 15·5′S, 110° 31·5′E (cf. map, Fig. 0·3). From Figure 4.4 it can be seen that the ice plateau rises steeply at first then more gradually further inland to the satellite station, S2, situated 80 km ESE of Wilkes at an elevation approximately 1166 m, latitude 66° 31′S, longitude 112° 12′E.

South of S2 the ice cap continues to rise to about 1230 m, 29 km south, then falls to 880 m by 90 km south. From here the plateau rises gradually less steeply to 2990 m by 480 km south of S2, latitude 71°. Plateau slopes measured in 1961 and further elevations obtained in March 1962 indicate that the Budd Coast has a high region with centre dome over 1500 m elevation at about 66° 33′S, 113°E.

To the south of this high region a low region less than 900 m elevation extends from the Totten Glacier to the Vanderford and John Quincy Adams Glaciers. Seismic soundings indicate bedrock surface reaching 3200 m below sea level in this region (Jewell (1962)). It will be seen that this topographical depression has a marked influence on the accumulation in the region.

4.2. STAKE SYSTEMS AND MEASUREMENTS

4.2.1. Wilkes local area

In November 1957 a set of more than 35 stakes was placed from the rock peninsular coast, up over the steep ice ramp to about 13 km inland on the plateau, elevation 380 m (Cameron *et al.* (1959)). The positions of these stakes are shown in the 'Northern Area' map of Figure 0.4. Except for several stakes which melted out in the summer months and had to be replaced, this stake system has been measured continually to 1962. In 1959 the accumulation stakes were hollow or of split bamboo. These tended to bend or break in strong winds and therefore were gradually replaced by solid cane stakes 2·5 cm in diameter. All these new stakes were painted white. This was found to greatly reduce melt water around the stakes in summer.

Although the relative change in plateau surface has been recorded on this stake system since 1957, the variation in net accumulation is difficult to determine precisely because of the extensive metamorphosis taking place at the surface. This metamorphosis has been described in detail by Hollin *et al.* (1961, pp. 194–5). Not only does the relative height of the firn surface change but, also, the density of the snow at and near the surface changes due to such processes as wind-packing, melting, refreezing, ice formation and crystal growth. Hence, in order to determine the net water equivalent accumulation, it would be necessary to keep a stratigraphic and density record for each stake throughout the year.

As this was impracticable the procedure adopted for 1960 and 1961 was to measure the height of the stake relative to both the surface and the top of the ice layer and record the density and type of surface snow. Often there were several different layers of snow above the ice and their depths and densities had to be recorded separately. The ice itself changed little except near the surface where the density was found to range from 0·65 g cm^{-3} for the small-grained "white" ice containing large bubbles to 0·85 g cm^{-3} for the large-grained "blue" ice containing small bubbles.

During 1959 few density measurements were made. However, for each stake at every measurement the type of snow at the surface was recorded by a standard classification ranging from freshly fallen snow to ice. In order to obtain an estimate of the change in net water equivalent accumulation during this year, density values were assigned to the various types of snow (to the nearest 0·05 g cm^{-3}) from the corresponding information including densities gathered during 1960 and 1961. Measurements of the 35 stakes were made monthly in 1959 and 1960 and fortnightly in 1961.

4.2.2. S2 trail

Inland from the local area a set of 8 stakes was emplaced in October 1957 at 8 km intervals along the route to S2 (Cameron *et al.* (1959)). With these stakes no summer melt-out was encountered and densities from pit and surface measurements were more accurately determined. The thickness and frequency of ice bands were found to gradually decrease with distance inland. Beyond S2 no ice lenses or bands were encountered in pits; instead only numerous fine wind crusts were observed.

From the pit studies it has been found that the snow is strongly wind-packed and hard, with densities ranging from 0·38 g cm^{-3} to 0·46 g cm^{-3} in different layers. The average density, however, showed no significant increase from the surface to 2·0 m (corresponding to more than 4 years' accumulation). This indicates that the effect of compaction to this depth is negligible. The average density to 2·0 m for the whole route was 0·41 g cm^{-3} and this has been used as a constant conversion factor for snow accumulation to water equivalent.

The accumulation results have been taken from the following measurements: two in 1957, eleven in 1958, four in 1959, two in 1960 and seven in 1961–2.

4.2.3. S2

At S2 two sets of stakes are used:

(i) A set of three 5 cm U.S. Weather Bureau stakes were emplaced in 1957 and a large number of measurements has been made on these to January 1962, although

the stakes have been replaced several times (to 200 m across wind from the station) to avoid general station build-up. These stakes give a detailed picture of how the accumulation rate has varied with time but can not be taken as representative of the area as a whole.

(ii) S2 strain grid. A set of 12 relative movement stakes (3 cm diameter) were emplaced over a 20 sq km area at S2 in March 1957 (Cameron *et al.* (1959)). Although fewer readings are available for this system than the above set of three stakes, they serve to give a more accurate estimate of the mean accumulation of the region and also its variation over this area.

The following measurements have been made: four in 1957, three in 1958, one in 1959, one in 1960 and six in 1961–2.

Cameron *et al.* (1959, p. 66) noted that the mean net accumulation rate measured from the three Weather Bureau stakes was higher than that of the mean of the relative movement network. It was suggested that this may be due to the influence of the station or to the larger cross-section of the Weather Bureau stakes. However, it will be seen below that, in view of the variability in net accumulation rates among the stakes of the relative movement network, due to slight topographic differences, the net accumulation rate at any one position (such as S2) can not be expected to be representative of the area as a whole.

4.2.4. South of S2

In November 1960 a total of 180 stakes were placed over a distance of 180 miles (290 km) due south from S2 to latitude 69°S. The interval between successive stakes was 1 statute mile (1·6 km) and the stakes were numbered 1 to 180 commencing at S2.

During 1961, stakes Nos. 1 to 120 were remeasured in February and again in March, and Nos. 1 to 180 were remeasured in November and again in December. In December 1961 the stake line was extended to 300 miles (480 km) south of S2, as far as latitude 71°S, for remeasurement in 1962 and 1963.

As described in Section 2, the properties of the firn were studied by a series of pits and surface measurements. In November 1961 eighteen 2 m pits were dug, one each 32 km next to an accumulation stake, from Wilkes to S2 and 480 km south of S2. Surface density was also recorded each 8 km. Because of the high accumulation over most of the route, the average densities of the annual layer (sometimes in excess of 2 m) obtained from the pits were needed for water equivalent calculations rather than the densities from the more closely spaced surface observations. The firn densities varied from an average of 0·44 g cm^{-3} in hard wind-packed winter layers, to 0·37 g cm^{-3} in softer summer layers. These values were found to be slightly higher for deeper layers more than one year old.

4.3. RESULTS

Tables of accumulation for the various stake networks are given in the appendix to this Section.

4.3.1. Wilkes local area

(a) Accumulation during the year. The pattern of accumulation during the year appears to depend largely upon the pattern of precipitation. The difficulties of measuring precipitation in Antarctica are well known. However, at Wilkes during 1961 most of the precipitation as recorded daily from the snow gauges occurred with light winds and, when totalled over a period without strong winds, agreed closely with the local increase in accumulation. Stronger winds following soon removed a large proportion of this new snow, the remainder being packed hard. This resulted in a net accumulation which increased with heavy precipitation but only as a proportion of it. This pattern is illustrated in Figure 4.1. When precipitation was small,

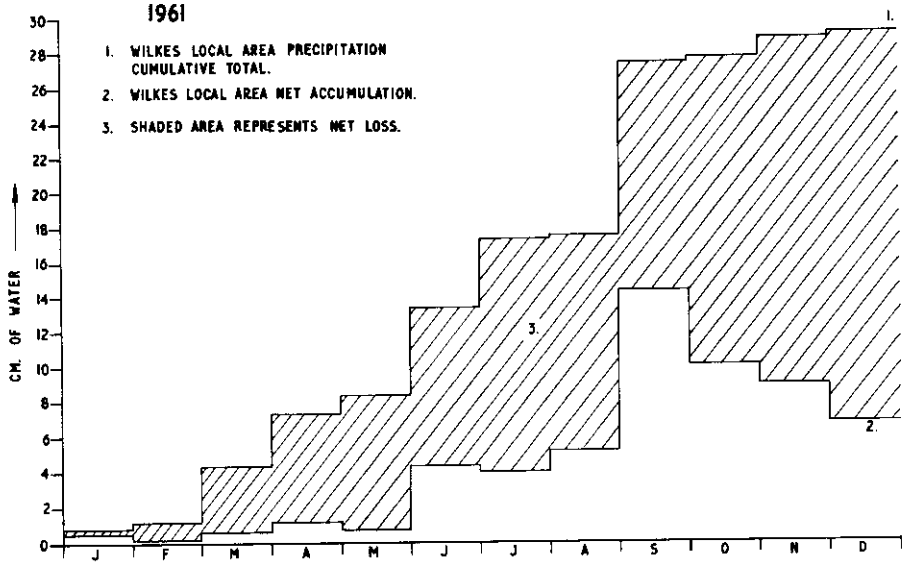

FIG. 4.1. 1. WILKES PRECIPITATION 1961, CUMULATIVE MONTHLY TOTALS.
2. WILKES LOCAL AREA AVERAGE NET ACCUMULATION.
The difference between the two values represents the cumulative net loss.

ablation still went on so that a decrease in net accumulation resulted. The difference between cumulative precipitation and net accumulation in Figure 4.1 represents the cumulative loss. The contributors to ablation are drift transport by wind, sublimation and melt. Of these, only drift transport has been directly measured. The measurements of drift transport carried out at Wilkes in 1959 (Dingle and Radok (1960)) were extended in 1960 and 1961. The analysis of the results (Section 3.4) shows how an estimate can be made of the loss of snow by wind from Wilkes to inland as far as S2. The results are in satisfactory agreement with the accumulation results measured over this region.

(b) Accumulation in different years. For the years 1957 and 1958 several points are noted from Hollin *et al.* (1961).

Firstly, for the summer of 1957–58 ablation was extensive, melt streams were observed below 150 m elevation, and the zone of ablation extended to 230 m.

Secondly, accumulation appears to have been relatively small during the first half of 1958. This has also been a feature of later years and so may be a general result for this region.

Thirdly, ablation in the summer of 1958–9 was far less than that of 1957–8. Few streams were observed and the whole of the area down to sea level remained in the accumulation zone. Average net accumulation from 24th February 1958 to 2nd February 1959 for stakes 402–429 (at elevations approximately 100 to 380 m) was about 10 g cm^{-2}. For the years 1959 to 1961 the pattern of net accumulation is illustrated in Figure 4.2. The general trends appear to be: ablation or little gain by

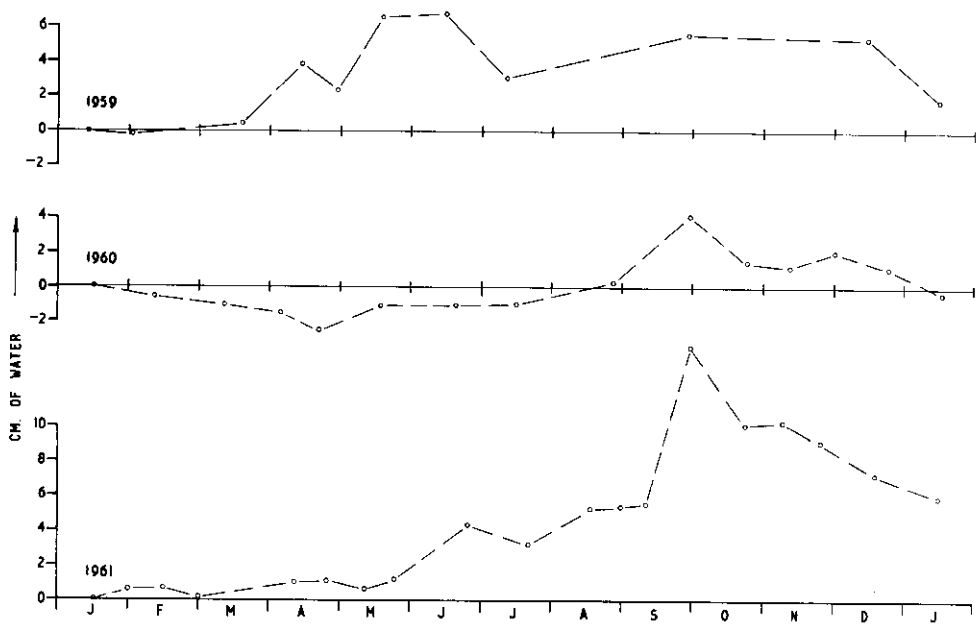

FIG. 4.2. WILKES LOCAL AREA AVERAGE NET ACCUMULATION 1959–1961.

April–May, then a steady build up to a maximum about September–October, after which summer ablation sets in and net loss continues until the following March–May.

In 1961 the average net accumulation from 15th January was only 0·6 g cm^{-2} by May, after which a continual build-up occurred to a maximum 11·5 g cm^{-2} in September, then ablating to 6·0 g cm^{-2} by 15th January, 1962. The corresponding figures from 15th January, 1960, are $-2{\cdot}5$ g cm^{-2} by April to $+4{\cdot}1$ in September to $-0{\cdot}3$ by January, 1961.

(c) The extent of the ablation zone. In 1960 the net ablation zone extended to about 260 m elevation—similar to the extent observed in 1957. The average net accumulation for the 3 km below this line was $-2{\cdot}0$ g cm^{-2} compared to $+2{\cdot}5$ g cm^{-2} for the 3 km immediately above. However, the ablation zone has no well-defined

limit for it gradually merges into the accumulation zone to different extents in different years. In 1961, as in 1958, there was a positive net accumulation over the whole of the local area extending down to sea level.

From this it is seen that the resultant change in the plateau surface in this area over 5 years has been small with annual net accumulation fluctuating from positive to negative in different years.

4.3.2. Wilkes to S2

The S2 trail stakes show a steady build-up of accumulation since 1957, with average annual net accumulation from 1958 to 1961 of: 13·5, 8·2, 8·8, and 10·1 g cm^{-2}, giving an average rate of 10·2 g cm^{-2} per annum over the four years.

The pattern of accumulation during the year is characterised by a rapid build-up from autumn to spring and slight loss from December to March, e.g. from December 1960 there was a loss of 1·6 cm of water by March 1961, then a gain of 11·0 g cm^{-2} to December 1961 and a loss of 1·2 g cm^{-2} by March 1962. This general pattern is similar to that of S2 which is discussed in the next section.

The variation in the average accumulation rate (10·1 g cm^{-2}) for different stakes along this profile is small, the standard deviation for the eight stakes being 1·3 g cm^{-2}. The mean rate of accumulation for the 4 stakes nearest the coast varied from 0·89 to 0·84 times that of the 4 stakes further inland from 1959 to 1961. Application of Student's '*t*' test to the difference between the two means shows this to be quite significant. Hence the rate of accumulation increases slightly with elevation and distance inland. This is in agreement with the results found for the coast and for S2.

4.3.3. S2 (80 km inland)

The accumulation at S2 from 1957 to 1962 is illustrated in Figure 4.3. This shows that net accumulation has been almost linear with time except for the cyclic variation during a particular year. This variation during the year appears similar from year to year and shows an autumn-spring build-up causing an excess above the average linear rate in spring, followed by a summer ablation causing a deficiency from the average rate, later summer to autumn. Variations from the overall linearity follow from variations in annual net accumulations, e.g., as with the more coastal regions, the net accumulation of 1958 was slightly higher than for other years.

The average rate over the whole period for the three stakes was 16·0 g cm^{-2}. This value, however, cannot be considered representative of the area because of the possible influence of station-built-up drifts. For a measure of the average accumulation of the area the results of the grid system are needed.

The 35 m pit at S2 (Cameron *et al.* (1959)) gave the average annual accumulation rate from 1783 to 1957 as 13·3 g cm^{-2} with five-year means varying from 9·0 to 17·4 g cm^{-2}.

The 12-stake strain grid network gives an average rate of accumulation over 20 sq. km (1957 to 1962) of 14·2 g cm^{-2} with a standard deviation of 3·1 g cm^{-2}. This relatively large variation among stakes, in contrast to that of the S2 trail, is not a random variation due, for example, to sastrugi (which are comparatively small in this region) but more a property of position. This follows from the result that the proportional differences in the accumulation rates for different stakes have varied

only slightly over the period. Although the maximum slope in the area is less than 40′ of arc, slight variations in surface topography appear to be responsible for the variation in accumulation rates. This is brought out more clearly by a closer examination of the accumulation figures for the "strain-grid" stakes.

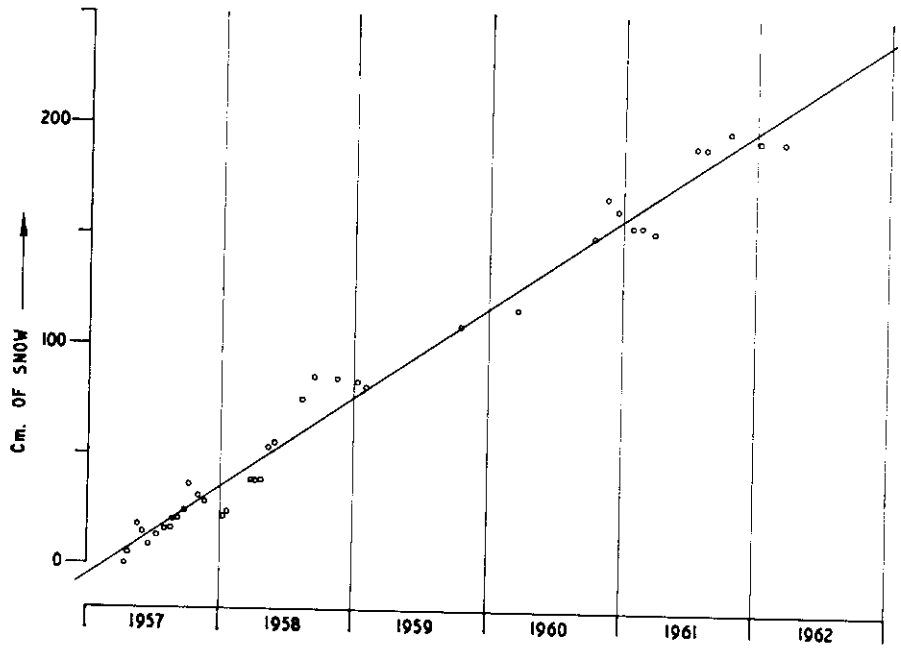

FIG. 4.3. AVERAGE NET SNOW ACCUMULATION AT S2, FROM 1957 TO 1962 MEASURED FROM THE THREE 5 cm × 5 cm STAKES. The straight line is the least squares regression line for net accumulation with time. The actual net accumulation total tends to be below this line in late summer, and above it over late winter and spring.

The network consists of 4 inner stakes surrounded by 8 outer stakes (cf. Fig. 6.13). The distance between neighbouring stakes is about 1·5 km. For the inner four stakes, *A*, *B*, *C*, *D*, the relative elevation of their surrounding neighbours are available. From these, estimates of the average slope of the line of greatest slope through each of *B*, *C*, *D*, have been made, together with the degree of convexity or concavity. The measure of curvature was taken as the average of the increases in slope going through the point in the direction of maximum slope and across this slope. (Stake *A* was omitted because it is in the station area.)

For each of these stakes the ratio of its accumulation rate to that of the mean of the network is listed in the following table for the period from 1957 to 1962, together with the slope and curvature of the stake position.

The accumulation rate has been consistently greatest for stake *C* in a relatively flat concave position, and least for stake *D* in a steeper convex position. For position *B*, of the same curvature as *C* but where the slope is greater, the accumulation rate has been midway between that of *C* and *D*.

TABLE 4.I.

RELATIVE ACCUMULATION RATES AND TOPOGRAPHY IN THE REGION OF S2.

Stake	*C*	*B*	*D*
Deviation from mean slope (27′)	−1·4′	+1·6′	+0·6′
Convexity(−), Concavity(+) (minutes per mile)	+7·0	+7·0	−18·7
Relative Accumulation Rate from			
20 Mar. 1957 to 18 Jan. 1958	1·24	1·17	0·49
18 Jan. 1958 to 10 Jan. 1959	1·20	0·82	0·42
10 Jan. 1959 to 1 Mar. 1961	1·01	0·94	0·83
1 Mar. 1961 to 2 Jan. 1962	1·26	1·11	0·69
20 Mar. 1957 to 2 Jan. 1962	1·13	0·99	0·67

From this it appears that both slope and curvature may play an important part in the topographical effect on accumulation rate. This becomes more evident south of S2 where the topographical variations and the corresponding accumulation rate variations are much larger.

4.3.4. South of S2

For this region only one year's data are available at this stage. Also, because of the high accumulation, the pits did not extend far into the past, so that the results cannot be taken as indicative of general trends as the above longer-term data. However, where the pits covered two or more years the pattern shows accumulation values of the same order as measured at the stake next to the pit from November 1960 to November, December 1961. Stakes numbers 0 to 50 which were remeasured in March 1962 gave an average of 13·1 g cm^{-2} accumulation from November 1961 compared to 13·7 g cm^{-2} for these stakes over the similar period 1960–61. This suggests the same order of accumulation may be expected for 1962.

The average overall accumulation from Wilkes to S2 and 480 km south was found to be 33 g cm^{-2}. This is of similar magnitude to that recorded south of Dumont D'Urville (Lorius (1962)) and south of Mirny (Dolgushin (1961)). However, south of S2 there is a region for which the profile over 200 km gave an average net accumulation in excess of 56 g cm^{-2}.

The stake tops on the southern trail from S2 were originally 214 cm above the surface; after 12 months several stakes were covered completely and many others protruded by only a few cms. The snow in this region was very hard and wind-packed with average density 0·42 g cm^{-3}. Hard wind-eroded sastrugi often reached heights of 1·5 m.

The most remarkable feature of the accumulation south of S2 is its apparent variation with topography on both major and minor scales.

(a) The variation of accumulation with major topography (illustrated in Fig. 4.4). South of S2 as the elevation increases to a high region between 20 and 29 km from S2 the average annual net accumulation (from November 1960 to November

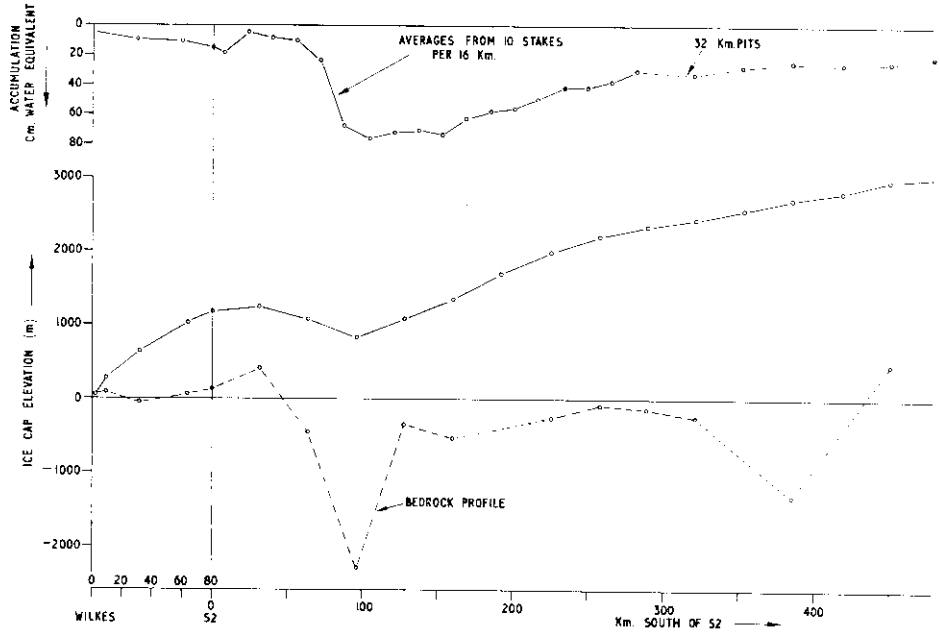

FIG. 4.4. ICE CAP PROFILE FROM WILKES ESE TO S2 AND SOUTH TO LATITUDE 71° ALONG THE TRAVERSE ROUTE OF FIG. 0.3. Above this is shown the net accumulation profile over this route for November 1960 to November 1961. Values are taken from the average of 10 stakes per 16 km, from S2 to 290 km south, and from data from pits 32 km apart from 290 km to 480 km south to S2. The bedrock profile is taken from Jewell (1962).

1961) decreases to 5 cm of water. From here on, the accumulation increases rapidly in the large trough about 90 km south and up the following slope to averages of 80 cm of water equivalent. This average gradually decreases to 30 cm of water by 290 km south of S2.

From 290 to 480 km south of S2 the pit data indicate a continued steady decrease to 20 g cm^{-2} per annum. Here, latitude 70° 52′S, the plateau elevation reaches 2,990 m and the plateau slope is less than 10′ of arc in any direction. Ram-hardness values to 4 m depth and lack of sastrugi indicate that this region is beyond the zone of strong surface winds.

The variation in accumulation rate during the year (for stakes 0 to 120) to 192 km south of S2 is illustrated in Figure 4.5. Over the summer period, November (1960) to March (1961), the high region 20 km south of S2 showed an average slight ablation of approximately 1 g cm^{-2}. Further south there was a substantial build-up over this period, the average rate overall being 1·7 g cm^{-2}/month. This can be compared with 2·8 g cm^{-2}/month during March, 2·3 g cm^{-2}/month from March 1961 and 1·8 g cm^{-2}/month from November 1961 to January 1962.

(b) Variation with minor topography. The elevation profile for each mile position in the region 90 to 300 km south of S2 shows, superimposed upon the steady slope (seen in Fig. 4.4), a series of irregualr undulations of wave lengths 5 to 15 km and amplitudes 7 to 50 m (cf. Fig. 4.6). These undulations caused large variations in accumulation (up to 215 cm in 3 km) with remarkable regularity.

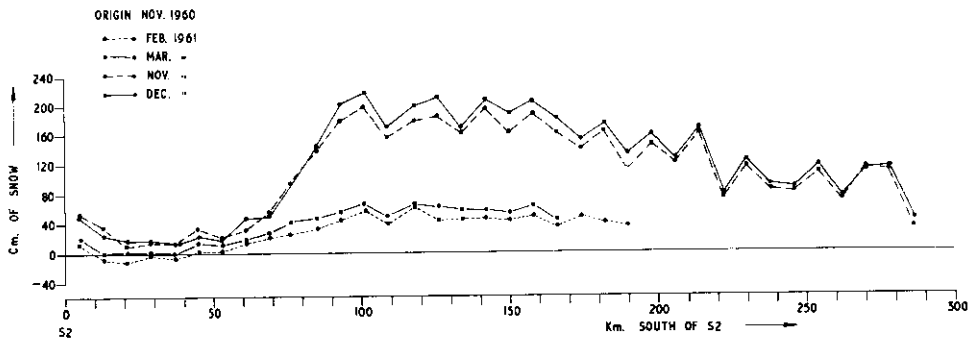

FIG. 4.5. VARIATION IN NET ACCUMULATION SOUTH OF S2 DURING THE YEAR. The net snow accumulation from November 1960 is plotted for the 4 measurements of 1961. The results are from the average of 5 stakes each 8 km.

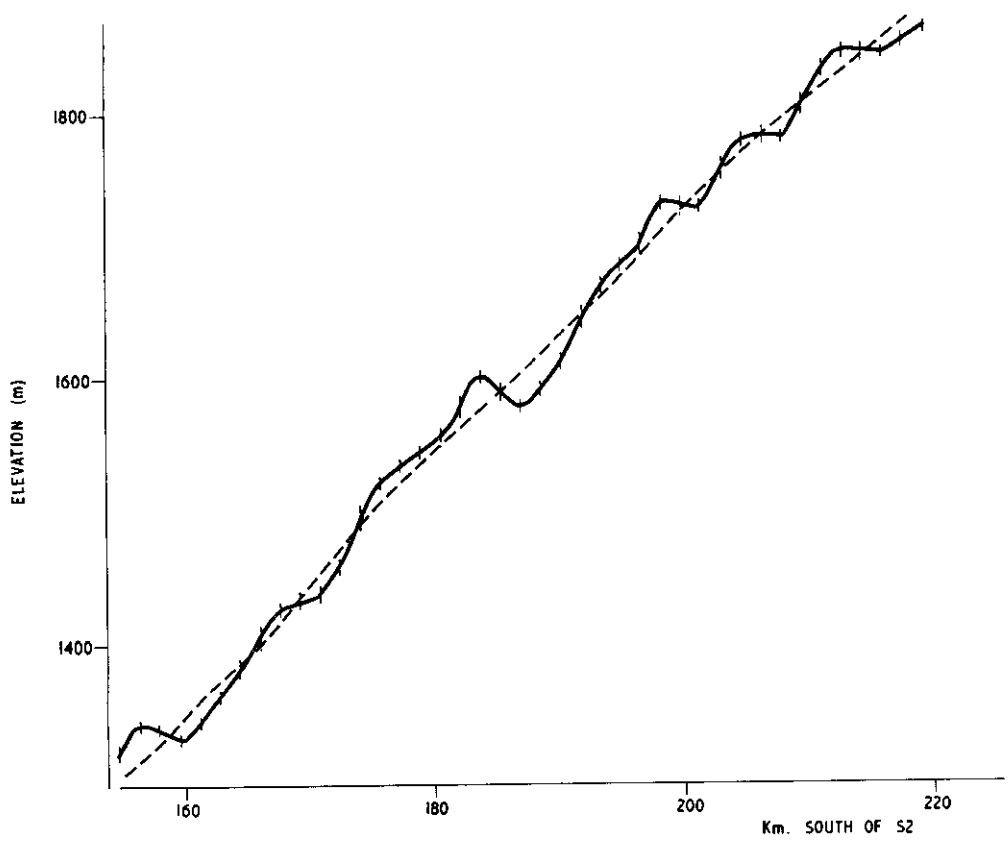

FIG. 4.6. UNDULATIONS ON A STEADY SLOPE. Between 150 and 200 km south of S2 the elevation for each mile (1.6 km) position is plotted. The broken line represents the 10-mile running mean elevation.

Dolgushin (1961) reported similar "waves" along a 150 km profile between Mirny and Pioneerskaya. These were observed to be between 2 and 6 km wide, perpendicular to the dominant direction of the wind, and to move slowly in the direction of the wind. In Terre Adélie, from the coast to Charcot, a distance of 500 km, accumulation was observed to vary greatly with local changes in slope (Cornet *et al.* (1960)). Inland of Maudheim, Swithinbank (1959) reported a series of stepped ridges on a slope. Over these, net accumulations variations were found of the same order as those south of S2. The accumulation stakes were too widely spaced to give an accurate picture of the net accumulation over these stepped ridges but Swithinbank noted that net accumulation appeared greatest where the slope was least. He concluded that the result would be a gradual smoothing of the topography, but that owing to movement, the irregularities would persist (Swithinbank (1959) p. 134).

After comparing the accumulation data south of S2 with the elevation profile it appeared that net accumulation maxima occurred near the bottom of depressions and minima occurred near the crests. However, closer analysis revealed that the net accumulation profile is more closely related to slope. A comparison of profiles '1' and '2' in Figure 4.7 shows that net accumulation minima tend to occur downwind of the troughs.

Comparing '2' and '3', it may be seen that the net accumulation profile closely follows slope not only in phase but also in relative magnitude. By least squares linear regression the following expression has been found for the deviation in accumulation A from its mean in terms of the deviation in slope S and deviation in relative elevation E (units used as in Fig. 4.7).

$$A = -0{\cdot}85\,S - 0{\cdot}21\,E.$$

This suggests that, rather than being filled in by the high accumulation, the "waves" would advance up slope, into the wind (in contrast to those reported by Dolgushin (1961)).

If it is assumed that the accumulation does not destroy the waves but just causes them to advance up-slope at a constant rate, together with an overall rise of the surface, then an estimate of the rate of movement may be made in terms of the variation of accumulation over a wave and the corresponding variation of slope.

For, suppose a series of waves is moving up a uniform slope at a constant speed, v, then the profile at a time, t, may be represented by an equation of the form

$$y = Ax + Bt + F(x - vt), \tag{4.1}$$

where x and y are the horizontal and vertical coordinates of the profile respectively, A is the uniform slope (assumed constant), B is the overall average rate of net accumulation of the surface as whole, and F a continuous periodic function with a continuous derivative and with zero integral over a period (e.g. for a series of regular waves of amplitude a and wave length $\frac{2\pi}{p}$, $F(x) = a \sin px$). Then the accumulation rate is given by

$$\frac{\partial y}{\partial t} = B - vF'(x - vt), \tag{4.2}$$

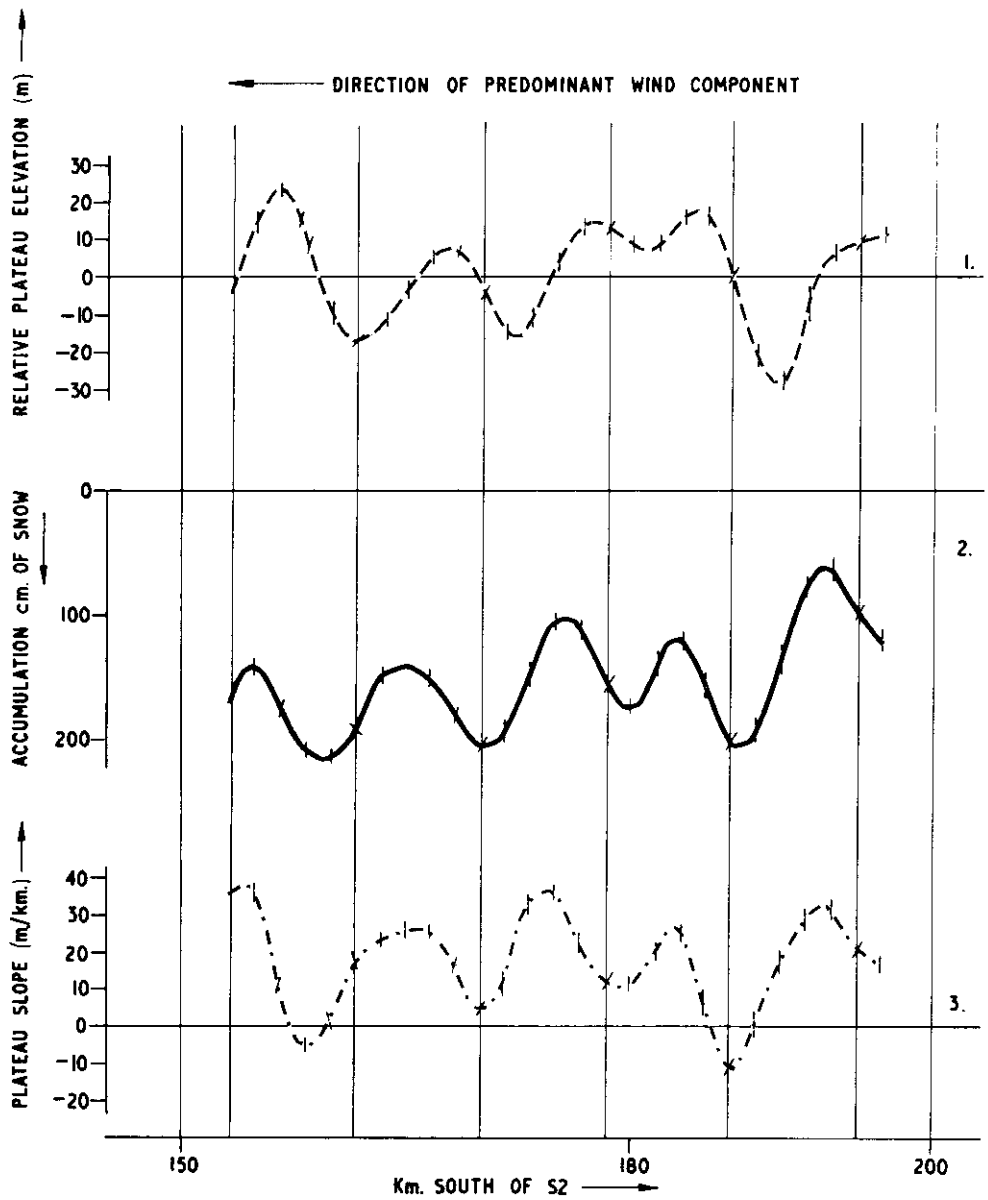

FIG. 4.7. ACCUMULATION OVER AN UNDULATING SLOPE. For a typical section of the traverse route in the region of high accumulation the following are plotted:

1. Relative elevation—obtained from the difference between the elevation at each stake and the 10-mile running mean (which represents the steady slope upon which the undulations are superimposed).
2. Annual net snow accumulation for each stake.
3. The average slope at each stake position.

Each profile has been smoothed according to $X_i' = \frac{X_{i-1} + 2X_i + X_{i+1}}{4}$.

and the slope by

$$\frac{\partial y}{\partial x} = A + F'(x - vt). \tag{4.3}$$

Hence

$$\frac{\partial y}{\partial t} = B + Av - v\frac{\partial y}{\partial x}. \tag{4.4}$$

This implies that the *variation* in net accumulation rate over the "waves" is proportional to the variation in slope. This appears to be in agreement with the net accumulation results obtained and is a condition for the preservation of the form of the waves.

To obtain v we note that over any wave

$$\left(\frac{\partial y}{\partial t}\right)_{\min} - \left(\frac{\partial y}{\partial t}\right)_{\max} = -v\left[\left(\frac{\partial y}{\partial x}\right)_{\max} - \left(\frac{\partial y}{\partial x}\right)_{\min}\right]. \tag{4.5}$$

Over the region considered in Figure 4.7 the average variation in net accumulation over a wave was 83 cm of snow, and the average change in slope was $\frac{31}{1000}$. Hence an estimate for v (in m/yr) is given by

$$0{\cdot}83 = v\frac{31}{1000}$$

or

$$v \doteqdot 27 \text{ m/yr}.$$

To obtain a more exact relationship for the variation of net accumulation over an undulating slope and to test the rate of movement it would be desirable to have a series of closely spaced stakes over a complete "wave". The study of the variation of drift transport with wind and the variation of wind down an undulating slope is expected to throw light on the cause of the phenomena.

4.3.5. Net accumulation isopleths

From the study of the relation between snow drift and wind speed and between wind speed and plateau slope, Section 3·4 showed how the net accumulation may be expected to be related to the plateau contours. General agreement with this was found for the accumulation line south of S2. Hence, from the accumulation near the coast, along the S2 trail, at S2 and south of S2 very generalised accumulation isopleths have been constructed for the Wilkes region. These are shown in Figure 4.8 and will be used for the mass balance calculation of Section 6.5.

4.4. CONCLUSION

4.4.1. Annual net accumulation

The Wilkes area from the coast to about 560 km inland may be considered in four main regions with merging boundaries.

(i) Within about 15 km of the coast, or below about 350 m elevation there is a region of very small net accumulation over the longer period because the

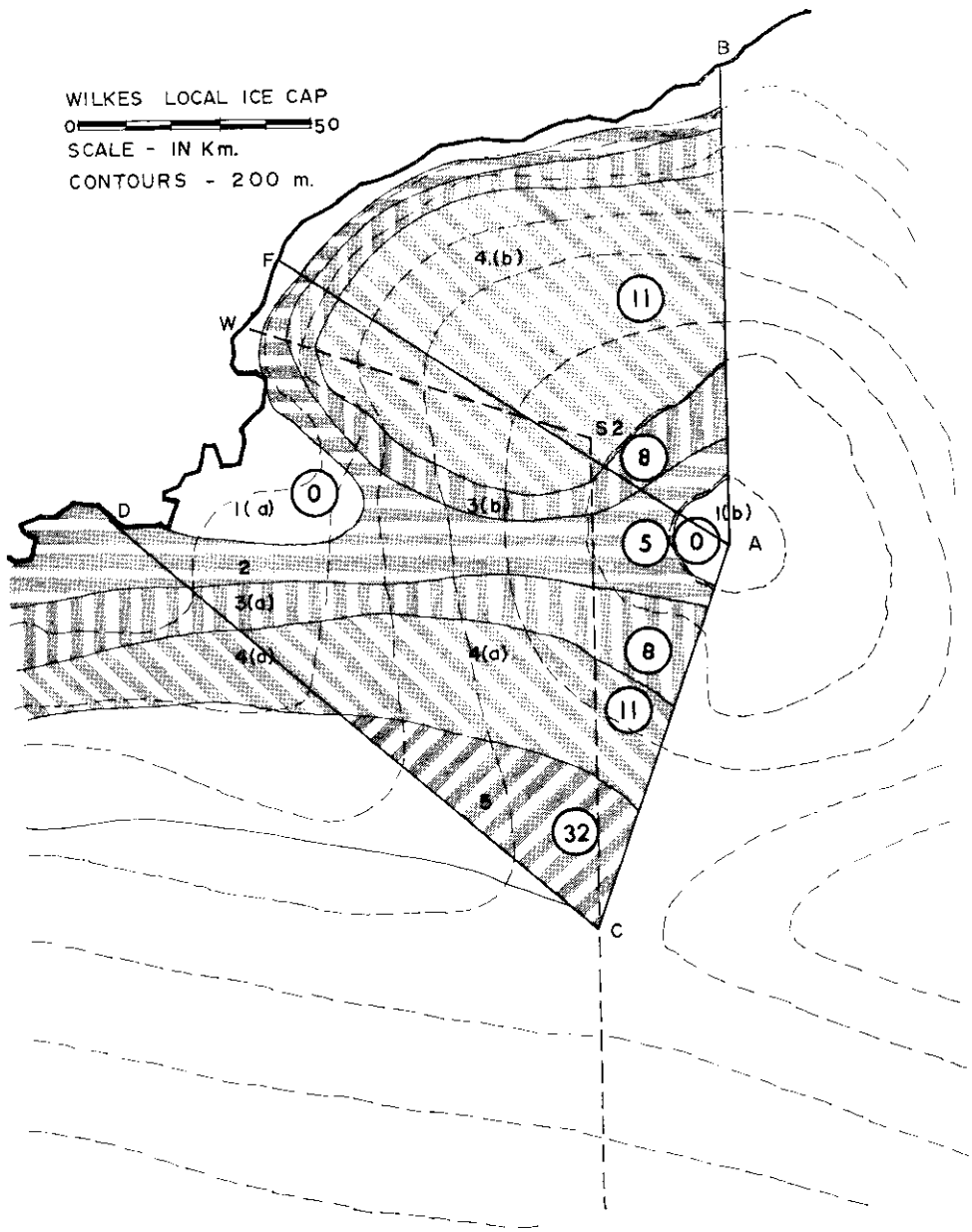

FIG. 4.8. ACCUMULATION ISOPLETHS OVER THE WILKES REGION. The accumulation values (circled) are in g cm^{-2} yr^{-1}. From the elevation contours it is expected that the regions *AFB* and *ACDB* are independent insofar as there is little or negligible inflow to them, and the only outflow is loss at the coast.

annual net accumulation varies from positive to negative values in different years.

(ii) From the coastal region going inland to about 100 km the net accumulation rate since 1957 has varied from about 10 g cm^{-2} yr^{-1} over most of the slope to 14 g cm^{-2} yr^{-1} in the vicinity of S2.

(iii) Further south from S2 over a topographical depression and up the following slope there is a region of very high annual net accumulation with averages from 80 to 68 g cm^{-2} between 90 and 200 km south of S2.

(iv) Still further south of S2 the annual net accumulation decreases gradually to about 18 g cm^{-2} by latitude 71°, at elevation 3,000 m, beyond the zone of strong surface winds.

4.4.2. Variation in accumulation rate during the year

The pattern of accumulation during the year is characterised by a period of rapid accumulation, autumn to spring, but net ablation during the summer. This net summer ablation varies from about 8 g cm^{-2} at the coast to 2 g cm^{-2} 100 km inland, elevation 1200 m. In the region further south there was no net ablation over summer (November to March) but the accumulation rate was only about $\frac{2}{3}$ of that from March to October.

4.4.3. Topography influence

The accumulation pattern is strongly influenced by topography on both large and small scales.

On the large scale the accumulation profile suggests that concave depressions gain accumulation at the expense of convex rises.

On the small scale, "waves" on a slope cause accumulation maxima near points of least slope (including negative values) and minima near points of maximum slope. This should perpetuate the waves, but move them up-slope into the wind at a rate of the order of 25 m/yr, for the slopes and accumulation rates observed inland.

(APPENDIX

APPENDIX TO SECTION 4

Snow accumulation tables

1. AVERAGE PROGRESSIVE ACCUMULATION ON S2 TRAIL STAKES (cm OF SNOW).

Year	Date	Average Stake Reading (cm)
1957	July 8	0·6
1958	January 2	0·0
	January 22	−1·5
	February 10	−2·4
	March 18	−0·8
	April 7	−1·0
	April 17	−1·0
	May 7	+7·0
	June 5	6·0
	July 14	15·1
	July 22	29·5
	August 4	27·4
	September 3	31·4
	November 3	34·0
1959	January 7	32·0
	January 30	32·1
	October	48·5
1960	March 19	56·0
	December 11	78·0
1961	January 31	80·6
	February 27	78·1
	March 28	83·0
	July 20	99·0
	August 13	98·4
	October	98·6
1962	January 3	102·4
	April 14	102·0

2. INDIVIDUAL STAKE ACCUMULATION VALUES ALONG S2 TRAIL.

Distance from the coast	miles	10	15	20	25	30	35	40	45	S2
Accumulation 2/1/58 to 3/1/62	cm snow	71	92	113	94	116	106	120	81	
Average rate/year	cm snow	17·7	23·0	28·2	23·5	29·2	26·5	30·0	20·2	
Average rate/year (density ·41 g cm^{-3})	g cm^{-2}	7·3	9·4	11·6	9·6	12·0	10·9	12·3	8·3	14·2

3. ACCUMULATION RATES FOR S2 GRID STAKES.

Stake	Stake Height Jan. 1962 cm	Average Accumulation Rate cm snow/yr	Position of original stake relative to marker cm	direction
A	25	48·5		
B	62	36·3	60	S
C	47	42·5	0	
D	109	25·4	78	E
E	24	45·2	105	E
F	59	36·3	100	SE
G	105	26·7	65	S
H	0	44·2	0	
I	28	41·5	60	SW
J	124	22·5	112	NW
K	53	37·5	126	N
L	−4	45·0	114	NE

4. AVERAGE ANNUAL NET SNOW ACCUMULATION ALONG SOUTHERN TRAIL.

Miles south of S2	Annual Accumulation Rate cm snow	cm water
Stake Measurements:		
5	44	18·5
15	12	5·4
25	23	9·6
35	26	10·9
45	61	25·6
55	159	61·8
65	176	74·0
75	181	76·0
85	178	74·8
95	175	73·5
105	150	63·0
115	137	57·5
125	133	55·9
135	118	49·6
145	96	40·3
155	97	40·7
165	90	37·8
175	70	29·4
Deduced from Pits:		
200	80	33
220	68	28
240	60	25
260	65	27
280	60	25
300	50	21

5. ICE PLATEAU TEMPERATURE PROFILES

5.0. INTRODUCTION

The study of temperature profiles at Wilkes was concerned with two main features:

A. The temperature profile to about 10 m depth reflects the local surface temperatures and gives a measure of the annual mean surface temperature, the amplitude of the annual temperature wave, and its variation with depth in the snow. These temperature profiles in the top 10 m of the firn also provide information on the heat parameters of the firn.

On the 1961 traverse from Wilkes to S2 and 480 km south of S2, temperatures were measured in the firn to 7 m depth. The calculation of the annual mean surface temperature from these data and simple heat conduction theory is complicated by the existence of a high accumulation rate (up to 2 m of snow per year) over much of the route, and a varying snow diffusivity with depth. The effect of these two complications on the heat conduction in the firn is analysed in this section and due allowance is made for them in the calculation of the annual mean temperature at the surface of the inland ice cap.

B. It is expected that the temperature profiles below 10 m depend largely upon the ice cap mean surface temperature, the basal temperature and geothermal heat flux, the accumulation rate, the movement of the ice, and the ice heat parameters, namely, conductivity, diffusivity and thermal capacitance. Temperature gradients below 10 m were obtained at five positions on the plateau between Wilkes and S2–80 km inland. These temperature gradients have been interpreted by an analysis of the relationships between the above variables for the Wilkes ice cap.

5.1. TEMPERATURES AT THE SURFACE

5.1.0. Temperature measurements at Wilkes

At S1, 9 km inland from Wilkes at an elevation of 260 m on the ice plateau, the U.S. party in 1957 (Cameron *et al*, (1959)) placed a set of thermocouples in the ice to measure temperatures at the following depths: 0, $\frac{1}{2}$, 2, 4, 7, 11, 16 m. These temperatures, which were observed approximately weekly until 1959, depict the temperature variation with depth and time at this position and are plotted in Figure 5.1 (from Cameron and Bull (1962)).

On the 1961 traverse, each 32 km, temperatures were measured in pits at 10 cm intervals, to 2 m; also, in a borehole, the temperature was measured at the 7 m level. To use these temperatures to estimate the annual mean temperature at the surface of the inland ice cap it is first necessary to consider theoretical profiles of temperature with depth for different models of the surface firn.

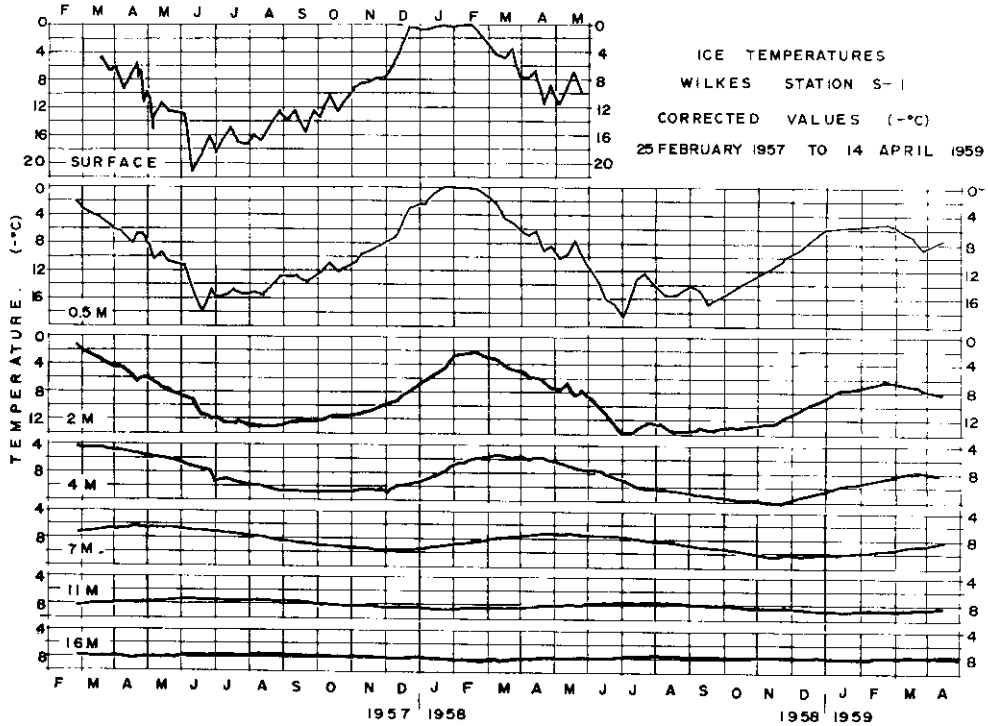

FIG. 5.1. DISSIPATION OF ANNUAL TEMPERATURE WAVE IN THE ICE AT S1, (taken from Cameron & Bull (1962)). The wave amplitude decreases with depth and small period fluctuations die out the most rapidly.

5.1.1. Temperature conduction in the firn

The first point to be considered is the dissipation of the annual temperature wave in the firn. This has been considered by many workers, including Koch and Wegener (1930), Sorge (1935), Loewe (1956), Schytt (1960), Bogoslovski (1960), Cameron and Bull (1962), Crary (1961) and Benfield (1951 and 1953).

5.1.1.1. Temperature profile for constant κ and zero accumulation

If it is assumed that the ice may be considered as a semi-infinite slab of constant diffusivity κ, then for no accumulation or movement the temperature θ at time t and depth x satisfies

$$\frac{\partial \theta}{\partial t} = \kappa \frac{\partial^2 \theta}{\partial x^2}. \tag{5.1}$$

(i) If the temperature-depth profile does not vary with time then $\dfrac{\partial \theta}{\partial x} = c$, a constant, so that $\theta = \theta_0 + cx$, where θ_0 is the surface temperature and the temperature varies linearly with depth.

Now, any periodic temperature variation in time may be superimposed upon this, and provided only steady state conditions are required, each may be treated and their

solutions added separately. Hence, for constant boundary conditions, if the geothermal flux q causes a constant gradient $\frac{q}{\kappa}$, this may simply be added to the effect of the periodic temperature variation. We now consider the simple periodic temperature variation separately.

(ii) For a periodic temperature variation at the surface of the form

$$\theta_0 = A_0 \cos(\omega t + \varepsilon_0) \tag{5.2}$$

with amplitude A_0 and period $p = \frac{2\pi}{\omega}$, the solution of equation (5.1), which is of period $\frac{2\pi}{\omega}$ and remains finite as $x \to \infty$, is

$$\theta = A_0 e^{-x\sqrt{\frac{\omega}{2\kappa}}} \cos\left(\omega t + \varepsilon_0 + x\sqrt{\frac{\omega}{2\kappa}}\right) \tag{5.3}$$

$$= A_x \cos(\omega t + \varepsilon_x),$$

where $$A_x = A_0 e^{-x\sqrt{\frac{\omega}{2\kappa}}} \text{ and } \varepsilon_x = \varepsilon_0 + x\sqrt{\frac{\omega}{2\kappa}}, \tag{5.4}$$

(e.g. cf. Carslaw and Jaeger (1959) p. 65).

This shows that the periodic temperature variation at the surface travels downwards into the firn with an amplitude that decreases exponentially with depth and a phase lag which increases linearly with depth. Furthermore, different periodic variations at the surface are superimposable for steady state conditions.

Benfield (1951) has pointed out that this steady state solution neglects transient effects. He has given a more complete solution involving error functions of a complex variable and which reduces to the above result for large values of time (cf. the Appendix to this section). However, for a permanently periodic effect, such as the annual temperature wave, the transient effects may be neglected.

Many workers have used the above analysis to determine the "effective diffusivity" of snow, firn or ice in the field from the amplitude decrease and phase shift of the annual temperature wave with depth. Some results are given below together with the relevant average densities.

	Effective Diffusivity $cm^2\ sec^{-1}$	Density $gm\ cm^{-3}$	
Greenland glacier ice	·0116	·911	(Koch & Wegener (1930))
Maudheim ice shelf	·00827	·525	(Schytt (1960))
Little America	·0075	·448	(Crary (1961))
Wilkes S1	·015	·87	(Cameron & Bull (1962))

The results most applicable to the region south of S2 are those for which the density varies with depth from about 0·40 at the surface to 0·63 at 10 m. In applying the results to temperatures measured in firn it is necessary to keep in mind the conditions assumed to be applicable in practice.

Besides the assumed constant density (therefore, diffusivity) with depth, a further assumption used, which in general does not strictly apply, is that the temperature at the surface may be represented by an annual sine wave. It can be seen from Figure 5.1

(and also from Fig. 1.1) that the actual surface temperature has many deviations from an ideal sine wave. Also the summer portion is shorter and more peaked than the longer (kernlose) winter.

This latter discrepancy has largely been taken into account, by e.g. Schytt, by representing the annual temperature variation at the surface by the sum of an annual and a semi-annual sine wave. The smaller short term fluctuations dissipate more rapidly with depth (as may be seen in Fig. 5.1) because of the higher value of ω in equation (5.4).

The validity of the application of this simple theory of conduction to the determination of effective diffusivity of the snow may be judged by comparison of the observed values with the theoretical expected values from the density profiles. Schwerdtfeger (1963; p. 81) derived a relationship for the diffusivity of an ice/air mixture (firn) in terms of its density and the conductivity and thermal capacitance of pure ice. The values of the observed effective diffusivities given above show generally close agreement with theoretical expected values, except for the value found at S1. This value is higher than that valid for pure ice (0·0116 $cm^2\ sec^{-1}$) and has been discussed in detail by Cameron and Bull (1962) with reference to the effects of (1) decreased temperature, (2) impurities, (3) crystal orientation, (4) convection in air bubbles, (5) thermal radiation and (6) solar radiation, but these still left the discrepancy largely unexplained.

A further factor affecting the application of the theory to the S1 data is that the mean temperatures for different depths are not equal and, furthermore, are changing with time. The reason for this appears to be that the overall *surface* temperature average has been falling; this effect also has a time lag with depth and results in a distortion of the annual temperature waves. The annual mean temperatures at Wilkes for 1957 to 1959 were −8·2, −9·7, −10·0°C (cf. Section 1).

The effect of a gradual variation of the annual mean temperature may be allowed for by superimposing a longer-term variation on the annual sine wave at the surface. Surface temperature variations of shorter period are more rapidly dissipated with depth in accordance with the second of equations (5.4). For example, Schytt (1960), taking a mean value of the diffusivity for the upper layers, finds the following depths for which the surface amplitude is less than 10% of the surface amplitude for different periods:

Period	*Depth*
24 hours	30 cm
7 days	80 cm
20 days	130 cm

In order to see the effect of the *daily* temperature oscillation on the temperature profile the monthly average daily ranges from 3 hourly observations at Mawson 1958 are listed below (taken from the Bureau of Meterology, ANARE REPORTS, Series D, Vol. X):

Month	J	F	M	A	M	J	J	A	S	O	N	D
Mean daily temperature range (°C)	3·2	4·1	3·2	1·5	0·8	0·3	1·1	1·4	2·2	3·9	4·7	3·5

The mean amplitudes are only half these values; it can therefore be seen from the above that the daily periodic temperature wave does not penetrate very deeply. Other temperature variations (besides daily and annual) do not have stable periods so are better treated by considering the transient effects. The dissipation of the surface temperature fluctuations may be observed in Figure 5.1 as the smoothing of the annual waves with depth.

So far, the accumulation has been considered as zero or negligible, and the snow diffusivity has been assumed constant with depth. Although this may apply at S1 it does not apply further inland, especially along the traverse route where the annual snow accumulation is between one and two metres and the density varies from about 0·40 at the surface to about 0·65 by 12 m depth. In the next section the effect of a steady accumulation rate on the temperature profile will be considered, and also the problem of varying diffusivity with depth. These two factors will be shown to have opposite and therefore partly compensating effects on the temperature profile.

5.1.1.2. Temperature profile in an accumulating snow field

A solution for this problem has been treated in detail by Benfield (1951) (cf. Appendix) who also gives some numerical values of temperature as a function of depth for accumulation rates of 8, 4, 0 m/yr.

Carslaw and Jaeger (1959) give a solution for a steady periodic temperature field in the region $x > 0$ which is moving with velocity U in the x direction and with temperature $\theta_0 = A_0 \cos(\omega t + \varepsilon_0)$ at $x = 0$. This solution may be applied to an accumulating snow field, where x represents the depth below the surface at time t and U the accumulation rate. It neglects transient effects, which are included in Benfield's solution, but applied to the periodic annual temperature wave will readily illustrate the effect of a constant accumulation rate.

The solution given by Carslaw and Jaeger for the temperature θ at depth x and time t is:

$$\theta = A_0 \exp\left(\frac{Ux}{2\kappa} - xa^{\frac{1}{2}} \cos\frac{\phi}{2}\right) \cos\left(\omega t - xa^{\frac{1}{2}} \sin\frac{\phi}{2} + \varepsilon_0\right), \tag{5.5}$$

where a and ϕ are defined by

$$\left(\frac{U^2}{4\kappa^2} + \frac{i\omega}{\kappa}\right) = ae^{i\phi}.$$

(Carslaw and Jaeger (1959); p. 389, Problem III).

Now, in order to be able to find the change in phase and amplitude with accumulation rate it is necessary to express $a^{\frac{1}{2}} \cos\frac{\phi}{2}$ and $a^{\frac{1}{2}} \sin\frac{\phi}{2}$ in terms of U. Complex number manipulation reveals

$$a^{\frac{1}{2}} \cos\frac{\phi}{2} = \frac{1}{\sqrt{2}}\left[\sqrt{\left(\frac{U^2}{4\kappa^2}\right)^2 + \frac{\omega^2}{\kappa^2}} + \frac{U^2}{4\kappa^2}\right]^{\frac{1}{2}}$$

and

$$a^{\frac{1}{2}} \sin\frac{\phi}{2} = \frac{1}{\sqrt{2}}\left[\sqrt{\left(\frac{U^2}{4\kappa^2}\right)^2 + \frac{\omega^2}{\kappa^2}} - \frac{U^2}{4\kappa^2}\right]^{\frac{1}{2}}.$$

Substitution of these in equation (5.5) gives for $U = 0$ the previous relation (5.3) valid for the case of zero accumulation. Comparing (5.3) with (5.5) after substitution shows that the effect of the movement (or accumulation) is to change the phase lag $\varepsilon_0 + xa^{\frac{1}{2}} \sin \frac{\phi}{2}$ and amplitude $A_x = A_0 \exp - \left(\frac{Ux}{2\kappa} - xa^{\frac{1}{2}} \cos \frac{\phi}{2}\right)$ by amounts depending on the depth x. It remains to substitute some typical values of U, κ, x, to see the effect of the accumulation on the snow temperature profiles.

Along the 1961 traverse route the accumulation maximum rate was about 2 m/yr. So, suppose

$$U = 200 \text{ cm snow yr}^{-1}$$
$$= 6{\cdot}3 \times 10^{-6} \text{ cm sec}^{-1},$$

and take average $\kappa = 0{\cdot}90 \times 10^{-2} \text{ cm}^2 \text{ sec}^{-1}$

and $$\omega = \frac{2\pi}{p} = 2{\cdot}0 \times 10^{-7} \text{ sec}^{-1}.$$

Now, for the accumulation to have a measurable effect on the temperature profile the value of

$$\frac{U}{2\kappa} - \frac{1}{\sqrt{2}}\left[\sqrt{\left(\frac{U^2}{4\kappa^2}\right)^2 + \frac{\omega^2}{\kappa^2}} \pm \frac{U^2}{4\kappa^2}\right]^{\frac{1}{2}} \tag{5.6}$$

must be significantly different from $\sqrt{\frac{\omega}{2\kappa}}$, the exponent of equation (5.4), for the temperature profile without accumulation. From the values of U, κ and ω given above, the magnitudes of the various terms in the expression (5.6) have been evaluated as follows:

$$*1 \quad \left(\frac{U^2}{4\kappa^2}\right)^2 = 1{\cdot}4 \times 10^{-13} \qquad *2 \quad \left(\frac{\omega}{\kappa}\right)^2 = 4{\cdot}8 \times 10^{-10};$$

$$*3 \quad \left(\frac{U}{2\kappa}\right)^2 = 1{\cdot}2 \times 10^{-7} \qquad *4 \quad \frac{\omega}{\kappa} = 2{\cdot}2 \times 10^{-5};$$

$$*5 \quad \frac{U}{2\kappa} = 3{\cdot}5 \times 10^{-4} \qquad *6 \quad \sqrt{\frac{\omega}{\kappa}} = 3{\cdot}3 \times 10^{-3}.$$

From this it can be seen that *1 is less than 0·1 % of *2, so may be neglected to this accuracy. Also *3 is less than 1 % of *4 so that, if this is also neglected, then expression (5.6) reduces to $\frac{U}{2\kappa} - \sqrt{\frac{\omega}{2\kappa}}$ as first approximation for the effect of the accumulation rate (U) on the temperature profile, with error less than 1 % for accumulation rates up to 2 m/yr.

The amplitude at depth x is then given by

$$A_x = A_0 e^{-x\left(\sqrt{\frac{\omega}{2\kappa}} - \frac{U}{2\kappa}\right)} \tag{5.7}$$

and the phase lag $\left(a^{\frac{1}{2}} \sin \frac{\phi}{2}\right)$ is insignificantly different from $x\sqrt{\frac{\omega}{2\kappa}}$, the phase lag without accumulation.

Equation (5.7) may now be used to correct the theoretical temperature profile for accumulation rates. This equation shows that the effect of the accumulation rate on the annual temperature wave in the snow is to slightly lessen the amplitude decrease with depth. This appears to agree qualitatively to the results obtained by Benfield (1951) for higher accumulation rates.

Taking $\sqrt{\frac{\omega}{2\kappa}} = 33 \times 10^{-4}$ cm^{-1}, Table 5.I below shows the ratio $\left(\frac{A_0}{A_x}\right)$ of the amplitude at the surface to the amplitude at depth x for accumulation rates of zero and 200 cm yr^{-1}.

TABLE 5.I.

x cm	$U = 0$ cm yr^{-1}	$U = 200$ cm yr^{-1}
0	1·00	1·00
100	1·39	1·34
200	1·93	1·80
400	3·74	3·25
700	10·1	7·90
1000	27·0	19·00

Table 5.II gives the ratio $\frac{A_0}{A_x}$ for the 7 m level for different accumulation rates taking $\sqrt{\frac{\omega}{2\kappa}} = 3{\cdot}3 \times 10^{-3}$.

TABLE 5.II.

U	$\frac{U}{2\kappa}$	$\alpha = \left(\sqrt{\frac{\omega}{2\kappa}} - \frac{U}{2\kappa}\right)$	$\frac{A_0}{A_{700}}$
0	0	$33{\cdot}0 \times 10^{-4}$	10·1
50	$0{\cdot}88 \times 10^{-4}$	$32{\cdot}2 \times 10^{-4}$	9·6
100	$1{\cdot}75 \times 10^{-4}$	$31{\cdot}2 \times 10^{-4}$	8·9
200	$3{\cdot}5 \times 10^{-4}$	$29{\cdot}5 \times 10^{-4}$	7·9

Thus, for example, if the amplitude at the surface is 10 C° then the amplitude at 7 m would be increased from 1·0 C° to 1·26 C° by an accumulation of 200 cm of snow per year.

Before using these values to correct the measured borehole temperatures for accumulation, to obtain the annual mean temperatures, it will be necessary to consider the effect of varying diffusivity with depth.

5.1.1.3. Effect of varying diffusivity

For the case of an accumulating snowfield with the snow diffusivity varying *linearly* with depth Benfield (1951) has shown that the temperature profile with depth

Loewe (1961) has shown that the temperatures of inland Antarctica are even lower than would be predicted from the normal decrease with elevation and latitude

Results from some sources, however, indicate that there may be a high geothermal flux in some parts of Antarctica. Rastorguyev (1961) reports that the presence of a high geothermal flux in the region of Victoria Land Coast has been confirmed. Zotikov (1961) obtains a thermal flux of $2{\cdot}5 \times 10^{-6}$ cal cm^{-2} sec^{-1} in a borehole drilled in the Mirny region through the ice and 2·5 m into the bedrock. This is also a high value, but Zotikov also reports that temperature measurements in lakes in the same region appear to indicate even higher values of geothermal flux.

From this, the value of $1{\cdot}4 \times 10^{-6}$ cal cm^{-2} sec^{-1} deduced above for the geothermal flux at Wilkes appears to be well within the range of

TABLE 5.VII.

Distance inland	km	15	30	63	80
Elevation	m	415	615	1015	1166
Ice thickness	m	345	701	961	1003
Accumulation ice	cm yr^{-1}	6	8	10	14
Temperature gradients:					
Calculated	°C/100 m	2·2	1·3	0·78	0·54
Observed	°C/100 m	2·0	1·4	0·4	

These gradients agree closely with the observed gradients near the coast but differ for 63 km inland. The movement rate near the coast for this profile may not be large (due to the obstruction provided by the Windmill Islands) so that the effect of movement on temperature profiles for the coastal positions has been disregarded. For the value at 63 km inland the observed gradient is lower and this may be due to the outward and downward movement of the surface, together with accumulation as suggested by Robin (1955). The effect of this movement on the temperature gradient will be considered shortly.

From equations (5.13) and (5.14) it may be seen that

(1) the *maximum* surface temperature gradient would be $\left(\frac{d\theta}{dh}\right)_{\text{base}} = \frac{q}{k}$, and would occur if $\dot{A} = 0$;

(2) the effect of an increase in the thickness (with accumulation held constant) is to cause a decrease in the *magnitude* of the surface temperature gradient;

(3) an increase in *accumulation* rate (with thickness held constant) also causes a decrease in the *magnitude* of the surface temperature gradient;

(4) the temperature gradient is always *positive* (ablation is not considered), hence the minimum value of temperature gradient is zero;

This velocity is small but is of the same order as that obtained from the movement survey for the region of S2, 32 km further inland.

5.2.5. Conclusion

and expected results, but further inland both movement and accumulation increase and so do the discrepancies. In the next section (5.2.3) the effect of accumulation and vertical movement will be considered and in section 5.2.4. the effect of horizontal movement.

5.2.3. Effect of accumulation and conduction on the ice temperature profile

Robin (1955) considers the effect of conduction and accumulation on the temperature profile, firstly with horizontal movement neglected. This situation will now be discussed and applied to the Wilkes ice cap.

Consider a part of the ice cap with thickness H and accumulation rate $\dot{A}$. If the rate at which the snow moves vertically downwards (while the shape remains constant) is taken as proportional to its distance from the base and if h is the height of the snow above the base at time t, then

$$-\frac{dh}{dt} = \frac{h}{H}\dot{A}. \tag{5.11}$$

The equation of linear heat conduction for the temperature θ at depth h and time t is

$$\frac{d\theta}{dt} = \kappa \frac{d^2\theta}{dh^2}, \tag{5.12}$$

where κ is the thermal diffusivity (assumed constant). Hence

$$\frac{d\theta}{dh}\frac{dh}{dt} = \kappa \frac{d^2\theta}{dh^2}$$

and substituting from equation (5.11) and integrating gives

$$\frac{d\theta}{dh} = \left(\frac{d\theta}{dh}\right)_{\text{base}} e^{-\frac{\dot{A}}{2H\kappa}h^2} \tag{5.13}$$

(Robin (1955)). This result gives the temperature gradient in the ice at any depth h, as a function of h, the thickness H, the accumulation rate $\dot{A}$, and the basal gradient $\left(\frac{d\theta}{dh}\right)_{\text{base}}$ which is equal to $\frac{q}{k}$ provided the basal temperature is not at melting point. It may be seen from this result that, in the case of zero accumulation, the temperature gradient reduces to that already considered, $\frac{q}{k}$, constant, throughout the thickness.

The temperature gradient at the surface is given for $h = H$ by

$$\left(\frac{d\theta}{dh}\right)_s = \left(\frac{d\theta}{dh}\right)_{\text{base}} e^{-\frac{\dot{A}}{2\kappa}H}. \tag{5.14}$$

From this equation values of $\left(\frac{d\theta}{dh}\right)_s$ have been calculated for the positions along the S2 trail.

Taking $\left(\frac{d\theta}{dh}\right)_{\text{base}} = 2{\cdot}8 \times 10^{-4}\ ^\circ\text{C cm}^{-1}$ we obtain the following temperature gradients shown in Table 5.VII.

TABLE 5.VII.

This velocity is small but is of the same order as that obtained from the movement survey for the region of S2, 32 km further inland.

5.2.5. Conclusion

A more complete analysis of the problem of temperature profiles could be carried out by making use of the analytical solution of the movement and conduction problem by Benfield (1949, 1951) (cf. also Radok (1959)) or by using the numerical solution of Jenssen and Radok (1960, 1963).

Alternatively, the effect of climatic change in absence of horizontal movement could have been studied, using the results of Wexler (1959) and Chi Tien (1960), However, it seems more realistic to consider *first* all the effects of the ice movement and accumulation and *then* attribute remaining discrepancies to climatic change.

As the results measured so far are well accounted for by the present treatment, more data will be required before the effect of climatic change could be analysed. In particular, a deep temperature gradient at the "centre dome" of the Budd Coast (approximately 112° 50′ E, 66° 40′ S) where horizontal movement is expected to be zero, should reveal the effect on the temperature profile of any recent climatic change.

However, at this stage, until inland ice velocities have been obtained, as well as deeper and more extensive temperature gradients, it is felt that a more advanced

6. SNOW AND ICE MASS FLUX IN THE WILKES REGION

6.0. Introduction

For the ice cap of the Budd Coast, cf. Figure 0.3, the Windmill Islands appear to form a blockage to the main ice flow from the plateau into Vincennes Bay. Consequently, the ice is channelled into the fast-moving ice streams to the south—the Vanderford and John Quincy Adams Glaciers—or to the north into the slower moving but more extensive ice cliffs from Cape Folger to Cape Poinsett.

The U.S. parties of 1957–8 (Cameron *et al* (1959) and Hollin *et al* (1961)) made measurements of the movement of Cape Folger, Vanderford Glacier and the plateau just above the moraine. Further inland at S2 a strain grid was set up, covering approximately 20 sq. km, to measure the relative deformation of the ice at the surface. A 35 m deep pit at S2 with a 2 m diameter tunnel at 30 m depth served to measure snow compaction and tunnel closure rates of the firn. These movement surveys were continued and extended in 1961.

The Budd Coast has a high centre dome approximately 30 km ESE of S2. From the contour pattern, cf. Figure 0.3, it appears that this whole region may have features of an independent ice cap, spreading at the boundaries and sinking at the centre, with supply being replenished by accumulation. The present movement survey will consider the processes involved in this mass flux, the ice lost by the movement process and the corresponding change in form. This will then be combined with the net accumulation pattern over the ice cap from Section 4 to give an estimate of the mass budget of the region.

First of all, from the measurements of firn compaction at S2, Section 6.1 studies the transition of the snow accumulated at the surface of the ice cap (density 0·4 g cm^{-3}) to the dense ice below. Section 6.2 analyses the results of the gradual contraction of the S2 ice tunnel, 30 m below the surface, throwing further light on the ice flow law parameters at this position. Section 6.3 analyses the movement measurements made on

$$\dot{\gamma} = \left(\frac{\tau}{B}\right)^n \tag{6.1}$$

(cf. Glen (1955)) where $\dot{\gamma}$ is the shear strain rate, τ is the shear stress and n and B are "flow law" parameters, largely dependent on temperature and type of ice. The fourth considers the horizontal and vertical movement in an ice model of non-uniform thickness in the line of motion.

These four types are as follows:

(i) Laminar flow of a flat sheet, or circular ice cap—partly applicable to the Cape Folger region.

(ii) Laminar flow of ice between two vertical boundaries at its edges—applicable to floating ice shelves or floating glacier tongues e.g. possibly the front of the Vanderford Glacier.

(iii) Laminar flow of a glacier over a bed of any prescribed cross-section—more generally used for the Vanderford Glacier.

(iv) Spreading of ice under its own weight and the resulting strain rates produced in particular in ice of decreasing thickness in the line of motion. This will be relevant to the ice plateau for the S2 strain grid and for the steep terminal region of the ice cap at Cape Folger.

Problems (i) and (ii) have been discussed, among others, by Nye (1952a, 1957) who also treated the particular case of a semicircular cross-sectional bed. An extension of the principle used for laminar flow in these studies has been found by the writer to permit the velocity distribution for other simple cross-sections to be calculated.

Problem (iv) has been dealt with by many writers, often with the aim of calculating the shape of the ice cap surface profile for balancing accumulation rates. As a rule however, only horizontal movement has been considered. Notable exceptions are the papers by Nye (1951, 1957) which treat the flow of a slab of ice of uniform depth on an inclined plane for steady state assuming a balancing accumulation rate. Most ice sheets and glaciers however, decrease in thickness as the terminus is approached (an example is the Wilkes ice cap at Cape Folger), so that the model of a uniform slab is inapplicable. The present study will consider the effect of this change in thickness, on the vertical and horizontal velocity distributions, the strain rates at the surface, the slide velocity at the base, and the resultant mass balance and change of shape of the glacier or ice cap. This will then be applied to the movement measurements made at S2 and Cape Folger.

The writer's theoretical analyses of (iii), the extension of the velocity profiles for laminar flow to that for an arbitrary cross-section, and (iv), the velocity distributions in an ice model of decreasing thickness, have proved rather lengthy. As the object of the present work is primarily the analysis and interpretation of the glaciological measurements carried out at Wilkes, only the major results of these theoretical studies will be given here for application to the ice movement data. The details of the derivation of the results will be presented in a more comprehensive survey of ice movement at a later date.

The two major results from the theoretical discussion which are to be used here are as follows:

(1) The velocity distribution for laminar flow in a glacier over a bed of arbitrary but constant cross-section.

Consider a glacier, density ρ, of constant cross-section moving down a slope α, under gravity g, such that the motion is everywhere parallel to the rock boundary. It is assumed that equal velocity surfaces are equidistant from the boundary and that the ice deforms according to a power law of the form $\varepsilon = \left(\frac{\sigma}{B}\right)^n$ with parameters n and B.

Then the velocity profile, perpendicular to the direction of flow, from the position of maximum velocity in the glacier to the boundary in the direction defined by a linear dimension, ξ_1 say, of the cross-section, is given by

$$u_c - u_\xi = C_{\xi_1}^n \left(\frac{\rho g \sin \alpha}{B}\right)^n \frac{\xi^{n+1}}{n+1}, \tag{6.2}$$

where u_c is the maximum velocity, u_ξ is the velocity at distance ξ from the maximum and C_{ξ_1} is the ratio of the cross-section area to the perimeter in terms of ξ_1.

(2) Velocity at the surface of an ice cap or glacier which decreases in thickness in the line of motion.

Consider a simple two dimensional model with a flat horizontal base and a linear sloping surface of small angle α. Take horizontal and vertical axes, x and y respectively, and let the surface profile be given by $y = H_0 - \alpha x$. Then if the ice is assumed to deform with constant viscosity η, the horizontal and vertical velocities at the surface, U_s and V_s respectively, at the point (x, y) are given by

$$U_s = U_0 + \frac{V_{s0}}{H_0} x + \frac{\rho g \alpha}{2\eta} H_0^2 - \frac{\rho g \alpha^4}{2\eta} x^2 \tag{6.3}$$

$$V_s = \frac{V_{s0}}{H_0} (H_0 - \alpha x), \tag{6.4}$$

where ρ is the ice density, g is the gravity acceleration, U_0 is the horizontal velocity at $x = 0$, $y = 0$, and V_{s0} the vertical velocity at the surface when $x = 0$. The longitudinal strain rate is given by

$$\frac{dU_s}{dx} = \frac{V_{s0}}{H_0} - \frac{\rho g \alpha^4}{\eta} x. \tag{6.5}$$

6.1. FIRN COMPACTION: S2 PIT

6.1.0. Introduction

In the 35 m deep pit at S2 measurements have been made of the vertical distances between dowels placed at various depths in the pit wall, cf. Figure 6.1. An initial measurement was made in January 1959, and subsequent measurements were made twice in 1960 and twice in 1961. From these the average compaction rates since 1959 have been calculated and are shown in Table 6.1. Their differences, however, are small and it is difficult to observe any change of compaction rate over small time

and expected results, but further inland both movement and accumulation increase and so do the discrepancies. In the next section (5.2.3) the effect of accumulation and vertical movement will be considered and in section 5.2.4. the effect of horizontal movement.

5.2.3. Effect of accumulation and conduction on the ice temperature profile

Robin (1955) considers the effect of conduction and accumulation on the temperature profile, firstly with horizontal movement neglected. This situation will now be discussed and applied to the Wilkes ice cap.

Consider a part of the ice cap with thickness H and accumulation rate $\dot{A}$. If the rate at which the snow moves vertically downwards (while the shape remains constant) is taken as proportional to its distance from the base and if h is the height of the snow above the base at time t, then

$$-\frac{dh}{dt} = \frac{h}{H}\dot{A}. \tag{5.11}$$

The equation of linear heat conduction for the temperature θ at depth h and time t is

$$\frac{d\theta}{dt} = \kappa \frac{d^2\theta}{dh^2}, \tag{5.12}$$

where κ is the thermal diffusivity (assumed constant). Hence

$$\frac{d\theta}{dh}\frac{dh}{dt} = \kappa \frac{d^2\theta}{dh^2}$$

and substituting from equation (5.11) and integrating gives

$$\frac{d\theta}{dh} = \left(\frac{d\theta}{dh}\right)_{\text{base}} e^{-\frac{\dot{A}}{2H\kappa}h^2} \tag{5.13}$$

(Robin (1955)). This result gives the temperature gradient in the ice at any depth h, as a function of h, the thickness H, the accumulation rate $\dot{A}$, and the basal gradient $\left(\frac{d\theta}{dh}\right)_{\text{base}}$ which is equal to $\frac{q}{k}$ provided the basal temperature is not at melting point. It may be seen from this result that, in the case of zero accumulation, the temperature gradient reduces to that already considered, $\frac{q}{k}$, constant, throughout the thickness.

The temperature gradient at the surface is given for $h = H$ by

$$\left(\frac{d\theta}{dh}\right)_s = \left(\frac{d\theta}{dh}\right)_{\text{base}} e^{-\frac{\dot{A}}{2\kappa}H}. \tag{5.14}$$

From this equation values of $\left(\frac{d\theta}{dh}\right)_s$ have been calculated for the positions along the S2 trail.

Taking $\left(\frac{d\theta}{dh}\right)_{\text{base}} = 2{\cdot}8 \times 10^{-4}\,^{\circ}\text{C cm}^{-1}$ we obtain the following temperature gradients shown in Table 5.VII.

TABLE 5.VII.

Distance inland	km	15	30	63	80
Elevation	m	415	615	1015	1166
Ice thickness	m	345	701	961	1003
Accumulation ice	cm yr^{-1}	6	8	10	14
Temperature gradients:					
Calculated	°C/100 m	2·2	1·3	0·78	0·54
Observed	°C/100 m	2·0	1·4	0·4	

These gradients agree closely with the observed gradients near the coast but differ for 63 km inland. The movement rate near the coast for this profile may not be large (due to the obstruction provided by the Windmill Islands) so that the effect of movement on temperature profiles for the coastal positions has been disregarded. For the value at 63 km inland the observed gradient is lower and this may be due to the outward and downward movement of the surface, together with accumulation as suggested by Robin (1955). The effect of this movement on the temperature gradient will be considered shortly.

From equations (5.13) and (5.14) it may be seen that

(1) the *maximum* surface temperature gradient would be $\left(\frac{d\theta}{dh}\right)_{\text{base}} = \frac{q}{k}$, and would occur if $\dot{A} = 0$;

(2) the effect of an increase in the thickness (with accumulation held constant) is to cause a decrease in the *magnitude* of the surface temperature gradient;

(3) an increase in *accumulation* rate (with thickness held constant) also causes a decrease in the *magnitude* of the surface temperature gradient;

(4) the temperature gradient is always *positive* (ablation is not considered), hence the minimum value of temperature gradient is zero;

(5) the temperature gradient increases with depth from a minimum at the surface to a maximum at the base.

Basal Temperatures. Integrating equation (5.13) Robin (1955) obtains for the temperature difference between the surface and height h

$$\theta_H - \theta_h = \left(\frac{d\theta}{dh}\right)_b \sqrt{\frac{2H\kappa}{\dot{A}}} \left[\operatorname{erf}\left(\sqrt{\frac{\dot{A}}{2H\kappa}} \cdot h\right)\right]_h^H,$$

where $\operatorname{erf} x = \int_0^x e^{-y^2}\, dy$, which for $h = 0$, at the bedrock, becomes

$$\theta_H - \theta_h = \left(\frac{d\theta}{dh}\right)_b \sqrt{\frac{2H\kappa}{\dot{A}}} \operatorname{erf} \sqrt{\frac{\dot{A}H}{2\kappa}}.$$

From this the basal temperatures have been calculated for the Wilkes ice cap and are shown for the respective positions inland in Table 5.VIII.

and expected results, but further inland both movement and accumulation increase and so do the discrepancies. In the next section (5.2.3) the effect of accumulation and vertical movement will be considered and in section 5.2.4. the effect of horizontal movement.

5.2.3. Effect of accumulation and conduction on the ice temperature profile

Robin (1955) considers the effect of conduction and accumulation on the temperature profile, firstly with horizontal movement neglected. This situation will now be discussed and applied to the Wilkes ice cap.

Consider a part of the ice cap with thickness H and accumulation rate $\dot{A}$. If the rate at which the snow moves vertically downwards (while the shape remains constant) is taken as proportional to its distance from the base and if h is the height of the snow above the base at time t, then

$$-\frac{dh}{dt} = \frac{h}{H}\dot{A}. \tag{5.11}$$

The equation of linear heat conduction for the temperature θ at depth h and time t is

$$\frac{d\theta}{dt} = \kappa \frac{d^2\theta}{dh^2}, \tag{5.12}$$

where κ is the thermal diffusivity (assumed constant). Hence

$$\frac{d\theta}{dh}\frac{dh}{dt} = \kappa \frac{d^2\theta}{dh^2}$$

and substituting from equation (5.11) and integrating gives

$$\frac{d\theta}{dh} = \left(\frac{d\theta}{dh}\right)_{\text{base}} e^{-\frac{\dot{A}}{2H\kappa}h^2} \tag{5.13}$$

(Robin (1955)). This result gives the temperature gradient in the ice at any depth h, as a function of h, the thickness H, the accumulation rate $\dot{A}$, and the basal gradient $\left(\frac{d\theta}{dh}\right)_{\text{base}}$ which is equal to $\frac{q}{k}$ provided the basal temperature is not at melting point. It may be seen from this result that, in the case of zero accumulation, the temperature gradient reduces to that already considered, $\frac{q}{k}$,constant, throughout the thickness.

The temperature gradient at the surface is given for $h = H$ by

$$\left(\frac{d\theta}{dh}\right)_s = \left(\frac{d\theta}{dh}\right)_{\text{base}} e^{-\frac{\dot{A}}{2\kappa}H}. \tag{5.14}$$

From this equation values of $\left(\frac{d\theta}{dh}\right)_s$ have been calculated for the positions along the S2 trail.

Taking $\left(\frac{d\theta}{dh}\right)_{\text{base}} = 2{\cdot}8 \times 10^{-4}\,^{\circ}\text{C cm}^{-1}$ we obtain the following temperature gradients shown in Table 5.VII.

TABLE 5.VII.

Distance inland	km	15	30	63	80
Elevation	m	415	615	1015	1166
Ice thickness	m	345	701	961	1003
Accumulation ice	cm yr^{-1}	6	8	10	14
Temperature gradients:					
Calculated	°C/100 m	2·2	1·3	0·78	0·54
Observed	°C/100 m	2·0	1·4	0·4	

These gradients agree closely with the observed gradients near the coast but differ for 63 km inland. The movement rate near the coast for this profile may not be large (due to the obstruction provided by the Windmill Islands) so that the effect of movement on temperature profiles for the coastal positions has been disregarded. For the value at 63 km inland the observed gradient is lower and this may be due to the outward and downward movement of the surface, together with accumulation as suggested by Robin (1955). The effect of this movement on the temperature gradient will be considered shortly.

From equations (5.13) and (5.14) it may be seen that

(1) the *maximum* surface temperature gradient would be $\left(\frac{d\theta}{dh}\right)_{\text{base}} = \frac{q}{k}$, and would occur if $\dot{A} = 0$;

(2) the effect of an increase in the thickness (with accumulation held constant) is to cause a decrease in the *magnitude* of the surface temperature gradient;

(3) an increase in *accumulation* rate (with thickness held constant) also causes a decrease in the *magnitude* of the surface temperature gradient;

(4) the temperature gradient is always *positive* (ablation is not considered), hence the minimum value of temperature gradient is zero;

(5) the temperature gradient increases with depth from a minimum at the surface to a maximum at the base.

Basal Temperatures. Integrating equation (5.13) Robin (1955) obtains for the temperature difference between the surface and height h

$$\theta_H - \theta_h = \left(\frac{d\theta}{dh}\right)_b \sqrt{\frac{2H\kappa}{\dot{A}}} \left[\operatorname{erf}\left(\sqrt{\frac{\dot{A}}{2H\kappa}} \cdot h\right)\right]_h^H,$$

where $\operatorname{erf} x = \int_0^x e^{-y^2}\, dy$, which for $h = 0$, at the bedrock, becomes

$$\theta_H - \theta_h = \left(\frac{d\theta}{dh}\right)_b \sqrt{\frac{2H\kappa}{\dot{A}}} \operatorname{erf} \sqrt{\frac{\dot{A}H}{2\kappa}}.$$

From this the basal temperatures have been calculated for the Wilkes ice cap and are shown for the respective positions inland in Table 5.VIII.

TABLE 5.VIII.

BASAL TEMPERATURES FOR THE WILKES ICE CAP.

Distance Inland	km	15	30	63	80
Elevation	m	415	615	1015	1166
Thickness	m	345	701	961	1003
Surface Temperature, θ_H	°C	−12·2	−14·2	−18·0	−19·6
$\theta_H - \theta_b$	°C	−8·9	−15·5	−15·7	−17·2
θ_b	°C	−3·3	+1·3	−2·2	−2·4

Unlike the basal temperatures obtained for a stationary ice cap of zero accumulation, the new basal temperatures appear to stay below zero inland, except for the position 30 km inland where the bedrock is below sea level. These lower basal temperatures are a result of the lowering of the temperature gradient due to accumulation. Consequently, the basal melting previously obtained would not occur. The temperatures, however, are not far below the pressure melting point and a higher value of geothermal flux, or friction due to movement (which has not been considered here), may provide sufficient heat for melting to occur. To test for these effects, temperature gradients measured to far greater depths would be necessary.

5.2.4. Effect of horizontal movement

Robin (1955) discusses the cause of a negative temperature gradient at the surface of an ice cap due to the outward and downward movement of the surface together with accumulation. Provided the boundary conditions are the same, i.e. for a steady state and slow movement, the effect of this negative gradient would be superimposable upon the gradient calculated from accumulation conduction and vertical movement only.

The result of the movement surveys at Wilkes indicate that the movement along the S2 trail is small, and as the observed temperature gradient is less than the gradient calculated from conduction, Robin's result will be used to obtain a velocity which would give a negative gradient to account for the discrepancy.

Robin's result is that for a steady state ice cap, where the surface velocity is V, the surface slope α, the accumulation rate $\dot{A}$, and where the rate of change of air temperature with height is λ, the temperature gradient at the surface is given by

$$\frac{d\theta}{dh} = -\frac{V\alpha\lambda}{\dot{A}}.$$

For the position 63 km inland of Wilkes we have $\alpha = 0{\cdot}011$, $\lambda = 0{\cdot}90$°C/100 m and $\dot{A} = 10$ cm water/yr. With these values the difference between the measured surface temperature gradient and that calculated for zero horizontal velocity becomes 0·38 °C/100 m. Then

$$V = \frac{d\theta}{dh}\frac{\dot{A}}{\lambda\alpha}$$

$$= \frac{0{\cdot}38 \times 10}{0{\cdot}90 \times 0{\cdot}011} \text{ cm yr}^{-1}$$

$$= 3.8 \text{ m yr}^{-1}.$$

This velocity is small but is of the same order as that obtained from the movement survey for the region of S2, 32 km further inland.

5.2.5. Conclusion

A more complete analysis of the problem of temperature profiles could be carried out by making use of the analytical solution of the movement and conduction problem by Benfield (1949, 1951) (cf. also Radok (1959)) or by using the numerical solution of Jenssen and Radok (1960, 1963).

Alternatively, the effect of climatic change in absence of horizontal movement could have been studied, using the results of Wexler (1959) and Chi Tien (1960), However, it seems more realistic to consider *first* all the effects of the ice movement and accumulation and *then* attribute remaining discrepancies to climatic change.

As the results measured so far are well accounted for by the present treatment, more data will be required before the effect of climatic change could be analysed. In particular, a deep temperature gradient at the "centre dome" of the Budd Coast (approximately 112° 50′ E, 66° 40′ S) where horizontal movement is expected to be zero, should reveal the effect on the temperature profile of any recent climatic change.

However, at this stage, until inland ice velocities have been obtained, as well as deeper and more extensive temperature gradients, it is felt that a more advanced account would be premature.

APPENDIX TO SECTION 5

1. Benfield's solution for zero accumulation

i.e. of

$$\kappa \frac{\partial^2 \theta}{\partial x^2} = \frac{\partial \theta}{\partial t}$$

with an imposed surface temperature, say,

$$\begin{aligned} \theta(o, t) &= A + B \cos(\omega t + \varepsilon) \\ &= A + R\{B \exp[i(\omega t + \varepsilon)]\}. \end{aligned}$$

The solution $\theta(x, t)$ has the form

$$\theta(x, t) = \theta_1 + \theta_2,$$

where

$$\theta_1 = A \operatorname{erf} \frac{x}{2\sqrt{\kappa t}}$$

and

$$\theta_2 = \frac{B}{2} \exp i(\omega t + \varepsilon) \left\{ \exp x \sqrt{\frac{i\omega}{\kappa}} \cdot \operatorname{erf} \left[\frac{x}{2\sqrt{\kappa t}} + \sqrt{i\omega}\, t \right] \right.$$

$$\left. + \exp - x \sqrt{\frac{i\omega}{\kappa}} \cdot \operatorname{erf} \left[\frac{x}{2\sqrt{\kappa t}} - \sqrt{i\omega}\, t \right] \right\}.$$

2. Benfield's solution for surface accumulation rate v

The differential equation is

$$\kappa \frac{\partial^2 \theta}{\partial x^2} - v \frac{\partial \theta}{\partial x} = \frac{\partial \theta}{\partial t}.$$

Surface temperature

$$T(o, t) = A + B \cos(\omega t + \varepsilon) = A + R[B\, e^{i(\omega t + \varepsilon)}].$$

We require the real part of

$$T = T_1 + T_2,$$

where

$$T_1 = \frac{A}{2}\left[e^{\frac{vx}{\kappa}} \operatorname{erf} \frac{x + vt}{2\sqrt{\kappa t}} + \operatorname{erf} \frac{x - vt}{2\sqrt{\kappa t}}\right]$$

and

$$T_2 = \frac{B}{2} e^{i(\omega t + \varepsilon)} e^{\frac{vx}{2k}} \left\{ e^{x\sqrt{\frac{i\omega}{k} + \frac{v^2}{4k^2}}} \cdot \operatorname{erf}\left[\frac{x}{2\sqrt{\kappa t}} + \sqrt{i\omega + \frac{v^2}{4\kappa^2}}\, t\right] \right.$$
$$\left. + e^{-x\sqrt{\frac{i\omega}{\kappa} + \frac{v^2}{4\kappa^2}}} \cdot \operatorname{erf}\left[\frac{x}{2\sqrt{\kappa t}} - \sqrt{i\omega + \frac{v^2}{4\kappa^2}}\, t\right]\right\}.$$

(The effect of the error function dies out as time increases, i.e. erf $t \to 1$ as $t \to \infty$.)

6. SNOW AND ICE MASS FLUX IN THE WILKES REGION

6.0. Introduction

For the ice cap of the Budd Coast, cf. Figure 0.3, the Windmill Islands appear to form a blockage to the main ice flow from the plateau into Vincennes Bay. Consequently, the ice is channelled into the fast-moving ice streams to the south—the Vanderford and John Quincy Adams Glaciers—or to the north into the slower moving but more extensive ice cliffs from Cape Folger to Cape Poinsett.

The U.S. parties of 1957–8 (Cameron *et al* (1959) and Hollin *et al* (1961)) made measurements of the movement of Cape Folger, Vanderford Glacier and the plateau just above the moraine. Further inland at S2 a strain grid was set up, covering approximately 20 sq. km, to measure the relative deformation of the ice at the surface. A 35 m deep pit at S2 with a 2 m diameter tunnel at 30 m depth served to measure snow compaction and tunnel closure rates of the firn. These movement surveys were continued and extended in 1961.

The Budd Coast has a high centre dome approximately 30 km ESE of S2. From the contour pattern, cf. Figure 0.3, it appears that this whole region may have features of an independent ice cap, spreading at the boundaries and sinking at the centre, with supply being replenished by accumulation. The present movement survey will consider the processes involved in this mass flux, the ice lost by the movement process and the corresponding change in form. This will then be combined with the net accumulation pattern over the ice cap from Section 4 to give an estimate of the mass budget of the region.

First of all, from the measurements of firn compaction at S2, Section 6.1 studies the transition of the snow accumulated at the surface of the ice cap (density 0·4 g cm^{-3}) to the dense ice below. Section 6.2 analyses the results of the gradual contraction of the S2 ice tunnel, 30 m below the surface, throwing further light on the ice flow law parameters at this position. Section 6.3 analyses the movement measurements made on the Vanderford Glacier to show how further information may be obtained regarding the ice flow law parameters and also the cross-section profile. Section 6.4 uses the movement measurements carried out at Cape Folger to estimate an "effective average viscosity" there. The strain grid movement at S2 is analysed to obtain an estimate of absolute velocity inland, on the assumption of a balanced mass flux, and also estimates are made of the effective average viscosity of the region. Finally, section 6.5 combines the results of the movement surveys to calculate the rate of net ice loss at the coast of the region; by comparing this with the measure of net accumulation over the area from Section 4 a measure of the mass budget for the region is obtained.

In order to carry out the analysis of Section 6.3 it has been necessary to make a study of four types of ice movement. The first three of these are concerned with laminar flow for a constant cross-section, under gravity, down a steady slope, assuming a flow law for ice of the form

$$\dot{\gamma} = \left(\frac{\tau}{B}\right)^n \tag{6.1}$$

(cf. Glen (1955)) where $\dot{\gamma}$ is the shear strain rate, τ is the shear stress and n and B are "flow law" parameters, largely dependent on temperature and type of ice. The fourth considers the horizontal and vertical movement in an ice model of non-uniform thickness in the line of motion.

These four types are as follows:

(i) Laminar flow of a flat sheet, or circular ice cap—partly applicable to the Cape Folger region.

(ii) Laminar flow of ice between two vertical boundaries at its edges—applicable to floating ice shelves or floating glacier tongues e.g. possibly the front of the Vanderford Glacier.

(iii) Laminar flow of a glacier over a bed of any prescribed cross-section—more generally used for the Vanderford Glacier.

(iv) Spreading of ice under its own weight and the resulting strain rates produced in particular in ice of decreasing thickness in the line of motion. This will be relevant to the ice plateau for the S2 strain grid and for the steep terminal region of the ice cap at Cape Folger.

Problems (i) and (ii) have been discussed, among others, by Nye (1952a, 1957) who also treated the particular case of a semicircular cross-sectional bed. An extension of the principle used for laminar flow in these studies has been found by the writer to permit the velocity distribution for other simple cross-sections to be calculated.

Problem (iv) has been dealt with by many writers, often with the aim of calculating the shape of the ice cap surface profile for balancing accumulation rates. As a rule however, only horizontal movement has been considered. Notable exceptions are the papers by Nye (1951, 1957) which treat the flow of a slab of ice of uniform depth on an inclined plane for steady state assuming a balancing accumulation rate. Most ice sheets and glaciers however, decrease in thickness as the terminus is approached (an example is the Wilkes ice cap at Cape Folger), so that the model of a uniform slab is inapplicable. The present study will consider the effect of this change in thickness, on the vertical and horizontal velocity distributions, the strain rates at the surface, the slide velocity at the base, and the resultant mass balance and change of shape of the glacier or ice cap. This will then be applied to the movement measurements made at S2 and Cape Folger.

The writer's theoretical analyses of (iii), the extension of the velocity profiles for laminar flow to that for an arbitrary cross-section, and (iv), the velocity distributions in an ice model of decreasing thickness, have proved rather lengthy. As the object of the present work is primarily the analysis and interpretation of the glaciological measurements carried out at Wilkes, only the major results of these theoretical studies will be given here for application to the ice movement data. The details of the derivation of the results will be presented in a more comprehensive survey of ice movement at a later date.

The two major results from the theoretical discussion which are to be used here are as follows:

(1) The velocity distribution for laminar flow in a glacier over a bed of arbitrary but constant cross-section.

Consider a glacier, density ρ, of constant cross-section moving down a slope α, under gravity g, such that the motion is everywhere parallel to the rock boundary. It is assumed that equal velocity surfaces are equidistant from the boundary and that the ice deforms according to a power law of the form $\varepsilon = \left(\frac{\sigma}{B}\right)^n$ with parameters n and B.

Then the velocity profile, perpendicular to the direction of flow, from the position of maximum velocity in the glacier to the boundary in the direction defined by a linear dimension, ξ_1 say, of the cross-section, is given by

$$u_c - u_\xi = C_{\xi_1}^n \left(\frac{\rho g \sin \alpha}{B}\right)^n \frac{\xi^{n+1}}{n+1}, \tag{6.2}$$

where u_c is the maximum velocity, u_ξ is the velocity at distance ξ from the maximum and C_{ξ_1} is the ratio of the cross-section area to the perimeter in terms of ξ_1.

(2) Velocity at the surface of an ice cap or glacier which decreases in thickness in the line of motion.

Consider a simple two dimensional model with a flat horizontal base and a linear sloping surface of small angle α. Take horizontal and vertical axes, x and y respectively, and let the surface profile be given by $y = H_0 - \alpha x$. Then if the ice is assumed to deform with constant viscosity η, the horizontal and vertical velocities at the surface, U_s and V_s respectively, at the point (x, y) are given by

$$U_s = U_0 + \frac{V_{s0}}{H_0} x + \frac{\rho g \alpha}{2\eta} H_0^2 - \frac{\rho g \alpha^4}{2\eta} x^2 \tag{6.3}$$

$$V_s = \frac{V_{s0}}{H_0} (H_0 - \alpha x), \tag{6.4}$$

where ρ is the ice density, g is the gravity acceleration, U_0 is the horizontal velocity at $x = 0$, $y = 0$, and V_{s0} the vertical velocity at the surface when $x = 0$. The longitudinal strain rate is given by

$$\frac{dU_s}{dx} = \frac{V_{s0}}{H_0} - \frac{\rho g \alpha^4}{\eta} x. \tag{6.5}$$

6.1. FIRN COMPACTION: S2 PIT

6.1.0. Introduction

In the 35 m deep pit at S2 measurements have been made of the vertical distances between dowels placed at various depths in the pit wall, cf. Figure 6.1. An initial measurement was made in January 1959, and subsequent measurements were made twice in 1960 and twice in 1961. From these the average compaction rates since 1959 have been calculated and are shown in Table 6.1. Their differences, however, are small and it is difficult to observe any change of compaction rate over small time

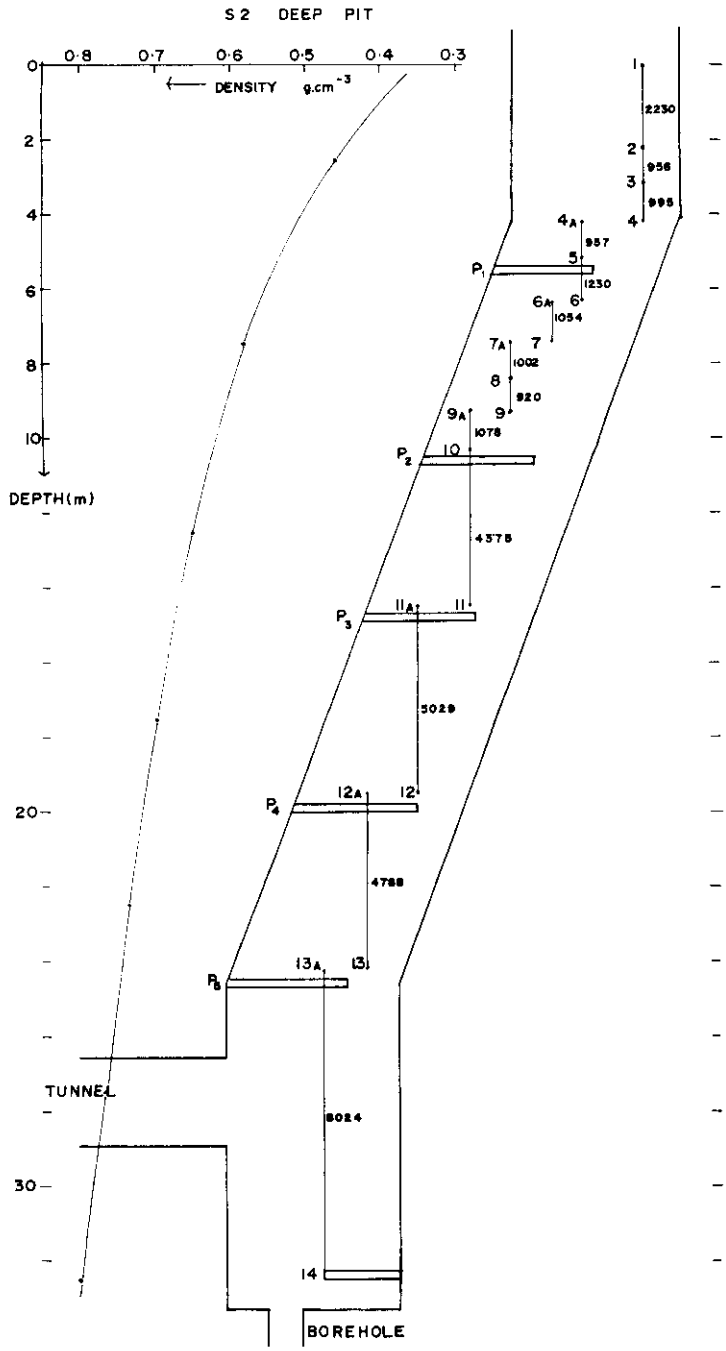

FIG. 6.1. S2 PIT AND TUNNEL (from Cameron et al. (1959)). The positions of the marker dowels and the platforms are shown with the vertical distances to scale as at January 1959.

TABLE 6.I.

S2 PIT FIRN COMPACTION MEASUREMENTS (l mm) AND RATES $\left(\frac{dl}{dx}\ \%\ \mathrm{yr}^{-1}\right)$.

Yrs. from Jan. 1959:		1·29		1·92		2·54		2·75	
Dowel Intervals	l	$\frac{dl}{dx}$	l	$\frac{dl}{dx}$	l	$\frac{dl}{dx}$	l	$\frac{dl}{dx}$	l
1–2	2230	2·92	2146	2·03	2143	1·98	2118	2·19	2096
2–3	956	1·38	939	1·36	931	1·36	923	1·22	924
3–4	995	1·25	979	1·41	968	1·11	967	1·54	953
4–4*A*	1		3		15		8		7
4*A*–5	957	1·94	933	1·58	928	0·45	946	0·80	936
5–6	1230	0·38	1214	0·72	1213	0·77	1206	0·89	1200
6–6*A*	23		22		40		26		27
6*A*–7	1054	0·52	1047	0·54	1043	0·60	1038	0·55	1038
7–7*A*	33		31		35		35		32
7*A*–8	1002	0·77	992	0·57	991	0·47	990	0·47	989
8–9	920	0·67	912	0·51	911	0·68	904	0·67	903
9–9*A*	31		27		65		30		30
9*A*–10	1018	0·46	1012	0·26	1013	0·31	1010	0·29	1010
10–11	4375	0·41	4352	0·38	4343	0·36	4335	0·36	4332
11–11*A*	13		13				9		15
11*A*–12	5029	0·42	5002	0·27	5003	0·23	4999	0·37	4978
12–12*A*	75		70		115		76		84
12*A*–14*A*	12822		12820		12820	0·23	12747	0·25	12733
Sum	32588		32360		32332		32183		32082
Average		0·68		0·63		0·55		0·54	

intervals. The two obtained for 1960 have therefore been averaged and similarly the two for 1961. These two average values were then smoothed and are shown in Table 6.II and are plotted in Figure 6.2.

TABLE 6.II.

S2 PIT SMOOTHED AVERAGE COMPACTION RATES.

Depth m	Interval mm	Compaction Rates % yr^{-1}	
Time yrs. →		1·6	2·64
1·12	2230	2·48	2·09
2·71	956	1·73	1·57
3·68	995	1·49	1·08
4·66	957	1·32	0·93
5·75	1230	1·06	0·68
6·90	1054	0·69	0·63
7·92	1002	0·59	0·57
8·88	920	0·54	0·49
9·85	1018	0·45	0·46
12·55	4375	0·37	0·34
17·25	5029	0·35	0·30
26·18	12820	0·25	0·24

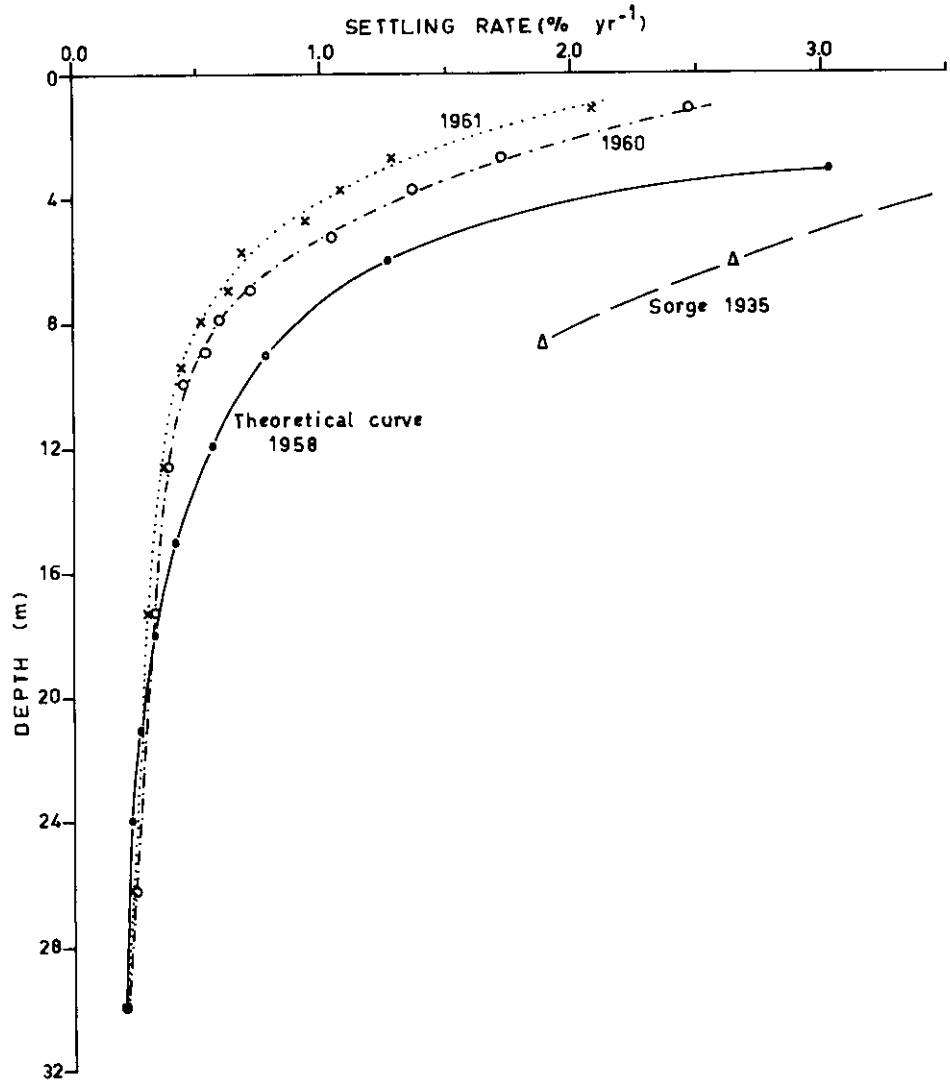

FIG. 6.2. S2 FIRN SETTLING RATES. The compaction rates smoothed from the measurements of 1960 and 1961 are plotted against the original depth of the positions in 1958. Since then the positions have become further below the surface by the amount of accumulation of snow at the surface. This corresponds to the vertical shift between the measured rates and the theoretical curve of 1958 of about 2.5 m of snow accumulation. Sorge's (1935) Greenland values are shown to be considerably higher.

There is no distinguishable difference in the rates at the lower levels, where the rate is slow and the density is high. The two curves diverge further as the surface is approached. If Sorge's law (cf. Bader (1954)) is applied (i.e. the density profile from the surface remains constant in time), the difference would be just the accumulation of snow over the period. The curves agree with this as well as can be expected from

the accuracy of the measurements, for if the top curve is moved downwards by 80cm it coincides very closely with the second curve. This value of 80 cm corresponds to an accumulation of 32 cm of water over the pit. The value at the stake of the relative movement network (about 50 m from the pit) gave an average of 19 cm of water (the average for the whole network being 14 cm water). Because of the large drifts built up in the station area an accurate measurement of the accumulation over the pit is not available.

6.1.1. Derivation of settling rate relation

The theory of the settling rate of the firn has been discussed, among others, by Bader (1954) and Schytt (1958). Schytt (1958, p. 54), defining the settling rate S at a depth x in the snow at time t as

$$S = \frac{dx}{x \,.\, dt},$$

obtained a relationship of the form

$$S = -\frac{1}{\rho}\frac{d\rho}{dt},$$

where ρ is the density at depth x.

The average thickness of annual strata in the 11 m pit, A cm, say, was taken by Schytt as the average accumulation rate $\frac{dx}{dt}$, so that the depth x became related to the time t by $x = At$ and hence

$$S = -\frac{A}{\rho}\frac{d\rho}{dx} \quad (\text{time}^{-1}).$$

This expression gives the *average* settling rate over the interval and Schytt found a value of $1{\cdot}6 \times 10^{-2}$ yrs^{-1} for the pit at Maudheim where the accumulation rate was 0·681 m of snow/year (as measured from pit strata).

Schytt's analysis, however, neglects the compression of the annual strata with depth, i.e. the fact that $v \equiv \frac{dx}{dt}$, the velocity of downward motion of a layer, is not constant with depth. (Schytt himself pointed out that this feature existed but his data were not sufficiently detailed to bring out the variation of settling rate with depth.)

Bader (1954) derived an expression for the settling rate at a given depth for a given constant accumulation rate, and the assumption that Sorge's density law applies, as follows:

Let σ_x be the total mass of snow above a depth x below the surface. If $\rho(x)$ again represents the density profile as a function of depth, then

$$\sigma_x = \int_0^x \rho \, dx. \tag{6.6}$$

Also, if t is the time taken by a layer to reach a depth x, after starting from the surface, and if A is the accumulation rate (in gm cm^{-2}) remaining constant with time, then

$$\sigma_x = At. \tag{6.7}$$

From this Bader finds

$$d\sigma = A\,dt \qquad \text{from (6.7)}$$

and

$$d\sigma = \frac{\rho + (\rho + \delta\rho)}{2}\,dx = \rho\,d\rho \qquad \text{from (6.6).}$$

Hence $\dfrac{dx}{dt} = \dfrac{A}{\rho} = v$, say, the velocity of downward travel of a layer at depth x. The settling rate is then given by

$$S = \frac{dv}{dx} = -\frac{A}{\rho^2}\frac{d\rho}{dx} \tag{6.8}$$

and is expressed in terms of the density profile and accumulation rate, both assumed constant.

An alternative derivation follows immediately from Sorge's law and the condition of continuity. Let ρ and v be the density and downward velocity of the firn distance x below the surface respectively. Now Sorge's law states that the density profile remains constant in time. Hence continuity demands

$$\frac{d(\rho v)}{dx} = 0.$$

Therefore $\rho v = c$, say a constant.
Now when $\rho = \rho_0$ (at the surface), $v = a$, the accumulation rate of *snow* at the surface,

Therefore $c = a\rho_0$

$$v = a\frac{\rho_0}{\rho} \tag{6.9}$$

and $$S \equiv \frac{dv}{dx} = -a\frac{\rho_0}{\rho^2}\frac{d\rho}{dx}. \tag{6.10}$$

In Bader's result $\left(v = \dfrac{A}{\rho}\right)$, A is the accumulation rate in water equivalent so that $A = a\rho_0$, showing the two results are identical. Further the above derivation shows that if Sorge's law were to hold for an accumulation rate that varied with time, the quantity c would be a function of time t, and the same result would hold except that a, and hence v, and S would be similarly dependent upon time.

6.1.2. *Theoretical density profiles*

Before Bader's theoretical results for settling rate can be used it is necessary to know the density profile with depth. Besides various empirical depth density profiles, Schytt (1958) discusses two theoretical profiles.

(1) "The fractional change in air space volume per unit depth is a constant" (Schytt (1958), p. 120).

Let V be the air space per unit volume of depth x and snow density ρ, and ρ_i be the density of ice. Then

$$V = \frac{\rho_i - \rho}{\rho_i}$$

gives

$$dV = -\frac{d\rho}{\rho_i},$$

and the postulate (1) implies

$$\frac{1}{V}\frac{dV}{dx} = c \text{ say, a constant.} \tag{6.11}$$

Hence

$$\frac{\rho_i}{\rho_i - \rho}\left(-\frac{d\rho}{\rho_i}\right) = c\,dx.$$

Integration gives

$$\log \frac{1}{\rho_i - \rho} = cx + c_1 \text{ another constant,}$$

so that

$$\rho_i - \rho = c_1 \mathrm{e}^{-cx},$$

where c_1 is a constant equal to $\rho_i - \rho_0$, ρ_0 being the density at the surface. Finally,

$$\rho = \rho_i - c_1 \mathrm{e}^{-cx} \tag{6.12}$$

and Schytt's values of the constants giving the best fit to his data were $c_1 = 0{\cdot}467$, $c = 0{\cdot}0258$.

(2) An alternative density profile was derived by Schytt from Robin's postulate (Schytt (1958), p. 120): "the proportional change in air space in the firn is in linear proportion to the change in stress due to the weight of material above a given level".

With the same symbols as before, and if $\sigma_x = \int_0^x \rho\,dx$ is the load above the level x, then

$$\frac{d\sigma_x}{dx} = \rho,$$

so that Robin's assumption becomes

$$\frac{1}{V}\frac{dV}{dx} = -c_2\frac{d\sigma_x}{dx} \qquad (c_2 \text{ a positive constant}),$$

hence

$$\frac{1}{V}\frac{dV}{dx} = -c_2\rho. \tag{6.13}$$

Substituting for V this becomes

$$\frac{d\rho}{\rho(\rho_i - \rho)} = c_2\,dx$$

and integrating we obtain

$$\frac{\rho}{\rho_i - \rho} = c_3 \, e^{cx} \qquad (c_3 \text{ constant}), \tag{6.14}$$

the other profile used by Schytt.

The relation between these two density profiles and their assumptions is brought out more clearly by expressing (6.14) in the form

$$\frac{1}{\rho} = \frac{1}{\rho_i} + c_4 \, e^{-c_2 x}, \tag{6.15}$$

where $c_4 = \dfrac{1}{c_3 \rho_i}$.

6.1.3. Calculation of theoretical settling rates.

All these theoretical formula, however, do not give a good fit to the S2 density profile obtained in 1957 (Cameron *et al* (1959)), especially in the top 10 m. Therefore, to obtain density and density gradient in Bader's relation,

$$S = -\frac{A}{\rho^2}\frac{d\rho}{dx},$$

the empirical values for density were taken from the smoothed curve of mean density of Cameron (1959). Similarly, the density gradients were obtained from the slopes of this curve at the various depths. The value of A used was 20 cm of water. The resulting curve, shown in Figure 6.2, has the same shape as the measured results, but gives slightly smaller compaction rates for greater depths. Also, the theoretical curve (calculated from the 1957 density values) and the empirical curve correspond closely to each other with a vertical shift of 2·5 m. This value is slightly higher than the estimated 2 m accumulation of snow over the pit during the period.

A difficulty in interpretation arises here because the accumulation rate since the construction of the pit has been considerably higher, due to local snow drifts in the station area, than the previous average rate, as measured from the pit strata. If the average annual accumulation of 13·7 cm of water as determined by Cameron had been used, then the curve (*c*) in Figure 6.3 would have been obtained. This curve gives values of compaction rate at the lower level which are considerably smaller than those actually obtained. The implication of this is that the compaction rate at depth may quickly react to the added load due to the new higher accumulation rate of 20 cm of water over the pit.

For future work longer-term measurements should be more accurate and will bring out more clearly the changes in compaction rates with time. An important project for the future will be to *remeasure the density-depth profile*; with such measurements Sorge's law can be readily tested for, if it holds, then the density will have increased in the pit by an amount required by the accumulation at the surface.

6.1.4. Comparison of settling rate for different localities

To compare the results of the S2 firn compaction rates with those of Maudheim, given by Schytt who obtained a mean settling rate, between 2 and 11·5 m, of 1·6 cm/m yr^{-1}, we need the *average* settling rate which, from equation (6.8), would be given by

$$S_{in} = \frac{1}{x_1 - x_2} \int_{x_1}^{x_2} -\frac{A}{\rho^2} \frac{d\rho}{dx}\, dx$$

$$= \frac{1}{x_1 - x_2} \int_{\rho_1}^{\rho_2} -\frac{A}{\rho^2}\, d\rho;$$

therefore

$$S_m = \frac{A}{x_1 - x_2} \frac{\rho_2 - \rho_1}{\rho_1 \rho_2}. \tag{6.16}$$

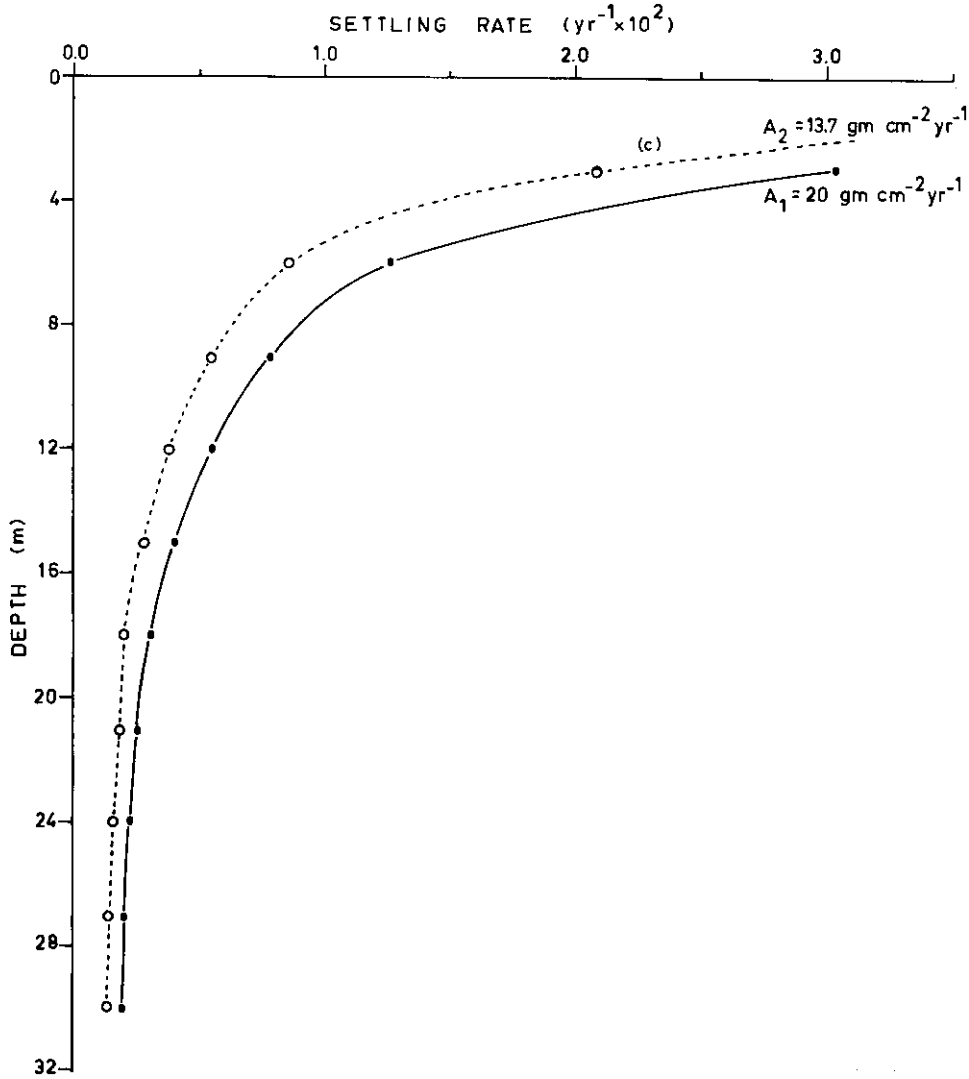

FIG. 6.3. SETTLING RATE VERSUS DEPTH. The two theoretical profiles have been calculated from accumulation rates of (i) 13.7 and (ii) 20 g cm^{-2} yr^{-1}. The latter gives the closer agreement to the measured values, indicating that the compaction rate follows the present accumulation rate rather than the past.

For the pit at S2 we have

at $x_1 = 2{\cdot}0$ m $\quad \rho_1 = 0{\cdot}45$ gm cm^{-3}

$x_2 = 11{\cdot}5$ m $\quad \rho_2 = 0{\cdot}64$ gm cm^{-3}

and $A = 0{\cdot}20$ gm cm^{-2} yr^{-1}

$$S_m = A \frac{\rho_2 - \rho_1}{x_1 - x_2} \frac{1}{\rho_1 \rho_2}$$

$$= 1{\cdot}4 \text{ cm m}^{-1} \text{ yr}^{-1}.$$

This rate is smaller than that measured by Schytt. The settling rate values at S2 are also smaller than those found by Sorge (1935) at Eismitte, Greenland, where the snow density was less at equivalent levels. Given more values of these compaction rates it may be possible to relate the density profile to other factors dependent on the location such as temperature, pressure, crystal size and accumulation rate.

Hoinkes (1962) discussed the settling in a pit at Little America, dug in 1940 and subsequently remeasured in 1947 and 1957. Some of his results are plotted together with the S2 curve in Figure 6.4. The settling rates found by Hoinkes were higher than those at S2 but appear to follow a similar pattern with depth as far as it goes (12·5 m). The reason why different values were obtained at the same depth for different times appears to be that the accumulation rate has been 19·4 gm cm^{-2} decreasing to 16·3 gm cm^{-2}; yet his curve still shows higher settling rates than that for S2. The reason for this may be seen from the density profiles. For the same layer (0 to 14 m) the density at S2 is higher than that at Little America, and since the settling rate,

$$S = -\frac{A}{\rho^2} \frac{d\rho}{dx},$$

depends on the square of density in the denominator, this may explain the discrepancy. The density values for Little America, however, appear to be too widely dispersed to warrant a more accurate analysis.

6.2. TUNNEL CONTRACTION AT S2

6.2.0. Introduction

The calculation of theoretical velocity profiles in moving ice has largely been hampered by the lack of information regarding the flow law of ice. To begin with, a simple viscous flow law was assumed (Lagally (1934)) and this appeared satisfactory to a first approximation. The apparent "viscosity" of ice, however, has been found to vary greatly with three variables, namely, (i) the applied stress, (ii) the temperature and (iii) the ice type; therefore different types of flow relations have been proposed to account for this (e.g. Glen (1952), (1956)). These more comprehensive relations have been tested over a limited range of stress and temperatures for various types of ice sample in the laboratory, cf. Glen (1956), Butkovitch and Landauer (1958), Mellor (1959c). A further means of deriving information on the flow laws of ice is by measuring strain rates of moving ice in its natural state in the field, e.g. horizontal and vertical

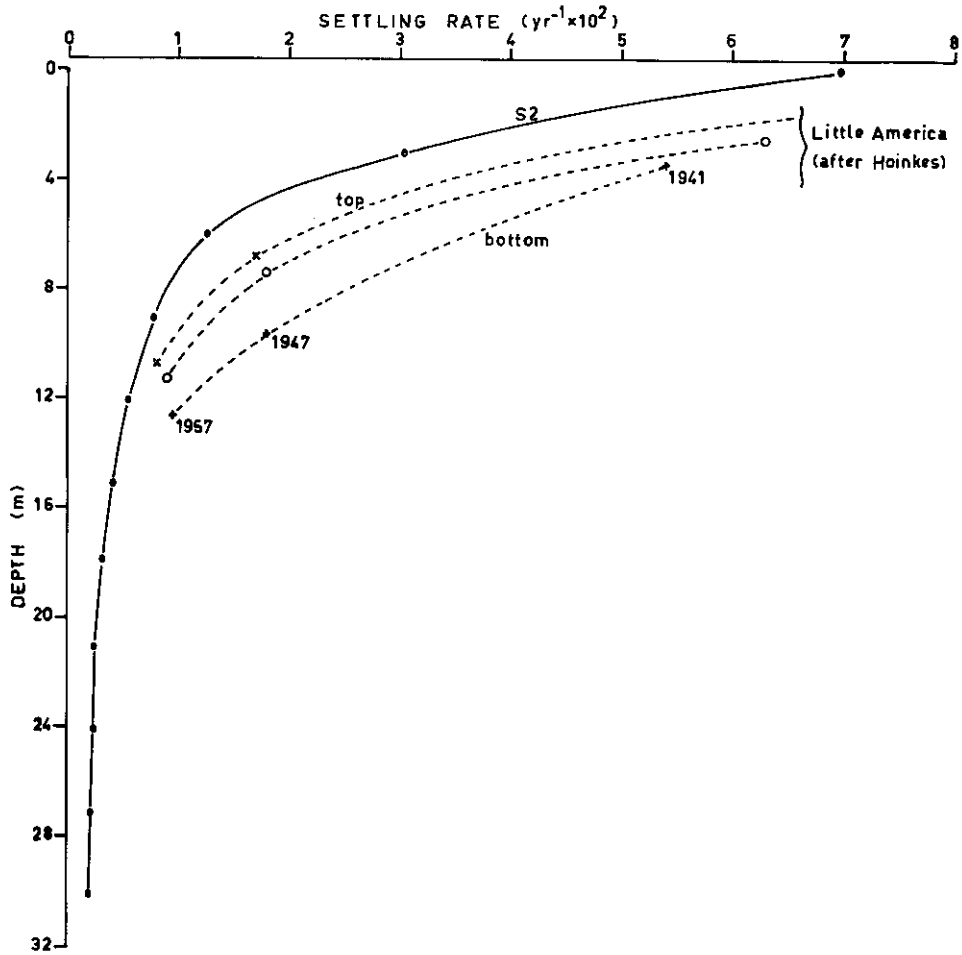

FIG. 6.4. FIRN SETTLING RATES FOR S2 AND LITTLE AMERICA. The value of the settling rates at S2 (from the theoretical curve in Fig. 6.2) are compared to those of Little America given by Hoinkes, from measurements in a pit from 1941 to 1957. The different curves for Little America, from top to bottom, are apparently due to the accumulation rate decreasing over the period from about 19 to 13 g cm^{-2} yr^{-1}.

velocity gradients through glaciers, and borehole or tunnel closure rates, and then relating these to the associated stress and temperature of the moving ice.

In this section the closure rates of the tunnel excavated at S2 in 1957 by Cameron *et al.* (1959) will be analysed with the aim of throwing further light on the parameters of the ice flow laws and, by comparing them with results from other locations, the effect of stress and temperature.

6.2.1. Observed closure rates in the S2 tunnel

At the 30 m level below the surface in the S2 pit a tunnel 6 m long and 2 m diameter extends horizontally into the firn, cf. sketch below.

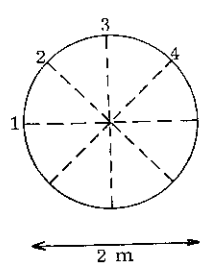

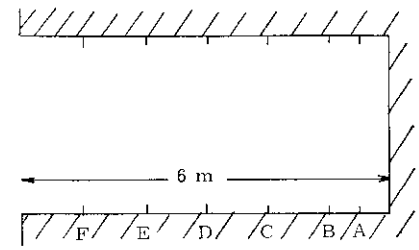

Measurements of the diameter of the tunnel have been made vertically, horizontally and diagonally at various distances from its end. For 12 measurements from October 1957 to October 1961 the average closure rates over the period have been calculated for each of the four directions and at the various distances along the tunnel. These are tabulated in Table 6.III.

TABLE 6.III.

S2 TUNNEL CONTRACTION RATES $\%\,yr^{-1}$,
MEASUREMENTS ACROSS TUNNEL AT DIFFERENT DISTANCES AND TIMES.

	0·44 yrs				1·40 yrs			
	1	2	3	4	1	2	3	4
A	0·87	0·81	1·11	0·61	0·61	0·71	0·92	0·72
B	0·64	0·94	1·15	0·70	0·62	0·78	1·10	0·78
C	0·81	0·89	1·16	0·90	0·67	0·79	1·11	0·86
D	0·77	1·14	1·26	0·90	0·73	0·85	1·15	0·83
E	0·91	0·91	1·20	0·97	0·78	0·86	1·10	0·91
F	0·93				0·96		1·16	
	2·54 yrs				3·85 yrs			
	1	2	3	4	1	2	3	4
A	0·49	0·67	0·92	0·65	0·45	0·58	0·92	0·49
B	0·51	0·69	0·98	0·68	0·50	0·67	0·96	0·63
C	0·55	0·72	1·03	0·79	0·56	0·66	0·96	0·76
D	0·62	0·76	1·09	0·80	0·60	0·72	0·95	0·75
E	0·67	0·78	1·02	0·83	0·61	0·71	0·98	0·78
F	0·82		1·06		0·77		0·98	

From this table it may be seen that (i) the vertical direction has the maximum closure rate, the horizontal direction the least; (ii) the rate of contraction increases away from the closed end, becoming stable at about *E*, 4 m from the closed end; and (iii) all rates have decreased slowly with time.

To interpret and analyse the results we first of all note that in 1957 the density of the firn at this level was 0·78 gm cm^{-3}, and that from the compaction data the average

vertical compaction rate at this depth was $0{\cdot}25 \times 10^{-2}$ yr^{-1}. This amount must be subtracted from the vertical closure rate, and half this amount from the diagonal rates (note that the amount of vertical compaction is small in comparison with the tunnel diameter). Average values have hence been obtained for the following times since the initial measurements: 0·44, 1·40, 2·54, 3·85 years and are listed in Table 6.IV.

These remaining contractions should be due to visco-plastic flow under hydrostatic pressure. The theory of this has been treated by Nye (1953) and will be discussed in detail in section 6.2.4.

TABLE 6.IV.

S2 TUNNEL CONTRACTION RATES % yr^{-1}, MEASUREMENTS CORRECTED FOR VERTICAL COMPACTION (OBTAINED FROM TABLE 6.III BY SUBTRACTING 0·13, 0·25, 0·13 FROM THE DIRECTIONS 2, 3, 4 RESPECTIVELY).

	0·44 yrs					1·40 yrs				
	1	2	3	4	Ave.	1	2	3	4	Ave.
A	0·87	0·68	0·86	0·48	0·72	0·61	0·58	0·67	0·59	0·61
B	0·64	0·81	0·90	0·57	0·73	0·62	0·65	0·85	0·65	0·69
C	0·81	0·76	0·91	0·77	0·81	0·67	0·66	0·86	0·73	0·73
D	0·77	1·01	1·01	0·77	0·89	0·73	0·72	0·90	0·70	0·76
E	0·91	0·78	0·95	0·84	0·87	0·78	0·73	0·85	0·78	0·78
F	0·93					0·96		0·91		
Ave.	0·80	0·81	0·93	0·69	0·805	0·68	0·67	0·83	0·69	0·717

	2·54 yrs					3·85 yrs				
	1	2	3	4	Ave.	1	2	3	4	Ave.
A	0·49	0·54	0·67	0·52	0·56	0·45	0·45	0·67	0·36	0·48
B	0·51	0·56	0·73	0·55	0·59	0·50	0·54	0·71	0·50	0·56
C	0·55	0·59	0·78	0·66	0·65	0·56	0·53	0·72	0·63	0·61
D	0·62	0·63	0·84	0·67	0·69	0·60	0·69	0·70	0·62	0·65
E	0·67	0·65	0·77	0·70	0·70	0·61	0·68	0·73	0·65	0·67
F	0·82		0·81			0·77		0·73		
Ave.	0·57	0·59	0·76	0·62	0·635	0·54	0·58	0·71	0·55	0·595

The measurements made so far provide data for an analysis to determine how the closure rate S, say, varies with three variables:

1. The direction across the tunnel (horizontal, diagonal, vertical), θ.
2. The distance along the tunnel (measured from the closed end), l.
3. The time from the initial measurement, t.

6.2.2. *Changes in closure rate with direction, position and time*

The measurements for different directions have not been taken over a sufficiently large number of values of θ to show a continuous dependence on that variable. Only the discrete values for the vertical, horizontal and diagonal directions are available.

Figure 6.5 shows the closure rates for each of the directions for the different times. From this it may be seen that (i) the closure rate for the vertical direction is significantly higher (even with the vertical compaction effect removed) than for other

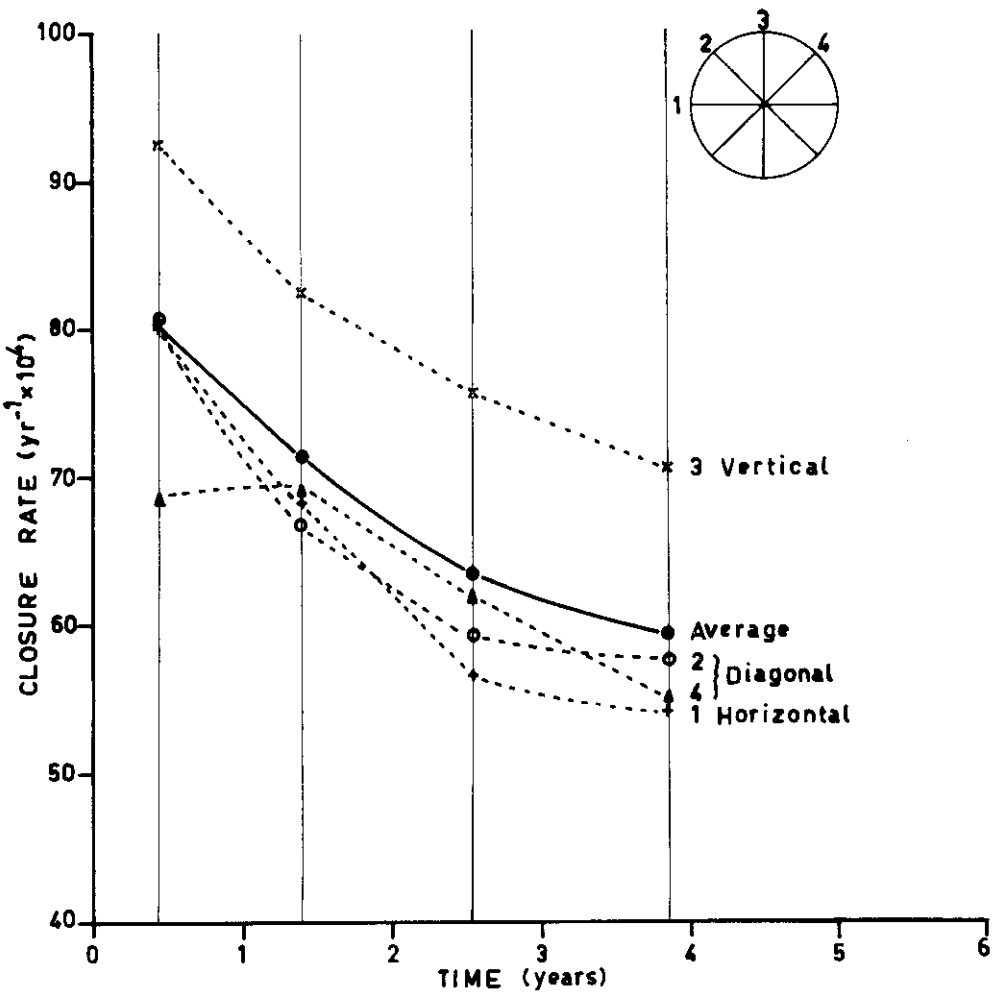

FIG. 6.5. CLOSURE RATE VERSUS TIME FOR DIFFERENT DIRECTIONS ACROSS THE S2 TUNNEL. The closure rate in each direction has been averaged over all the distances from the end for each of the four directions. The form of the decrease of closure rate with time appears to be similar for all directions.

directions; (ii) the closure rates for the other directions do not appear to be significantly different; and (iii) the slowing down of the closure rate with time appears to be of the same form for the different directions.

Figure 6.6 shows the variation in closure rate along the tunnel for the different directions. From this it can be seen that the closure rate increases with distance from the closed end but slightly more slowly for the vertical than for the other directions. However, the errors of measurements at this stage are too large to establish any difference between the directions beyond doubt.

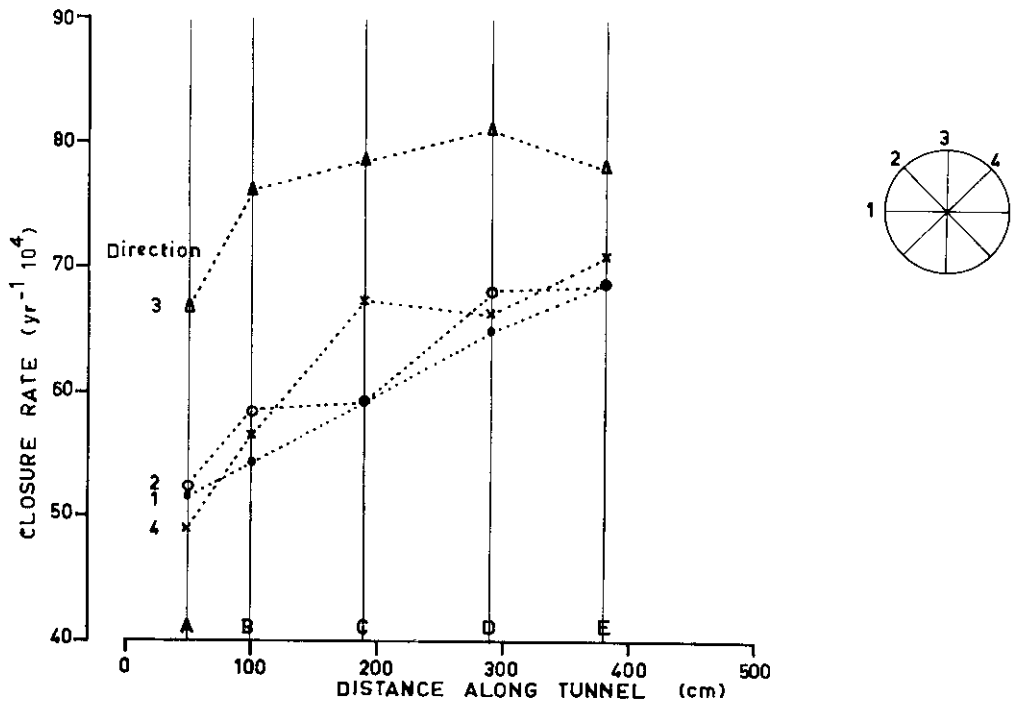

FIG. 6.6. CLOSURE RATE VERSUS DISTANCE ALONG TUNNEL FOR DIFFERENT DIRECTIONS. For each direction the closure rate at each position along the tunnel has been averaged over all times and then plotted against the distance from the closed end. The scatter is large and the curves are not smooth but there appears to be no evidence for a difference in *form* of the relation for the different directions.

We have seen already from Figure 6.5 that for all directions the closure rate has been decreasing with time in the same way. Figure 6.7 shows even more clearly that (iv) the closure rate is decreasing with time in a similar way for all distances from the closed end.

The decrease of closure rate with time is not constant, but becoming gradually smaller, suggesting that the closure rate may be asymptotic to some final steady value. The reason for the decrease in the closure rate is not yet certain. If the closure rate depended only upon the hydrostatic pressure from the overburden snow it would be expected to increase with time because the overburden increases from accumulation. An effect of compaction on the decrease of closure rate can be ruled out, for although the compaction rate is also decreasing with time, as the snow densifies, the previous

section indicates that at the 30 m level this is too small to be considered. This leaves as alternative a decaying readjustment in response to the sudden pressure discontinuity created by the excavation.

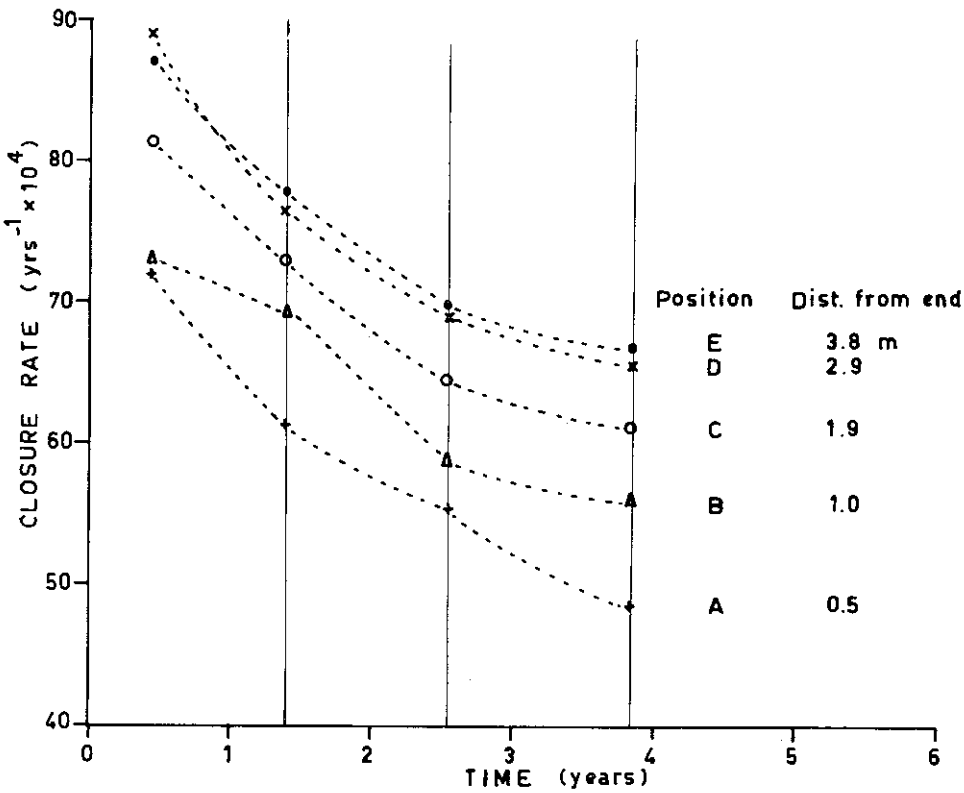

FIG. 6.7. CLOSURE RATE VERSUS TIME FOR DIFFERENT DISTANCES FROM THE CLOSED END. For each position along the tunnel the closure rate has been averaged over the four directions and plotted against time. The closure rate appears to have been decreasing in time similarly for all distances from the closed end.

Figure 6.8 shows the increase in closure rate going along the tunnel from the closed end for each of the four average time intervals from the commencement. From this it can be seen that (v) the pattern of increase in closure rate along the tunnel from the closed end has remained the same with time.

For the initial profile measured 0·44 years after commencement the percentage errors are large so that the values are erratic. The accuracy of measurement was to the nearest millimeter and the differences were about 3 mm. Hence the errors at this stage could be up to 30%. For the later measurements the errors should drop to below 5%. Again longer-term results will raise the accuracy and it is therefore important that these measurements should be continued as long as possible.

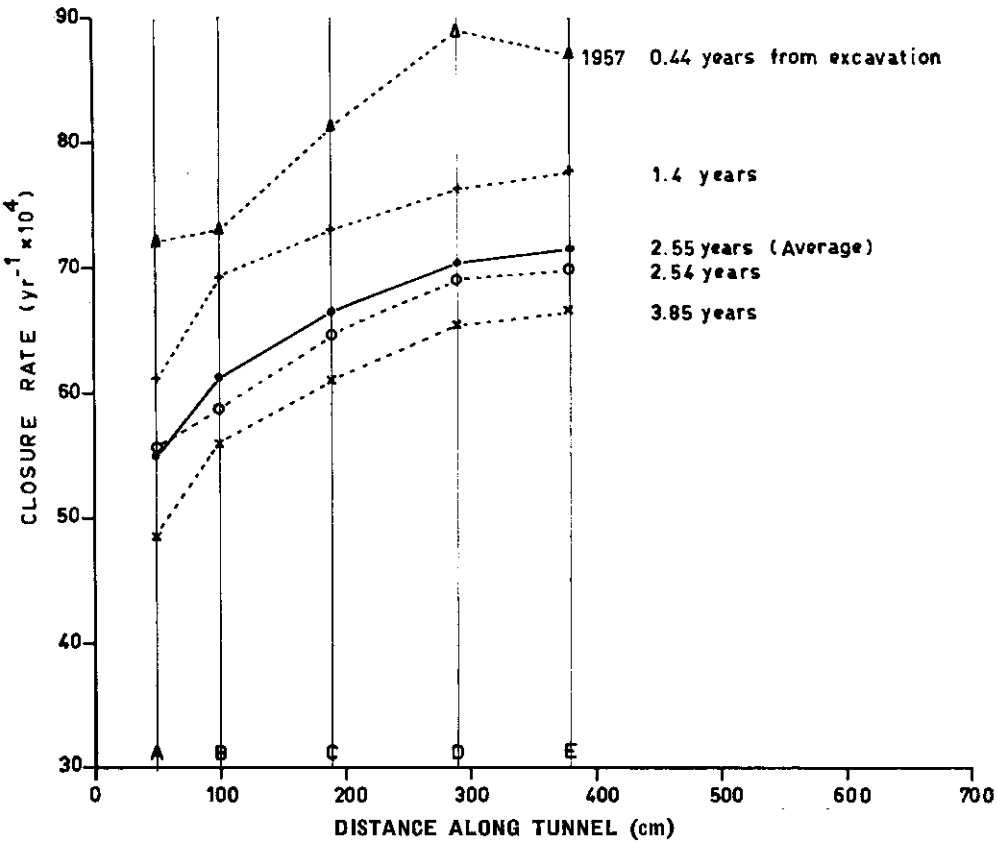

FIG. 6.8. CLOSURE RATE VERSUS DISTANCE ALONG TUNNEL FOR DIFFERENT TIMES. For each time the closure rate has been averaged over all directions for each position along the tunnel then plotted against the distance from the closed end. The scatter in the early measurements are due to the small differences obtained and the consequent high probable error. The form of the change of closure rate along the tunnel appears to be independent of time, hence the average over all times (2.55 years) has been used as the general variation.

6.2.3. *Estimation of flow parameters from tunnel contraction data*

Nye's (1953) analysis gives an expression for the closure rate S for a tunnel of radius a at a depth d as

$$S = \left(\frac{p}{nB}\right)^n, \tag{6.17}$$

where $p = \rho g d$, ρ being the ice density and g the gravity acceleration, and the flow law for the ice has the form

$$\dot{\gamma} = \left(\frac{\tau}{B}\right)^n, \tag{6.1}$$

where τ is the shear stress, $\dot{\gamma}$ is the shear strain rate and n and B are parameters which may depend on temperature, stress and ice type.

Equation (6.17) shows how the value of closure rate varies with the hydrostatic pressure, so that if values of closure rate are available for different pressures the parameters n and B may be determined. At S2, however, the whole tunnel is at the same depth so that only one value of p is available. If we take the value of n as 3, the value of the parameter B may then be determined from equation (6.17).

Now for the S2 tunnel at a depth of 30 m below the surface, the average density of the overburden firn (from Section 6.1) is 0·65 gm cm^{-3} and the average closure rate at the open end 0·64% yr^{-1}. Hence we have

$$n = 3$$
$$S = 0{\cdot}64 \times 10^{-2}\ \text{yr}^{-1} = 2{\cdot}02 \times 10^{-10}\ \text{sec}^{-1}$$
$$\rho = 0{\cdot}65\ \text{gm cm}^{-3}$$
$$g = 0{\cdot}98 \times 10^{3}\ \text{cm sec}^{-1}$$
$$d = 3 \times 10^{3}\ \text{cm}$$

and hence

$$p = \rho g d = 1{\cdot}91 \times 10^{6}\ \text{dynes cm}^{-2}.$$

Solving equation (6.17) for B and substituting from these values yields

$$B = \frac{p}{nS^{\frac{1}{3}}}$$
$$= \frac{1{\cdot}91 \times 10^{6}}{3 \times (2{\cdot}2 \times 10^{-3})^{\frac{1}{3}}}$$
$$= 2{\cdot}9 \times 10^{9}\ \text{c.g.s.}$$

The values obtained by Glen (1952) at various temperatures, using $n = 3{\cdot}03$, were

Temperature °C	0	−1·5	−6·7	−13
B c.g.s. × 10^9	0·381	0·711	1·01	1·61

The temperature average in the S2 tunnel is −20°C; thus the high value of B obtained appears to be consistent with the increasing values obtained by Glen for decreasing temperatures.

6.2.4. Exponent for power law and apparent viscosity

The closure rate increase with distance from the closed end provides a means for estimating the parameter n in the flow law.

$$\dot{\gamma} = \left(\frac{\sigma}{B}\right)^{n}. \tag{6.1a}$$

If it is assumed that the relative shear strain rate along the tunnel is proportional to the nth power of the distance from the end, then the average closure rate, relative to that at the position of maximum closure rate, would depend on the $(n + 1)$th power of the distance from this position, i.e.

$$V = ad^{m}, \tag{6.18}$$

where V is the velocity relative to the maximum, d is the distance from that position, $m = n + 1$, and a is a constant. Hence

$$\log V = \log a + m \log d. \tag{6.18a}$$

Plotting the values of log V against log d, cf. Figure 6.9, gives a value of $m = 1{\cdot}85$. This implies that the value of n for the flow is just below 1, the value required for constant viscosity. Because of this low value of n the closure rate will be used to calculate a value of apparent viscosity. In this case we have, putting $n = 1$ and $B = 2$ in Nye's formula

$$S = \frac{\rho g h}{2\eta},$$

where $\rho = 0{\cdot}65$ gm cm^{-3}, $g = 0{\cdot}98 \times 10^3$ cm sec^{-2}, $h = 3 \times 10^3$ cm, $S = 0{\cdot}64 \times 10^{-2}$ yr^{-1} $= 2{\cdot}02 \times 10^{-10}$ sec^{-1} and $p = 1{\cdot}9\text{x} \times 10^6$ dynes cm^{-2},

$$\eta = \frac{\rho g h}{2S}$$

$$= \frac{0{\cdot}65 \times 0{\cdot}98 \times 10^3 \times 3 \times 10^3}{2 \times 2{\cdot}02 \times 10^{-10}}$$

$$= 4{\cdot}7 \times 10^{15} \text{ poises.}$$

The values obtained by Haeffli and Bretani (1955) for the Z'Mutt tunnel and the Jungfraujoch tunnel are as follows:

1. Temperate ice, Z'Mutt tunnel (approximately at melting point):

(i) $p = 39t$ m^{-2} $= 3{\cdot}8 \times 10^6$ dynes cm^{-2}, $\eta = 2{\cdot}5 \times 10^{14}$ poises;

(ii) $p = 22t$ m^{-2} $= 2{\cdot}16 \times 10^6$ dynes cm^{-2}, $\eta = 7{\cdot}5 \times 10^{14}$ poises.

Here the effective viscosity is smaller where the stress is greater, as expected from the power law relation.

2. Jungfraujoch "cold ice" (annual mean air temperature -8°C, ice temperature -2°C):

Over-burden: 28 m of snow and ice;

$p = 24 \times 10^3$ kg m^2 $= 2{\cdot}36 \times 10^6$ dynes cm^{-2}, $\eta = 1{\cdot}18 \times 10^{15}$ poises.

Here the stress is between those of the temperate cases but the apparent viscosity is much larger due to the lower temperature, as would be expected from the results of Glen.

The overburden pressures in these different cases cause some differences in the value of η. From the power law it can be seen that, as the stress increases, the actual strain rate will increase more rapidly than if the substance were perfectly viscous. This implies that the "effective viscosity" appears to decrease with stress; hence for S2, where the overburden pressure is less, the apparent viscosity would be expected to be greater. The temperature and ice type must also play an important part. The closure rate at S2 was $2{\cdot}02 \times 10^{-10}$ sec^{-1} whereas that of the Jungfraujoch tunnel mentioned above was $1{\cdot}0 \times 10^{-9}$ sec^{-1}. The resulting apparent viscosity at S2 is much higher. This appears to be due mainly to the lower temperature of -20°C at

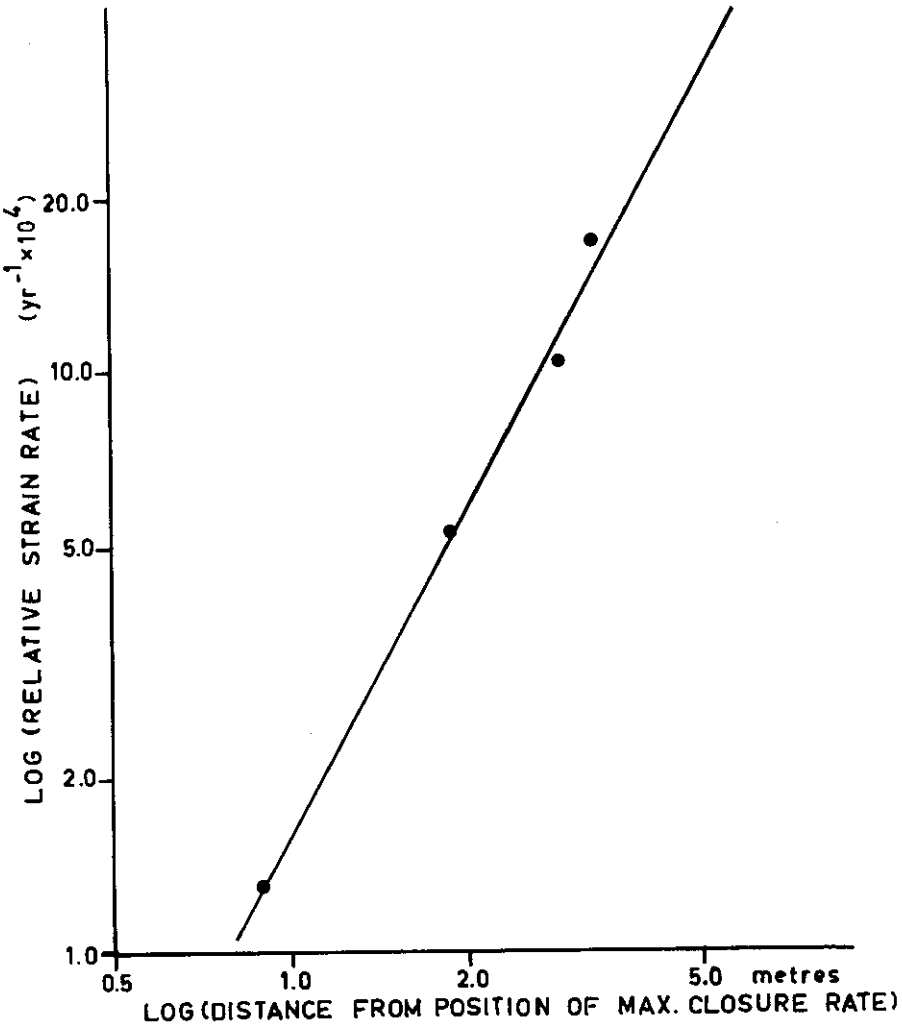

FIG. 6.9. LOG RELATIVE CLOSURE RATE VERSUS DISTANCE FROM THE POSITION OF MAXIMUM CLOSURE RATE. The relative closure rate (u) has been obtained for each position by the difference between the maximum closure rate and the closure rate at that position. This has then been plotted against the distance (d) from the position to the position of maximum closure rate. Plotting these on log-log scales, and assuming a relation of the form $u = ad^{n+1}$, gives a value of $n + 1 = 1.85$.

S2, but also to the lower stress at S2. Finally, the smaller-crystalled firn may show greater resistance to movement than larger-crystal glacier ice.

Thus it can be seen that the limited data so far available agree qualitatively with the theoretical laws. Furthermore, by making some assumptions regarding the form of the flow law for the ice, the various flow parameters of the ice type can be calculated.

When a large number of closure rates become available for different conditions of stress, temperature and crystal type, a functional relationship may be found or tested for the flow law of ice of various kinds occurring in the field. Such results form a comparable and necessary supplement to the empirical flow laws obtained from laboratory experiments.

6.3. THE MOVEMENT OF THE VANDERFORD GLACIER

6.3.1. The velocity profile and flow parameters

From the relation (cf. Introduction to this chapter)

$$u_c - u = \left(C_\xi \frac{\rho g \alpha}{B}\right)^n \frac{\xi^{n+1}}{n+1} \tag{6.2}$$

for the velocity change from the position of fastest movement in the direction of ξ, an estimate may be made of the parameters n and B (on the assumption of laminar flow) provided that the cross-section profile and a velocity profile are known. Alternatively if n and B are known the velocity profile will provide an estimate for the dimensions of the cross-sectional area.

The value of horizontal velocity profiles in glaciers does not seem to have been fully exploited in the determination of flow parameters. The measurements on Highway Glacier (Baffin Island) provided two horizontal velocity profiles and also seismically determined cross-sections. Ward (1955) used the flow parameters from Glen's laboratory tests to estimate the vertical velocity profile. It is here suggested that the horizontal velocity profile should first be used to determine the flow parameters; these could then be used for determining the vertical velocity profile, provided the cross-section profile of the glacier is known. For the Vanderford Glacier no cross-section profile is available as yet so the following two procedures will be adopted:

(i) A cross-section profile for the glacier will be assumed and the flow parameters calculated and compared with Glen's laboratory results.

(ii) Taking values from Glen's laboratory results which appear applicable to the Vanderford Glacier an effective glacier thickness will be determined.

For the Vanderford Glacier we have a velocity profile from the centre across the glacier. Figure 6.10 shows the initial positions of the stakes placed on the Vanderford Glacier by the U.S. party in 1957 (Cameron *et al.* (1959)) and their subsequent measured displacements. Also shown are the estimated positions of the wave crests to which angles were observed relative to the base-line AB on Haupt Nunatak. The subsequent positions of the wave crests, as measured in 1961, are also shown. From these displacements the velocity profile of the glacier has been calculated. Figure 6.11 shows the graph of the velocity of the glacier at the various distances from the edge. The wave crests appear to be at the centre and the velocity reaches a maximum at this position, as implied by equation (6.2).

If V represents the velocity relative to the centre at a distance d from the centre then the following empirical relation (found by plotting log V against log d) holds for the velocity profile of the Vanderford Glacier:

$$V = K d^{3.2},$$

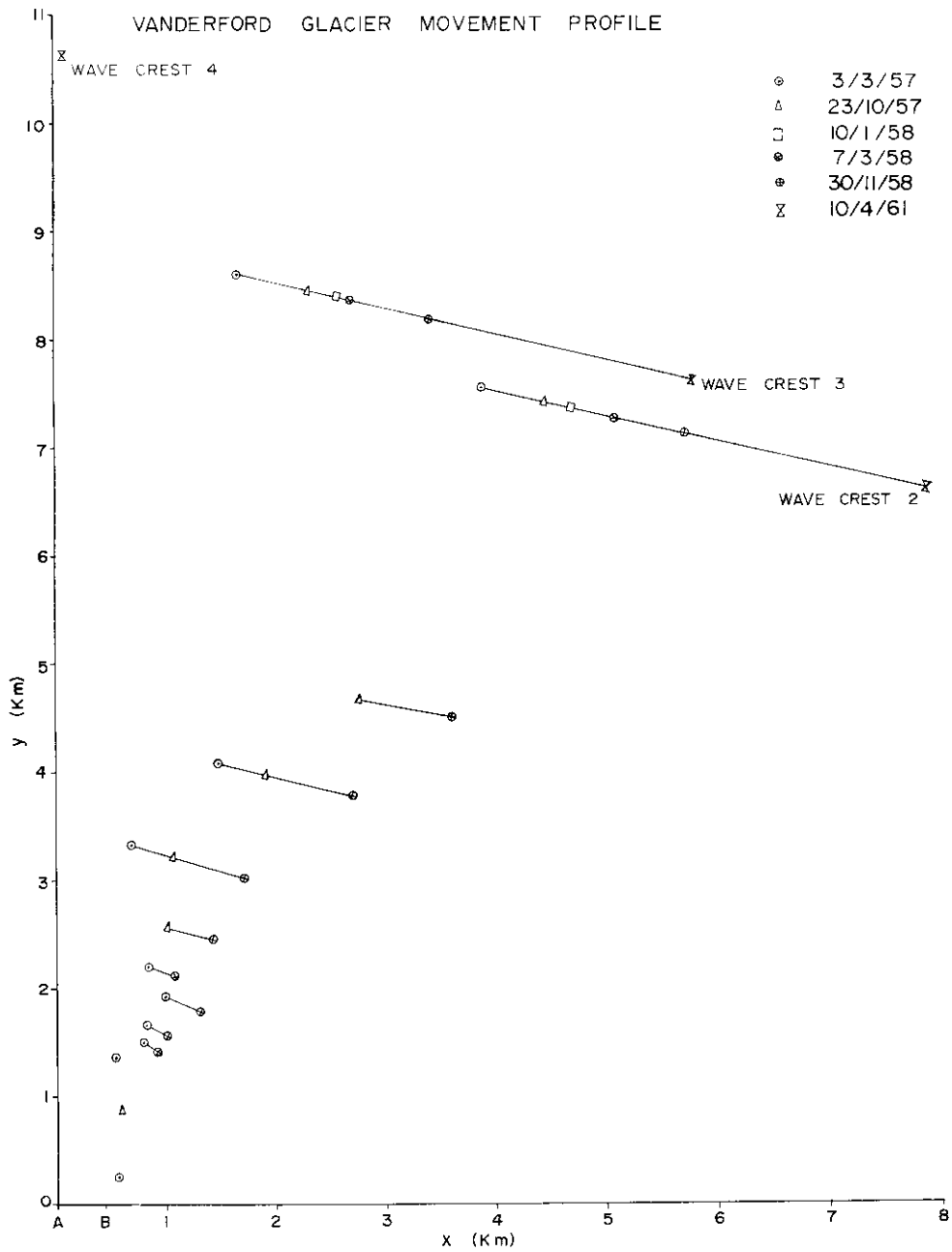

FIG. 6.10. POSITIONS OF MOVEMENT MARKERS ON THE VANDERFORD GLACIER. The positions of the stakes set out by the U.S. parties in 1957–58, and their subsequent positions, are shown. Further inland, the approximate position of the wave crests are shown as determined in 1961 and their positions estimated from the U.S. parties' angle measurements in earlier years.

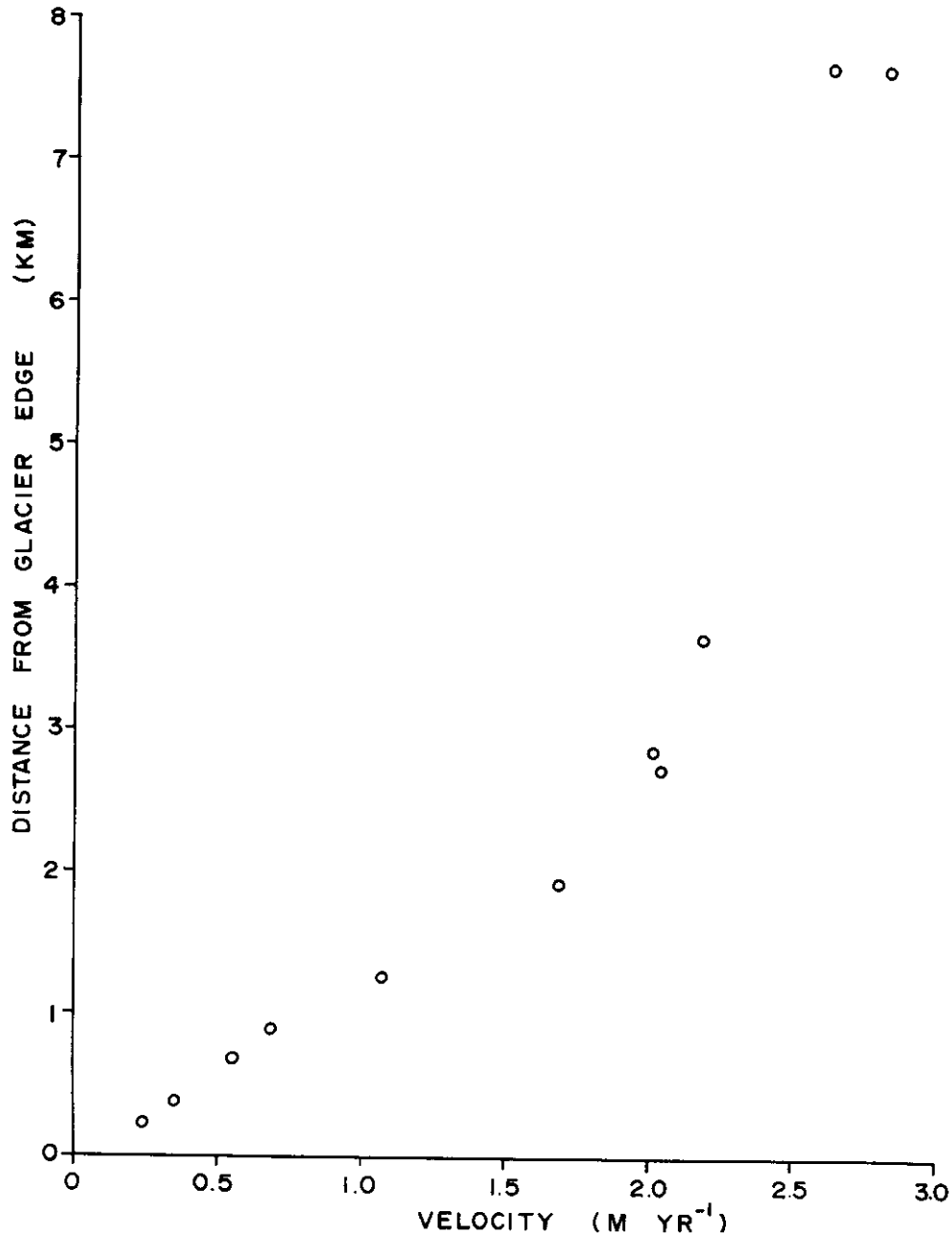

FIG. 6.11. VANDERFORD GLACIER VELOCITY PROFILE. From the movement measurements made over 1957–58 and the wave crest movement measured in 1961 a velocity profile has been plotted from the edge to the wave crests of the Vanderford Glacier. The points furthest inland correspond to two different wave crests.

where $K = 4{\cdot}18 \times 10^{-22}$ c.g.s. units. This implies a value of $n = 2{\cdot}2$ which is somewhat lower than that obtained from other sources (e.g. by Glen (1952) and Mathews (1959), cf. below).

From equation (6.2) we see that

$$K = \left(C_\xi \frac{\rho g \alpha}{B}\right)^n \frac{1}{n+1},$$

so that

$$C_\xi \frac{\rho g \alpha}{B} = [(n+1)K]^{1/n}.$$

If the glacier were infinitely deep, or if it were floating at the position measured (making the velocity approximately constant with depth), then $C_\xi = 1$ and B could be calculated.

On the other hand, if the glacier were assumed to have an approximately rectangular cross-sectional shape, of half width W and depth h, then C_d is given by

$$C_d = \frac{h}{h + W}.$$

Now, if h is much smaller than W (for the Vanderford Glacier W is 8 km), then $C_d \approx \frac{h}{W}$, so that using

$$\frac{h}{W}\frac{\rho g \alpha}{B} = [(n+1)K]^{1/n}$$

with a known B, an estimate of the effective depth, h, can be made.

Before trying either of these alternatives (to estimate B or h) the values of B obtained from other sources will be considered.

6.3.2. Values of flow parameters from other sources

(i) Laboratory measurements. Glen (1952) gives the flow law parameters in the form

$$\dot{\varepsilon} = k\sigma^n, \tag{6.19}$$

where $\dot{\varepsilon}$ is in years^{-1} and σ is in bars and found from laboratory experiments on ice samples just below the pressure melting point, with the result that $n = 4$ and $k = 0{\cdot}0074$. To convert this value of k to c.g.s. units we note that 1 year $= 3{\cdot}16 \times 10^7$ sec and 1 bar $= 10^6$ dynes cm^{-2}, and then to put equation (6·19) in the form to derive equation (6.2), i.e.

$$\dot{\varepsilon} = \left(\frac{\sigma}{B}\right)^n,$$

we obtain

$$\dot{\varepsilon} = \left(\frac{\sigma}{2{\cdot}6 \times 10^8}\right)^4$$

and hence

$$B = 2{\cdot}6 \times 10^8 \text{ c.g.s.}$$

By experimenting with compressive loads, between 1·5 and 10 bars, on samples of randomly oriented ice at various temperatures Glen, (1954) found that the formula $\dot{\varepsilon} = k\sigma^n$ would apply with $n = 3{\cdot}2$ and that this value was independent of stress.

The value of k was found to vary markedly with temperature and the following values were given for k, with $\dot{\varepsilon}$ in years^{-1} and σ in bars for various temperatures:

Temperature (°C)	0	−1·5	−6·7	−13
k (bars^n years^{-1})	0·17	0·023	0·008	0·0017.

Now k and B as used previously are related by

$$B = \left(\frac{1}{k}\right)^{1/n} = \left(\frac{1}{k}\right)^{1/3.2},$$

provided that both B and k are in c.g.s. units. To convert k to c.g.s. units we have

$$\dot{\varepsilon} = k\sigma^{3.2}$$

in the above units which implies

$$3{\cdot}16 \times 10^7\,\dot{\varepsilon} = k\left(\frac{\sigma}{10^6}\right)^{3.2} \text{ in c.g.s. units.}$$

$$\text{Therefore } k' = \frac{k}{3{\cdot}16 \times 10^{19.2} \times 10^7} = \frac{k}{5{\cdot}05 \times 10^{26}};$$

$$\text{therefore } B = \left(5{\cdot}05 \times 10^{26}\right)^{1/3.2}\left(\frac{1}{k}\right)^{1/3.2}$$

$$= 2{\cdot}19 \times 10^8 \times \left(\frac{1}{k}\right)^{1/3.2}.$$

From this we find the following values for B:

Temperature (°C)	0	−1·5	−6·7	−13
B (c.g.s. × 10^9)	0·381	0·711	1·01	1·61.

Glen's earlier value, $n = 4$, gave a value of B slightly lower than these, namely, $0{\cdot}26 \times 10^9$ at a temperature just below zero.

(ii) Field measurements. From the vertical velocity profile near the centre of the Salmon Glacier, Mathews (1959) gave a result from which B may be calculated. Mathews adopted Nye's equation in the form

$$u_0 - u = \frac{K}{n+1}\sin^n \alpha\, d^{n+1}$$

and found that the values of n and K needed to obtain the best fit to the measured velocity profile from the glacier surface to its bedrock were $n = 2{\cdot}8$ and $K = 1{\cdot}25 \times 10^{-4}$ for u in m yr^{-1} and d in metres.

From the above formula it appears that $K = \left(C_d \frac{\rho g}{B}\right)^n$ where all units are converted to c.g.s. The cross-section of the glacier is also given so that C_d may be estimated. With the cross-sectional area $A = 975{,}000$ m^2 (given), the cross-sectional

perimeter $p = 3{,}200$ m (as estimated from the scale diagram given by Mathews (1959)) and depth $d = 500$ m,

$$C_d = \frac{A}{pd} = 0{\cdot}61.$$

To convert K (given above) to c.g.s. units

$$v = K d^{n+1}$$
$$(m/yr) \quad (m)$$

$$\frac{3{\cdot}16 \times 10^7}{10^2}\left(\text{cm/sec}\right) = K\left(\frac{\text{cm}}{10^2}\right)^{3.8};$$

therefore

$$K' = \frac{1{\cdot}25 \times 10^{-4}}{3{\cdot}16 \times 10^5 \times 10^{7.6}} = 0{\cdot}99 \times 10^{-17}.$$

Hence B may be found from

$$\frac{C_d \rho g}{B} = (K)^{1/n} = (0{\cdot}99 \times 10^{-17})^{1/2.8} = 8{\cdot}7 \times 10^{-7};$$

therefore

$$B = \frac{0{\cdot}61 \times 0{\cdot}9 \times 0{\cdot}98 \times 10^3 \times 10^7}{8{\cdot}7}$$
$$= 0{\cdot}61 \times 10^9 \text{ c.g.s. units.}$$

Mathews states that no temperature measurements were made in the borehole but that measurements by Miller in a similarly situated glacier gave a temperature of $-0{\cdot}1$°C below 20 m from the surface. The temperature in the glacier was found to be certainly above $-6{\cdot}0$°C and probably just below zero.

It is seen that the values obtained for the flow law parameters from the Salmon Glacier profile agree well with the laboratory values of Glen quoted in the preceding section. The value of n found is slightly smaller, and the value of B larger, than the laboratory values for the corresponding temperature range.

6.3.3. Flow parameter estimates for the Vanderford Glacier

From the Vanderford Glacier results a maximum value of B can be obtained if the tongue is assumed afloat in the section studied. Then

$$\frac{\rho g \alpha}{B} = (3{\cdot}2K)^{1/2.2} = (3{\cdot}2 \times 4{\cdot}8 \times 10^{-22})^{1/2.2}$$
$$= 3{\cdot}26 \times 10^{-10}.$$

The slope of the glacier is difficult to obtain exactly because the centre is higher than the edges. Taking the average slope over the section measured to the tongue edge the slope is $\alpha = 1{\cdot}7 \times 10^{-3}$ therefore

$$B = \frac{0{\cdot}9 \times 0{\cdot}98 \times 10^3 \times 1{\cdot}7 \times 10^{-3}}{3{\cdot}26} \times 10^{10}$$
$$= 4{\cdot}6 \times 10^9 \text{ c.g.s. units.}$$

This value is almost three times as large as the largest value given by Glen (for the temperature of $-13°C$). The temperature at the surface of the Vanderford Glacier is expected to average $-9°C$, the average temperature at Wilkes, and if the tongue is floating as assumed above, then the temperature at the base should be close to sea temperature. This indicates that B is definitely higher than the values obtained by Glen (1952). This high value may be partly due to the lower value of n. For $n = 1$, constant viscosity, B represents η, the coefficient of viscosity, and is of the order of 10^{14}.

6.3.4. Estimation of effective thickness of Vanderford Glacier

The alternative way of interpreting the Vanderford Glacier data is to take a value of B, say $1{\cdot}0 \times 10^9$, obtained by Glen for ice at $-6°C$, and from this calculate an effective ice depth h. Using

$$\frac{h}{W}\frac{\rho g \alpha}{B} = [(n+1)K]^{1/n} = 3{\cdot}2 \times 10^{-10},$$

where $W = 8$ km $= 8 \times 10^5$ cm and $\alpha = 1{\cdot}7 \times 10^{-3}$.
Then

$$h = \frac{8 \times 10^5 \times 1{\cdot}0 \times 10^9}{0{\cdot}9 \times 0{\cdot}98 \times 10^3 \times 1{\cdot}7 \times 10^{-3}} \text{ cm}$$
$$= 1{\cdot}7 \times 10^4 \text{ cm}$$
$$= 1700 \text{ m}.$$

The ice cliffs, 22 km towards the sea from the measured section, are about 30 m high. With a density ratio of 0·90 to 1·03 for ice to sea water the ice thickness there is calculated to be 250 m.

The value of the thickness h can not be regarded as much better than an order of magnitude, but it represents the depth required for the base to be fixed to bedrock and the glacier to be moving in laminar flow with the flow law parameter assumed.

6.3.5. Conclusion

The two interpretations given for the Vanderford Glacier movement data make it clear, that before an exact treatment of flow can be given, a more precise knowledge of flow parameters will be required. Alternatively, in order to obtain empirical values of the flow parameters from glacier flow, it is necessary to have a complete surface profile and thickness profile as well as the velocity distribution across the glacier. Furthermore, because the flow parameters depend greatly on temperature it is necessary to have a knowledge of the temperature distribution in the ice in order to reconcile measurements from glaciers in different localities.

6.4. ICE MOVEMENT OF CAPE FOLGER AND S2 STRAIN GRID

6.4.1. Cape Folger

The angular displacements of the Cape Folger ice cliffs and the drum marker (2·4 km inland from the cliffs) were measured from a survey point situated at Wilkes Base, 16·0 km from the ice cliffs. Both positions at Cape Folger are moving approxi-

mately at right angles to the line of sight from Wilkes, so that the angular displacements are proportional to the surface velocities of the ice. The mean velocity for each over the period was 53 m yr^{-1} for the ice cliffs and 32 m yr^{-1} for the drum.

Gravity and elevation measurements for the drum marker were carried out and used by D. Walker of the Australian Bureau of Mineral Resources to determine the thickness of the ice at the drum as 200 m approximately (personal communication). The surface slope from the drum to the cape is 0·037.

From the measurements of surface velocity 2·4 km apart in the line of motion the longitudinal surface strain rate has been calculated as

$$\frac{53 - 32}{2400} \approx 10^{-2}\ \mathrm{yr}^{-1}.$$

To interpret the value of the observed strain rate by means of the theory summarized in equations (6.3) to (6.5) an estimate will be needed for the value of the vertical surface velocity, V_s. From the Wilkes local area accumulation measurements it appears that the average accumulation rate of the region may be considered as zero. It is not known whether the surface profile is remaining the same or not. But if it is assumed that the surface profile is constant, then an estimate of the vertical velocity may be made in terms of the horizontal velocity.

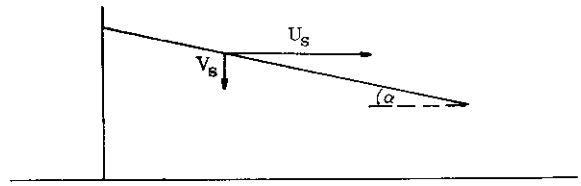

Then from equations (6.3) to (6.5)

$$V_s = \alpha U_s$$

for constant surface shape and zero accumulation and

$$U_s = \frac{\rho g \alpha}{2\eta}(H_0^2 - \alpha^2 x^2) + \frac{V_{s0}}{H_0} x + U_0;$$

therefore

$$V_s = \frac{\rho g \alpha^2 H_0}{2\eta} + \alpha U_0,$$

since the terms with α^4 and $\frac{V_s \alpha}{H_0} x$ are very much smaller, over the distances to be studied.

$$\frac{dU_s}{dx} = \frac{V_s}{H_0} - \frac{\rho g \alpha}{\eta}$$

and substituting for V_s this becomes

$$\frac{dU_s}{dx} = \frac{\rho g \alpha^2 H_0}{2\eta} + \frac{U_0}{H_0} + \frac{\rho g \alpha^3}{\eta} x \sec^{-1}.$$

For Cape Folger we have $\rho = 0{\cdot}90$ gm cm^{-3}, $H_0 = 200$ m $= 2 \times 10^4$ cm, $g = 0{\cdot}98 \times 10^3$ cm sec^{-2}, $\alpha = 0{\cdot}037$ and $x = 2{\cdot}4 \times 10^5$ cm. Thus

$$\frac{dU_s}{dx} = \frac{2}{220}\,\mathrm{yr}^{-1} = \frac{2}{220} \times \frac{1}{3{\cdot}16 \times 10^7}\,\mathrm{sec}^{-1}.$$

$\frac{\alpha U_0}{H_0}$ is more than an order of magnitude less than $\frac{dU}{dx}$ since U_0 (the initial slide velocity) must be less than the surface velocity, 23 m yr^{-1}. Also, the term in α^3 is an order of magnitude less than

$$\frac{\rho g \alpha^2 H_0}{2\eta}.$$

Therefore an estimate of the effective viscosity can be made:

$$\frac{\rho g \alpha^2 H_0}{2} = \tfrac{1}{2} \times 0{\cdot}9 \times 0{\cdot}98 \times 10^3 \times (3{\cdot}7)^2 \times 10^{-4} \times 2{\cdot}0 \times 10^4$$
$$= 1{\cdot}2 \times 10^4;$$

therefore

$$\eta = 1{\cdot}2 \times 10^4 \times \frac{240}{2{\cdot}0} \times 3{\cdot}16 \times 10^7$$
$$= 4{\cdot}6 \times 10^{13} \text{ poises.}$$

This value is 2 orders of magnitude smaller than the estimates obtained in section 6.2.5. for the colder ice at S2. On the other hand, Dorsey (1940, p. 456) lists values of effective viscosity found by various workers as ranging from $0{\cdot}6 \times 10^{13}$ to $14{\cdot}8 \times 10^{13}$ poises.

The viscosity increases greatly with decreasing temperature (by a factor of about 26 for a 10°C temperature decrease, in the case of glacier ice). The temperature of the ice in the Cape Folger region ranges from −8°C at the surface to approximately zero at the base, as estimated from the temperature gradients near Wilkes (cf. Section 5). From this it appears that the calculated effective viscosity is of the right order.

The spreading of the ice has not been considered, but where the slope is steep, as at the coast, this is expected to be small in comparison with the longitudinal strain rate. Further inland where the slope is small the spreading may be far greater. This will be seen to apply to the ice cap in the vicinity of S2, treated in the next sub-section.

6.4.2. Surface movement at S2

To obtain an estimate of the rate of movement and resulting lateral spread at S2 the value of the surface velocity of the ice inland would be required. As this is not yet known the value of the velocity which would be necessary for balance for the known accumulation will be calculated.

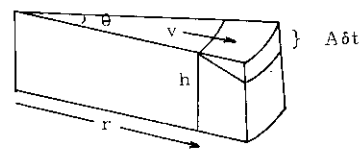

For a uniform circular ice cap consider an element of a sector $r\theta$ distance r from the centre, between vertical planes through the centre enclosing an angle θ. Let h be the thickness and v the mean horizontal velocity at distance r from the centre. Let A be the accumulation rate. If the effect of purely vertical motion is neglected, and if at time $t + \delta t$ $h = h + \delta h$, $v = v + \delta v$ and $r = r + \delta r$, then continuity demands

$$r\theta vh = \theta(r + \delta r)(v + \delta v)(h + \delta h - A\delta t),$$

that is

$$rvh = rvh + rh\delta v + rv\delta v - rvA\delta t \qquad \text{(to 1st order)}$$

or

$$\delta(rvh) = r\frac{dr}{dt}A\,\delta t \qquad \left(\text{since } v = \frac{dr}{dt}\right),$$

so

$$d(rvh) = rA\,dr.$$

Now ,if A is a constant over the range considered, then

$$vh = \tfrac{1}{2}Ar + \text{constant.} \tag{6.20}$$

In general, when A varies with distance from the centre

$$rvh = \int rA\,dr \tag{6.21}$$

and A must be specified as a function of r. This corresponds to the two-dimensional

$$hv = \int ax\,dx.$$

If $v = 0$ when $r = 0$ (i.e. at the centre) then the constant in the above equation is zero.

To apply the above results to S2 we can consider the Wilkes dome region (37 km ESE of S2) as the centre of the sector and as the thickness and accumulation rates are known, the required velocity can be calculated.

Using $v = \dfrac{Ar}{2h}$ and $A = 0{\cdot}13$ m yr^{-1}, $h = 1{,}000$ m and $r = 37 \times 10^3$ m

$$v = \frac{0{\cdot}13 \times 37 \times 10^3}{2 \times 10^3} = 2{\cdot}4 \text{ m yr}^{-1}.$$

If the velocity profile were parabolic and the slide velocity zero at this position then surface velocity would be $\frac{3}{2}$ times the mean horizontal velocity, hence

$$v_{\text{surface}} = \tfrac{3}{2} \times 2{\cdot}4 = 3{\cdot}6 \text{ m yr}^{-1}.$$

The lateral strain in time δt is given by

$$\frac{(r + \delta r)\theta - r\theta}{r\theta} = \frac{\delta r}{r}.$$

For the strain rate per year we take $\delta r = v(\text{m yr}^{-1})$

$$\frac{v}{r} = \frac{3{\cdot}6}{37 \times 10^3} = \frac{1}{10^4}.$$

This is slightly smaller than the result obtained from the S2 baseline, discussed below.

S2 strain grid

The strain of the S2 baseline has been measured since 1957. This baseline shows, cf. Figure 6.12, a fairly linear increase in length from 1957 at an average rate of 26 cm in 1587 m per year, giving as strain rate $\frac{0{\cdot}26}{1587}\,\mathrm{yr}^{-1} = \frac{1}{6{\cdot}1 \times 10^3}\,\mathrm{yr}^{-1}$. This value is about 160% of the value estimated from the horizontal velocity required for mass balance under steady state conditions.

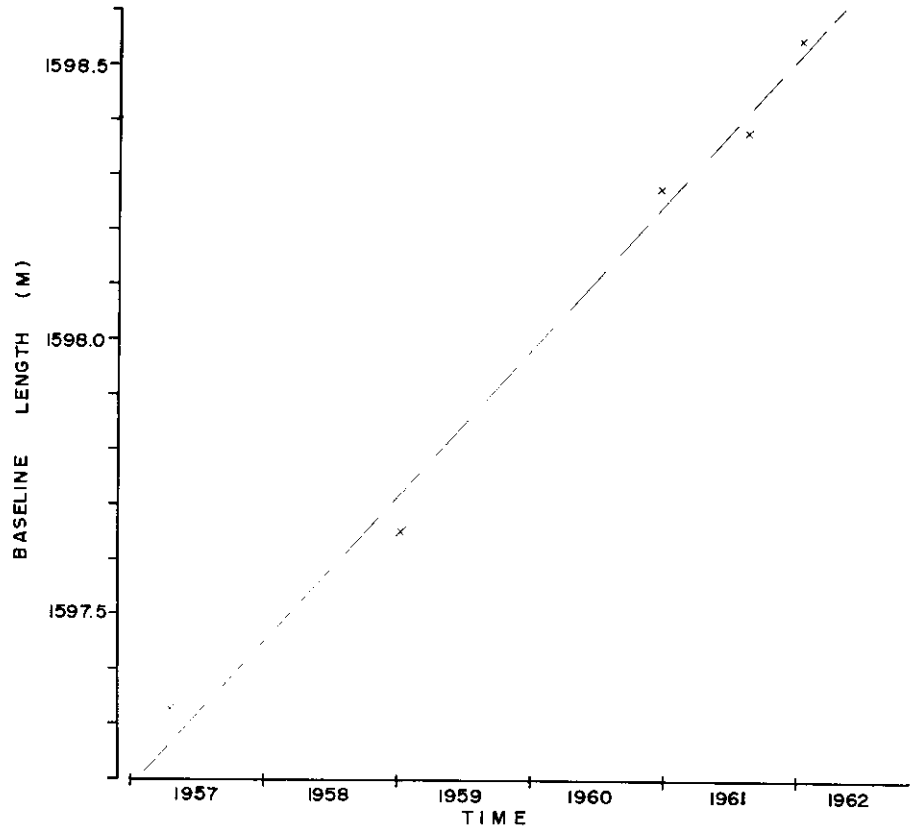

FIG. 6.12. EXTENSION OF S2 STRAIN GRID BASELINE AB, 1957–62. The measurements of the S2 baseline by Cameron et al. (1959), Hollin et al. (1961), Black (1960) and Budd (in 1961 and 1962) have been plotted against time. The strain rate appears to have been approximately linear with time, with the average extension rate of 26 cm yr^{-1}.

The results for the remainder of the S2 strain grid system are illustrated in Figure 6.13. This shows the initial positions of the stakes in 1957 and their displacement vectors in 1961. The change in length of each line joining two stakes is also shown. The average extension in the direction *AB*, which is across the line of greatest slope (and hence probably across the direction of absolute movement), has been 0·88 m over 4·5 years at an average rate of about 20 cm yr^{-1}. The corresponding average extension perpendicular to this line was about -8 cm yr^{-1}.

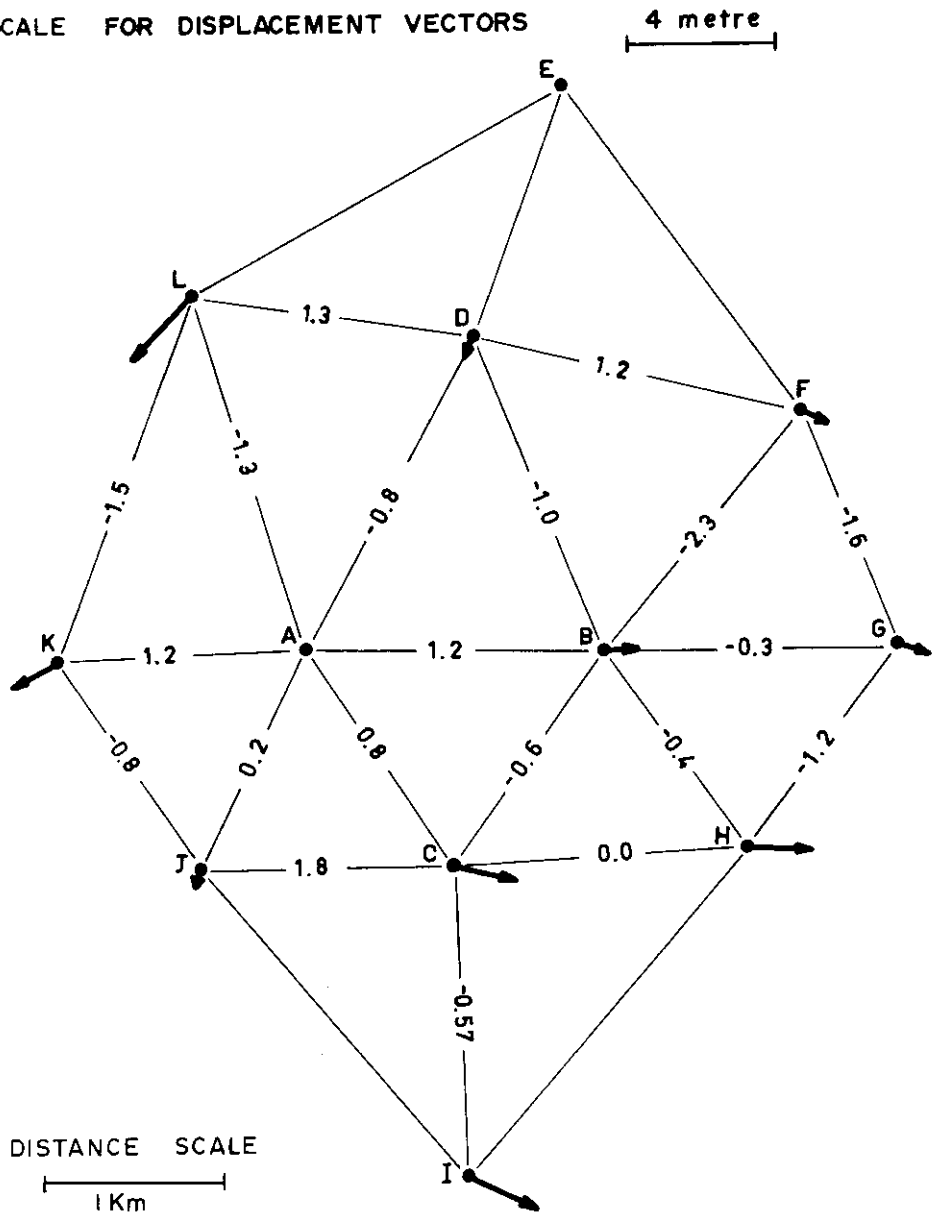

FIG. 6.13. S2 STRAIN GRID MOVEMENT RELATIVE TO A. From the survey of 1961 the new positions of the strain grid stakes have been calculated. Then, by comparing these new positions with the original positions in 1957, movement vectors have been calculated over the period of 4 years.

These rates are small and it will be important to continue the grid measurements until the differences become significant. The average errors at this stage are relatively high; namely, 0·2 m/1000 for lines other than the baseline. For the baseline the error should be less than 0·05 m/1000 m.

Much more precise estimates will be possible when the actual velocity of S2 has been determined. Furthermore the differential motion can then be calculated and a comparison of the change in surface elevation with the accumulation rate should then reveal whether or not this part of the ice cap is in a state of balance.

From the two-dimensional theory summarized in equations (6.3) to (6.5), using a coefficient of viscosity of the order of 10^{14}, an estimate can be made of the order of magnitude of the equivalent longitudinal strain rate that would apply in the absence of lateral spread.

For S2 we take $H_0 = 1000\text{ m} = 10^5\text{cm}$, $x = 0$, $\eta = 10^{14}$, $\alpha = 0{\cdot}008$. The surface strain rate is given by (6.5) as

$$\frac{dU_s}{dx} = \frac{\rho g \alpha^2 H_0}{2\eta} + \frac{\alpha U_0}{H_0} - \frac{\rho g \alpha^3}{\eta} x \text{ sec}^{-1}.$$

Here again we assume U_0 to be only a small fraction of surface velocity so that $\frac{\alpha U_0}{H_0}$ is an order smaller than the first term. Also the term in α^3 is again negligible. Hence

$$\frac{dU_s}{dx} = \frac{0{\cdot}9 \times 0{\cdot}98 \times 10^3 \times (0{\cdot}008)^2 \times 10^5 \times 3{\cdot}16 \times 10^7}{2 \times 10^{14}}$$

$$= \frac{0{\cdot}8}{10^3} \text{ yr}^{-1}.$$

This is about three times higher than the result for the lateral strain rate at S2, suggesting that the effective viscosity is higher than here assumed. In fact, an effective viscosity of 3×10^{14} poises. well in the range quoted by Dorsey (1940), would account for the strain rate observed. The average temperature through the ice cap at this position, from Section 5, is about $-10°$C. Hence, from section 6·2 the required effective viscosity is in accord with the value of $4{\cdot}7 \times 10^{15}$ found for the S2 tunnel where the temperature average is approximately $-20°$C.

Because both the velocity and surface slope are small, the lowering of the surface with advancement is small and thus the longitudinal strain rate is small in comparison with the lateral spread. It should be stressed that this lateral spread rate depends only on the forward velocity and the distance from the dome centre. To account fully for the flow conditions in the S2 region a three-dimensional analysis will be necessary.

6.5. MASS BALANCE

6.5.0. Regions and measurements considered

The section to be considered for mass balance extends (cf. Fig. 4.8) from the centre dome, *A*, 115 km inland from Wilkes, due north to the ice cliffs at *B*, south-west of the dome to a "saddle point" *C*, then west to the coast near the Vanderford glacier at *D*.

If it is assumed that ice flow in general is along movement lines down slope, i.e. perpendicular to the contours, then it follows that the flow in the section considered will be outwards from *A* in all directions. At the saddle point *C* we may also assume a stationary point. This then implies that the flow between longitudes 110° and 116°E would be diverted at this point to either an easterly flow into the area of the Totten

Glacier, or westerly into the region of the Vanderford and John Quincy Adams Glaciers.

The region *ACDB* defined above appears from the contours to have no ice flow into it and hence represents an isolated system. Thus its mass budget may be considered separately. The section *ABF*, where *F* is at Cape Folger, also appears to be an isolated system and will also be treated separately.

Accumulation measurements have been made in detail at Wilkes, from Wilkes to S2, at S2, and from Wilkes due south, to latitude 71°. From these and surface observations made en route to Cape Folger and the Vanderford Glacier in 1961, and from surface observations made by the U.S. parties (Cameron *et al.* (1959)) due east of Wilkes in 1957, and south-east of the Vanderford and John Quincy Adams Glaciers in 1958 (Hollin *et al.* (1961)) accumulation contours of the region have been drawn up (cf. Fig. 4.8).

Measurements of outflow of ice have been made at Cape Folger and across the Vanderford Glacier. These will be taken as representative of the two types of coastal flow of the area.

6.5.1. Mass budget calculations

6.5.1.1. Section ACDFB

(a) Accumulation. The accumulation contours are shown in Figure 4.8. The following table gives the total net accumulation rate over the whole area for one year.

TABLE 6.V.

Region	Area km²		Accumulation Rate gm cm⁻² yr⁻¹	Product gm yr⁻¹ × 10¹⁴
1 *A*	1316)	1568	0	0
B	207)			
2 *A*	2205	2205	5	1·10
3 *A*	1223)	2721	8	2·17
B	1498)			
4 *A*	4272)	6477	11	7·13
B	2205)			
5 *A*	1188	1188	32	3·80
Total		1416		14·20

From this the total gain comes to $1{\cdot}4 \times 10^{15}$ gm yr^{-1}.

(b) Outflow of Ice. Because of the barrier formed by the Windmill Islands the flow between *E* and *F* is negligible. Hence the two regions to be considered are the ice cliffs from *F* to *B*, and across the Vanderford Glacier *E* to *D*.

(1) Sheet flow *E* to *F*. Over the boundary *F* to *B* the ice cliffs are approximately the same height and the ice surface contours follow the same pattern as the coast, so

the measurements of thickness and speed made at Cape Folger will be used as typical results for this coastline.

The speed of movement of the Cape Folger ice cliffs is 53 m yr^{-1}. The thickness at the cliff edge has not been measured. At the drum marker 2·4 km inland the thickness was measured at 200 m. An estimate of thickness of the ice can be made from the height of the ice cliffs. Just before calving, the height of the ice cliffs was approximately 17 m above the water. The tabular berg produced was also approximately the same height. Using 0·90 to 1·03 as the ratio of ice to sea water densities, the estimated thickness comes to 136 m. The flow rates per unit length of coast line then become, with $\Phi = \rho \times v \times h$ (ρ density, v velocity) at the cliff edge,

$$\Phi_1 = 0{\cdot}9 \times 53 \times 10^2 \times 136 \times 10^2$$
$$= 6{\cdot}5 \times 10^7 \text{ gm yr}^{-1},$$

and at the inland marker,

$$\Phi_2 = 0{\cdot}9 \times 32 \times 10^2 \times 200 \times 10^2$$
$$= 5{\cdot}8 \times 10^7 \text{ gm yr}^{-1}.$$

This suggests that the estimated thickness at the cliff edge may be too high because the accumulation rate in the area is close to zero and may even be negative. For this reason the smaller figure will be used to calculate the total outflow for the whole coastline.

The length of the coastline from F to B is 110 km. Hence the total outflow becomes

$$\Phi = 5{\cdot}8 \times 10^7 \times 110 \times 10^5$$
$$= 6{\cdot}4 \times 10^{14} \text{ gm yr}^{-1}.$$

(2) Vanderford Glacier flow. The measurements on the Vanderford Glacier provide a velocity profile from one boundary, near Haupt Nunatak, into the centre of the glacier. However, it is not known how far the region of rapid movement (2·6 m per day) of the centre extends across to the other side. The region between the Vanderford and John Quincy Adams Glaciers is a large, smooth, flat expanse with the characteristics, as seen from the air, of a small floating ice shelf. The ocean depth soundings show deep areas in front of the fast moving Vanderford Glacier tongue but less deep regions in front of the coast beyond (cf. Cameron *et al.* (1959)), Maps for Report 825–1, Part III, 2. Windmill Islands).

This suggests that the Vanderford and John Quincy Adams Glaciers are faster-moving streams with a larger, more slowly moving shelf between them. A mean velocity of 1·5 m/day will be taken for the 20 km of coastline E to D. The actual mean velocity of this region may be from 1·0 to 2·0 m/day.

The other unknown variable is the ice thickness. If the region considered is assumed to be a floating tongue, then although the amount of bottom melting is unknown (but should be included with the thickness for outflow considerations), the approximate thickness can be calculated from the heights of the cliff fronts and icebergs. On the other hand, if the glacier were considered as resting on bedrock, then it may be very deep. This follows from the flow considerations in Section 6.3.4 and also from the observations that the ice thickness at point C is approximately

3,200 m (cf. Jewell (1962)) and that the submarine trench in front of the Vanderford tongue reaches a depth of 1250 fathoms (2,228 m). However, from the height of the cliffs in front of the Vanderford it appears unlikely that this part of the glacier is more than 250 m thick.

In the absence of further data the thickness at the positions measured (22 km inland) will be taken as 500 m. This value however may easily be in error by a factor of two. The total flow over the 20 km would then be

$$\begin{aligned}\Phi &= \rho vhl \\ &= 0{\cdot}9 \times 550 \times 10^2 \times 500 \times 10^2 \times 20 \times 10^5 \\ &= 5{\cdot}0 \times 10^{15} \text{ gm yr}^{-1}\end{aligned}$$

with a range from $1{\cdot}5 \times 10^{15}$ to $1{\cdot}5 \times 10^{16}$ gm yr^{-1}.

Even taking the lower estimate, the total combined outflow from sheet flow and glaciers becomes $2{\cdot}1 \times 10^{15}$ gm yr^{-1} as compared to a gain from net accumulation of $1{\cdot}4 \times 10^{15}$ gm yr^{-1}. From this it appears that the outflow can cope with the accumulation in this isolated region. The contours inland of the glaciers, however, are not well defined and a large part of the drainage system considered may include outflow from the great plateau further south. This will be considered later, but first the mass balance of the sector *AFB* will be studied.

6.5.1.2. Sector AFB

All the outflow from this region has been calculated in the previous section for the *FB* coastline as $6{\cdot}4 \times 10^{14}$ gm yr^{-1}. The accumulation is given below.

TABLE 6.VI.

Region	Area km^2	Accumulation Rate gm cm^{-2} yr^{-1}	Product $10^{14} \times$ gm yr^{-1}
1	491	0	
2	479	5	0·239
3	890	8	0·712
4	3256	11	3·575
Total	5116		4·5

From this it appears that the ice flow may be slightly greater than that needed to balance the accumulation of the area. But as the accumulation and movement have been extrapolated beyond regions of measurements the difference of $1{\cdot}9 \times 10^{14}$ gm yr^{-1} is well within the range of errors. More extensive measurements will be needed for a definite answer.

6.5.1.3. The ice cap further inland

Because of the high movement rates of the glaciers and their possibly considerable depth, it will be interesting to determine from the measurements of the accumulation further inland just how much of the ice cap the glaciers can drain.

From the map it appears that all the ice between longitudes 109° and 112°E at least must flow out through the Vanderford and John Quincy Adams systems. If we

assume the whole 80 km of coastline of the glacier fronts has a speed of 1·5 m/day (as assumed for the earlier case) and a thickness of 500 m, then the total annual loss amounts to

$$0{\cdot}9 \times 80 \times 10^5 \times 550 \times 10^2 \times 500 \times 10^2 = 2{\cdot}0 \times 10^{16} \text{ gm yr}^{-1}$$

From the 1961 traverse we have accumulation measurements along longitude 112° E as far as 71° S. If we consider the section south of the saddle point *C*, and assume that the average accumulation between these longitudes and as far as 71° S is the same as the average along the traverse route, then the total accumulation amounts to

$$140 \text{ km} \times 386 \text{ km} \times 40{\cdot}0 \text{ gm cm}^{-2} \text{ yr}^{-1} = 2{\cdot}1 \times 10^{16} \text{ gm yr}^{-1}$$

Already at this distance inland there accumulates as much as flows out in the glacier systems. This still leaves as surplus all the accumulation further inland. Even though the accumulation rate decreases from 18 gm cm^{-2} yr^{-1} at latitude 71° S to 8 gm cm^{-2} yr^{-1} at Vostok, latitude approximately 78° S, the coastal movement rate would need to be considerably higher than here assumed in order to produce a balanced mass flux in this region of the Antarctic ice cap.

Summing up the limited results available at this stage it appears that the flow at the coast may be greater than would be balanced by the accumulation in the immediate inland region (*ACDFB*). However, the accumulation further inland between longitudes 110° and 116° appears to easily outweigh the discrepancy because the only outlet for the ice of this sector is provided by the ice streams of the Totten, Vanderford and John Quincy Adams Glaciers. The possible errors in the estimates make it not unlikely for balance to exist in the coastal region, but further accumulation and movement data will be required to reach a firm conclusion.

ACKNOWLEDGEMENTS

The author wishes to acknowledge the active support given by the members of the ANARE who helped with the glaciological program at Wilkes during 1961.

The results of the work carried out in 1960 have been supplied by Mr. H. P. Black, the officer-in-charge of Wilkes for 1960. Mr. Black extended the accumulation stakes to 300 km south of S2 and later assisted in the analysis of the accumulation results reported in Section 4. The results of the measurements carried out during 1959 were supplied by Mr. W. R. J. Dingle, the officer-in-charge at Wilkes 1959.

Dr. J. T. Hollin and Dr. R. L. Cameron, the leaders of the glaciological teams at Wilkes in 1958 and 1957 respectively, readily provided the detailed reports and information of the work of the United States parties at Wilkes during 1957 and 1958. This information provided an excellent basis for the work of later years.

The author was fortunate in having the guidance of Dr. F. Loewe and Dr. U. Radok of the Department of Meteorology, University of Melbourne, while preparing for the expedition. The Meteorology Department has organised and co-ordinated the glaciological programs of the ANARE each year. During the analysis of the data Dr. Radok readily offered his advice and the frequent discussions enabled many difficulties to be overcome.

Approval to publish the information in this report was given by the Director of the Antarctic Division of the Department of External Affairs, Dr. P. G. Law.

Finally, the author wishes to thank Miss Judith Martin of the Meteorology Department for her care with the typing of the final manuscript and her help in organising the production.

REFERENCES

BADER, H. (1954). Sorge's law of densification of snow on high polar glaciers. *Journal of Glaciology*, Vol. 2, p. 319–323.

BAGNOLD, R. A. (1941). *The physics of blown sand and desert dunes.* London, Methuen & Co.

BALL, F. K. (1956). The theory of strong katabatic winds. *Australian Journal of Physics*, Vol. 9, p. 373–386.

BALL, F. K. (1960). Winds on the ice slopes of Antarctica. *Antarctic Meteorology*, Pergamon Press, Oxford.

BENFIELD, A. E. (1949). A problem of the temperature distribution in a moving medium. *Quarterly Journal of Applied Mathematics*, Vol. 6, p. 439.

BENFIELD, A. E. (1951). The temperature in an accumulating snowfield. *Monthly Notices of the Royal Astronomical Society*, Geophysical Supplement, Vol. 6, p. 139–147.

BENFIELD, A. E. (1953). The effect of accumulation on temperatures within a snowfield. *Journal of Glaciology*, Vol. 2, p. 250.

BLACK, H. P., and BUDD, W. (1964). Accumulation in the region of Wilkes, Wilkes Land, Antarctica. *Journal of Glaciology*, No. 37.

BUDD, W. F. (1963). Glaciology of the Budd Coast and its hinterland—a progress report. *Glaciological Notes*, No. 13, p. 33.

BUDD, W. F. (1966). The drifting of non-uniform snow. *Antarctic Research Reports*, American Geophysical Union, (to be published).

BUDD, W. F., DINGLE, W. R. J., *and* RADOK, U. (1966). The Byrd snow drift project—outline and basic results. *Antarctic Research Reports*, American Geophysical Union (to be published).

BUTKOVICH, T. R., *and* LANDAUER, J. K., (1958). The flow law for ice. International Union of Geodesy and Geophysics, International Association of Scientific Hydrology, Symposium of Chamonix, p. 318–327.

CARSLAW, H. S. *and* JAEGER, J. C. (1959). *Conduction of heat in solids.* Oxford.

CAMERON, R. L., LOKEN, O. H., *and* MOLHOHM, J. R. T. (1959). Wilkes station glaciological data 1957–1958. *Ohio State University Research Foundation Project* 825, Report No. 1, Part 3.

CAMERON, R. L., *and* BULL, C. B. (1962). The thermal diffusivity and conductivity of glacial ice at Wilkes station, Antarctica. American Geophysical Union, Antarctic Research Reports, Maury Memorial Symposium.

COLLINS, B. G., *and* SUMNER, C. J. (1963). An instrument for measuring vertical temperature profiles in small boreholes. *Geofisica Pura e Applica—Milano*, Vol. 54, p. 77–83.

CORNET, A., LORIUS, C., *and* RICOU, G. (1960). Accumulation de neige en Terre Adélie. *La Météorologie*, Ser. 4, No. 57, p. 77–87.

CHI TIEN. (1960). Temperature distribution of an idealised ice cap. *U.S. Army S.I.P.R.E. Research Report* 64.

CRARY, A. P. (1961). Glaciological studies at Little America station, Antarctica, 1957 and 1958. *I.G.Y. Glaciological Report* No. 5.

CRARY, A. P., ROBINSON, E. S. BENNET, H. F., *and* W. W. BOYD, JR. (1962). Glaciological studies of the Ross Ice shelf, Antarctica, 1957–1960. *I.G.Y. Glaciological Report* No. 6.

CROHN, P. W. (1959). A Contribution to the geology and glaciology of the western part of Australian Antarctic Territory. *ANARE Reports*, Series A, Vol. III, 103 p. (Publication No. 49.)

DINGLE, W. R. J., *and* RADOK, U. (1961). Antarctic snow drift and mass transport. International Union of Geodesy and Geophysics, International Association of Scientific Hydrology, Symposium of Helsinki, p. 77–87.

DIUNIN, A. K. (1954). Vertical distribution of solid flux in a snow-wind flow. Technical Translation 999 (from Russian), National Research Council of Canada, Ottawa, 1961.

DIUNIN, A. K. (1956). Struktura metelevogo snega i zakonomernosti snegovogo potoka. (The structure of blowing snow and the laws governing its flow.) *Questions of the utilisation of snow*, Institut Geografii, Akademii Nauk S.S.S.R.

DOLGUSHIN, L. D. (1961). Zones of snow accumulation in Eastern Antarctica. International Union of Geodesy and Geophysics, International Association of Scientific Hydrology, Symposium of Helsinki, p. 63–69'

DORSEY, N. E. (1940). Properties of ordinary water-substance in all its phases: water-vapour, water and all the ices. *American Chemical Society Monograph*, Series No. 81.

GLEN, J. W. (1952). Experiments on the deformation of ice. *Journal of Glaciology*, Vol. 2, p. 111–114.

GLEN, J. W. (1955). The creep of Polycrystalline Ice. *Proceedings of Royal Society*, Series A, Vol. 228, p. 519–538.

HAEFLI, R. (1961). Contribution to the movement and form of the ice sheets in the Arctic and Antarctic. *Journal of Glaciology*, Vol. 3, p. 1133.

HAEFLI, R., *and* BRETANI, F. (1955). Observations in a cold ice cap. *Journal of Glaciology*, Vol. 2, p. 571–580; Vol. 2, p. 623–630.

HOINKES, H. C. (1961). Studies in glacial meteorology at Little America V, Antarctica. International Union of Geodesy and Geophysics, Internation Association of Scientific Hydrology, Symposium of Helsinki, p. 29–48.

HOINKES, H. C. (1962). The settling of firn at Little America III, Antarctica, 1940–1958. *Journal of Glaciology*, Vol. 4, p. 111.

HOLLIN, J. T., *and* CAMERON, R. L. (1961). I.G.Y. glaciological work at Wilkes station, Antarctica. *Journal of Glaciology*, Vol. 3, p. 833–844.

HOLLIN, J. T., CRONK, C. T., *and* ROBERTSON, R. (1961). Wilkes station glaciology 1958. *Ohio State University Research Foundation Report* 825–2, Part X.

JEFFREYS, H. (1952). *The Earth*. Cambridge.

JENSSEN, M. J. D., *and* RADOK, U. (1961). Transient temperature distributions in ice caps and ice shelves. International Union of Geodesy and Geophysics, International Association of Scientific Hydrology, Symposium of Helsinki, p. 112.

JENSSEN, M. J. D., *and* RADOK, U. (1963). Heat conduction in thinning ice sheets. *Journal of Glaciology*, Vol. 4, p. 347.

JEWELL, F. (1962). Wilkes ice thickness measurements 1961. *Australian Bureau of Mineral Resources Records* No. 1962/162, (unpublished).

KOCH, J. P., *and* WEGENER, A. (1930). Wissenschaftliche Ergebnisse. *Koch and Wegener Expedition*, Abteilung I, Meddelelser om Grönland LXXV.

LAGALLY, M. (1934). Mechanik und Thermodynamik des stationären Gletschers. *Ergebnisse der Kosmischen Physik*, Akad. Verlagsgesellschaft, Leipzig, Bd. 2.

LIED, N. T. (1963). Notes on sastrugi and snow dunes observations, satellite station, Vestfold Hills, 1961. *Australian Meteorological Magazine*, No. 40, p. 35–46.

LILJEQUIST, G. H. (1957). Energy exchange of an Antarctic snowfield: Wind structure in the lower layer. *Norwegian–British–Swedish Antarctic Expedition 1949–1952, Scientific Results*, Vol. II, Part I.

LISTER, H. (1960). Solid precipitation and snow drift. *Trans-Antarctic Expedition 1955–1958, Scientific Reports* 5, Glaciology I.

LOEWE, F. (1956). Etudes de glaciologie en Terre Adélie 1951–1952. *Expédition Polaires Française*, IX, Paris.

LOEWE, F. (1957). Precipitation and evaporation in the Antarctic. *Meterology in the Antarctic*, Chapter 5, Ed. M. P. van Rooy, Weather Bureau, Department of Transport, Pretoria, South Africa.

LOEWE, F. (1961). Fortschritte in der Physikalisch-Geographischen Kenntnis der Antarktis. *Erdkunde, Archiv für weissenschaftliche Geographie*, Bd. XV, Lfg. 2, 1961, Bonn.

LORIUS, C. (1962). Contribution to the knowledge of the Antarctic ice sheet: a synthesis of glaciological measurements in Terre Adélie. *Journal of Glaciology*, Vol. 4, p. 79.

MATHER, K. B. (1962). Further observations on sastrugi, snow dunes and the pattern of surface winds in Antarctica. *Polar Record*, Vol. 11, p. 158–171.

MATHER, K. B., *and* GOODSPEED, M. J. (1959). Australian Antarctic ice thickness and sastrugi observations, Mac. Robertson Land, 1957–1958. *Polar Record*, Vol. 9, p. 436–45.

MATHEWS, W. H. (1959). Vertical distribution of velocity in Salmon Glacier, British Columbia. *Journal of Glaciology*, Vol. 3, No. 26.

MELLOR, M. (1958). Australian glaciological contributions in Antarctica—Preliminary report. *Journal of Glaciology*, Vol. 3, p. 279.

MELLOR, M. (1959a). Ice flow in Antarctica. *Journal of Glaciology*, Vol. 3, p. 377.

MELLOR, M. (1959b). Mass balance studies in Antarctica, *Journal of Glaciology*, Vol. 3, p. 522.

MELLOR, M. (1959c). Creep tests on Antarctic glacier ice. *Nature*, Vol. 184, p. 717.

MELLOR, M. (1959d). A study of factors governing the mass economy of Antarctica. Master of Science Thesis, Meteorology Department, University of Melbourne, (unpublished).

MELLOR, M. (1960). Temperature gradients in the Antarctic ice sheet. *Journal of Glaciology*, Vol. 3 p. 773.

NYE, J. F. (1951). The flow of glaciers and ice sheets as a problem in plasticity. *Proceedings of the Royal Society*, A, Vol. 207, p. 554–572.

NYE, J. F. (1952a). The mechanics of ice flow. *Journal of Glaciology*, Vol. 2, p. 82.

NYE, J. F. (1952b). A comparison between the theoretical and the measured long profile of the Unteraar Glacier. *Journal of Glaciology*, Vol. 2, p. 103.

NYE, J. F. (1953). The flow law of ice from measurements in glacier tunnels. laboratory experiments and the Jungfraufirn. *Proceedings of the Royal Society*, A, Vol. 219, p. 477–489.

NYE, J. F. (1957). The distribution of stress and velocity in glaciers and ice sheets. *Proceedings of the Royal Society*, A, Vol. 239, p. 113–133.

NYE, J. F. (1958). A theory of wave formation in glaciers. International Union of Geodesy and Geophysics, International Association of Scientific Hydrology, Symposium of Chamonix, p. 139–154.

NYE, J. F. (1959a). A method of determining the strain rate tensor at the surface of a glacier. *Journal of Glaciology*, Vol. 3, p. 409–419.

NYE, J. F. (1959b). The motion of ice sheets and glaciers. *Journal of Glaciology*, Vol. 3, p. 493.

RADOK, U. (1959). Temperatures in polar ice caps. *Nature*, Vol. 184, p. 1056.

RASTORGUYEV, V. (1961). Teplaya voda v zamerzshikh ozerakh (Warm water in frozen lakes). *Information Bulletin*, No. 31, p. 56.

ROBERTSON, R. (1959). Preliminary report on the bedrock geology of the Windmill Islands. *Ohio State University Research Foundation Project* 825, Report No. 2, Part 6.

ROBIN, G. DE Q. (1955). Ice movement and temperature distribution in glaciers and ice sheets. *Journal of Glaciology*, Vol. 2, p. 523–532.

SHCHEPILOV, F. P. (1963). Quoted in: Soviet activities in the Antarctic, 1961–1962. *Polar Record*, Vol. 11, p. 452.

SCHNEIDER, T. R. (1959). Snow drifts and winter ice on roads. National Research Council of Canada, Technical Translation 1038, Ottawa, 1962.

SCHWERDTFEGER, P. (1963). Theoretical derivation of the thermal conductivity and diffusivity of snow. International Union of Geodsey and Geophysics, International Association of Scientific Hydrology, Symposium of Berkeley, p. 75–81.

SCHYTT, V. (1958). Snow studies at Maudheim; snow studies inland; The inner structure of the ice shelf at Maudheim as shown by core drilling. *Norwegian–British–Swedish Antarctic Expedition 1949–1952, Scientific Results*, Vol. IV, Glaciology II, A to C.

SCHYTT, V. (1960). Snow and Ice Temperatures in Dronning Maud Land. *Norwegian–British–Swedish Antarctic Expedition 1949–1952, Scientific Results*, Vol. IV, Glaciology II, D.

SHAW, P. J. R. (1960). Local winds in the Mawson area. *Antarctic Meteorology*, p. 3, Pergamon, Oxford.

SHIOTANI, M., *and* ARAI, H. (1953). A short note on the snow storm. Proceedings of Second Japanese National Congress for Applied Mechanics.

SORGE, E. (1935). Glaciologische Untersuchung in Eismitte. *Wissenschaftliche Ergebnisse der Deutschen Grönland Expedition Alfred Wegener 1929 und 1930/31*, Bd. III, Leipzig.

SUTTON, O. (1953). *Micrometeorology*. McGraw & Hill, New York.

SWITHINBANK, C. (1958). The morphology of the inland ice sheet and nunatak areas of Western Dronning Maud Land; The regime of the ice sheet of Western Dronning Maud Land as shown by stake measurements. *Norwegian–British–Swedish Antarctic Expedition 1949–1952, Scientific Results*, Vol. III, Glaciology I, D and E.

TAUBER, G. M. (1960). Characteristics of Antarctic katabatic winds. *Antarctic Meteorology*, p. 52–64, Pergamon, Oxford.

VALTAT, B. (1960). Loewe's phenomenon. *Antarctic Meteorology*, p. 65–66, Pergamon, Oxford.

VICKERS, W. W. (1961). The Use of statistical analysis for tracing of firn layers. International Union of Geodesy and Geophysics, International Association of Scientific Hydrology, Symposium of Helsinki, p. 71.

WARD, W. H. (1955). Studies in glacier physics on the Penny Ice Cap, Baffin Island, 1953, Part IV: The flow of Highway Glacier. *Journal of Glaciology*, Vol. 2, p. 592.

WEERTMAN, J. (1957). On the sliding of glaciers. *Journal of Glaciology*, Vol. 3, p. 33.

WEERTMAN, J. (1961). Equilibrium profile of ice caps. *Journal of Glaciology*, Vol. 3, p. 953.

WEXLER, H. (1959). Geothermal heat and glacier growth. *Journal of Glaciology*, Vol. 3, p. 420.

WEXLER, H. (1960). Heating and melting of floating ice shelves. *Journal of Glaciology*, Vol. 3, p. 626.

WEXLER, H. (1961). Growth and thermal structure of the deep ice in Byrd Land, Antarctica. *Journal of Glaciology*, Vol. 3, p. 1075.

UNITED STATES WEATHER BUREAU. Monthly Climatic Data for the World (Published monthly).

ZIMMERMAN, F. R. (1960). Wilkes climatology. *Antarctic Meteorology*, p. 415, Pergamon, Oxford.

ZOTIKOV, I. A. (1961). Izmerenie geotermicheskogo potoka tepla v Antarktide. (Measurement of the geothermal heat flow in Antarctica). *Information Bulletin*, No. 29, p. 30–32.

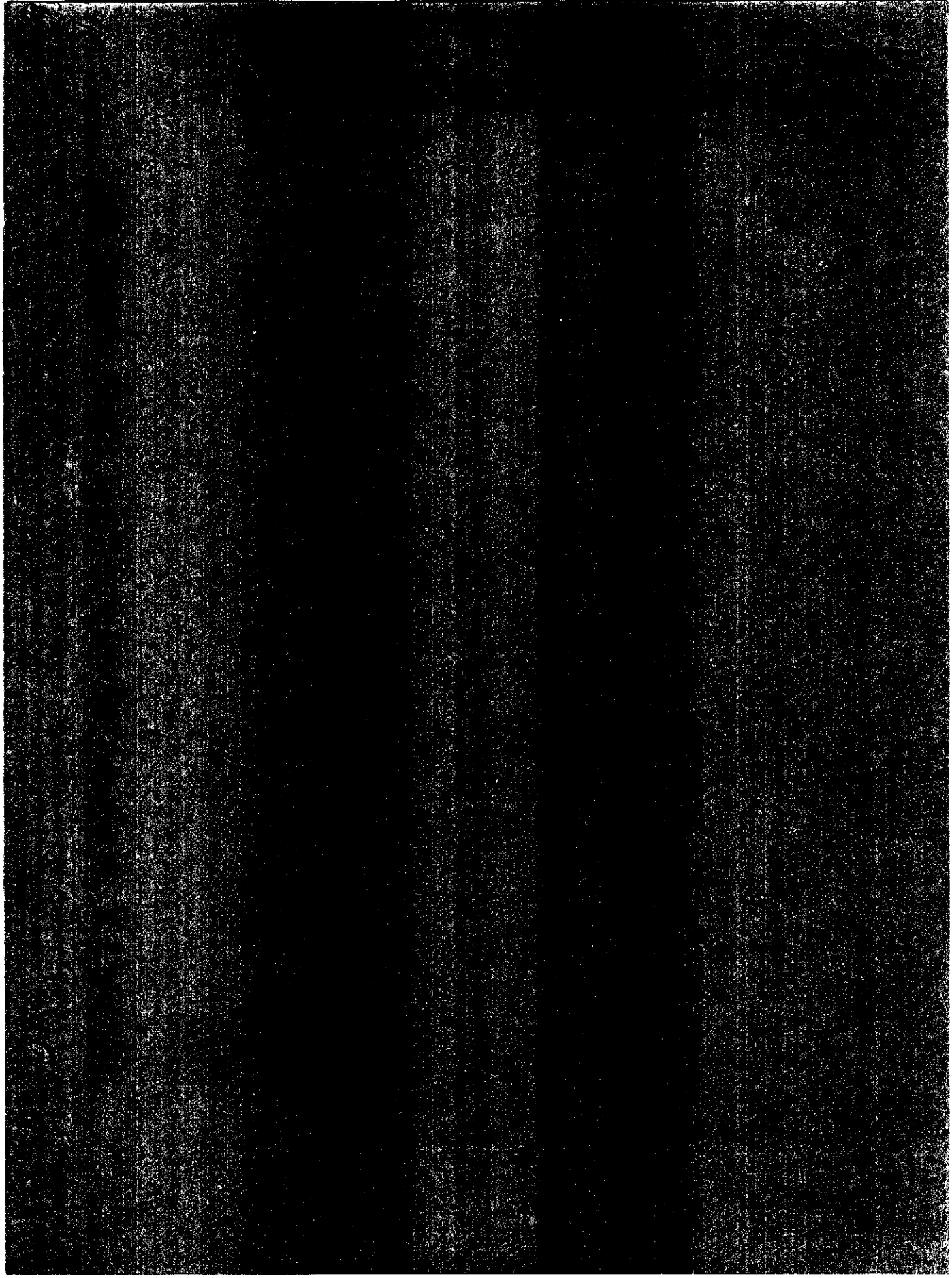

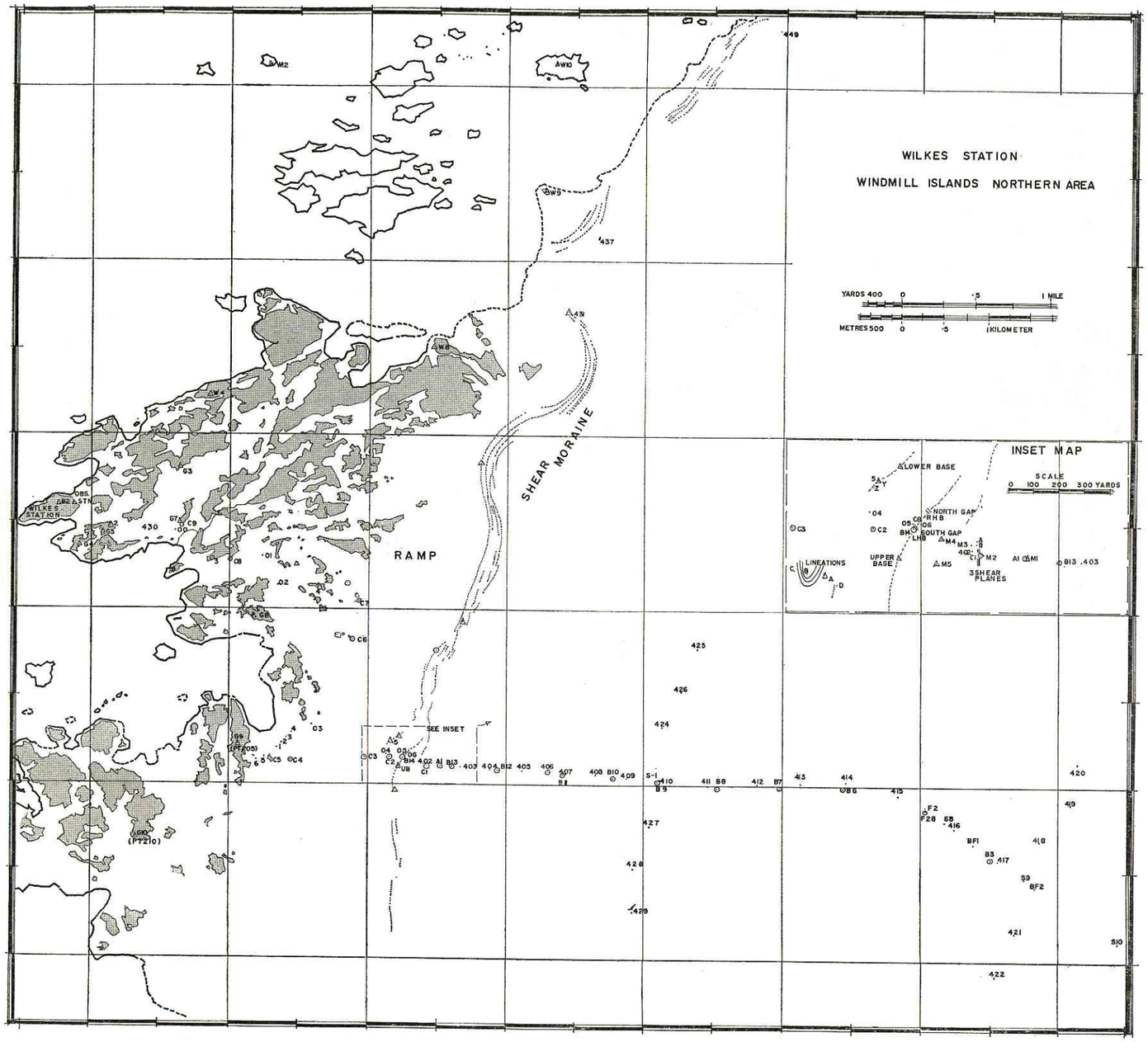

FIG. 0.4. THE WINDMILL ISLANDS NORTHERN AREA MAP. From Fig. (ii) of Cameron et al. (1959). The positions of the major survey stations are shown. together with the local area movement markers and accumulation stakes.

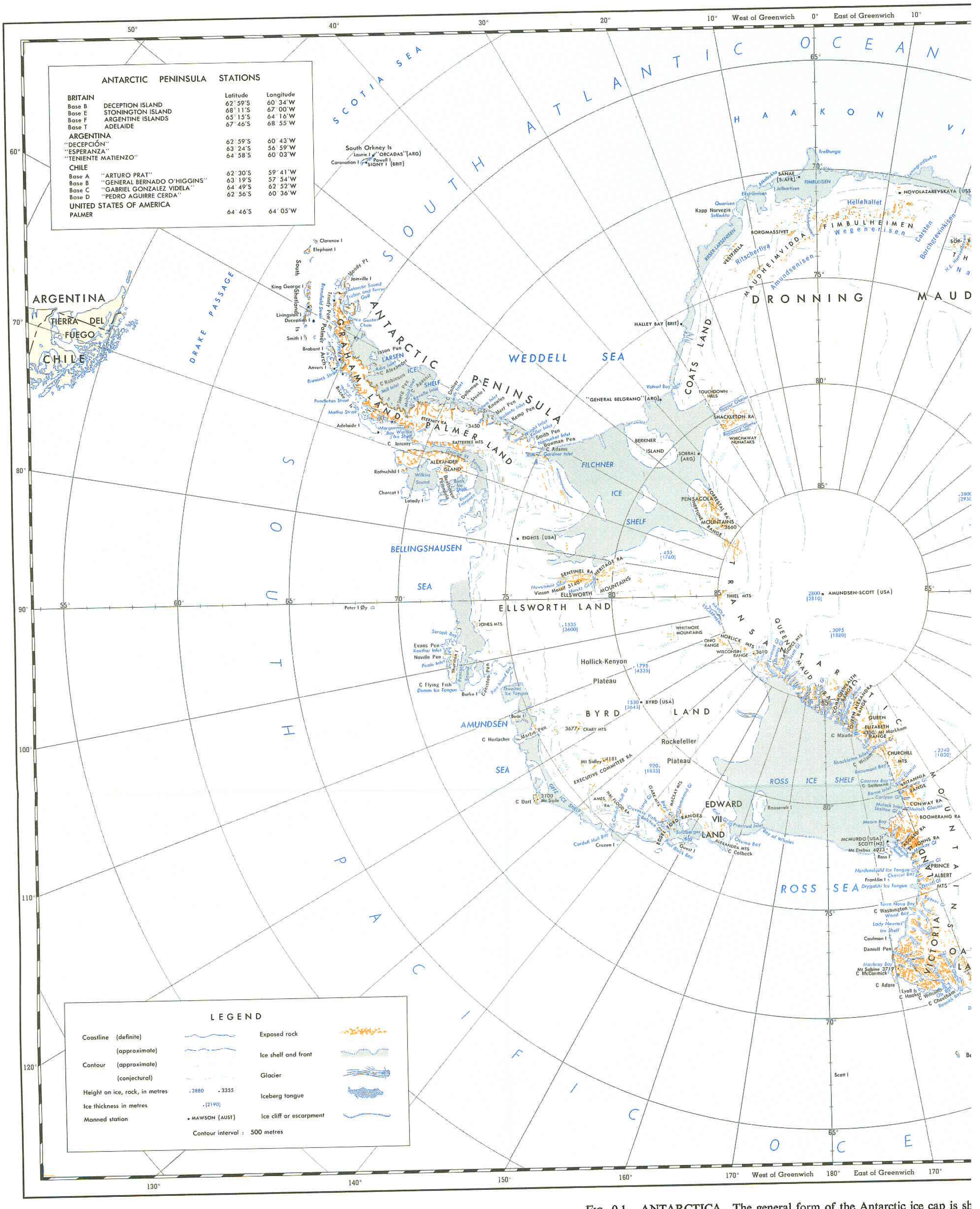

FIG. 0.1. ANTARCTICA. The general form of the Antarctic ice cap is sh
contours drawn at intervals of 500 m. The relative position of the Wilkes re
respect to its eastern Antarctic neighbours: Dumont d'Urville, Mirny, D

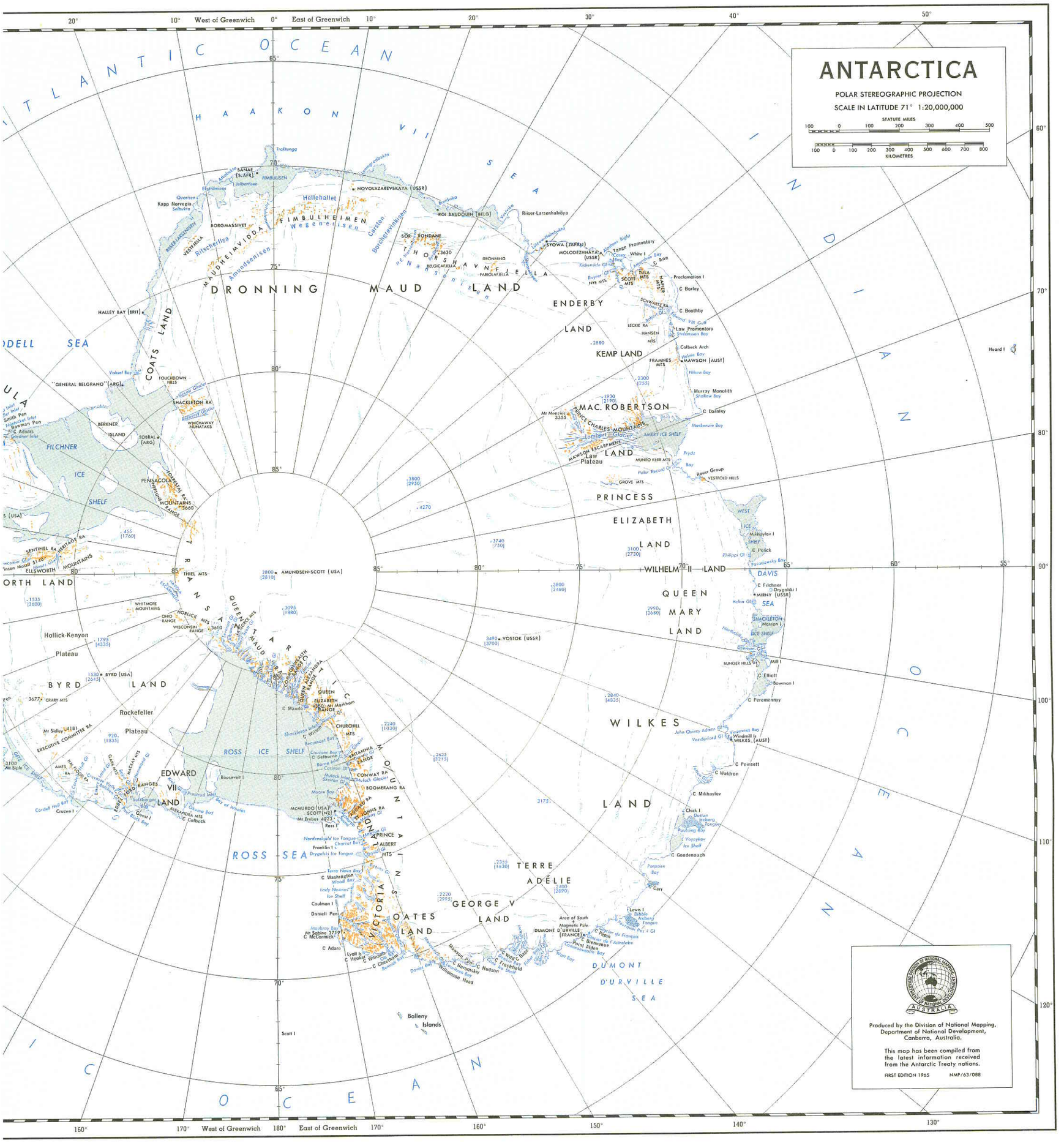

FIG. 0.1. ANTARCTICA. The general form of the Antarctic ice cap is shown by the elevation contours drawn at intervals of 500 m. The relative position of the Wilkes region can be seen with respect to its eastern Antarctic neighbours: Dumont d'Urville, Mirny, Davis and Mawson.